TOXICOLOGY: BIO-NANO INTERACTIONS OF POLYMER COATED TITANIUM DIOXIDE NANOTUBES

A THESIS PRESENTED BY

ATHIRA S S

TO

THE SREE CHITRA TIRUNAL INSTITUTE FOR MEDICAL SCIENCES AND TECHNOLOGY, TRIVANDRUM

Thiruvananthapuram

IN PARTIAL FULFILLMENT OF THE REQUIREMENTS

FOR THE AWARD OF

DOCTOR OF PHOLOSOPHY

2024

CERTIFICATE

I, **Athira S S**, hereby certify that I had personally carried out the work depicted in the thesis entitled *"**Toxicology: Bio-nano interactions of polymer coated titanium dioxide nanotubes"***.No part of the thesis contains any matter previously published or written by another person, nor any material that has been submitted for the award of any other degree or diploma of any University or Institute of higher learning, except where due acknowledgement has been made in the text.

Place: Thiruvananthapuram

Signature: 

Date: 19/10/2024

Name: ATHIRA S S

Reg. No.: 2017/PHD/14

Dr. P V Mohanan

Toxicology Division

This is to certify that, ***Ms. Athira S S*** in the Division of Toxicology of this institute has fulfilled the requirements prescribed for the Ph.D degree of the Sree Chitra Tirunal Institute for Medical Sciences and Technology, Trivandrum. The thesis entitled, ***"Toxicology: Bio-nano interactions of polymer coated titanium dioxide nanotubes"*** was carried out under my direct supervision. No part of the thesis was submitted for the award of any degree or diploma prior to this date.

* Clearance was obtained from the Institute Animal Ethics Committee (IAEC) for carrying out the study. IAEC Approval No.: SCT/IAEC-381/NOVEMBER/2020/107.

On behalf of

Signature:

Dr. MANOJ KOMATH
Scientist G & HOD, LBST

Date: 17.10.24

The thesis entitled

TOXICOLOGY: BIO-NANO INTERACTIONS OF POLYMER COATED TITANIUM DIOXIDE NANOTUBES

Submitted by

Athira S S

For the degree of

Doctor of Philosophy

of

SREE CHITRA TIRUNAL INSTITUTE FOR MEDICAL SCIENCES AND TECHNOLOGY, TRIVANDRUM

Thiruvananthapuram

Is evaluated and approved by

.....

for

Dr. P V Mohanan

(Research supervisor)

04.10.24

Dr. MANOJ KOMATH, Ph.D (Senior DAC member)
Scientist G & HOD,
Chief of Biomaterials Science & Technology
Biomedical Technology Wing, SCTIMST
Poojappura, Trivandrum - 695012

25.09.2024

.....

Thesis examiner

डॉ. एस. के. रथ/Dr. S. K. Rath
मुख्य वैज्ञानिक एवं प्रमुखाध्यक्ष/Chief Scientist & Head
विष विज्ञान एवं प्रायोगिक चिकित्सा प्रभाग
Division of Toxicology & Experimental Medicine
सीएसआईआर-केन्द्रीय औषधि अनुसंधान संस्थान
CSIR-Central Drug Research Institute

ACKNOWLEDGEMENT

I would like to express my sincere gratitude to our Director Dr. Sanjay Behari and Dr. H.K. Varma, Head, Biomedical Technology Wing, Sree Chitra Tirunal Institute for Medical Sciences and Technology, for providing all the necessary support and facilities for completing my PhD work.

I express my sincere thanks to our former Director Dr. Jayakumar K, Former Dean Dr. Sankara Sharma P, Dean Dr. Roy Joseph, Associate Dean Dr. Uma Shankar, Registrar Dr. Santhosh Kumar, Deputy Registrar Mrs. Radha M and all the staffs of the academic division for their academic assistance.

I would like to acknowledge the Council of Scientific and Industrial Research (CSIR-New Delhi) for the financial support with Junior and Senior research fellowship (Award file No. 09/523(0090)/2017-EMR-I).

I am very much grateful to my Doctoral Advisory Committee (DAC) members: Dr. Manoj Komath, Dr. Rekha M R and Dr. Kamalesh K Gulia for their comments of encouragement and valuable suggestions throughout the period of my PhD work.

I would like to express my gratitude and respect to all the Departments and Divisions Heads, Dr. T V Anilkumar (HOD, DAB), Dr. Maya Nandkumar (SIC Toxicology Division), Dr. H K Varma, Dr. Rekha M R, Dr. Anugya Bhatt and Dr. Harikrishnan V S for providing their support in completing my work.

I express my sincere thanks to Dr. Sabareeswaran A and lab members (Histopathology facility), Mr. Suresh Babu S (Bioceramics), Mr. Willi Paul, Mr. Pradeep Kumar S S and lab members (Microbiology), Mrs. Susan Mani, Mr. Prem Mohan M and lab members (DIMT), Dr. Rajalekshmi and other lab members (BST), Mr. Amal Wilson and Ms. Swathi (Molecular Medicine) for all the timely support and facilities.

I would like to extend my gratitude for the support provided by Dr. Remya N S, Dr Sangeetha Vijayan P, Dr Megha K B, Mrs. Vandana Unnikrishnan, Mr. Shaji, Mr. Harikumar G, Mrs. Aparna, Mr. Sudeesan, Mrs. Sreedevi, Former members Mrs. Varsha and Mrs. Shiny. I also thank my former members in research lab, Dr. Syama S,

Dr. Biby T Edwin, Dr. Reshma V G, Dr. Prajitha N, Dr. Anju Surendranath and Dr Ashtami Jayakumar, Mr Akhi Venugopal and Mrs. Aarathi Ashok kumar for their immense support and friendship. I specially thank my labmates Mr. Joseph Xavier, Ms. Reshma, Mr. Amir S, Mr. Ajai Krishnan, for all the support.

I would like to acknowledge with a deep sense of gratitude to my family and friends who stood behind me in the midst of all ups and downs. I am at loss of words to express how grateful I am towards my Amma (Mrs. Sairanthry), Achan (Mr. Suku) and my brother (Mr. Aneesh S S for the never ending love and affection. I consider the immortal loving soul of my younger brother Mr. Anu S S as the light in every path of my journery. I express my deepest affection and thankfulness to my father-in-law, Mother-in-law, Brother-in-law for their enormous support, love and encouragement. Not least of all, I am eternally grateful to my better half Mr. Nabendhu Raj and our daughter Nadhi Nabendhu for the overwhelming support, love and care.

I bow my head with immense gratitude and dedicate this dissertation to the eternal soul of my beloved supervisor Dr. P V Mohanan for his relentless support, guidance and encouragement throughout the journey.

Finally, thank you God Almighty for all the blessings you have bestowed.

Athira S S

CONTENTS

Declaration by the student…… ii
Certificate of guide…… iii
Approval of thesis…… iv
Acknowledgements…… v
Table of contents…… vii
List of figures…… xv
List of tables……... xviii
Abbreviations…… xix
Synopsis…….. xxiii

1 CHAPTER 1: INTRODUCTION 1
1. Introduction 2
1.1 Nanomaterials…… 2
1.2 Types of nanomaterials …… 4
1.2.1 Carbon-based nanomaterials…….. 4
1.2.2 Metal-based nanomaterials……. 5
1.2.3 Dendrimers……. 6
1.2.4 Composite nanomaterials……..... 6
1.3 Nanotubes and their importance in present era……. 7
1.4 Type of nanotubes and derivatives…… 9
1.5 Nanomaterial toxicity…… 12
1.6 Cell line used……. 13
1.6.1 Glial cells and nanotoxicity…… 14
1.7 Motivation of the study……. 16
1.8 Objectives…….. 17

2 CHAPTER 2: REVIEW OF LITERATURE 20
2. Review of literature 21
2.1 Nanotubes: different dimensions……... 21
2.2 Different types of synthesis of nanotubes……. 22

2.2.1 Sol-gel methods…….. 23
2.2.2 Template assisted method…….. 23
2.2.3 Hydro or Solvo thermal approaches……... 24
2.2.4 Electro chemical anodization…… 24
2.2.5 Chemical vapour deposition (CVD) ……..…… 26
2.3 Structure and characterization of nanotubes……. 27
2.3.1 Different structures of nanotubes……..... 29
2.3.1.1 Hydrothermal tubes……. 29
2.3.1.2 Anodic tubes…… 29
2.3.2 Characterization techniques for nanotubes…… 30
2.4 Different applications of nanotubes…….. 31
2.4.1 Photocatalytic applications……. 32
2.4.2 In solar cells……..... 33
2.4.3 In electro-chromic devices……. 34
2.4.4 Biomedical applications……. 35
2.4.4.1 Cell interaction and biomedical coatings…… 35
2.4.4.2 Tissue engineering based on TNT arrays…… 36
2.4.4.3 Drug delivery from TNT arrays…….. 37
2.4.4.4 Biosensing mediated by nanotubes……. 38
2.5 Toxicity or safety of nanotubes……. 39
2.5.1 Cellular toxicity……. 39

3 CHAPTER 3: MATERIALS AND METHODS 41
3. Materials and Methods…… 42
3.1 Chemicals…….. 42
3.2 Equipments…… 42
3.3 Animal husbandry and welfare……. 44
3.4 Animal ethics……. 44
3.5 Synthesis of titanium dioxide (TiO_2) nanotubes using solvothermal route and physico-chemical characterization……. 45
3.5.1 Synthesis of TiO_2 nanotubes…….. 45
3.5.1.1 PHASE I: Synthesis of TiO_2 nanoparticles (TNPs)…… 45

3.5.1.2 PHASE II: Synthesis of TNTs using solvothermal method……. 45
3.5.1.3 PHASE III: Surface coating of TNTs with Pluronic F-127……..... 48
3.5.2 Physico-chemical characterization……. 49
3.5.2.1 Dynamic light scattering (DLS) ……. 50
3.5.2.2 Zeta potential analysis……. 50
3.5.2.3 Fourier transform infrared spectroscopy (FTIR)…… 50
3.5.2.4 X-Ray diffraction (XRD)…… 50
3.5.2.5 Micro Raman spectroscopy……. 51
3.5.2.6 Transmission electron microscopy (TEM)……. 51
3.5.2.7 Thermo gravimetric analysis (TGA)……..... 51
3.5.2.8 Differential thermal analysis (DTA)……..... 51
3.5.2.9 Evaluation of surface coating of TNTs using FTIR Spectroscopy……..... 52
3.6 Evaluation of *in vitro* toxicity of TiO_2 nanotubes using C6 cell line…… 52
3.6.1 C6 glial cell culture and nanomaterial exposure…… 52
3.6.2 Cellular phenotypic observation by phase contrast microscopy…… 52
3.6.3 Cellular uptake study using imaging flow cytometry ……..... 53
3.6.4 Evaluation of cell viability or mitochondrial activity by MTT assay…..……... 53
3.6.5 Mitochondrial membrane potential (MMP) evaluation by JC1 staining…….. 54
3.6.6 Evaluation of lysosomal stability using neutral red uptake (NRU) assay……..... 54
3.6.7 Assessment of lysosomal integrity using acridine orange staining…… 55
3.6.8 Evaluation of cellular morphology using non-fluorescent staining methods…….. 56
3.6.8.1 Coomassie Brilliant Blue (CBB) staining for TNP exposure of C6 cells…… 56
3.6.8.2 Giemsa staining for TNT exposure of C6 cells…….. 56
3.6.9 Evaluation of cytoskeletal integrity or actin filament organization by rhodamine-phalloidin staining……... 56
3.6.10 Investigation of intracellular oxidative stress……..... 57
3.6.10.1 Evaluation of Reactive Oxygen Species (ROS) by DCFH-DA Assay……..... 57
3.6.10.2 Evaluation of Reactive Nitrogen Species (RNS) by Griess reagent Assay…… 58
3.6.11 Evaluation of cell membrane integrity using lactate dehydrogenase (LDH) release assay ……. 58

3.6.12 Live/dead cell study for TNPs using acridine orange (AO) / ethidium bromide (ETBR) dual staining method……... 59
3.6.13 Live/dead study for TNTs using calcine AM/PI staining method……..... 59
3.6.14 DNA laddering assay for nuclear integrity by agarose gel electrophoresis (AGE) ……... 60
3.6.15 Evaluation of nuclear condensation by DAPI staining…… 60
3.6.16 *In vitro* toxicity studies for TNT-P……..... 61
3.6.16.1 Evaluation of cell viability upon TNT-P exposure by MTT Assay……... 61
3.6.16.2 Study on effects of P-F127 polymer on C6 cell viability……... 61
3.6.16.3 Lysosomal integrity study for TNT-P – C6 cells interaction…… 61
3.6.16.4 Evaluation of ROS generation for C6 cells – TNT-P interaction……..... 61
3.7 Investigation of acute toxicity of surface coated TiO_2 nanotubes using wistar rat…….. 62
3.7.1 Experimental design and dosage…… 62
3.7.2 Visual examination for signs of behavioral changes…….. 63
3.7.3 Body weight of rats…… 63
3.7.4 Euthanization and sample collection…….. 63
3.7.5 Gross pathology analysis…… 63
3.7.6 Wet weight of rat organs…… 63
3.7.7 Hematology analysis…….. 64
3.7.8 Serum biochemistry analysis…….. 64
3.7.9 Determination of antioxidant levels in the brain and liver …….. 64
3.7.9.1 Estimation of total protein by Lowry's method…….. 64
3.7.9.2 Detection of reduced glutathione (GSH) by DTNB method…….. 65
3.7.9.3 Detection of lipid peroxidation (LPO) by thiobarbiturate reaction…… 66
3.7.10 urine analysis……..... 66
3.7.11 Biodistribution study using inductively coupled plasma mass spectroscopy (ICPMS) …….. 67
3.7.11.1 Sample digestion…….. 68
3.7.11.2 ICPMS analysis…… 68
3.7.12 Immunotoxicity study……. 68
3.7.12.1 Splenocyte proliferation Assay by Tritiated (^3H) Thymidine 69

incorporation…….....
3.7.13 Histopathology analysis……..... 70
3.7.13.1 Tissue processing…….. 70
3.7.13.2 Eembedding…….. 71
3.7.13.3 Preparation of glass slides……. 71
3.7.13.4 Sectioning of paraffin blocks…… 72
3.7.13.5 Tissue staining using Haematoxylin and Eosin (H&E)…… 72
3.8 Statistical analysis……. 73

4 CHAPTER 4: RESULTS 74
4. Results……. 75
4.1 Synthesis of titanium dioxide (TiO_2) nanotubes using solvothermal route and physico-chemical characterization……. 75
4.1.1 Synthesis of TNTs and polymer coating…… 75
4.1.2 Physico-chemical characterization……. 75
4.1.2.1 Dynamic light scattering (DLS) ……. 76
4.1.2.2 Zeta potential Analysis…… 76
4.1.2.3 Fourier transform infrared spectroscopy (FTIR)…… 76
4.1.2.4 X-ray diffraction (XRD)…… 77
4.1.2.5 Micro Raman spectroscopy……. 79
4.1.2.6 Transmission electron microscopy (TEM)…….. 80
4.1.2.7 Thermo-gravimetric analysis (TGA)…….. 81
4.1.2.8 Differential thermal analysis (DTA)……..... 82
4.1.2.9 FTIR Spectroscopy for surface coating……. 84
4.2 Evaluation of *in vitro* toxicity of TiO_2 nanotubes using C6 cell line…… 86
4.2.1 C6 glial cell culture and nanomaterial exposure…… 86
4.2.2 Phenotypic observation by phase contrast microscopy…….. 86
4.2.3 Cellular uptake study using imaging flow cytometry…… 87
4.2.4 Cell viability study by MTT assay……. 87
4.2.5 Mitochondrial membrane potential (MMP) analysis by JC1 staining…….. 87
4.2.6 Lysosomal integrity study using NRU assay……. 88
4.2.7 Acridine orange (AO) staining……..... 90

4.2.8 Evaluation of cellular morphology…… 92
4.2.8.1 Coomassie brilliant blue (CBB) staining…… 92
4.2.8.2 Giemsa staining……..... 92
4.2.9 Actin filament staining using rhodamine phalloidin……. 94
4.2.10 Investigation of intracellular oxidative stress……..... 95
4.2.10.1 Detection of ROS by DCFH-DA assay……. 95
4.2.10.2 Detection of RNS by Griess reagent assay…… 96
4.2.11 Cell membrane integrity by LDH release assay……..... 97
4.2.12 Live/dead cell study for TNPs……. 98
4.2.13 Live/dead cell study for TNTs……. 99
4.2.14 DNA laddering by agarose gel electrophoresis (AGE) …….. 99
4.2.15 Nuclear condensation by DAPI staining…….. 99
4.3 *In vitro* toxicity studies for TNT-P…… 100
4.3.1 Cell viability study by MTT assay……. 100
4.3.2 Effects of P-F127 on C6 cell viability…… 100
4.3.3 Lysosomal integrity by NRU assay…… 103
4.3.4 ROS generation by DCFH-da assay……..... 104
4.4 Investigation of acute toxicity of surface coated TiO_2 nanotubes using wistar rat…….. 105
4.4.1 Visual examination of behavioural changes……..... 105
4.4.2 Body weights of rats……..... 106
4.4.3 Gross pathology evaluation…… 106
4.4.4 Wet weight of organs……. 107
4.4.5 Hematology analysis…….. 109
4.4.6 Serum biochemistry…… 109
4.4.7 Antioxidants in brain and liver……..... 110
4.4.8 Urine analysis……. 112
4.4.9 Biodistribution study by ICPMS…… 113
4.4.10 Immunotoxicity…… 116
4.4.11 Histopathology……. 118

5 CHAPTER 5: DISCUSSION 121

5. Discussion……... 122

5.1 Synthesis and physico - chemical characterization of TiO_2 nanotubes……. 122

5.1.1 Synthesis of TNTs and bio-polymer coating…….. 122

5.1.2 Physico-chemical characterization……. 123

5.1.2.1 Physico-chemical characterization…….. 123

5.1.2.2 Zeta potential Analysis…… 124

5.1.2.3 Fourier transform infrared spectroscopy (FTIR) …… 124

5.1.2.4 X-ray diffraction (XRD) ……. 125

5.1.2.5 Micro Raman spectroscopy……. 125

5.1.2.6 Transmission electron microscopy (TEM) ……. 126

5.1.2.7 Thermo gravimetric analysis (TGA) …….. 126

5.1.2.8 Differential thermal analysis (DTA) …….. 127

5.1.2.9 FT/IR Spectroscopy for surface coating……. 127

5.2 *In vitro* toxicity of TiO_2 nanotubes using C6 glial cells…… 128

5.2.1 C6 glial cell culture and nanomaterial exposure…… 128

5.2.2 Phase contrast microscopy……. 129

5.2.3 Imaging flow cytometry……. 129

5.2.4 MTT assay…….. 130

5.2.5 JC1 staining…… 131

5.2.6 NRU assay…….. 131

5.2.7 Acridine orange (AO) staining……... 132

5.2.8 Cellular morphology…….. 132

5.2.8.1 Coomassie brilliant blue (CBB) staining…… 132

5.2.8.2 Giemsa staining……... 133

5.2.9 Rhodamine phalloidin staining…….. 133

5.2.10 Intracellular oxidative stress……. 134

5.2.10.1 DCFH-DA assay……... 134

5.2.10.2 Griess reagent assay…….. 135

5.2.11 LDH release assay…… 135

5.2.12 AO/EtBR DUAL STAINING…….. 136

5.2.13 Calcian am/pi staining…….. 136

5.2.14 DNA laddering assay……..... 136
5.2.15 DAPI staining……..... 137
5.2.16 *In vitro* toxicity studies for TNT-P……..... 137
5.2.16.1 MTT assay……. 137
5.2.16.2Effects of P-F127 on C6 cell viability…….. 138
5.2.16.3 NRU assay……. 138
5.2.16.4 DCFH-DA assay……... 138
5.3 *In vivo* experiments for acute toxicity response of TNT-P……... 139
5.3.1 Behavioural changes…….. 139
5.3.2 Body weight……... 140
5.3.3 Organ weight…….. 140
5.3.4 Hematology…… 141
5.3.5 Serum biochemistry…… 141
5.3.6 Antioxidants in brain and liver……..... 142
5.3.7 Urine analysis……. 143
5.3.8 Biodistribution by ICP-MS…… 143
5.3.9 Immunotoxicity…….. 144
5.3.10 Histopathology……. 144

6 CHAPTER 6: SUMMARY AND CONCLUSION 146
6. Summary and Conclusion……..... 147
6.1 Summary……... 147
6.2 Methodology adapted for the study…….. 151
6.3 Major findings of the study……... 153
6.4 Conclusion…… 155
6.5 Future directions…… 156
References……. 157
Annexure…… 174
List of publications…….. 174
Online Reports……. 175
Book chapters…….. 175
Conference presentations…… 176

LIST OF FIGURES

1.1 General applications of nanotubes……. 10

1.2 Cellular toxicity induced by nanoparticles in general…… 14

1.3 Various uptake pathways for nanoparticles into brain parenchyma……... 15

1.4 Proposed pathway for nanoparticle-induced onset of neurodegenerative disease……..... 17

1.5 Overall work plan of the study……... 19

2.1 Solvo thermal formation of TiO_2 nanotubes and their applications……... 22

2.2 Structure of single-walled graphene and CNTs and multi-walled graphene & CNTs……... 28

2.3 Basic mechanism involved in TiO_2 driven photo catalytic removal of organic pollutants…… 33

2.4 Adhesion complex formation of TNT surface by ECM components around cells……. 36

3.1 Synthesis of TNPs using urea precipitation method……... 46

3.2 Two-step formation of TNT from TNP through Solvo thermal method…… 47

3.3 Steps and principle involved in Solvo thermal synthesis of TiO_2 nanotubes…. 48

3.4 Flow chart for P-F127 coating of TNTs (PhaseIII)…… 49

3.5 Biochemical reaction involved in DCFH-D Aassay…….. 57

3.6 *In vivo* acute toxicity work plan using Wistar rat liver samples by Lowry's method…… 62

3.7 Procedure for estimation of total proteins using Wistar rat…… 65

3.8 Procedure for cleaning glass slides for H&E staining…… 72

4.1 Zeta potential measurement of TNPs……. 77

4.2 FT/IR Spectroscopy…… 78

4.3 X-Ray diffraction of TNPs and TNTs…… 79

4.4 Micro Raman spectra of TNPs and TNTs…….. 82

4.5 TEM images of TNPs at different magnifications and that of TNTs……. 83

4.6 TGA analysis plots for TNPs and TNTs…… 84

4.7 DTA analysis for TNPs and TNTs……. 84

4.8 FT/IR spectroscopy for surface coating of TNTs, P-F127 and TNT-P…….. 85

4.9 Phase contrast images of cultured C6 glial cells…… 86

4.10 Imaging flow cytometry for identification of cellular uptake of TNPs into C6 cells upon 24h exposure…… 88

4.11 MTT assay for C6 cells after 24h exposure with TNPs and TNTs…….. 89

4.12 MMP analysis using JC1 staining for C6 cells treated with TNPs and TNTs 90

4.13 Cell viability or lysosomal integrity study by Neutral red uptake assay for cells exposed with TNPs and TNTs…… 91

4.14 Lysosomal integrity study using AO staining for cellular exposure with. TNPs and TNTs…….. 92

4.15 Morphological evaluation of C6 cells using non-fluorescent CBB staining method for 24h cellular exposure with TNPs……... 93

4.16 Giemsa staining for C6 cells after exposure with TNTs for 24h…….. 93

4.17 Actin filament organization study using Rhodamine phalloidin staining…… 94

4.18 DCFH-DA assay for ROD detection after 24h cellular exposure with TNPs and TNTs…….. 95

4.19 Griess reagent assay for detection of intracellular RNS after exposure with TNPs and TNTs…… 96

4.20 Cell membrane damage study using LDH release assay for cells treated with TNPs and TNTs…….. 97

4.21 Live/dead study by AO/EtBr dual staining for cells exposed with TNPs for 24h…… 98

4.22 Live/dead study by Calcein AM/PI staining for cells treated with TNTs for 24h……... 101

4.23 DNA laddering assay by Agarose gel electrophoresis……. 102

4.24 Nuclear condensation study by DAPI staining for cells exposed with TNPs at various concentrations……... 102

4.25 MTT assay for cellular exposure with TNT-P……. 103

4.26 Effects of P-F127 on cell viability by MTT assay……... 103

4.27 Lysosomal integrity study for TNT-P using DCFH-DA assay…… 104

4.28 Oxidative stress evaluation for TNT-P using DCFH-DA assay……... 105

4.29 Body weight assessment of Wistar rats…… 107

4.30 Gross pathology evaluation of Wistar rats treated with TNT-P……... 107

4.31 Wet weight of organs isolated from Wistar rats after TNT-P administration.. 108

4.32 Plots showing hematology parameters mean value for Wistar rats treated with TNT-P……... 111

4.33 (i) Biochemistry evaluation for metabolic enzymes from Wistar rats exposed with TNT……. 113

4.33 (ii) Analysis for biochemical parameters for Wistar rats exposed with TNT-P…….. 114

4.34 Evaluation of antioxidant levels in brain and liver from Wistar rats exposed with TNT-P…….. 115

4.35 Biodistribution study of samples isolated and collected from Wistar rats after TNT-P administration…….. 117

4.36 Immunotoxicity study by splenocyte proliferation assay for Wistar rats after TNT-P exposure…… 118

4.37 Histopathology evaluation of tissue samples from Wistar rats exposed with TNT-P using H&E staining (Brain and Liver)……. 119

4.38 Histopathology evaluation for tissue samples from Wistar rats exposed with TNT-P (Spleen and Kidney)…… 120

LIST OF TABLES

3.1 Procedure for GSH estimation in brain and liver samples by DTNB method... 66

3.2 Procedure for LPO assay…… 67

3.3 Elemental analysis conditions for Inductively Couples Plasma Mass Spectroscopy (ICPMS)…….…….. 69

3.4 Embedding procedure for H&E staining…… 71

3.5 Steps in Hematoxylin & Eosin (H&E) staining for tissue sections…… 73

4.1 Influence of dispersion media in terms of Z-average dm & PDI for TNPs….. 76

4.2 Diffraction angles (2θ values) of each XRD peak & corresponding hkl indices……. 78

4.3 Raman spectroscopic parameters for TNPs & TNTs……. 80

4.4 Visual examination of Wistar rats for behavioral changes……. 106

4.5 Wet organ weight of Wistar rats exposed with TNT-P…….. 108

4.6 Hematology parameters count for Wistar rats exposed with TNT-P……. 110

4.7 Serum Biochemistry analysis for Wistar rats treated with TNT-P……. 112

4.8 Urine analysis of Wistar rats exposed with TNT-P…… 116

ABBREVIATIONS

µg	: Microgram
µL	: Microliter
µM	: Micromolar
0D	: Zero Dimensional
1DNMs	: One Dimensional Nanomaterials
2D	: Two Dimensional
3D	: Three Dimensional
AB/AM	: Antibiotic/Antimycotic
AD	: Alzhiemer's Disease
ALP	: Alkaline Phosphatase
ALT	: Alanine Transaminase
AO	: Acridine Orange
AST	: Aspartate Transaminase
BBB	: Blood Brain Barrier
BSA	: Bovine Serum Albumin
C	: Control
CBB	: Coomassie Brilliant Blue
CNS	: Central Nervous System
CNTs	: Carbon Nanotubes
CO_2	: Carbon dioxide
CPCSEA	: Committee for the Purpose of Control and Supervision of - Experiment on Animals
CTAB	: Cetyltrimethyl Ammonium bromide
CVD	: Chemical Vapour Deposition
D.I water	: De-Ionized water
DAPI	: 4', 6-diamidino-2-phenylindole
DCFH-DA	: 2′,7′-dichlorofluorescin diacetate
DLS	: Dynamic Light Scattering
DMEM F12	: Dulbecco's Modified Eagle Medium/ Nutrient Mixture F12

DMSO	: Dimethyl Sulfoxide
DNA	: Deoxyribonucleic Acid
DSSC	: Dye-sensitized Solar Cells
DTA	: Differential Thermal Analysis
DTNB	: Bis (3- carboxy, 4-nitrophenyl) disulfide
ECM	: Extra Cellular Matrix
EtBr	: Ethidium Bromide
ETC	: Electron Transport Chain
FBR	: Foreign Body Response
FBS	: Fetal Bovine Serum
FSC	: Forward Scatter
FT/IR	: Fourier Transform Infrared Spectroscopy
GSH	: Reduced Glutathione
H&E	: Hematoxylin and Eosin
H_2O	: Water
HCT	: Hematocrit
HGB	: Hemoglobin
i.p	: Intraperitoneal
IAEC	: Institute Animal Ethical Committee
ICPMS	: Inductively Coupled Plasma Mass Spectroscopy
IL-1α	: Interleukin-1 Alpha
IL-4	: Interleukin-4
IR	: Infra-Red
LDH	: Lactate Dehydrogenase
LPO	: Lipid Peroxidation
MCH	: Mean Corpuscular Hemoglobin
MCHC	: Mean Corpuscular Hemoglobin Concentration
MCV	: Mean Corpuscular Volume
MDA	: Malondialdehyde
min	: Minute
MMP	: Mitochondrial Membrane Potential

MOS_2 : Molybdenum Sulfide

MS : Mass Spectroscopy

MTT : 3-(4, 5-Dimethylthiazol-2-yl)-2,5-diphenyltetrazolium- : bromide

MWCNTs : Multi-Walled Carbon Nanotubes

N : Normal

$Na_2Ti_3O_7$: Sodium Titanate

NaOH : Sodium hydroxide

NCCS : National Center for Cell Science

NF-κB : Nuclear Factor- Kappa B

nm : Nanometer

NMs : Nanomaterials

NPs : Nanoparticles

NRU : Neutral Red Uptake

NTs : Nanotubes

PBS : Phosphate Buffered Saline

PC : Positive Control

PD : Parkinson's Disease

P-F127 : Pluronic F-127

pH : Potential of hydrogen

PI : Propidium Iodide

PLT : Platelet

PNS : Peripheral Nervous System

PTT : Photothermal Therapy

R/P : Rhodamine phalloidin

RBC : Red Blood Cells

RES : Reticulo Endothelial System

RFU : Relative Fluorescence Unit

RNA : Ribonucleic acid

RNS : Reactive Nitrogen Species

ROS : Reactive Oxygen Species

SAED : Selected Area Electron Diffraction

SDS	: Sodium Dodecyl Sulfate
SnS_2	: Tin (IV) Sulfide
SSC	: Side Scatter
SWCNTs	: Single-Walled Carbon Nanotubes
TBA	: Thiobarbiturate
TCA	: Trichloro Acetic acid
TEM	: Transmission Electron Microscopy
TGA	: Thermo gravimetric Analysis
TiO_2	: Titanium Dioxide
TMCH	: Transition Metal Chalcogenides
TNF	: Tumour Necrosis Factor
TNPs	: TiO_2 nanoparticles
TNT-P	: Pluronic F-127 coated TiO_2 nanotubes
TNTs	: TiO_2 nanotubes
UV	: Ultra Violet
WBC	: White Blood Cells
WS_2	: Tungsten (IV) Sulfide
XRD	: X-Ray Diffraction
ZnO	: Zinc Oxide
ZrO_2	: Zirconium Dioxide

SYNOPSIS

Title: 'Toxicology: Bio-nano interactions of polymer coated titanium dioxide nanotubes'

People of the recent era require devices which can accommodate all the properties and informations at a high density using only negligible energy. However, it was quite challenging to miniaturize components into tiny sizes using available techniques. This further ignited the notion of nanotechnology which holds the concept of achieving fascinating properties exhibited by materials in their nanoform. The term 'Nanotechnology' comprises an emerging branch of science dealing with the manipulation and control of matter at the atomic or molecular level. The materials forming the base of nanotechnology are termed as 'Nanomaterials' (NMs); which all belong to the size range of 1-100 nanomater (nm). The downsizing of matter to the nanometer level allows accomplishing certain inherent properties of materials such as quantum effect or surface effect. This is principally not attainable when materials are in their bulk form and this fact justifies the relevance of nanotechnology. There exist a long list of criteria based on which the NMs classification can be made. For example, based on dimensionality, composition, type of material and the route of fabrication *etc*. Considering dimensionality, one dimensional nanomaterials (1D NMs) offers immense application potentials. Especially 1D NMs synthesized from metallic nanoparticles (NPs) are of extreme importance because of their unique physico-chemical properties and biocompatibility. 1D nanostructures formed from titanium dioxide (TiO_2) have been gaining considerable attention among scientific community in recent years. In particular; nanotubes, nanofilaments, nanowires, nanorods *etc.*

TiO_2 is generally considered as the most prominent photocatalyst with Ultra Violet (UV) absorption properties and it has been globally accepted as one of the major transition metal oxides. Far exceeding commercial acceptability of this material can be exemplified like; in self-cleaning surfaces, paints and sunscreens, cosmetics, dye-sensitized solar cells, water purification systems, electrical devices *etc.* Most of these applications relay mainly on the wide band gap energy of their crystalline forms (Anatase, Rutile & Brookite). There are enough evidences for the observation that, it is crucial to have higher surface area to volume ratio for the complete utilization of the

inherent properties of the NMs. This further stimulated the demand of 1D NMs in various applications. Ever since the discovery of Carbon Nanotubes (CNTs), researchers have witnessed the exciting properties of nanotubes (NTs) because of their unique molecular geometry. NTs formed from TiO_2 were identified to be offering a perfect combination of metallic properties and nanotubular morphology. Biomedical field has been benefited from such advantageous features of TiO_2 nanotubes (TNTs) in various scenarios. For example, targeted drug delivery and unloading of other biomolecules, as tissue implants (bone, cartilage, dental, knee *etc.*), as intravascular stents, photothermal therapy (PTT) and other anti-cancerous treatments, for improvisation of electrostatic interaction and tissue regeneration, cardiovascular therapies *etc*.

Despite the increasing application potentials of NMs, huge concerns about human biosafety have also been raised considerably. Owing to their extremely smaller size, NMs are capable of invading into the deeper premises of the body. Further physiological fate of the material is crucially dependent on the physico-chemical properties of the material; particularly the morphology. Regarding biosafety of TiO_2 nanostructures, numerous arguments still exist as it have already been proven to cause deleterious toxic effects in some *in vitro* and *in vivo* systems. For instance, studies have confirmed significant toxic outcomes such as lipid peroxidation, oxidative stress, DNA damage, apoptosis *etc*. However, a generalization of these toxic effects cannot be derived as it depends on several physico-chemical properties. Considering this fact and the increasing therapeutic applicability of TNTs in neuronal tissue, an effort was made to evaluate the safety limits of TNTs using a neuronal cell line (C6 glial cell) and the acute toxicity was also studied using rat model. C6 glial cells were used for the study as it denotes one of the key regulators of immune response of the brain tissue. The study includes a comparative toxicity evaluation of nano TiO_2 in NP and NT forms. Also a safety assessment of a polymer coated TNTs were also performed based on the concept that, surface coating can contribute to increasing dispersion stability of the material.

In view of existing literatures, present study was designed hypothesizing that TiO_2 in the form of NP and NT can compromise cellular viability in terms of oxidative stress, organelle functionality as well as nuclear integrity. In addition, polymer

functionalization can alleviate the toxic response caused by the bare form. In order to test the hypothesis, three objectives were formed and are mentioned below:

1] Objective I: Synthesis of titanium dioxide (TiO_2) nanotubes using Solvo thermal route and physico-chemical characterization:

- Phase I: Synthesis of TiO_2 nanoparticles (TNPs)
- Phase II: Synthesis of TiO_2 nanotubes (TNTs) from TNPs
- Phase III: Surface coating of TNTs with Pluronic F-127

2] Objective II: Evaluation of *in vitro* toxicity of TiO_2 nanotubes using C6 cell line

3] Objective III: Investigation of acute toxicity of surface coated TiO_2 nanotubes using Wistar rat

Overall, the thesis includes six chapters. **First** one is the **Introduction chapter**; which initially covers the fundamental aspects of nanotechnology including a detailed narration about NMs and their types. Then a comprehensive detailing about the concepts of NTs and their importance in present era is given. Certain types of NTs and their derivatives are also explained here. A note on C6 glial cells and their relevance in the neuronal tissue along with generalized concept of TiO_2 induced toxic response is also explained.

The **second chapter** comprises the **Review of literature**. Detailed information on the available literatures on NTs, their synthesis approaches, structure and characterization techniques and different applications of NTs (non-medical and medical applications) are given here. Major emphasis is provided for toxicity or safety of NTs. Studies focusing on cellular toxicity in various cell lines are also detailed in this chapter.

Materials and methodologies adapted for the study is included in the **third chapter**. The chapter is prepared corresponding to the objectives and is divided into three major portions. First portion corresponds to objective I and can again be sub-divided into two parts. Part-I contains the detailed synthesis procedures adapted for three forms of nanoTiO_2 and Part-II contains various physico-chemical characterization techniques used for the material. Part-I comprises three major divisions denoted as Phase-I, Phase-II and Phase-III. In Phase-I, urea precipitation protocol for TiO_2 nanoparticles (TNPs) is explained. Followed by Phase-II in which solvo thermal synthesis approach for the

conversion of TNPs into TNTs is given. The surface coating protocol of as synthesized TNTs from Phase-II is detailed in Phase-III. In Part-II, characterization of nano TiO_2 obtained from Part-I is explained in detail. Major characterizations performed were in terms of hydrodynamic diameter (Dynamic Light Scattering or DLS method), surface charge (Zeta potential analysis), functional groups (Fourier Transform Infrared Spectroscopy or FT/IR), crystalline phase (X-Ray diffraction or XRD), and molecular pattern (Micro Raman Spectroscopy), surface morphology (Transmission Electron Microscopy or TEM) and thermal stability (Thermo Gravimetric Analysis or TGA & Differential Thermal Analysis or DTA). Surface coating of TNTs were confirmed using FT/IR for the identification of major characteristic peaks of TiO_2 and P-F127 in the coated form of TNTs.

The second objective includes *in vitro* toxicity evaluation. C6 glial cells were cultured in Dulbecco's Modified Eagle Medium/ Nutrient Mixure F-12 (DMEM F12) medium and obtained the characteristic spindle shaped morphology. Initially, two forms of TiO_2 (TNPs and TNTs) were subjected to toxicity studies. After the confirmation of cellular uptake of TNPs using imaging flow cytometry, cell viability was studied using MTT assay for the interaction of C6 cells and the NMs for 24h. Mitochondrial membrane potential (MMP) was further evaluated using JC1 staining for both TNPs and TNTs. Neutral red uptake (NRU) study was conducted for the detection of percentage of lysosomal stability. Lysosomal integrity was confirmed afterwards using acridine orange (AO) staining. Cellular morphology after TNP and TNT exposure was studied using Coomassie Brilliant Blue (CBB) and Giemsa staining respectively. Cytoskeletal integrity or actin filament organization was analyzed using Rhodamine phalloidin (R/P) staining. NM induced intracellular oxidative stress was evaluated using DCFH-DA assay and Griess reagent assay respectively for both TNPs and TNTs. Cellular integrity of TNP and TNT exposed cells was evaluated using Lactate Dehydrogenase (LDH) release assay. A qualitative live/dead study was conducted using AO / ethidium bromide (AO/EtBr) dual staining for TNP exposed cells. Similarly, TNT induced cell death was qualitatively and quantitatively measured using Calcein AM/PI staining. Nuclear integrity of both TNP and TNT exposed cells was evaluated using Agarose Gel Electrophoresis of isolated genomic Deoxy Ribose Nucleic Acid (DNA) for each tested concentration of both types of materials. For ensuring the level of morphological

changes associated with cellular nuclei, DAPI staining was done. Cellular viability after exposure with surface coated TNTs (TNT-P) was studied thereafter using MTT and NRU assays. Interference of Pluronic F-127 with assay reagent was checked separately by treating C6 cells with the polymer alone for 24h. This was for detecting the interference limit of the polymer with assay reagents. Intracellular oxidative stress was then analyzed for the cells exposed with Pluronic F-127 (P-F127) for analyzing the change of Reactive Oxygen Species (ROS) production levels after polymer coating of TNTs.

The third objective of the study is included as final part of this chapter, which explains the acute toxic response of TNT-P in Wistar rats. The rats were divided into four groups: Group-1 served as the control group and was exposed with normal saline instead of TNT-P. Rest of the animal groups (Group 2-4) was categorized on the basis of observation periods. All of the test groups were treated with TNT-P through intraperitoneal route (i.p.) and were sacrificed on days 3, 7 and 14 respectively. Home cage observation of the animals was done throughout the experimental period of over 14 days in terms of various signs of behavioral changes. Body weight of the experimental animals was checked on all observation periods prior to sacrifice. Gross pathology and wet organ weight was also analyzed prior to other experiments on all the days mentioned.

Urine, blood and fecal matter were collected prior to sacrifice and four key organs were isolated. They include: brain, liver, spleen and kidney. Blood samples were evaluated in terms of hematology and serum biochemistry. Urine was evaluated for several urinary parameters. Collected spleen was subjected to immunotoxicity analysis using splenocyte proliferation assay. Brain and liver samples were evaluated for antioxidant levels via quantitatively measuring the hallmarks of oxidative stress such as protein, reduced glutathione (GSH), and lipid peroxidation (LPO). Biodistribution of the exposed NM was analyzed in all of the four organs, urine, blood as well as fecal matter using Inductively Coupled Plasma Mass Spectroscopy (ICPMS).In addition, induced pathological lesions in all the experimental groups were evaluated using Hematoxylin and Eosin (H&E) staining method.

The next two chapters (**fourth and fifth**) include **Results and Discussion** respectively. Both of these chapters are divided into three sections in accordance with the order of objectives. First section describes the synthesis and characterization of two morphological forms of nano TiO_2 (TNPs and TNTs) and the surface coated form of TNTs (TNT-P). The hydrodynamic diameter of TNPs was found to be varying depending on the dispersion medium used (33.92nm, 36.19nm and 68.68nm for distilled water, Phosphate- buffered Saline (PBS) and DMEM F12 medium respectively). Zeta potential study confirmed the positive surface charge of TNPs with a magnitude of 12.9. Major characteristic functional groups in both TNPs were identified around at positions 3415.6cm^{-1}, 1634.9$cm^{-1}$and 587.4 cm^{-1} corresponding to O-H and Ti-O bonds respectively. Comparable peaks were obtained for TNTs as well and hence confirmed that there was no change in functional groups occurred after phase transformation. Crystalline phase of TNPs was studied using XRD; which indicated that the material is a heterogeneous mixture of anatase and rutile phases. Definite deflection peaks were obtained for each of these phases and the occurrence of anatase was observed to be dominated. The phase identification was further confirmed using micro Raman spectroscopy; in which phase transformation was noted from relative broadening of peaks obtained for TNTs than TNPs. Dominance of anatase phase was noticed; corresponding to the XRD pattern. Surface morphology of TNPs and TNTs was confirmed using TEM and it was confirmed to be roughly round and tubular in shape with average diameters of 22nm and 24.6nm respectively. Thermal stability of the materials was evaluated in terms of decomposition or percentage weight loss using TGA over a temperature range of 0-750°C. Three major surface reactions were identified which corresponds to removal of water molecules from the surface of the material, dehydroxylation and phase transformation respectively. Comparable surface reaction peaks were noted in DTA analysis also which correspond to exothermic and endothermic event temperatures and showed phase transition below 200°C. The effectiveness of polymer coating of TNTs was identified using FT/IR spectroscopy; in which TNT-P contained major characteristic peaks from both P-F127 and TNTs.

The second section of the chapter describes *in vitro* toxicity study of nano TiO_2 using C6 cells. Cellular uptake of TNPs was evaluated using flow cytometry in which increase in side scattering of cells were noticed corresponding to increase in TNP

concentration. This confirmed cellular uptake of NPs. Cell viability study indicated that, both TNP and TNT showed significant toxic response for 160microgram/milli litre (160µg/ml) compared to control. MMP analysis by JC1 staining also indicated toxic response for highest tested concentration. Lysosomal stability study using NRU assay and AO staining confirmed non-significant toxic response upto 160µg/ml after 24h of exposure. Cellular morphology study after 24h TNP exposure confirmed cytoplasmic shrinkage at 160µg/ml; whereas TNT did not cause any toxic changes in cellular morphology at any of the tested concentrations. Cytoskeletal integrity or actin filament organization was analyzed using R/P staining and comparable observation to that of non-fluorescent staining was obtained. Cytoskelatal shrinkage was noticed for TNP exposure at highest concentration. Intracellular oxidative stress study by DCFH/DA assay indicated significant generation of ROS for both TNPs and TNTs at higher concentrations of respective materials. However, none of the materials showed any signs of Reactive Nitrogen Species (RNS) production at any of the concentrations. A noticeable amount of cytoplasmic LDH was not obtained for both of the materials and this further confirmed the fact that, the cell membrane integrity remained intact without any structural damage. Qualitative evaluation of live/dead cell level for TNP exposure showed signs of necrotic cell death for 160µg/ml. This was evident from selective uptake of EtBr into a major population of cells. Similarly, live/dead study performed for TNT exposed cells also indicated evidence of induced cell death in highest tested concentration. Both TNPs and TNTs did not produce any toxic response with nuclear compartment of C6 cells as there was no observable laddering of genomic DNA was found. However, DAPI staining indicated slight level of nuclear condensation. Basic cell viability study using MTT assay for TNT-P point out that, cell viability was markedly improved compared to the non-coated form of TNTs. This was further substantiated from the increase in cell viability obtained for C6 cell-polymer interaction for 24h. Moreover, intracellular ROS levels were also diminished distinctly compared to bare NTs. Therefore from the observations of *in vitro* toxicity studies, it is evident that polymer coating can improve the biocompatibility of TNTs in glial cells.

The third and final section of the chapter narrates the outcomes of *in vivo* bio-nano interaction of TNT-P. Animals were injected with TNT-P through i.p. route and sacrificed on days 3, 7 and 14. No signs of behavioral changes were observed in any of

the experimental groups. Whole body weight of the rats showed a normal increment. Gross pathology also did not indicate any visible changes on surface of body or organs. Wet organ weight was also assessed and a discernable change in weight was not obtained for the isolated tissues except the liver. However, a time-dependent increase in weight was evident for liver. Hematology parameters exhibited some significant variations on 7^{th} day; wherein, significant decline and elevation was observed for Hematocrit (HCT) and Mean Corpuscular Volume (MCV) respectively. Regarding antioxidant study, level of total protein indicated an increasing pattern on 3^{rd} day compared to the control and was normalized on subsequent observation periods. GSH level increased only on 14^{th} day; whereas LPO did not change over 14 days of observation. Serum biochemistry showed evidence of liver cell damage in which both Alanine Transaminase (ALT) and Aspartate Transaminase (AST) showed significant increase on 7^{th} day. Alkaline Phosphatase (ALP) level also exhibited a time-dependent increase in pattern. Rest of the biochemistry parameters level was found to be not significantly deviating from the control values. ICPMS analysis indicated the evidence of metabolic clearance of TNT-P from brain, liver and kidney on 14^{th} day. Blood and urine also showed a decreased value on day-14; whereas fecal matter contained relatively high level of TNT-P on final observation period. Urine parameters were found to be normal and significant increase in splenocyte proliferation was noticed on 7th day in response to particle exposure. H & E staining signifies the fact that, three of the isolated tissues (brain, spleen and kidney) exhibited normal histology and were comparable to that of the control tissues. However, signs of cellular damage were evident for the liver from 3^{rd} to 14^{th} day. Occurrence of cellular infiltration and pathological lesions justifies this observation.

The **final chapter (sixth)** of the thesis includes **summary and conclusion** of the study. Two morphologically different nano forms of TiO_2 (TNPs and TNTs) were synthesized through precipitation and solvo thermal routes. The materials were physico-chemically characterized in terms of hydrodynamic diameter, surface charge, functional groups, surface morphology, crystallographic nature and thermal stability. The surface of TNTs was coated using P-F127 polymer and characterized using FT/IR. *In vitro* toxicity of the materials was studied using C6 glial cells. TNPs and TNTs were compared in terms of cell viability, MMP, lysosomal stability, oxidative stress, cell membrane and nuclear

integrity. Both of the materials were found to be non-toxic except at 160µg/ml concentration. Polymer coating of TNTs could markedly improve the percentage of cell viability and observed to be capable of decreasing intracellular ROS levels. This supports the applicability of TNT-P for neuronal therapeutic approaches than uncoated form. A single i.p. administration of TNT-P resulted in hepatic toxicity; whereas rest of the tested parameters remained unharmed. AST and ALT levels justifies hepatocellular damage on 7^{th} day. Histopathology evaluation showed symptoms of hepatic toxicity including cellular infiltration. In conclusion, present study confirms relatively non-toxic response of polymer coated TNTs in both *in vitro* and *in vivo* systems. However, some of the *in vivo* experiments showed symptoms of hepatotoxicity and further repeated dose toxicity studies will be required to declare TNT-P as a validated safe material for medical or clinical applications.

CHAPTER 1. INTRODUCTION

1. INTRODUCTION

1.1 NANOMATERIALS

The Nanoworld comprises a precise intermediary between atoms and solid objects which relies largely on the relationship between surface and volume. The concept of a nano world existed a long time back itself. The detailed study of its structure and properties was given by chemists (with the help of physicists), for which newer dimensions began to appear with the adventure of many observation tools including electron microscopes, atomic force microscopes and scanning-tunneling microscopes [Ducker *et al*., 1991]. A certain number of analysis tools like X-ray, neutron, and mass spectroscopy also have been some of the deciding factors behind the development of nanoworld. Even though the scientific community has been captivated widely by nanoscience and nanotechnology, debates are still going on for attaining a meaningful definition. In short, nanotechnology is defined as the fabrication of nanostructures and NMs based on atomic precision. Whereas, nanoscience comprises the branch of science dealing with the study of properties and behavior of matter at the nanoscale range or their behavior when changed from bulk to nanosized forms. Primarily nanoscience investigates the uniqueness of nanosystems [Mansoori *et al*., 2005]. The individuality of nanoscience lies in the fact that the optical, mechanical, electrical, physical as well as chemical properties of NMs differ widely from their bulk counterparts.

Studies support the theory that compared to respective macro forms; NMs exhibit enhanced performance when used for similar applications. The demand and thereby the fabrication of NMs is constantly improving as is the case with the application of nanocatalysts and on surfaces with improved properties [Ghorbanpour *et al*., 2015]. The role of NPs and materials are posing a higher pace in application as catalysts as they are capable of improving the performances of chemical processes. The underlying reason for this phenomenon is the dependence of catalytic reactions on the size distribution of materials and their size-to-volume ratio. The morphology and physico-chemical properties of nano forms vary widely and such beneficial effects are getting explored in innumerable fields [Mansoori *et al*., 2015]. The renowned American physicist Richard Philips Feynman, the former Nobel Prize winner for physics in 1965 proposed the brilliant concept of nanotechnology during his speech at a

conference by the American Physical Society in 1959. He conveyed the concept beginning with the statement: “There is plenty of room at the bottom”. Later the statement became one of the most studied and path-breaking perception around the world [Tekmen *et al*., 2018].

The word “nano" is reported to be of Greek origin (meaning 'dwarf') and conceptually it refers to the reduction of size by 10-9. i.e., 1000 times smaller than a micron. 1 nanometer (1nm) is equivalent to one billionth of a meter or ten Angstroms. In other words, 1nm=10-9m and it is 10,000 times smaller than the diameter of a human hair. The average diameter of human hair is reported to be about 50µm. i.e., it is having 1000 times larger size than a 50nm object. The size of a single nanosized particle can be correlated with a basketball when compared with the size of the earth [Mansoori *et al*., 2018]. United States National Science Foundation defined nanoscience and nanotechnology as studies dealing with materials possessing properties including (1) atleast a single dimension in the range of 1-100nm, (2) fabricated with technologies ensuring proper control over molecular level behavior of matter, (3) ability to form larger structures when combined without losing inherent properties, (4) ability to interact even with biological structures like DNA, Ribonucleic acid (RNA), proteins, amino acids, carbohydrates, *etc*., and also with microorganisms including viruses. Varying properties of NMs can be attributed to mainly two reasons: One is their larger surface area than corresponding bulk forms with the same mass. This further contributes to increased chemical reactivity. Occasionally, some inert macromolecules become reactive when they changed to nanoscale dimensions. Another reason is the dominance of quantum containment effects which all markedly elevate the behaviour of NMs in various aspects [*Prasad et al*., 2016].

Fundamental agents making nanoscience attractive are NMs; which are at being subjected to continuous modifications to explore their characteristic features. These structures can be fabricated either by a top-down approach (synthesis beginning from bulk forms) or by a bottom-up approach (NPs are formed from gas-phase or liquid-phase methods). NMs are of numerous origins including; metals and metal oxides, semiconductors, dielectrics, magnetic materials, polymers, or other organic and inorganic compounds. Among these categories, semi-conductive NMs are the best candidates for generating electronic and photonic nanodevices [Bromley *et al*., 2008]. As the higher number of surface atoms contributes abundant levels of surface active phenomena, NMs have attracted enormous attention in the scientific community;

especially in biomedical and optoelectronic fields. In optical applications, NMs are used as perfect agents presenting upgraded illumination properties than conventionally used materials. Such specific industrial requirements are satisfied by fabricating nanostructures via different synthesis strategies which permit fine control over size, shape, and composition. Nevertheless, assembling NPs to form a functional NM or nanodevice is a tedious process. One of the major obstacles observed during most of the synthesis procedures is the undesirable agglomeration property of NPs which may lead to altered behavior of the final products [Koch *et al*., 2006].

1.2 TYPES OF NANOMATERIALS

Based on organization and many characteristic properties, NMs have been classified into four major categories: (i) Carbon based materials, (ii) metal-based materials, (iii) dendrimers and (iv) composites. Depending on the application (diagnosis, imaging or therapy), each of these are being used; while some are employed for more than one application [Cartaxo *et al*., 2018].

1.2.1 CARBON BASED NANOMATERIALS

Carbon is conventionally known to exist in nature as two crystalline allotropic forms: Graphite and Diamond. Notably, the chemistry between these two differs widely; especially in their crystalline formation and properties. The peculiarity of carbon valence allows the formation of other allotropes also. This occurs mainly due to the covalent bond formation between carbon and other carbon atoms. Chemically speaking, allotropes are formed when two compounds share similar chemical structures and properties with different physical characteristics. Hence in addition to graphite and diamond, carbon forms other allotropes including graphene, CNT, fullerenes, *etc*. [Geim *et al*., 2010]. Some other known derivatives also exist like graphene oxide, reduced graphene oxide, graphene quantum dots, *etc*.

The exceptionality of carbon-based NMs which makes the group attractive among researchers is their intrinsic strength compared to any other materials (especially graphene), ~ 97% transparencies in pure form, higher stability, and chemical inertness with other compounds. The best advantage of carbon NMs is that, they are comparatively cheaper than other metal-based

catalysts like platinum. The presence of high surface area and sp2 hybridized carbon atoms make these NMs a perfect candidate for a wide range of biomedical application fields.

A noteworthy potential includes excellent drug-loading capacity on both sides of the layered structure [Zhu *et al*., 2010]. In the field of biosensors, carbon NMs are gaining significant attention which work either via optical or electrochemical signaling mechanisms. This can be because of their ease of operation, exceptional sensitivity limits, inexpensiveness, and reliable outputs. Such innumerable characteristic features make carbon-based materials a hot topic in biomedicinal as well as pharmaceutical research.

1.2.2 METAL BASED NANOMATERIALS

Owing to the uniform and sharp size distribution, metal NPs and materials have attracted immense attention. The presence of functional groups on metallic surfaces presents a platform that allows selective binding of specific targeting moieties including ligands, drugs, macromolecules, *etc*. Also, it exhibits surface plasmon resonance and optical properties which highlights their applicability in the optoelectronic field. The existence of this exciting group of NPs was discovered for the first time by Faraday in 1857 [Venkatesh *et al*., 2018]. Industrial application potentials of metallic NPs are growing at a rapid pace mainly due to high mechanical strength, surface area, lower melting point, optical and magnetic properties. Compared to others, the synthesis of metallic NPs should be finely tuned and it strongly depends on experimental conditions, stabilizing agents used, and kinetic interaction of metal precursor molecules with reducing agents.

The foremost advantages of employing metal NPs are: (a) Promotes Rayleigh scattering, (b) surface-directed and enhanced Raman scattering, (c) durable plasmon adsorption, (d) allows laid-back biological imaging, (e) regulates chemical identity on a metallic substrate within the nanoscale range [Li *et al*., 2007]. Conversely, there are some disadvantages exist during its usage including (a) particles instability is occasionally possible in which NPs undergo phase transformations, (b) impure environments barely seen by the production of undesirable by-products, (c) not always suitable for biological applications due to toxic or carcinogenic properties, (d) rare occasions of exothermic combustions and (e) difficulty in control over synthesis [Granqvist *et al*., 1976]. Application fields gaining benefit from metallic NMs include optical sensors, photocatalysis, optical detectors, biomedicines, in lasers, as high-temperature

superconductivity material, improvement of mechanical properties of NT-like carriers after filling with metal NPs, advanced magnetic characteristics, as catalytic agents like in fuel cells, in material science, in surface active agents (as in paints), in sunscreen lotions, for removing environmental pollutants, *etc*. [De Gusseme *et al*., 2010].

1.2.3 DENDRIMERS

Dendrimers are highly branched polymeric macromolecules their highly branched organization allows a multitude of application potentials. These three-dimensional (3D) branched molecules are generally termed "polymers of the 21st century". Structural advantages allow dendrimers to perform several advantageous roles in nanotechnology, pharmaceutical, and medicinal chemistry. Three architectural components of dendrimers include an interior core, interior generations surrounding the core, and an exterior part radially attached with the generations (with functional groups presenting sites for ligand attachment) [Pushkar *et al*., 2006]. Certain key properties of dendrimers include: (a) Nanoscale size comparable to many of the bio-building groups like proteins, nucleic acids, *etc*. (b) presence of surface functional groups allowing conjugation of drugs, signaling groups, targeting moieties and other biocompatibility groups, (c) interior void space allowing encapsulation of moieties of interest, (d) lower or no immunogenic response; mostly during coating with compatible polymers, (e) possibility of tailoring surface conjugated groups for biodistribution, site-specific targeting, and receptor-mediated endocytosis *etc*. [Svenson *et al*., 2012].

Major dendrimer-based medicinal applications include oral drug delivery, ocular drug delivery, transdermal drug delivery, targeted gene delivery, and targeted delivery of drugs into the central nervous system (CNS) by crossing the Blood-Brain Barrier (BBB) via additional conjugation with cell-penetrating protein or other analogous moieties.

1.2.4 COMPOSITE NANOMATERIALS

Composite materials encompass a novel class of materials formed by the specific combination of one or more materials at the nanoscale to establish a nanosystem showing improved characteristics. Members of this large family can be of various origins. These include 3D metal matrices, lamellar composites (two dimensional or 2D), nanowires (1D), or core-shell materials (zero dimensional or 0D) [Sahay *et al*., 2014]. The overall properties of the final composite

form depend not only on the components mixed; but also on the morphology and interphase characteristics. Beneficial results of the combination process include improved mechanical strength, dimensional stability, thermal/chemical stability, and electrical conductivity. In a biomedical scenario, nanocomposites promise solutions to problematic situations via performing gas/liquid sensors, self-repair nanostructures, catalytic initiators or inhibitors, and biomedical engineering applications.

1.3 NANOTUBES AND THEIR IMPORTANCE IN PRESENT ERA

Shape controlling of NPs is generally considered to be an important aspect of nanotechnology as it brings various functional alterations within the primitive form. NPs can attain a variety of morphologies and corresponding properties which could be applied for different purposes according to the requirement. This includes nanospheres, nanowires, nano reefs, nano boxes, nanoclusters, NTs, *etc*. The switching of parental morphologies occurs primarily as an impact of the templating or shape-directing agent used. Amorphous particles obtained immediately after synthesis usually adopt a spherical shape which upon calcination or a suitable aging process gives the crystalline nature of respective shapes [Pothukuchi *et al*., 2004].

Multi-faceted aspects of sizes and shapes of NPs have always been an interesting topic among researchers as it holds a diverse range of application potentials. Studies provide enough support for the fact that a NP's shape influences greatly cellular uptake, rate, and/or site specificity during targeted drug delivery. Moreover, preferential attachment to specifically targeted cell surface moieties including membrane receptors, other proteins, carbohydrates, nucleic acids, macromolecules, *etc*. can be achieved via tuning particle shape either before or after synthesis.
From a biomedical perspective, tubular-shaped NPs or NTs share abundant valuable properties to be applied. As the name implies, NTs are hollow tube-like entities composed of an element in the nanoscale range. Many variants of NTs possibly exist which are categorized based on the number of walls, element of origin, route of synthesis, *etc*. One of the widely employed and studied NTs is CNTs which are made of carbon with diameters typically measured in the nano range. CNTs are either single-walled (SWCNTs) or multi-walled (MWCNTs). SWCNTs were discovered initially by Iijima and Ichihashi in 1993 [Iijima *et al*., 1993].

NTs synthesized from different elements exhibit numerous gainful properties including an ordered arrangement with a high aspect ratio, ultra-light weight, elevated degrees of mechanical strength, electrical and thermal conductivities, higher surface areas, semi-conducting properties, *etc*. The unique combination of these peculiarities makes it an ideal platform to be cherished for various biomedical applications [Kostarelos *et al*., 2007]. The exponential increase in patents documented in the past few years mirrors the range of research interest for NTs globally. Nevertheless, their applicability is facing some obstacles like difficulty in purification, lack of accurate control over properties of the material, *etc*. Exact purification strategies are not yet explored and thereby most of the NT preparations contain undesirable contaminants either of precursor origin or coming from reagents used.

In early periods of discovery, researchers focused on deriving the inherent properties of NTs rather than polishing the advanced possibilities residing in them. Later on, scientists tried to modify the existing scenario principally via specific surface modifications to meet a selective purpose. Most of the trending biomedical applications are experiencing complications including; physiological barriers for tissue targeting, diminished rate of drug/material delivery, undesirable biodistribution and cellular uptake, control over drug release, acute or chronic toxic impacts, difficulty in sensing antigenic moieties, *etc*. [Lynam *et al*., 2007]. According to current observations, NTs can be employed to rectify such drawbacks as it offers a bunch of beneficial characteristics like high surface area/volume ratio, tunable surface properties, functionalization possibilities, incorporation of biocompatible agents for improved performance, long-term functionality and non-toxic response, the possibility of responsive drug release by both external and internal stimuli, *etc*. Various biomedical applications of NTs are illustrated in Figure 1.1.

NT arrays on a suitable template are widely used as biosensors with ultimate accuracy and specificity. Compared to conventional sensors, NTs ensure nanoscale detection precision which can detect foreign DNA or RNA strands; also helps to screen minute mutations in the genome. This finds useful applications in the detection of inheritable and infectious diseases which are difficult to identify by other means. As the present era is facing impediments in identifying pathogenic microorganisms (most of which, no antibodies are present in humans like the COVID-19 pandemic), biosensors incorporating NTs present incredible policy to be utilized.

Genetic-level consequences of pathogens entering the human body can also be easily identified; hence further extends the research possibilities in developing vaccines for such dreadful pandemics [Ferancová *et al*., 2006].

1.4 TYPE OF NANOTUBES AND DERIVATIVES

The term 'nanotube' usually refers to CNTs which are the most studied and explored forms of tubular nanostructures. Two broad classes of NTs known are: (a) Inorganic NTs such as those deriving from Group III nitrides, oxides of some metals, (b) Organic NTs formed from cyclic protein components and some naturally occurring heat shock proteins (obtained from microorganisms existing in extreme environmental conditions). As mentioned earlier, based on the number of walls present, CNTs can be classified mainly into two categories: SWCNTs and MWCNTs.

SWCNTs consist of a single cylindrical shaped wall; whereas MWCNTs have cylinders within cylindrical walls. Depending on the route of synthesis, the lengths of the two types vary. Unlike other NMs, these are microscopic rather than nanoscopic. i.e., they possess a size greater than 100nm, extending up to 10,000nm. Studies claim that tight winding of these NTs gives nanofibers with micrometer-sized dimensions. Post-fabrication thermal treatments can significantly increase the strength of these fibers [Wilder *et al*., 1998].

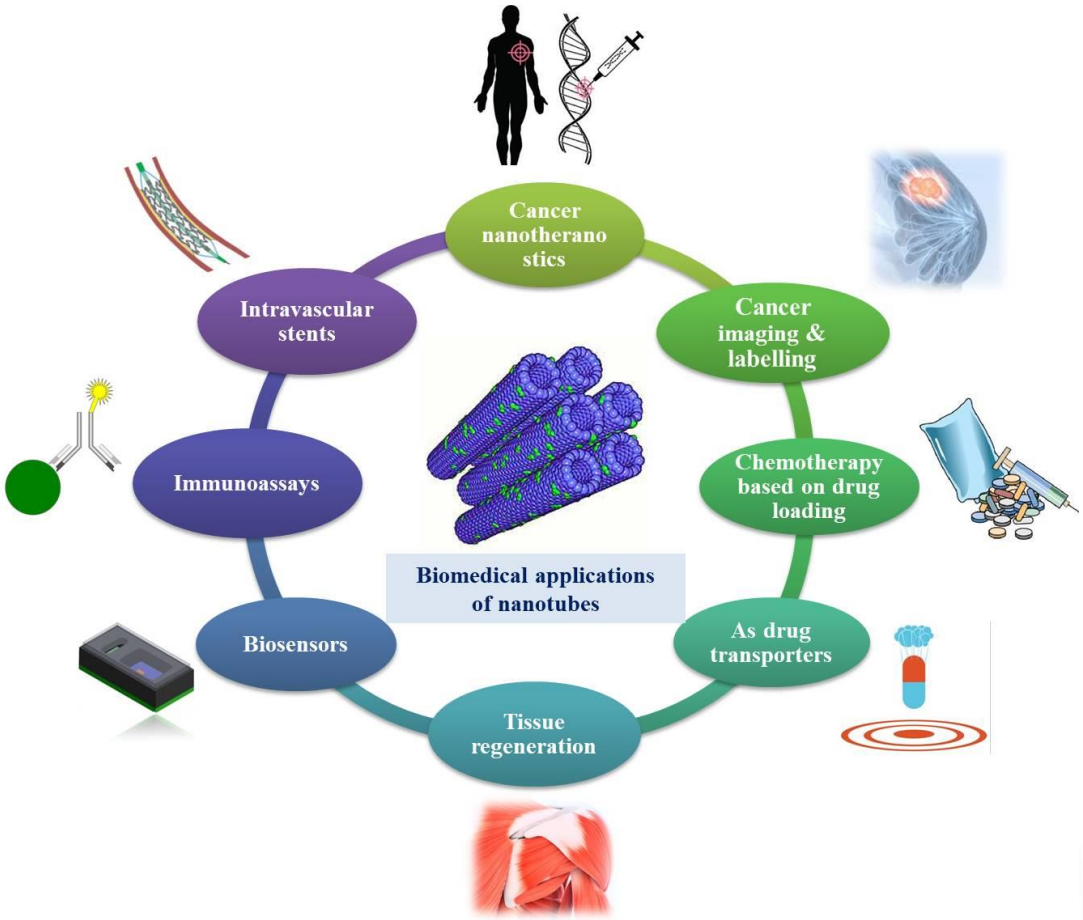

Figure 1.1 General biomedical applications of nanotubes.

Theoretically, the minimum diameter of a NT falls in the range of 0.4-0.5nm. This is comparable to the length of two silicon atoms arranged side by side. NTs with single walls are relatively more flexible and can bend at any angle without causing any breaks within the overall structure. In addition, the properties of NTs are studied mostly by using single-walled tubes. Considering the electrical behavior of NTs studies so far, metallic NTs are conducting materials; whereas semi-conducting NTs are also present like oxides of metals including TNTs. In the case of later, the conductivity can be altered step down or step up by changing the electric field. This indicates its suitability in circuits and other electronic types of equipment and devices [Karousis *et al*., 2010].

Many biomolecules such as lipids, proteins as well as peptides have been identified to form NTs; with extensive biomedical applications. Undesirable degradation of lipids is generally

considered one of the hurdles during their application. For example, they are susceptible to uptake by the lymphatic system of the Payer's patches upon oral administration of these nanocarriers. Also, there occurs a possibility of morphological alterations by calcium ions in circulation. Likewise, protein NTs are highly vulnerable to chemical degradation via acidic pH in the gastrointestinal tract, heat, enzymes, and oxidative reactions. Compared to these NTs, peptide NTs are regarded as simple, biocompatible, and biodegradable with numerous smart features [Gao *et al*., 2005]. One of the most attractive features of peptide NTs is the possibility of incorporating hydrophilicity and hydrophobicity without further surface functionalization. Two sub-categories of this group of NTs are linear polypeptide NTs and cyclic polypeptide NTs. Increasing biomedical applications of these NTs can be attributed to ease of control over the internal diameter of tubes by altering the amino acid composition, pH or polymeric combination, *etc*. [Chapman *et al*., 2012].

Inorganic NTs are morphologically comparable to CNTs and are primarily observed in mineral deposits of natural origin. Synthetic forms of this category of NTs were firstly discovered by Reshef Tenne in 1995 [Tenne *et al*., 1995]. Most such inorganic NTs can be derived from compounds like tungsten (IV) sulfide (WS_2), molybdenum disulfide (MOS_2), and tin (IV) sulfide (SnS_2). WS_2 and SnS_2 can be fabricated in microscales. In addition, established ceramic materials like TNTs, zirconium dioxide (ZrO_2), Zinc oxide (ZnO), *etc*., can also form inorganic NTs. In recent times, some modified versions of NTs have also been synthesized like transition metal/ chalcogen/ chalcogenides (TMCH), denoted by the formula TM6CYHZ (TM= Transition metals like molybdenum, tungsten, tantalum, niobium, C= Chalcogens like sulfur, selenium, tellurium, H= Halogen like iodine). The composition is expressed by $8.2 < (y+z) <10$. TMCH NTs are characterized by excellent dispersity contributed via poor mechanical coupling between individual tubes [Kis *et al*., 2003].

Inorganic NTs are widely considered as an excellent alternative to CNTs owing to their ease of synthesis and crystallinity, improved homogeneity and dispersity, pre-determined and tunable electrical conductivity depending on the nature of the precursor material, sharp needle-like morphology, good adhesion property on various polymers, *etc*. Thus, they are used as fillers in polymer composites showing excellent performance. Inorganic NTs are heavier than CNTs and exhibit lower strength under tensile stress. However, they are exceptionally strong under

compression and hence are applied widely for impact-resistant applications like bullet-proof vests. The optical properties of NTs can be markedly increased by generating composites with quantum dots (QDs); wherein resonance energy gets transferred from QDs to inorganic NTs during photoexcitation [Zhu *et al*., 2003].

1.5 NANOMATERIAL TOXICITY

Based on research outcomes focusing on NM toxicity, it was interesting to note a strong relationship between NM exposure to humans and the occurrence of various acute and chronic diseases. Nevertheless, the basic factors contributing to such toxicity imparted by NMs are still under investigation. Launching newer characterization techniques for NMs significantly promoted the field of nanotoxicology. As per reports, physico-chemical characteristics of NMs lie close to their toxicity features. Cellular uptake, sub-cellular interaction, and the further cytoplasmic fate of NMs are crucially dependent on their route of synthesis, the extent of purification, physico-chemical characters like crystallinity, surface topography, individual crystal size, shape, aspect ratio, electron distribution over a surface, *etc*. [Zoroddu *et al*., 2014]. The generation of ROS is the foremost toxic consequence of NM exposure. This ROS can result in oxidative stress, inflammation as well as structural and functional damage of proteins, cell membranes, and other key cellular organelle. The basic element forming the NM can directly take part in determining the type of cellular toxicity mechanism. For instance, NMs formed from metal oxide precursors such as TNPs can develop oxidant species from the TNP surface via a specific 'Fenton-type reaction'; which can specifically hamper mitochondrial functioning. Some metallic NPs can selectively disrupt cell membrane ionic transporters and thereby result in an influx of undesirable moieties such as water molecules, ions and other biomolecules, *etc*. This would consequently cause intracellular ionic imbalance, cytoplasmic swelling, sub-cellular organelle damage, and finally cell disruption.

Considering the size of NPs, those having a size of below 10nm can effortlessly enter into the nuclear premises of cells rather than just residing in the cytoplasm. This can further increase the probability of a genotoxic response; based on the NM's characteristics. Toxic symptoms generated by NMs include; chromosomal aberrations, nuclear condensation, DNA

fragmentation, micronuclei formation, *etc*. Whereas, those NPs having a higher size range (50-250nm) can be captured by the phagocytic population of cells and hence accumulate or present more in the liver or spleen [Garcés *et al*., 2021]. A general concept of NP-induced cellular toxicity is illustrated in Figure1.2.

1.6 CELL LINE USED

The current study uses glial cells as the *in vitro* toxicity model; which is generally accepted as 'non-neuronal cells in the central anxious framework formed by brain and spinal network. They do not directly take part in driving electric impulses, whereas they perform an array of certain other key functions in CNS as well as in PNS (peripheral nervous system). Major functions of the glial cell population can be listed as,

- To maintain a structural framework to CNS and PNS via holding neurons and other components in place
- Ensures nutritional and oxygen supply to neurons
- Provide protection to neurons from each other
- Protect brain and associated structures from pathogen invasion and act as major immunoregulatory cell community
- Assist in proper functioning of neurotransmission and synapsis formation
- Support early-stage neurogenesis (plasticity)
- Help to vacate dead neurons

There exist different categories of glial cells based on their function, structure, and location of origin. They are astrocytes, oligodendrocytes, ependymal cells, and microglia. Other minor forms of glial cells include Schwann cells and toady cells (Lie *et al*., 2005). The former type or astrocytes are capable of forming contact with both blood capillaries and nearby neurons. They also play a central role in the development of BBB and provide an ionic/chemical balance in an extracellular matrix (ECM). Astrocytes stabilize the flow of calcium waves upon neurotransmission throughout the network. Oligodendrocytes deliver an insulating action on neuronal axons by forming a myelin sheath over their cell body. This further coordinates the

functioning of synapses and regulates proper neurotransmission. Microglia is the major component in the category and regulates the elimination of dead neurons; along with the regulation of immune activity. Ependymal type of glial cells maintains the production of cerebrospinal fluid which acts as a cushion for the brain. The category of glial cells lines the fluid-filled deep ventricles of the brain and the central canal of the spinal cord.

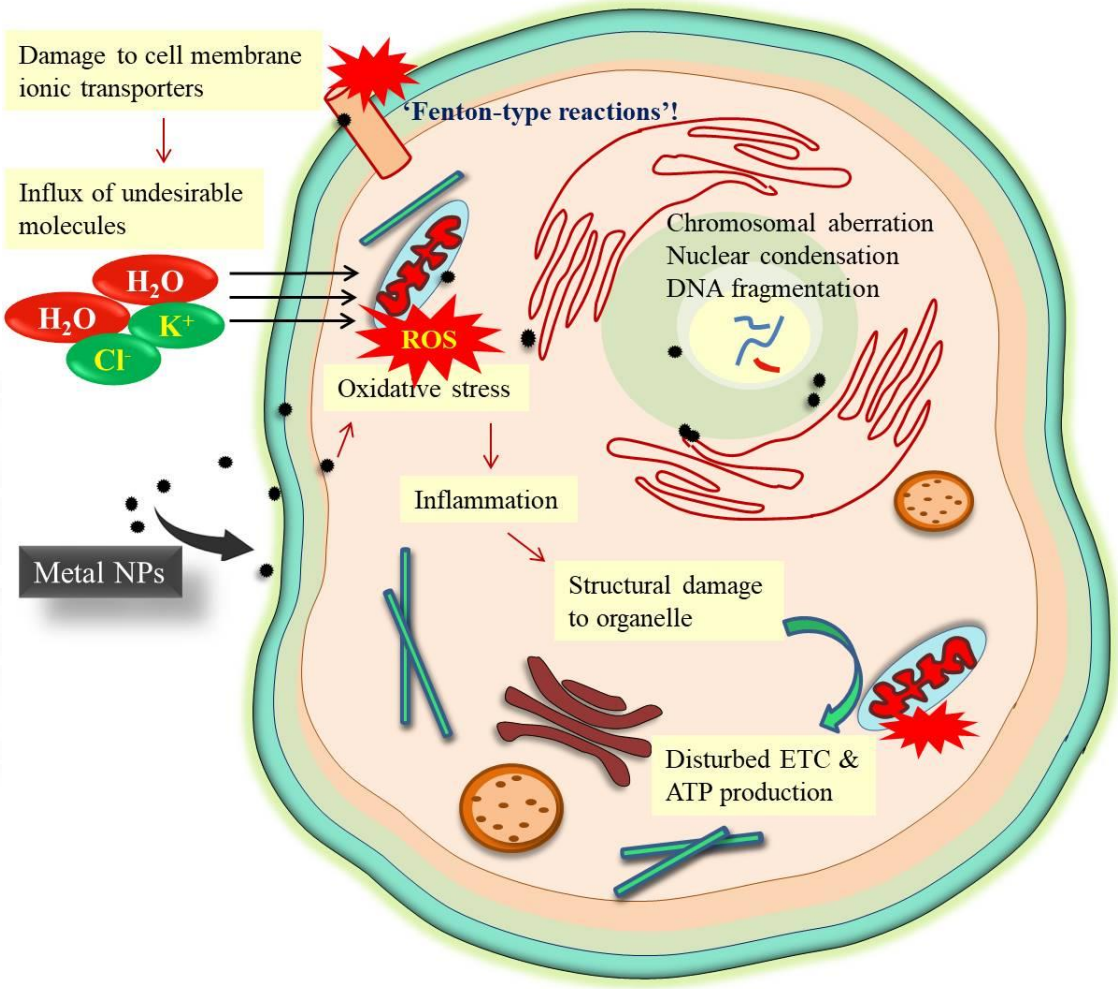

Figure 1.2 Cellular toxicity induced by nanoparticles in general.

1.6.1 *GLIAL CELLS AND NANOTOXICITY*

Owing to the extremely smaller size and characteristic properties including a high aspect ratio, NMs can cross biological barriers such as BBB quite easily. There is a long list of NPs that can

bypass BBB in the animal body including iron oxide NPs, ZnONPs, TNPs, *etc*. Several uptake pathways have been proposed for nanomaterials to enter neuronal tissue and are pictured in Figure 1.3. Major such pathways include; carrier-mediated transport, receptor-mediated transport, adsorptive transcytosis, paracellular aqueous pathway, transcellular lipophilic pathway, *etc*. (Chen *et al*., 2011).

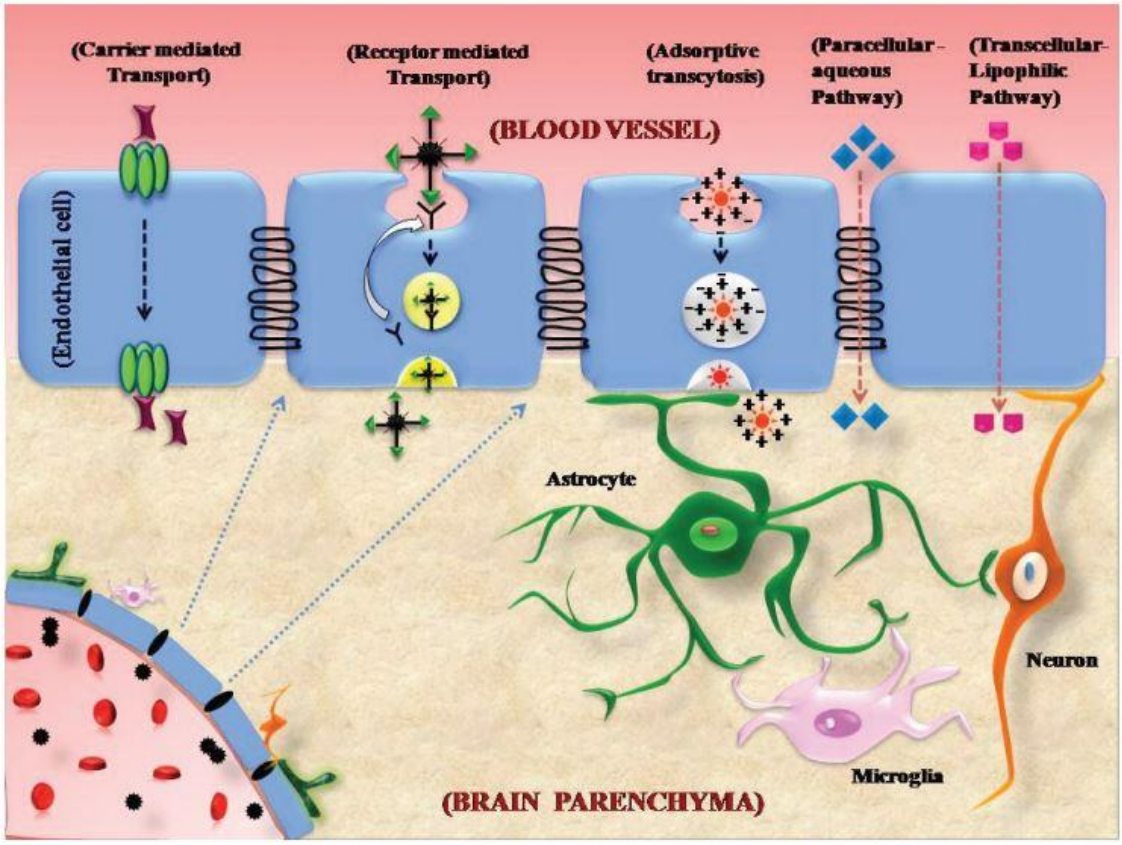

Figure 1.3 Various uptake pathways for NPs into brain parenchyma (Adapted from Athira *et al*., 2018).

Upon translocation into neuronal tissue, these NPs can induce mild to severe neurotoxic effects such as oxidative stress, activation of apoptotic signals in the hippocampus, organelle disintegrity, structural deviations in neurons, lipid peroxidation, attenuation of cognitive ability in animals, poor spatial recognition ability, *etc*. Glial cells represent one of the first and major categories of CNS cells with which NPs come in primary contact upon crossing BBB. Since glial cells are the mediators of the neuronal immune system, any functional ceasing of those cells would severely affect the rest of the CNS components. It has been reported that glial cell

encounter with NPs is likely to be causing phagocytic overload, leading to a rise in local tissue temperature and compromised immunity (Von Bohlen *et al*., 2007). Relatively lower degradation rates of nanomaterials cause them to accumulate in CNS premises and subsequently damage neurons.

In contrast to other bodily tissues, damages in CNS are relatively difficult to repair or regenerate. Although debates are going on regarding possible links between NP exposure and neurodegenerative diseases including Alzheimer's disease (AD), Parkinson's disease (PD), *etc*., supporting shreds of evidence are available that demonstrate such probabilities. Figure 1.4 illustrates one of the conceivable routes of NP-induced onset of neurodegenerative disorders such as AD; in which NP-induced aggregation and post-translational modification of proteins are shown. There is evidence for swollen astrocytes and structural transformation of glial cells into filamentous form after interaction with metal-based NMs (Tang *et al*., 2009).

1.7 MOTIVATION OF THE STUDY

Owing to the elevating application potentials of NMs, the nanotoxicology arena equally requires to be expanded to ensure safer applicability of materials; irrespective of the field of interest. The ultrafine size of NMs makes them capable of invading deeper premises of tissues and organs via highly efficient, easy passage through biological barriers. Nanoforms of TiO_2 have already been well–established in accomplishing passive diffusion across BBB. This phenomenon can lead to a dual situation such as achieving various beneficial roles for which it had administered, along with a plethora of deleterious effects. Some examples of such effects include; lipid peroxidation, cell membrane integrity loss, oxidative damage, morphology changes, DNA damage, *etc*.

Similar to any other NMs, the actual physiological fate of nano TiO_2 depends crucially on their physico-chemical properties; exclusively their morphology. TNTs have been identified to be possessing extremely high application potential in various therapeutic applications. Particularly, TNTs are applied at huge levels for neuronal applications such as targeted drug delivery vehicles, PTT for brain tumors, intravascular stent, *etc*. Most of these applications have witnessed immense advantageous results compared to other nanomaterials like CNTs, dendrimers, and nanocomposites; which all occasionally result in objectionable side effects.

Such compatible nature of TNTs in neuronal tissue requires to be scrutinized thoroughly as the brain represents the most sensitive region in a living body. A comprehensive toxicity report on TNTs with a neuronal tissue model or animal model is relatively scarce and needs to be elucidated. The current study has been planned in this context and a comprehensive *in vitro* toxicity study for TNPs, TNTs, and polymer-coated TNTs was performed; followed by an elaborative acute toxicity study for polymer-coated TNTs or TNT-P using Wistar rats. To the best of the knowledge acquired for the study, the research topic presented here is the first *in vitro* toxicity study for TNTs as well as TNT-P using glial cells. Moreover, the acute toxicity study of TNT-P is hypothesized to be valuable information for the validation of such a novel material for medical applications.

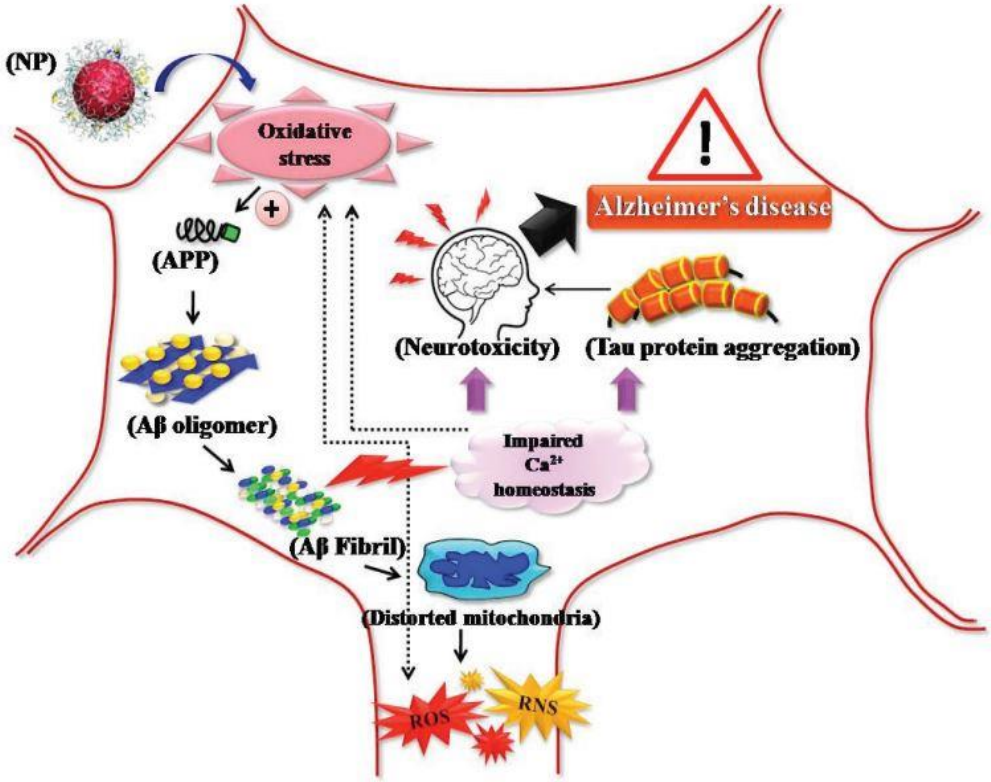

Figure 1.4 Proposed pathway for NP-induced onset of neurodegenerative disease (Adapted from Athira *et al.,* 2018). APP- Amyloid precursor protein, Aβ- Amyloid beta.

1.8 OBJECTIVES

Nano forms of TiO_2 have attracted a noteworthy level of attention among researchers since it finds immense application possibilities in various medical and non-medical fields. Particularly,

therapeutic strategies targeting CNS involve the active participation of Ti-based nanomaterials such as TNPs, TNTs, their functionalized forms, derivatives, *etc*. TNTs have gathered remarkable attention in this context; where, different unmet neurological treatment procedures have reached a point of success. In the meantime, a detailed perception of the toxicity profile of TNTs is lacking at this time point and requires to be elucidated in detail. In view of this fact, the current study addresses a basic toxicity evaluation of three nano forms of TiO_2 using glial cells after short term exposure period. Three forms of nano TiO_2 employed were: TNPs, TNTs and TNT-P.

Major objectives formulated for the study are mentioned below:

[1] Objective I: Synthesis of titanium dioxide (TiO_2) nanotubes using solvothermal route and physico-chemical characterization:

- Phase I: Synthesis of TiO_2 nanoparticles (TNPs)
- Phase II: Synthesis of TiO_2 nanotubes (TNTs) from TNPs
- Phase III: Surface coating of TNTs with Pluronic F127 (TNT-P)

[2] Objective II: Evaluation of *in vitro* toxicity of TiO_2 nanotubes using C6 cell line

[3] Objective III: Investigation of acute toxicity of surface coated TiO_2 nanotubes using Wistar rat

TNTs are the major material of interest for the study, and they were produced from the nanoparticle form of TiO_2 via a solvo thermal route. Studies suggest that the dispersion stability of insoluble NMs can be increased multifold by providing surface functionalization or coating with biocompatible molecules. This can significantly expand the acceptability of materials for biomedical applications. Based on this, TNTs developed for the study were surface coated with a biopolymer; P-F127. *In vitro* and *in vivo* toxicity report assimilated through this study is hypothesized to be very useful as a note of caution before any commercial or medical applications. A detailed illustration of the overall study plan is given in Figure 1.5.

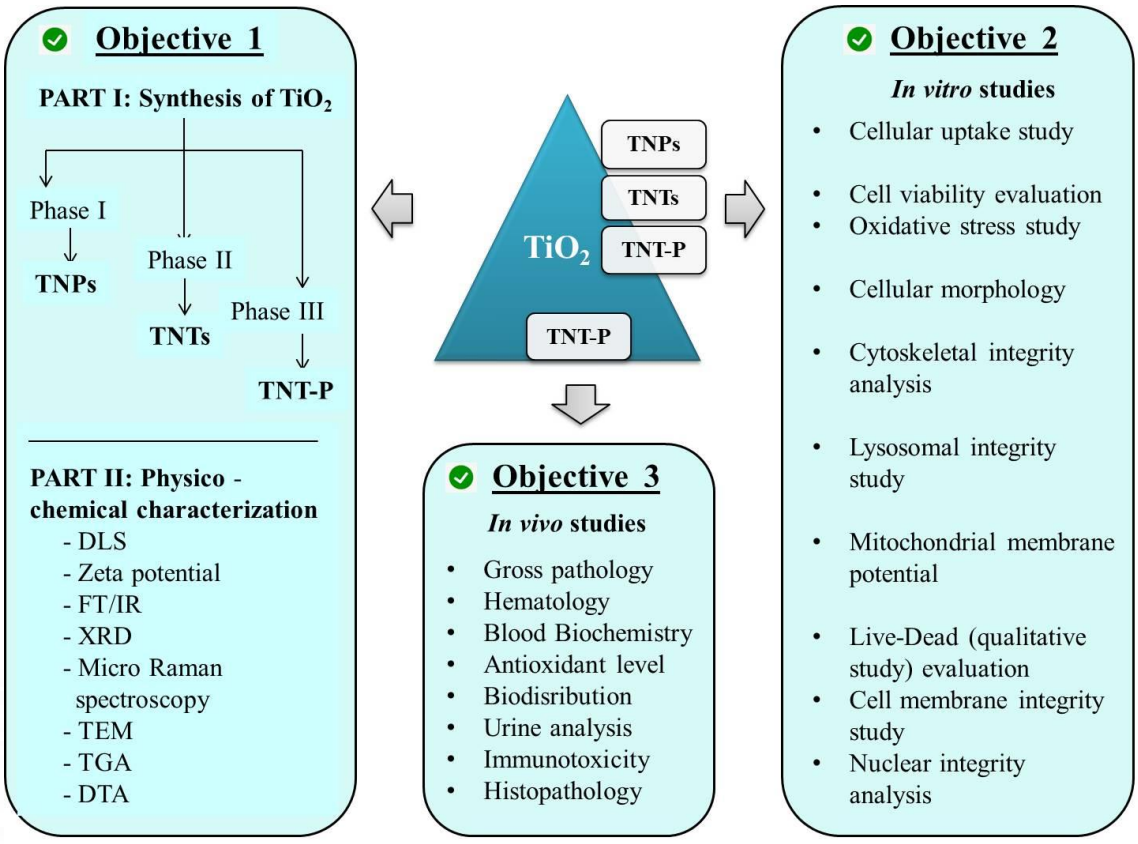

Figure 1.5 Overall work plan of the study.

CHAPTER 2: REVIEW OF LITERATURE

2. REVIEW OF LITERATURE

2.1 NANOTUBES: DIFFERENT DIMENSIONS

The physico-chemical characteristics of a material are greatly influenced by its dimensionality. Parallel to the advancement of nanotechnology, there has been a hike in progression with the fabrication of NMs in which electrons are confined in such a way to occupy within reduced dimensional systems. Considering single-walled NTs, they are essentially 3D NM formed via rolling up corresponding 2D forms in an extremely controlled atmosphere. For example, SWCNTs are formed via the rolling up of 2D graphene sheets. Graphenes are naturally formed by controlled networking of sp2 hybridized carbon atoms arranged like a hexagonal honeycomb-like pattern with two atoms per unit cell [Camilli *et al*., 2014].

Comparable observation can be seen in the formation of TNTs during the hydrothermal method of synthesis. In the initial step, 1D sodium titanate nanosheets will be formed ($Na_2Ti_3O_7$) under an extremely high alkaline environment (~10M Sodium hydroxide or NaOH). This 1D nanosheet will be rolled up into TNTs via ion exchange phenomena during the subsequent acid-washing step. This demonstrates the influence of material dimensionality on morphology and the switching of material properties. According to Wei *et al*., (2004) [Wei *et al*., 2004], the $Na_2Ti_3O_7$ nanosheets in TNT synthesis are formed by the following reaction:

$$3TiO_2 + 2NaOH \rightarrow Na_2Ti_3O_7 + H_2O$$

The basic concept of TNT formation via solvothermal treatment and their applications are given in Figure 2.1. Among the transition metal oxides, TNTs have attracted immense attention because of the functional and structural peculiarities of their 1D organization. An exceptionally high aspect ratio of these materials promises not only different biomedical applications but also industrial applications such as in Gratzel-solar cells and photocatalytic materials. Confinement within 1D pattern markedly increases their band gap into higher levels and thus elevates the semi-conducting behavior [O'Regan *et al.,* 2000]. Other morphologies of TiO_2 involve NPs (0D), 1D (nanowires, rods and tubes), 2D (layers and sheets), and 3D titania structures which offer a unique combination of very high surface areas as well as interconnected networks of bulk titania phase.

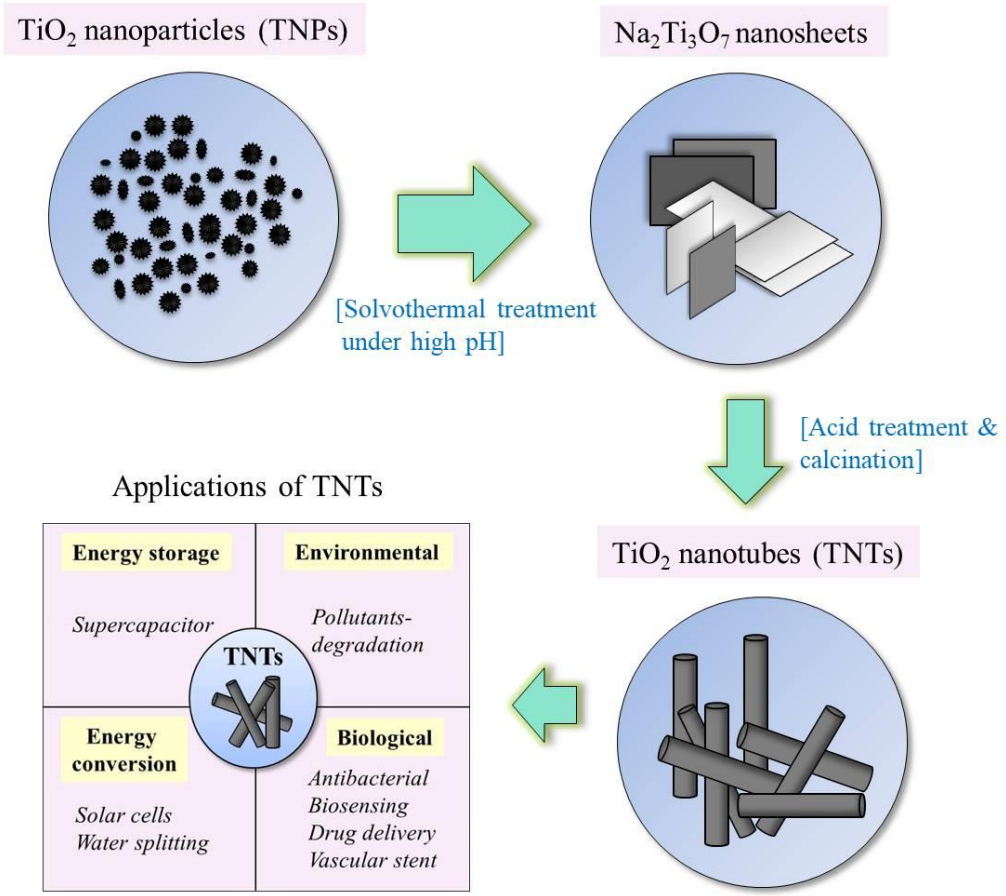

Figure 2.1 Solvo thermal formation of TNTs and their applications.

According to Roy *et al*. (2011) [Roy *et al*., 2011], empty organization of 3D titania serves to incorporate additional features such as tunable anisotropy and possibility to control interaction with light via photonic effects.

2.2 DIFFERENT TYPES OF SYNTHESIS OF NANOTUBES

The synthesis of NTs can be achieved via different methods mentioned below:

1. Sol-gel methods
2. Template assisted methods

3. Hydro/solvo thermal approaches
4. Electro chemical anoidization
5. Chemical vapour deposition.

2.2.1 SOL-GEL METHODS

Sol-gel methods have been widely employed for the fabrication of 1D nanostructures in the past two decades [Zhou *et al*., 2004]. Conceptually, the sol-gel method denotes a wet chemical technique (also known as wet solution deposition) and it involves two major reactions: (1) Hydrolysis of the precursor in an acidic or basic medium, (2) Polycondensation of the hydrolyzed products obtained in the first step. Afterward, the amorphous NMs will be subjected to gelation, aging, drying, densification, and crystallization [Yilmaz *et al*., 2020]. Researchers are highly dependent on this method for fabricating functional nanostructures. Wu *et al*., 2005 synthesized ZnO nanowires and NTs via this approach in which they used porous anodic alumina templates [Wu *et al*., 2005]. Wang *et al*. (2016) have developed TiO_2-coated CNTs via a modified sol-gel method. Such MWCNT-TiO_2 nanocomposites exhibited higher photocatalytic activity than conventional materials [Wang *et al*., 2016].

2.2.2 TEMPLATE ASSISTED METHOD

Template-based synthesis of NMs has been considered one of the pioneering methods since the early 1990s. South Korean scientists Kim *et al*. (2005) used mesoporous silica (MCM-48) as the template for the synthesis of 3D cubic mesoporous carbon CMK-1 [Kim *et al*., 2005]. During the same year, Japanese scientist Moriguchi *et al*. developed disordered carbon materials using CTAB or Cetyltrimethylammonium bromide (a cationic surfactant) as a template while using phenolic resin as the carbon source [Moriguchi *et al*., 1999]. The template method is generally observed to be non-sensitive to synthesis conditions, trouble-free to operate and implement and it controls the structure, morphology, and material properties using a template. The method involves two sub-categories: Soft template and Hard template methods; based on the difference in the template structure. NM synthesis via template methods consists of three key steps in common: (1) Preparation of the template, (2) Synthesis of the target material under conventional approaches like hydrothermal method/ precipitation method/sol-gel method in presence of the prepared template material, (3) Removal of the template. The

preference for template material is the quality-determining factor in the entire synthesis route. Traditionally used template materials can be of two sources: Natural type (nano mineral, biological molecules, cells/tissues, *etc*.) or Synthetic type (Surface active agents, porous materials or nanoparticles, *etc*.) [Nielsch *et al*., 2002].

2.2.3 HYDRO OR SOLVO THERMAL APPROACHES

The hydrothermal route of NM synthesis has gained tremendous consideration globally by R&D administrations and laboratories. It occurs at higher pressure solvents with high degrees of temperature and often occurs in closed atmospheres. When the solvent used is an aqueous medium, it is termed the hydrothermal route of synthesis; whereas if the solvent used is any other organic or inorganic solution, it is referred to as the solvo thermal method. Both ways involve an artificial route to synthesize individual crystals of NMs of varying morphologies (*e.g*. NPs, nanowires, NTs, *etc*.) [Vu *et al*., 2014]. The reaction will be performed within closed containers within a hydrothermal reactor (mostly Teflon-lined autoclave) filled with reaction medium. The accomplishment of the process is highly dependent on the aqueous solubility and thermal stability of the starting material. The entire reaction will be by the maintenance of temperature difference between opposing ends of the crystallizing compartments. The reaction container consists of a thick and sealed cylindrical portion roomed within a suitable coating material that should be resistant to high pressure and temperature. Also, it should not be reactive with the solvent used. The protective coatings normally are made up of gold, platinum, silver, carbon-free iron, titanium, glass, copper or Teflon. Major attractive features of this route of NM synthesis are: (1) the possibility of generating proper crystallinity to materials that are normally not stable at higher temperatures, (2) allows controlled growth of materials having higher vapor pressures closer to melting points, (3) produce high-quality crystals and NPs which can be easily controlled in terms of composition and functionalities [Chen *et al.,* 2005].

2.2.4 ELECTRO CHEMICAL ANODIZATION

Compare to other synthesis protocols, the electrochemical anodization method has gained significant attention as it gives specially ordered nanostructures having a precise periodic

pattern of semi-conductor arrays. From the perspective of NTs, they can be fabricated with homogenous distribution onto the surface of metallic foils; which is a highly desirable factor as it ensures efficient charge separation and transfer [Zhu *et al*., 2007]. One of the major advantages is, 1D NT arrays prepared by the anodization method have shorter carrier diffusion lengths than the bulk semiconductor; hence distinctly minimizes the energy loss possible during electron transition among NPs. The size of the anodized NT arrays can be accurately monitored and controlled by altering the reaction parameters like applied voltage, anodization time as well as the composition of the components in an electrolyte solution (*e.g*. Ammonium fluoride, water, *etc*.). Albu *et al*. in 2007 synthesized dense and free-standing membranes consisting of vertically oriented both-side open TNTs. The key steps governing the entire fabrication process were: (1) growth of a specifically ordered TNT layer on Ti metal with a high aspect ratio, (2) careful dissolution of the metallic substrate, (3) chemical etching of the closed tube bottom. A suitable mixture of fluoride-containing ethylene glycol solution served as the medium in which anodization of TNT arrays occurred. For the selective metal dissolution, a mixture of CH_3OH/Br_2 solution was employed; which removed the Ti metal from formed TNT arrays. According to the authors, the TNT arrays obtained via this process can be effectively used as a photoactive membrane for environmental cleaning or other biomedical applications because of the promising biocompatibility [Albu *et al*., 2007].

In another report, TNTs were fabricated by an anodization method in which electrolytes consisted of an organic solution and double-distilled water at a ratio of 100:2 and 0.3M ammonium fluoride. For obtaining tubes of different geometry, the organic solution was used at varying concentrations (combinations of ethylene glycol and glycerol in 1:1 ratio and 7:3 ratios). The effect of electrolyte concentrations was evident from the NT dimensions based on the glycerol content. Glycerol content increased the viscosity in an electrolyte solution; thereby slowing down the movement of electrons across the system and hence reducing the length of NTs. While using electrolyte with lower glycerol content, the perfect anatase crystalline form of the NTs was evident [Tamilselvan *et al*., 2016].

2.2.5 CHEMICAL VAPOUR DEPOSITION (CVD)

The underlying mechanism of CVD is a chemical reaction occurring under the influence of thermal induction on the surface of a heated substrate in the presence of reagents supplied in gaseous form. CVD offers many advantages over the deposition process. These include many types of coating materials used like metals, alloys, and ceramics. The coating process offers materials with very low porosity and utmost purity levels [Banerjee *et al.*, 2020]. The CVD process involves a reaction temperature in a range of 600-1100˚C. At this high temperature, significant effects may occur in the substrate material. A commonly employed modification of CVD is plasma-assisted CVD or plasma-activated CVD. Here, a lower electrical discharge in presence of low gas pressures is used to activate the CVD reaction kinetics. This further helps to lower the reaction temperature to several hundreds of degrees Celsius. However, lower gas pressure minimizes the coating rates of the whole process.

Han *et al.* (1998) fabricated TiO_2 thin films by growing on InP(100) and GaAs(100) substrates via metal-organic CVD. Those films that were grown on InP(100) surface gave dominantly rutile crystalline forms, whereas GaAs(100) gave polycrystalline structures in anatase form [Han *et al*., 1998]. Another attractive feature of such deposition phenomena is that plasma used for the heating process can effectively deliver reacting moieties that further accelerate on substrates. This helps to lower high temperature-driven material degradation otherwise. In the case of TiO_2 deposition, numerous studies reported that, there are different precursor materials available for TiO_2 fabrication including titanium tetra isopropoxide (Ti $[OCH\ (CH_3)_2]_4$, TTIP), titanium tetra chloride ($TiCl_4$), titanium ethoxide $[Ti_4\ (OCH_2CH_3]_{16}$, $Ti(OEt)_4$, TEOT) and titanium bis(acetylacetonate) diisopropoxide ($[(CH_3)_2CHO]_2Ti(C_5H_7O_2)_2$, TIPO). This TEOT and TIPO offer some advantages as they provide lesser contamination possibilities with a minimum content of carbon [Takahashi *et al*., 2014]. Although deposition techniques have been introduced widely for the fabrication of TiO_2 nanostructures, most of the procedures are facing a drawback of lower reproducibility of the crystalline phases of TiO_2; which may hamper its applicability. In addition, compared to other methods, the applicability of the deposition technique in the fabrication of NTs is lower; hence requires more detailed research and possibility studies in terms of many features.

2.3 STRUCTURE AND CHARACTERIZATION OF NANOTUBES

The research on multi-walled NTs has been initiated since the discovery of NTs in the early 1950s. Since that period, broadened studies on the elucidation of NT structures had begun. According to pioneer researchers, two main approaches came into the field to describe the structure of NTs. The first approach postulates that NTs are formed by the transfer of the layered structure of a bulk material onto the tubular phase of the corresponding circular or spiral cross-section of the same material [Butler *et al*., 1987]. Some examples of such NTs and the corresponding bulk forms include: CNT versus graphite, SnS_2 NT versus berndtite, SnS versus herzenbergite, WS_2 NT versus tungstenite *etc*. However, the postulates of this first approach were not satisfactory since they described the nanotubular structure based on a rectangular, non-primitive unit cell. The major drawback was that often the unit cell can cause the loss of structural peculiarities of nanotubular forms and hence their intrinsic properties. Also, it may cause to loss of the geometrical arrangement of atoms in a unit cell [Whittaker *et al*., 1956].

Followed by the first approach, another perceptible approach was put forward after the discovery of CNTs by Iijima in 1993 [Iijima *et al*., 1993]. Nevertheless, this came within reach of NTs having a hexagonal pattern of distribution. It is hard to generalize every NT into hexagonal symmetry; hence this approach also could not find a comprehensive description of NT structural peculiarities. Also, it was striking that, both of these approaches differ only in the selected unit cell for structural analysis of NTs [Dresselhaus *et al*., 1998]. Meanwhile, some authors have proposed works showing unit cell possibilities that could explain both single and multi-walled NTs; provided some additional requirements for multi-walled ones. Such unit cells can be termed ‘universal unit cells’ since it refers to both the categories of NTs in terms of their organization [Bernaerts *et al*., 1998].

Considering CNTs, SWCNTs are formed by the rolling up of a single graphene layer into a seamless cylinder (or long-wrapped graphene sheets). Similar to SWCNTs, most of the other classes of single-walled NTs consist of two phases with entirely different chemical and physical properties. The first phase is the smooth surfaced side walls, and the second is the end caps of the tubes. Multi-walled tubes are generally formed by rolling up of multiple single-

walled tubes around themselves and exhibit different internal diameters. The length and diameters of these multi-walled tubes vary widely from single-walled ones and hence the structural and functional features [Iijima *et al*., 1993]. An illustration of single and multi-walled forms of graphene and CNTs are given in Figure 2.2. The interlayer distance found in multi-walled tubes can be near to that of the distance between individual layers of the single-walled tubes (~3.3 Å).

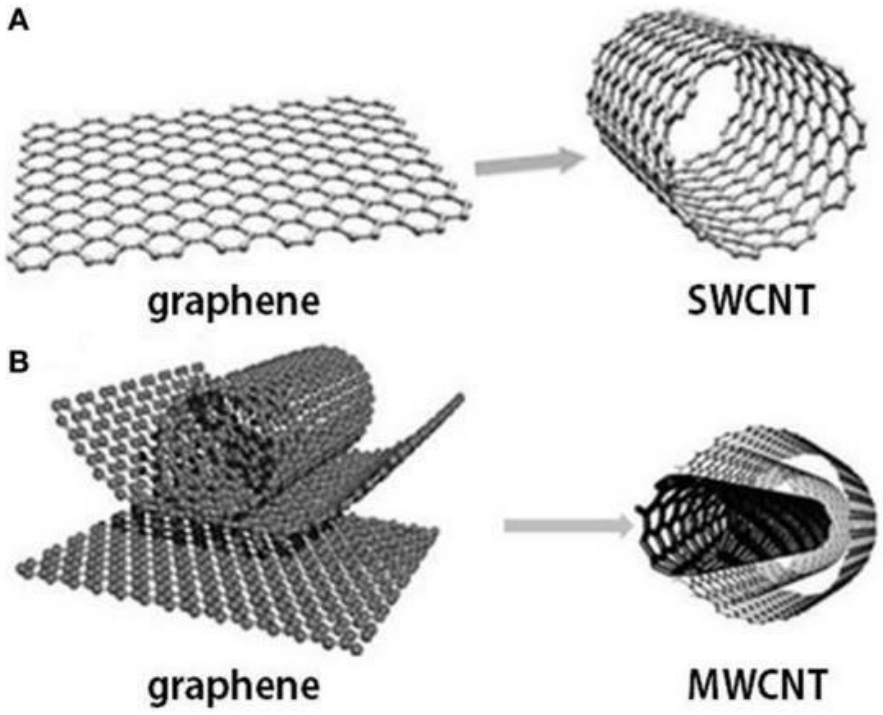

Figure 2.2 Structure of single walled graphene and CNTs (A) and multi-walled graphene and CNTs (B).Adapted from (Vidu *et al.*, 2014).

Hydrothermally synthesized TNTs and CNTs have certain properties in common; including they consist of the rolled atomic or molecular plane with monomolecular thickness. In a physical sense, these NTs are referred to as 'true tubes' as they possess appropriate quantum size and dimensionality in support of perfect NT properties like electron mobility, wide band gap as well as surface reactivity. The average wall diameter of NTs generated via the hydrothermal route is ~ 10-100nm. Hydrothermally synthesized NT exhibits extraordinary properties like high surface area, size exclusion effects, desirable diffusion behavior, biological interactions, and ion transport properties [Law *et al*., 2004].

In nature, TiO_2 exists predominantly in three crystalline forms: Anatase, Rutile, and Brookite. Certain synthetic layered phases are also seen. For example, TiO_2 (B); was produced via a hydrothermal route by Marchand *et al*. (1980) [Marchand *et al*., 1980]. In general, TiO_2 nanostructures synthesized at lower temperatures such as in the sol-gel technique exhibit amorphous morphology. Post-synthesis treatments like calcination at temperatures 300-400˚C help to convert amorphous forms to anatase crystals and increasing the treatment temperature to a range of 500-700˚C helps to have anatase to rutile transformation. Considering application possibilities, anatase and rutile crystals are widely used.

2.3.1 DIFFERENT STRUCTURES OF NANOTUBES

2.3.1.1 Hydrothermal tubes

A generalized recounting of hydrothermal NT structure is still under debate and it is strongly determined by preparation conditions. According to Morgado *et al*. (2007), hydrothermal tubes formed under highly alkaline conditions initially consists of TiO6 octahedral layers and the unit cell structure at this stage will be more co-relatable with sodium titanate. Selected Area Electron Diffraction (SAED) patterns reveal that most of the crystals are in anatase crystalline form [Morgado Jr *et al*., 2007]. A similar observation was obtained by Zhang *et al*. (2003) in which hydrothermal tubes exhibited titanate ($H_2Ti_3O_7$) [Zhang *et al*., 2003]. During the annealing procedure, the diffraction peak intensity 2θ decreases with increasing temperature. Moreover, peaks corresponding to anatase crystals dominate as phase transformation occurs. The specific surface area was also noted to be decreasing as the annealing proceeded. By providing sufficient annealing temperature, the full stoichiometry of TiO_2 nanoforms can be obtained as anatase-like morphology.

2.3.1.2 Anodic tubes

Unlike hydrothermal tubes, anodic tubes demonstrate mostly amorphous morphology which begins to change into anatase forms when the temperature rises to 280˚C. Due to the possibility of heat transfer reactions, annealing of anodic NTs in ordinary furnaces occurs in presence of Ti substrate. Phase transformation is mainly possible via the thermal oxidation of Ti metal

beneath the sample. Rutile crystalline forms predominate at a temperature of around 500˚C. Thermo gravimetric studies revealed that; upon annealing, surface hydroxyl groups coming from surface-absorbed water on TNTs will get completely lost at 200˚C. Further increase in temperature around 500˚C contributes to the loss of carbon coming from the incorporation of organic electrolyte decomposition products [Mirabolghasemi *et al.,* 2013]. Most of the anodic synthesis procedures revealed that single-walled NTs display drastically different physical properties compared to multi-walled tubes. A prominent feature is the improved electrical property in single-walled tubes by around 10-100 times. In addition, both amorphous and anatase TNTs show strikingly similar band gap (~3.3 eV); wherein their magnitude and recombination kinetics distinctly change [Murata *et al*., 2000].

2.3.2 CHARACTERIZATION TECHNIQUES FOR NANOTUBES

For the physico-chemical characterization of NTs, a bunch of global characterization techniques is available. They include electron microscopy, X-ray XRD, FT/IR, XPS, Raman spectroscopy, *etc*. Electron microscopy is considered as the key characterization tool as it allows to address the morphological features, and shape as well as the average size of NTs. Nanometer and sub-nanometer size of NTs can be obtained by various types of electron microscopy tools like TEM, Scanning Electron Microscopy (SEM), Atomic Force Microscopy (AFM), Scanning Tunnelling Microscopy (STM), High-Resolution Transmission Electron Microscopy (HRTEM), *etc*. Each of these microscopic techniques differs in terms of working principle and mode of action. TEM and SEM are the preliminary types of microscopy techniques that cause damage to the sample due to the influence of electron beam striking the material [Flygare *et al*., 2019].

XRD is a non-destructive technique used to analyze the structure of crystalline materials. Analysis of the crystalline phase of the material allows identifying the chemical composition of the material. In the case of TNTs, phase transformation stages of the NTs before and after annealing can be determined via this technique and hence the purity levels. The technique is based on constructive interference of monochromatic X-rays which are generated and focused onto the crystalline material with the aid of a cathode ray tube. Before striking the material, the rays will be made monochromatic using suitable filters. The peak intensity measured via this

technique endows with extend of crystallinity of the particular plane [Jackman *et al*., 2015]. FT/IR technique is used to identify the functional groups present in NM by the support of infrared (IR) light colliding onto its surface. It can be applied to materials of polymeric, organic, or inorganic origin. It gives an IR spectrum of molecular bonding in materials. FT/IR usually measures light absorption in the range of wavelengths of 4000-400 cm^{-1}. The presence of undesirable contaminants and other moieties can easily be identified using this. The composition of the material can be identified via XPS also. Here, the bombardment of samples with an electron beam leads to the selective excision of surface electrons. Measurement of energy levels of these electrons can describe the chemical composition of the sample. Principally, it determines the elemental composition and chemical bonding state of electrons. XPS provides improved resolution for heavier elements, in particular inorganic trace impurities of a diverse group of NMs including NTs [Thostenson *et al*., 2001].

Raman spectroscopy comprises a family of spectral identification methods in which the inelastic scattering of incident light is used to identify the molecular pattern of the NM. Upon initiation of the technique, the energy will be exchanged between the photon and the material. The energy level of the scattered electron can be lesser or greater than the incident light based on the rotational or vibrational motions of the molecule. The major technical drawback of Raman spectroscopy is that, there may be lower intensity due to inelastic scattering and higher intensities due to Rayleigh scattering. Due to the prevalence of improvements in research for numerous characterization techniques and analytical tools in the past few decades, inherent application possibilities of NMs became unveiled. Moreover, a precise understanding of the material characteristics made it achievable to modify the existing systems of nanotechnology in a useful way. Fabrication methodologies also find immense possibilities as they can be fine-tuned via the emergence of these sophisticated techniques.

2.4 DIFFERENT APPLICATIONS OF NANOTUBES

Many investigators and researchers have paid much dedication and effort to expand the number of possible applications of NTs in various fields including material science, optoelectronics, pharmaceutics, medicines, *etc*. More attractive applications of NTs include which require higher conductivity and absorption capacity and for the fabrication of high-strength fuel cells,

energy conversion devices, field emission devices, conduction devices, hydrogen storage devices, and semi-conducting devices. Some other environmental applications like water and air purification also have attracted immense interest. Potential applications of TNTs involve the exploitation of some of the unique features including electronic, ionic, or biocompatibility properties. Moreover, significant enhancement of reaction and transport rates is possible using small-scale dimensions like large surface area, short diffusion path, or size confinement effects [Song *et al*., 2010]. The presence of defined top openings allows NTs to be used as size-selective applications like filters or templating secondary material.

2.4.1 PHOTOCATALYTIC APPLICATIONS

TiO_2 is generally considered as the most effective material for the photocatalytic removal of organic contaminants from different surfaces. The basic principle for photocatalysis is shown in Figure 2.3. Upon exposure to UV rays, electrons in the valence band will get excited and move toward conduction band; hence creating an electron-hole pair. While the conduction band electrons come in contact with redox species of the nearby environment (including H_2O), highly reactive species will be generated [Linsebigler *et al*., 1995].

For example, $H_2O + h^+ \rightarrow OH^{\cdot}$ (Reactionin valence band)

$O_2 + e^- \rightarrow O_2^-$: (Reaction in conduction band)

These reactive radicals are capable of eliminating virtually every organic pollutant into CO_2 and H_2O. Selective degradation of absorbed moieties starts when direct transfer of h+ present in valence band occurs.

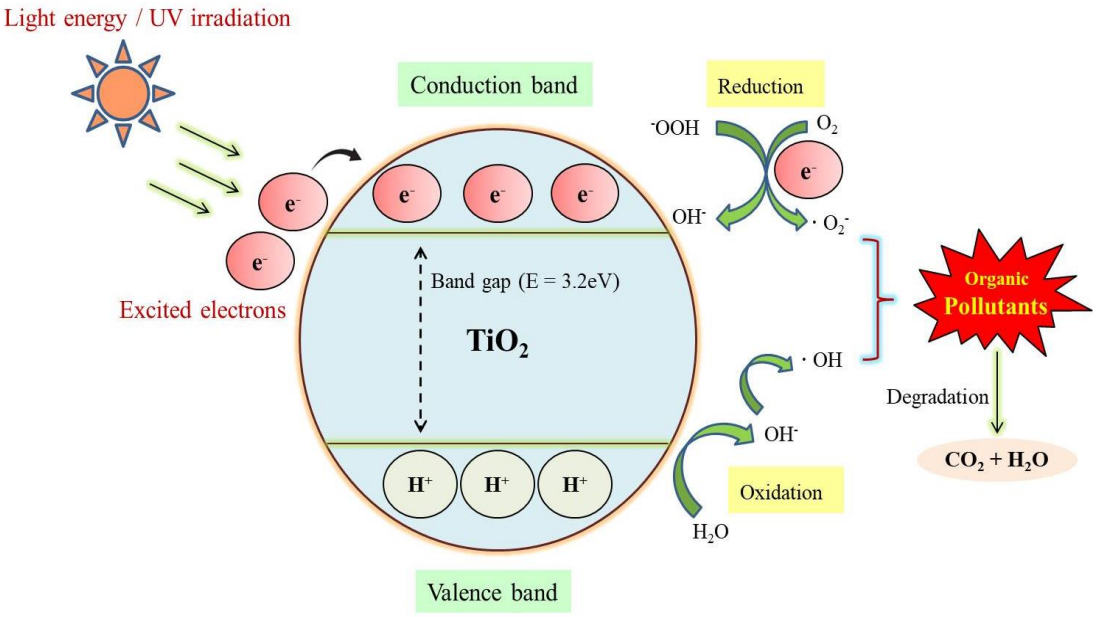

Figure 2.3. Basic mechanism involved in TiO_2 driven photocatalytic removal of organic pollutants.

Often certain N-doping procedures and visible light-induced photocatalysis are since UV light-driven photocatalysis may create toxic side effects occasionally. Ordered assemblies of NTs present many advantages from the perspective of photocatalytic reactions due to their high surface area and higher retention times than nanoparticulate assemblies. This improved catalytic effect in nanotubular assemblies of TiO_2 was firstly reported by Macak *et al*. in 2007 [Macak *et al*., 2007]. Another interesting concept behind photocatalysis is the possibility of combining NT surfaces with specific molecule-selective binding units. For example, a combination of TNTs with zeolites markedly improves the accumulated amount of organic pollutants and thereby accelerating their removal via photo degradation. Recovery of zeolites further improves the degradation efficiency on long term basis [Paramasivam *et al*., 2009].

2.4.2 IN SOLAR CELLS

The application of TiO_2 layers as a photon-absorbing layer in dye-sensitized solar cells (DSSC) has been under thorough research since the 1970s. A remarkable number of reports have previously been published; including the first report by Gerischer and Tributsch in 1968 by which they proposed the application of TiO_2 layering on ruthenium bipyridyl coating [Gerischer *et al*., 1968]. This approach reached an efficiency of 11%. The underlying principle in DSSC is comparable to that mentioned in photocatalysis in which electron excitation occurs

while the dye absorbs photons and the corresponding oxidation of components in electrolytes occurs. Since the rate-limiting factor in DSSCs is the path traveled by excited electrons, NTs can contribute additional benefits in the way it provides longer diffusion lengths than nanoparticulates. Anatase NTs are more efficient in this context than other crystalline phases because of the far exceeding path length of electrons and hence the indented objective of the system [Tang *et al*., 1998].

2.4.3 IN ELECTRO-CHROMIC DEVICES

In the branch of ion-intercalation devices, transition metal oxides hold an indispensable position because of the excellent host lattice it possesse. This category of metal oxides includes MnO_2, WO_3, Nb_2O_5, MoO_3, TiO_2, *etc*. Lithium-ion batteries and electro-chromic devices are worth mentioning in this circumstance. These devices depend on the selective intercalation of Li^+ and H^+ ions in between the space created by the metal oxides. The reversible uptake of such ions by metal ions significantly alters the redox state of the material. Hence, the corresponding change in the electronic and optical behavior of the material can turn into a beneficial way for the device. For example, in the case of lithium-ion batteries, Li^+ ions selectively intercalate between TiO_2 tubular layers and thereby accelerate the reduction of Ti^{4+} at the lattice into Ti^{3+}. This further changes the band gap of the material from UV to visible range, which contributes to the blue coloration of the device [Cronemeyer *et al*., 1959]:

Eg ~ 3eV (Trasnsparent) $\quad \underset{\text{Cathodic}}{\overset{\text{Anodic}}{\mathbf{TiO_2 + Li^+ \rightleftharpoons Ti^{3+} + LiO_2}}} \quad$ Eg ~ 2eV (Blue)

The rate-limiting step is the diffusion/migration process of the small ion into the lattice space. The switching kinetics in this step is extremely slower (only seconds). To achieve short diffusion paths, most commercial devices employ layers of compacted NMs. The optimal applied voltage and period for achieving proper intercalation are 1-2 V and seconds respectively. Conventional NTs including TNTs offer such a system that is workable within these prerequisites. Vertical alignment in NTs also permits to have ideal geometry for maximizing optical contrast. For the fabrication of transparent effective electrochromic devices, TNT layers can be easily lifted off from the titanium metallic substrate and be transferred onto conducting glass [Ghicov *et al*., 2008].

2.4.4 BIOMEDICAL APPLICATIONS

The major content of TNT applications is in association with the biomedical field. About 40% of implant materials used nowadays is made up of titanium and their derivatives like titanium alloys. TNT surfaces have been identified to be applied in the medicinal field not only because of their size properties but also due to the peculiarities of the tunable surface present. Studies claim that, the complex TNT surfaces can be adjusted to any value between 10-250nm. Wide-ranging applicability can be attributed to their self-organizing nature and versatility. Even complex-shaped surfaces can be easily coated with TNT layers because of this property.

2.4.4.1 Cell interaction and biomedical coatings

The first investigation on size-dependent cell interaction of TNTs in 2007 has shown that mesenchymal stem cells were able to grow by the diameter of the NTs. TNTs having ~15nm diameter promoted cell adhesion, differentiation, and proliferation in a highly regulated manner. However, tubes with diameters exceeding 100nm induced programmed cell death in stem cells (apoptosis) [Park *et al*., 2007]. Following several conflicting investigatory reports, Bauer et al. in 2009, have shown that the size-dependent (diameter of ~15nm) cell proliferating property of TNT layers is nearly a universal property of NTs. In addition to mesenchymal stem cells, certain other types of cells also showed similar size-directed responses such as hematopoietic stem cells, endothelial cells, osteoblasts and osteoclasts, chondrocytes, neuronal cells, *etc*. [Bauer *et al*., 2009]. Tubes created from other metals such as ZrO_2 also showed a similar property. The reliable explanation for this observation is that, integrin complex formation on the cell membrane and corresponding adhesion complex having a diameter of about 10nm creates a perfect fit to accommodate within the geometry of TNTs and in this way elicit an accelerated cell growth promotion and differentiation (Figure 2.4).

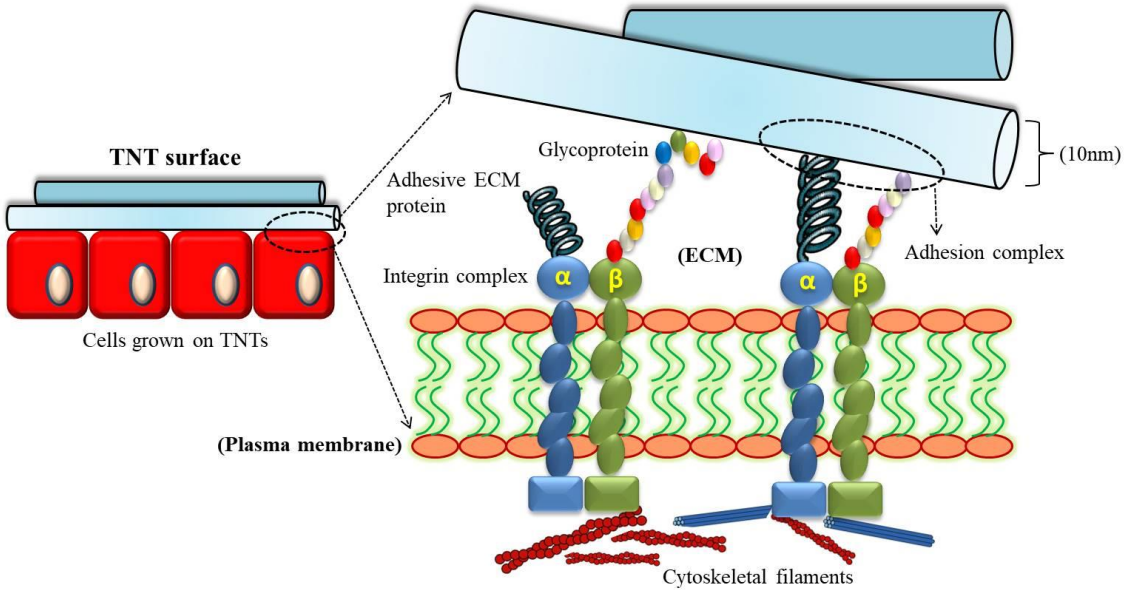

Figure 2.4 Adhesion complex formation on TNT surface by ECM components around cells.

2.4.4.2 Tissue engineering based on TNT arrays

The use of TNTs as active devices for physical support to tissue in biological systems has attracted immense interest in recent years. 2007 is considered one of the relevant years in the perspective of TNT-based tissue engineering applications since it provided a certain number of significant reports. The investigators tried to study the impact of TNT surface topography on cellular adhesion, apoptosis, proliferation, and differentiation and to activate biological responses exactly mimicking the physiological system. For instance, Popat *et al.* (2007) have demonstrated the long-term influence of 80nm TNTs in the proliferation and related cellular activities using rat MSCs. After subcutaneous implantation, they analyzed that there occurred a marked increase in cellular ALP activity and accumulation of cellular calcium levels without any undesirable immunological response [Popat *et al.*, 2007].

In another report, TNTs loaded with gentamycin significantly reduced the adhesion of Staphylococcus epidermidis and thereby nourished the differentiation of pre-osteoblastic MC3TC-E1 cells. The study proved the role of TNTs as wonderful substrates for tissue engineering applications [Popat *et al.*, 2007]. The applicability of TNT arrays for coating vascular implants have been demonstrated by Peng et al. in 2009. According to the study, TNTs having a diameter of 30nm notably resulted in an improved proliferation of bovine aortic endothelial cells by simultaneously maintaining vascular smooth muscle cells in differentiated

status. A prominent increase in the secretion of prostaglandin E2 was also noticed in endothelial cells grown on this TNT substrate [Peng *et al*., 2009]. Genomic analysis of the particular observation was analyzed further by Peng et al. in 2010; wherein an increase in the expression of endothelial cells and smooth muscle cells was confirmed. In addition, the study reported that TNTs caused the downregulation of genes associated with inflammation and coagulation related to restenosis and thrombosis in both cell types [Peng *et al*., 2010].

2.4.4.3 Drug delivery from TNT arrays

Titanium devices can be surface coated with vertically aligned NTs for drug releases such as in bone screws, titanium stents, and wires. Desorption and diffusion of drugs on the TNT surface is the major driving force for drug release in target sites. The rate of drug release is strongly dependent on certain properties like NT surface chemistry, surface area, pore size, molecular size, surface charge, drug solubility, stability, diffusion coefficient, *etc*. Comparable to the conventional drug release processes, TNT also follows certain series of events before drug release. This was demonstrated by Peng *et al*. (2009), who analyzed the release kinetics of certain proteins (albumin and lysozyme) and antibiotics (sirolimus and paclitaxel). The study observed the sequence of release events beginning from burst release. i.e., the majority of the loaded drugs were released within the initial period of administration and then followed by a prolonged release over a week [Peng *et al*., 2009].

Recent advances allowed scientists to use specific biodegradable coatings for NT capping. Polymeric micelles were later used for drug encapsulation, since most of the drugs may undergo undesirable leakage and distribution otherwise. Some other reports exploited the photocatalytic property of TiO_2 for controlled drug release in target sites. The ability of TNTs to create a redox environment when stimulated by a light source of a suitable wavelength has been employed in a large number of studies. The external stimuli used for such excitation include; magnetic stimuli, radio frequencies, ultrasound waves, *etc*. [Schneider *et al*., 2014]. Another study used a suitable cross-linking molecule (siloxane) for the loading of a fluorescent-labeled drug. Upon application of external UV light stimulation, chain scission of siloxane cross-linker occurred followed by drug release from the NT. The system can be used instead by filling the NT interior or exterior with magnetic NPs; thereby guiding the system toward the target site by applying static external magnetic stimuli. Poor tissue penetration or

payload degradation often creates an obstacle in UV-based drug release. Therefore, studies paid attention to using visible light or IR light stimulation for induced drug release from TNTs [Shrestha *et al*., 2009].

2.4.4.4 Biosensing mediated by nanotubes

TNTs can act as excellent substrates for the quantification of several biomolecules in samples owing to their role as probe-free analytical devices or immobilization platforms. They are routinely used for the detection of various molecules like antibodies, antioxidants, metabolic by-products, neurotransmitters, peptides or proteins, xenobiotics, *etc*. Low-cost metal NPs like Cu_2O, noble metal NPs like Ag, Au, Pt, *etc*., or their various combinations can be conjugated onto TNTs to improve their physico-chemical properties. In recent decades, different analytes in biological samples can be detected using TNTs based on various amperometric methods as well as photocatalytic properties. For instance, other methods have also been used like immunohistochemistry, interferometry, spectroscopy, *etc*. The likelihood of chemical reactions occurring both on the NT surface as well as deeper tube channels allows a high magnitude of analyte detection limits. This enhances the biosensor applicability of NTs compared to other nanostructures [Kang *et al*., 2008].

Easier electron transfer reactions occurring on the surface of TNTs allow scientists in the detection of different types of analytes like glucose, hydrogen peroxide, ascorbic acid, glutathione, and immunoglobulins. An *et al*., in 2010 developed highly reproducible and stable Au-doped TNTs allowing defined detection of α-synuclein protein in a neuronal tissue sample of PD patients [An *et al*., 2010]. Au NPs were doped onto the TNT array surface for improved photocurrent performance. Primary antibodies for the detection of α-synuclein were immobilized on TNT arrays which acts like highly active bioagent for protein detection. Enhanced sensitivity was obtained by conjugation of the secondary antibody and glucose oxidase enzyme. Hydrogen peroxide (H_2O_2) released by the conjugated enzyme performs as a scavenger of valence band electrons upon photoexcitation. Such highly organized systems using NTs can generate high throughput performances in the field of biosensing applications [Vander Wal *et al*., 2003].

2.5 TOXICITY OR SAFETY OF NANOTUBES

One of the major struggles in the field of nanotoxicology is that, the toxicity of a specific NM cannot be predicted when it exists in different morphological forms. For instance, toxicity limits of relatively inert systems like iron oxide, gold, or silver change widely between their NP, filamentous and tubular forms. As the usage of NTs with improved modifications and performance is at a rapid pace in various biomedical fields, human beings are susceptible to higher exposure risks and associated health consequences. Hence, it is becoming indispensable to investigate toxicity levels and physiological outcomes caused by NTs. Numerous works have been published based on the nature of toxicity arising due to the application of NTs in biological systems, especially in the context of drug delivery. CNTs denote the major category of NTs which denote one of the hot topics for toxicity studies among researchers. There exist a large number of *in vitro* toxicity studies for the interaction of CNTs with different cell lines [Francis *et al*., 2018]. Lack of thorough knowledge and deepened research has contributed negatively to picturizing the exact reason behind NT-driven toxic impacts in tissues.

Researchers are now focussing at the fate of inorganic NTs as well in the body. Generalizing reports from various studies, one can make a statement that; the geometry of NMs plays a crucial role in cytotoxicity. Nevertheless, certain defects occurring on the surface of nanofilament structures and chemical moieties adsorbing onto their surfaces may turn out to be toxicity determining factor when applied [Wani *et al*., 2011].

2.5.1 CELLULAR TOXICITY

Studies focused initially on finding pathways by which NTs enter into cells; as it can vary based on the difference in aspect ratios. Regarding CNTs, the vital pathway of cellular uptake is via endocytosis. There are reports available on developing inflammation and oxidative stress accompanying endocytosis. Since the body recognizes NTs as foreign entities, there would be an associated immunological response mediated by the release of several immune mediators including cytokines. Generally, such immune responses are termed as ‘foreign body response’ or FBR. Oxidative stress eliciting during CNT uptake leads to the induction of a chain reaction associated with the generation of protein kinases and nuclear factor- Kappa B (NFκB) thereby producing immune mediators. The basic cellular mechanism leading to oxidative stress is the production of free radicals. These free radicals further lead to the oxidation of DNA, proteins,

amino acids, lipids, *etc*. In addition, these reactive molecules are responsible for the activation of transcription factors and activator protein-1; thereby stimulating NT-mediated oxidative stress. Di Giorgio *et al*., in 2011 have shown that it is often difficult to eliminate nanotubes from circulation and they may get accumulated in major tissues and organs; leading to hazardous consequences [Di Giorgio *et al*., 2011]. Since the brain, spleen, kidney, and lungs are the key organs susceptible to oxidative stress difficulties, nanotubes are more likely to cause oxidative stress in these organs; mainly via the generation of reactive oxygen species (ROS).

Under normal circumstances, ROS are generated as by-products of oxygen metabolism. Up to optimal ranges, these moieties are essential to the body. However, a misbalancing of ROS levels; such as that induced by NTs may cause structural and functional damage to tissues. Functional loss of tissues can mainly be attributed to NM-driven selective programmed cell death or apoptosis, detrimental effects in genetic material, and oxidative damage to proteins or enzymes.

CHAPTER 3: MATERIALS AND METHODS

3. MATERIALS AND METHODS

3.1 CHEMICALS

Titanium tetra (IV) chloride ($TiCl_4$) (M.W. 189.68), Urea powder (CH_4N_2O) (M.W. 60.06), Sodium hydroxide (NaOH) (M.W. 40.0), Hydrochloric acid fuming (HCl) 37% (M.W. 36.46), Pluronic® F-127 powder, 3-(4,5-Dimethylthiazol-2-yl)-2,5-diphenyltetrazolium bromide (MTT), Neutral red powder (Bioreagent for cell culture), Dimethyl Sulfoxide (DMSO), Trypan Blue powder (Bioreagent for cell culture), Griess reagent, Histopaque, Sodium Dodecyl Sulfate (SDS), L-Glutathione reduced (GSH) and Thiobarbituric acid were purchased from Sigma Aldrich (USA).High Glucose (HG)- Dulbecco's Modified Eagle's Medium Ham's F12 medium (DMEM F12), Acridine orange, Propidium Iodide (PI), 4',6-diamidino-2-phenylindole (DAPI), Ethidium Bromide (EtBr), RPMI 1640 cell culture media, were purchased from Himedia, India. Fetal Bovine Serum (FBS) was obtained from Invitrogen, USA.Ca^{2+}, Mg^{2+}free Phosphate Buffered Saline (PBS),Trypsin-EDTA and Antibiotic and Antimycotic solution [Streptomycin (10,000 g/ml), Penicillin (10,000 units/ml), Fungizone® (25 g/ml)]were purchased from Gibco, USA.JC1 dye (mitochondrial membrane potential probe) and Calcein AM was obtained from ThermoFisher Scientific (USA), Rhodamine Phalloidin (F-actin probe) was purchased from Cytoskeleton Inc. (USA). Folin's reagent and Coomassie® Brilliant Blue stain, and Bis(3-carboxy, 4-nitrophenyl) disulfide (DTNB) was obtained from Merck (USA),2′,7′-dichlorofluorescin diacetate (DCFH-DA) was purchased from Molecular Probes Invitrogen, Carlsbad, CA (USA). Genomic DNA ladder kit was obtained from Gen Elute ™ Mammalian genomic DNA miniprep kit, Sigma Aldrich (USA). ^{3}H-tritiated thymidine was bought from American Radiolabelled Chemicals Inc. (USA). Reagents for biochemical analysis of urine and blood samples were obtained from Erba mannhiem (Germany). Hematology analysis reagents were bought from Horiba (Japan).

3.2 EQUIPMENTS

Synthesis of NMs was performed using the hot plate (IKA RCT basic) (India). Synthesized materials were dried using Innova™ 4080 Incubator shaker (Denmark). Dynamic Light Scattering (DLS) and zeta potential analysis was done using Malvern zetasizer nano ZS (UK).

Fourier Transform Infrared (FTIR) spectra were obtained from IR Tracer 100 Shimadzu (Singapore). Crystallographic study by X-Ray diffraction (XRD) was done using Bruker D8 advanced PXRD(Germany). Micro Raman mapping of the crystalline phases of the nanomaterial was performed using Confocal Raman Microscope, alpha 300A, Witec Inc. (Germany). Morphology study was done using Transmission Electron Microscope (TEM) (JEOL JEM 2100, China). Thermo gravimetric study and Differential thermal analysis (TGA and DTA) was done using SDT Q600 V8.3 Build 101 (USA). C6 cells were cultured in laminar air flow (Mark Air particulars, India) and incubated inSanyo inCu safe CO_2 (USA) and Panasonic CO_2 incubators (Japan). Various sonication steps were done using the Bath sonicator, Maxsell Professional Ultrasonic cleaner (India). Cellular uptake study was performed using Amnis FlowSight® imaging flow cytometer. Spectrophotometric reading of various assays was obtained from Lambda 25, UV/Vis spectrophotometer (Perkin Elmer, USA). Colorimetric reading for cell culture assays (MTT, NRU, Griess reagent and LDH assays) were taken using ELx 808 Ultra Microplate reader, Bio-Tek Instruments (USA). Quantitative fluorescence readings (DCFH-DA and Calcein AM/PI staining) were taken from Infinite F Nano + TECAM Fluorescence micro plate reader (Switzerland). Phase contrast images of C6 cells were obtained from Leica DMIL, (Germany). Non-fluorescent images of the cells (CBB and Giemsa stainings) were taken from the compound microscope Olympus CX31 (Japan). Fluorescent images for all the staining experiments were obtained from Axio Scope A1 microscope, Carl Zeiss (Germany). Gel documentation after electrophoresis was done using the imaging system [Alpha innotech, (USA)]. Hematological readings for the rat blood samples were done using Horiba Vet abc (Japan). Serum biochemistry evaluation was done using Erba Mannheim XL300 (Germany). Collected urine samples were checked using Uro-dipchek 300 (Erba Mannheim, Germany). Antioxidant studies were carried out using Polytron P 3100tissue homogenizer. Elemental analysis was done using Inductively coupled plasma mass spectrophotometer iCAP RQ(Thermo Scientific, USA).Thymidine uptake in splenocyte proliferation study was determined using the scintillation counter (Hidex, Finland). All centrifugation steps for the study were conducted using refrigerating centrifuge (Eppendorf, USA).

3.3 ANIMAL HUSBANDRY AND WELFARE

Wistar rats were obtained from the Division of Laboratory Animal Sciences, Biomedical Technology Wing, Sree Chitra Tirunal Institute for Medical Science Technology (Govt. of India), Trivandrum. Healthy male and female Wistar rats weighing 200-250g were employed for the acute toxicity study of the nanomaterial. Total 12 numbers of animals were used for the study which was divided into four different groups comprising three animals in each group.

The rats were conserved in an atmosphere of 12h light and dark cycle provided with a constant temperature of 22 ± 2°C and humidity range of 30-70%. Animals were fed with a standard pellet diet and water *ad libitum*. For easier identification, all of the animals were marked with picric acid. Moreover, individual animal cages were provided with a label describing the experiment number, name, animal number(s), date of exposure, and the date of the experiment. All the animals were acclimatized for 5 days prior to the experiment. Home cage observation of the experimental animals was done throughout the period till the end of the 14th day. All the animals were handled humanely to avoid any kind of pain or stress and for ensuring their welfare.

3.4 ANIMAL ETHICS

Constant care about the maintenance and management of the animals were taken in accordance with rules and regulations of CPCSEA (Committee for the Purpose of Control and Supervision of Experiments on Animals), Govt. of India. Approval from the Institute Animal Ethics Committee (IAEC) was obtained before the commencement of the study. All the experiments were in conformance with the approved Institutional protocol. IAEC approval No: SCT/IAEC-381/NOVEMBER/2020/107.

3.5 SYNTHESIS OF TITANIUM DIOXIDE (TIO_2) NANOTUBES USING SOLVOTHERMAL ROUTE AND PHYSICO-CHEMICAL CHARACTERIZATION

3.5.1 SYNTHESIS OF TIO_2 NANOTUBES

3.5.1.1 PHASE I: Synthesis of TiO_2 nanoparticles (TNPs)

TNPs were synthesized in Phase I using the classical and simplest approach proposed by Seo *et al*., [2003] using the precipitation method. The method includes a metal halogen of Ti ($TiCl_4$) as the precursor compound. $TiCl_4$ and de-ionized (D.I) water were taken (1:4 molar ratio) in a round bottom three-neck flask. The reaction mixture was placed in an oil bath and the temperature was slowly increased from room temperature to 150°C in a controlled manner to regulate the proper nucleation of the NPs. Once the temperature reached 150°C inside the flask (monitored using an external thermometer inserted along the side neck of the reaction flask), the reaction was allowed to proceed for 3.5h. A white colloidal solution was obtained after the completion of the reaction. The NPs in the colloidal solution were precipitated by the addition of 5M Urea solution slowly along the sides of the flask. The flask was then kept to cool down to room temperature and it aided complete precipitation of the NPs to the bottom (Figure 3.1). The settled NPs were recovered from the flask and washed thoroughly with a large volume of D.I water until the pH reaches 7 (by centrifugation at 12000rpm for 5min). The product obtained was dried at 80°C for 5h in a hot air oven. Proper crystallization of the product was obtained after calcination of the NPs at 400°C for 1h. TNPs were physico-chemically characterized before proceeding to Phase II of the synthesis step.

3.5.1.2 PHASE II: Synthesis of TNTs using solvothermal method

TNTs were synthesized using the method proposed by Kasuga *et al*., (1998). 0.3g of TNPs synthesized from Phase I was added into 30ml of 10M NaOH solution taken in a beaker. The mixture was allowed to stir for 1h at room temperature and placed in a bath sonicator for another 1h at 37°C. The reaction mixture was poured into a 100ml Teflon-lined autoclave, sealed, and allowed to react for 48h at 130˚C. This step was

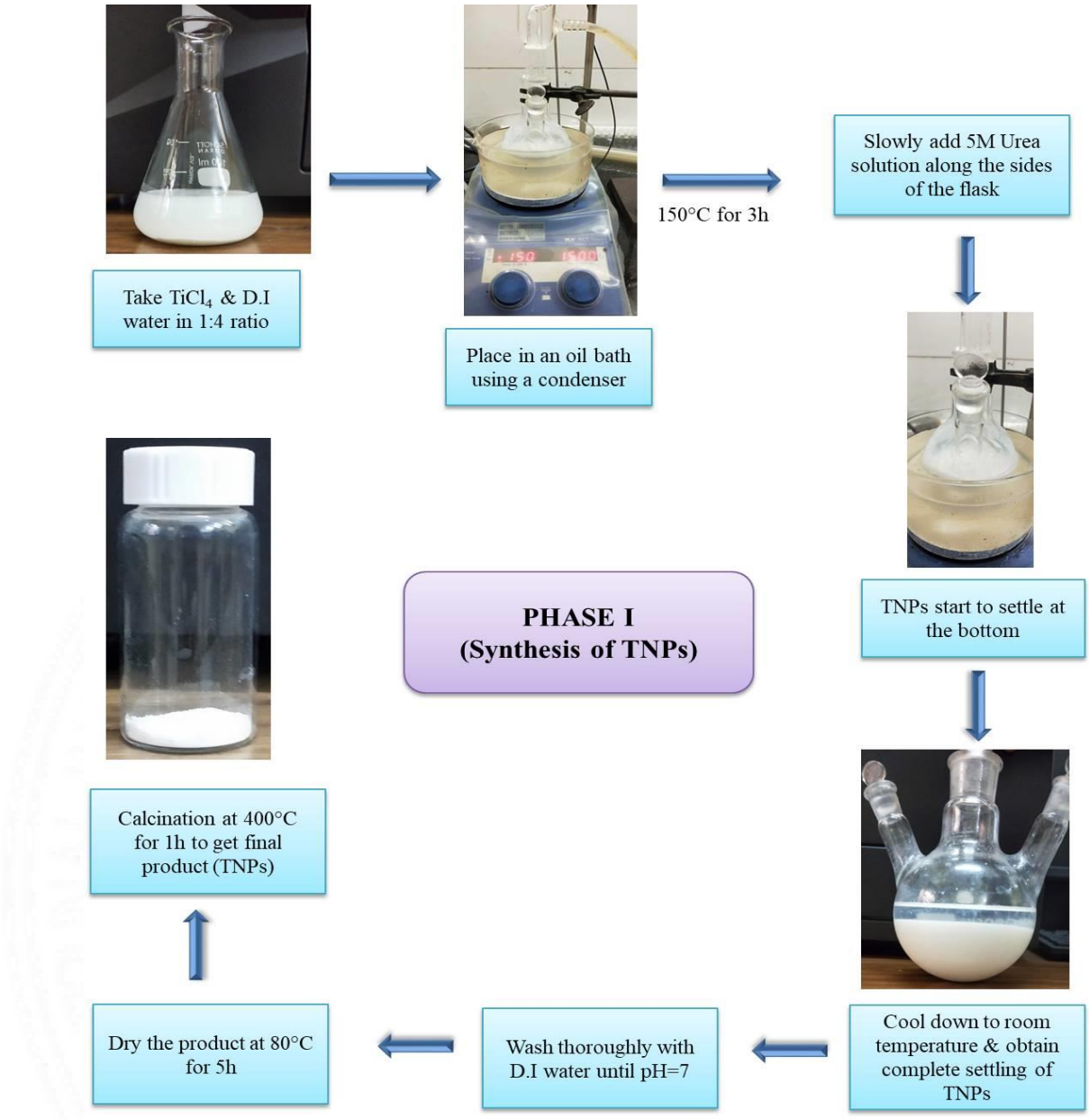

Figure 3.1 Synthesis of TNPs using urea precipitation method (Phase I).

conducted firstly by placing the tightly sealed Teflon autoclave into a milk cooker poured internally with silicon oil. Next, the cooker along with the autoclave was immersed into a silicon oil bath maintained at a temperature of 135˚C (5˚C more than the required temperature to ensure proper diffusion of the temperature into the reaction mixture) [Kasuga *et al.*, 1998]. In principle, the Ti-O-Ti bond will break at this stage in the highly alkaline atmosphere and Ti-O-

Na and Ti-OH bonds will be formed. This leads to the formation of Sodium titanate ($Na_2Ti_3O_7$) nanosheets in solution (Step 1 in Figure 3.2). The reaction product was then washed thoroughly with a large volume of D.I water until the pH=7. Sodium titanate nanosheets were then immersed into a dilute HCl aqueous solution (pH=2) for 8h at room temperature. Through selective dehydration of $Na_2T_iO_3$ in an acidic medium, Ti-O-H-O-Ti hydrogen bonds are generated. This leads to the rolling up of sheets by connecting the ends of each between themselves; resulting in the formation of a tube-like structure (Step 2 in Figure 3.2).

Step 1 $3TiO_2 + 2NaOH \longrightarrow Na_2Ti_3O_7 + H_2O$

Step 2 $Na_2Ti_3O_7 + 2HCl \longrightarrow H_2Ti_3O_7 + 2NaCl$

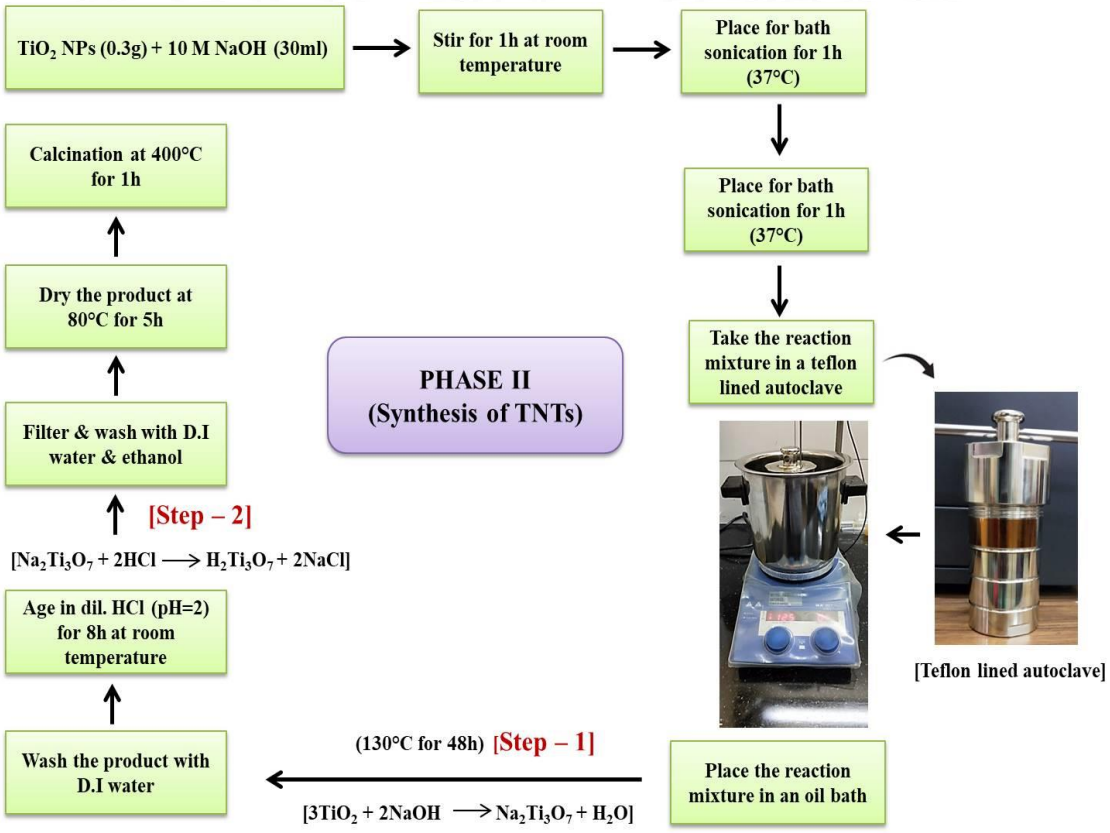

Figure 3.2 Two-step formation of TNT from TNP through solvo thermal method (Phase II).

The white-colored product was then filtered using Whatman filter paper and washed repeatedly with DI water and ethanol respectively until the pH reaches 7. The product obtained after

washing was dried at 80˚C for 5h and calcined at 400˚C for 1h. A schematic representation of the principle involved in the solvo thermal synthesis of TNTs is shown in Figure 3.3. TNTs were then physico-chemically characterized before proceeding to Phase III of the synthesis steps.

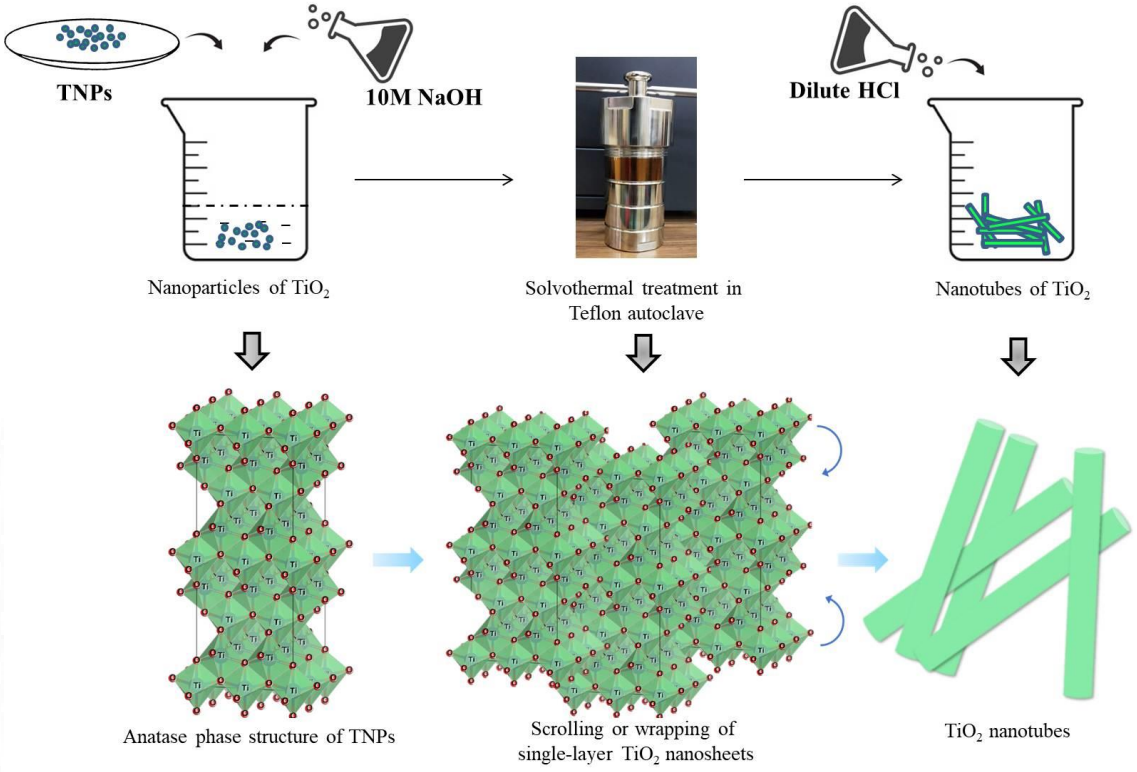

Figure 3.3 Steps and principle involved in solvo-thermal synthesis of TiO_2 nanotubes

3.5.1.3 PHASE III: Surface coating of TNTs with Pluronic F-127

TNTs were surface coated with P-F127 polymer according to the method proposed by Ludtke *et al*., [2009]. P-F127 and TNTs were mixed at a 2:1 ratio in 2ml DI water taken in a screw-capped bottle. It was vortexed well at room temperature and placed for bath sonication at 37°C for 30min. The reaction mixture was then placed in an oil bath and allowed to react for 1h at 65°C at 350rpm. Surface-coated TNTs were then transferred into pre-hydrated cellulose membrane dialysis tubing (average flat width of 33nm or 1.5inches) and placed for dialysis

overnight against D.I water. The product obtained was then dried at 80°C for 5h. A flowchart showing steps in Phase III of the synthesis protocol is illustrated in Figure. 3.4.

3.5.2 PHYSICO-CHEMICAL CHARACTERIZATION

TNPs were characterized for hydrodynamic diameter, surface charge, and crystallographic study by DLS, zeta potential analysis, and XRD respectively. FT/IR, micro Raman spectroscopy, TEM, TGA, and DTA were performed for both TNPs and TNTs in a comparative manner. Polymer coating on the TNT surface was characterized

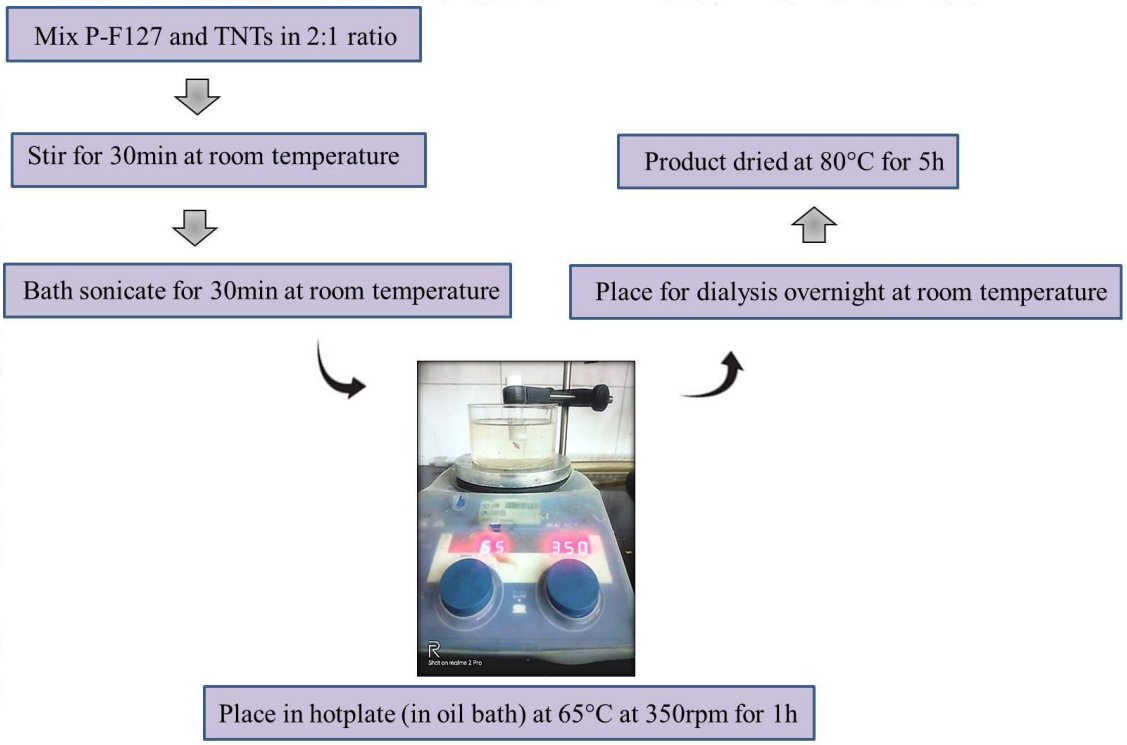

Figure 3.4 Flow chart for P-F127 coating of TNTs (Phase III).

using FT/IR spectroscopy; wherein TNT-P was scrutinized for the presence of characteristic peaks from TNTs and P-F127. Three of the materials were dried into a fine powder before every characterization procedure.

3.5.2.1 Dynamic Light Scattering (DLS)

The hydrodynamic diameter of TNPs in two different dispersion media such as distilled water and phosphate-buffered saline (PBS) was determined using Malvern Zetasizer Nano ZS (UK) with DTSNano V4.2 software. The variation in hydrodynamic diameter and the corresponding Poly Dispersity Index (PDI) of TNTs by the dispersion medium was noted. PDI was noted down to analyze the dispersity of the material in different suspensions. The procedure was done for TNPs alone. Because in general, 1DNMs like NTs exhibit a high degree of agglomeration and hence it becomes relatively more difficult to achieve a homogenous dispersion than NPs.

3.5.2.2 Zeta potential analysis

The surface charge of TNPs was determined using zeta potential analysis using Malvern Zetasizer Nano ZS (UK) with DTSNano V4.2 software. The zeta potential of the sample was obtained from the electrophoretic mobility measurements which were obtained from the instrument software.

3.5.2.3 Fourier Transform Infrared Spectroscopy (FT/IR)

FT/IR permits the analysis of interphases to determine the surface adsorption of functional groups on NMs. Typically the FT/IR spectrum does not alter even though there is any phase transformation occurring within the NM. For the confirmation of such chemical stability after phase transformation, both TNPs and TNTs were subjected to FT/IR analysis using IR Tracer 100 Shimadzu (Singapore). The spectrum was obtained using ATR module for a range of 400-4000 cm-1.

3.5.2.4 X-Ray diffraction (XRD)

Major crystalline phases of the synthesized TNPs were detected using XRD. Vital parameters obtainable through XRD include; crystalline structure, nature of the phases and lattice parameters. Here, XRD pattern was assessed using Bruker D8 advanced PXRD (Germany). The crystalline peaks were identified from the corresponding deflection angles (2θ) and their respective hkl values. The identified XRD peaks were compared with the JCPDS (Joint Committee on Powder Diffraction Standards) online database and the card numbers for detected crystalline phases were noted.

3.5.2.5 Micro Raman Spectroscopy

The phase transition from NPs to NTs was identified using micro-Raman spectroscopy. This technique aids to identify the chemical structure of the material depending on the inelastic scattering of light after colliding on the molecule's surface. Also, it helps to distinguish two different forms of the same material in terms of their molecular organization. Here, the technique was performed using a Confocal Raman Microscope, alpha 300A, Witec Inc. (Germany) over a range of 100-3500cm-1 of the Raman spectra.

3.5.2.6 Transmission Electron Microscopy (TEM)

Surface topography and the average diameter of TNPs and TNTs were determined via TEM analysis using JEOL JEM 2100 (China). The calcined form of both of the samples was dispersed in water and bath sonicated for 20min at room temperature. Dispersed samples were then dropped cast on a TEM 200 mesh Copper (Cu) microgrid and air dried at room temperature overnight. Casted samples were then viewed under TEM at an accelerated voltage of 80kV at two different magnifications (50,000X and 60,000X).

3.5.2.7 Thermo Gravimetric Analysis (TGA)

TGA allows determining the thermal stability of NMs by the identification of percentage weight loss over a controlled temperature range. This aids in identifying the fraction of volatile components on the material surface and their change over the given temperature range. The TGA curves for TNPs and TNTs were assessed using SDT Q600 V8.3 Build 101 (USA) by heating the dried samples between 0°C to 800°C.

3.5.2.8 Differential Thermal Analysis (DTA)

Apart from the measurement of thermal behavior, DTA additionally allows the identification of specific chemical reactions such as exothermic and endothermic events occurring from the NM surface. The DTA curves of TNPs and TNTs were obtained using SDT Q600 V8.3 Build 101 (USA) over a temperature range of 0°C to 800°C. The materials were inspected for the difference in thermal reactions and were compared with the weight loss pattern obtained for TGA analysis.

3.5.2.9 Evaluation of surface coating of TNTs using FT/IR Spectroscopy

The efficacy of P-F127 coating over the TNT surface was characterized using FT/IR spectroscopy using IR Tracer 100, Shimadzu (Singapore). The peaks obtained for TNT-P were compared with the FT/IR peaks of P-F127 and that of bare TNTs. The presence of major characteristic peaks corresponding to the Ti-O bond and P-F127 specific bonds was considered to be indicative of the surface coating of TNTs with the polymer. IR spectra were obtained at a frequency range of 400-4000cm-1.

3.6 EVALUATION OF *IN VITRO* TOXICITY OF TiO_2 NANOTUBES USING C6 CELL LINE

3.6.1 C6 GLIAL CELL CULTURE AND NANOMATERIAL EXPOSURE

C6 glial cell is a type of cancerous cell line isolated from the nervous tissue of rat glioma and has major importance in neuronal research. The C6 cell line for the study was obtained from National Center for Cell Science (NCCS), Pune. The cell line was cultured in DMEM F12 medium supplied with 10% FBS, 1% antibiotic-antimycotic solution, 1% Glutamax, and 1mM sodium pyruvate. Cells were used for toxicity studies once they reach 80-85% confluence. All three forms of TiO_2 NMs were prepared in DMEM F12 before exposure (freshly prepared) and were prepared in a series of concentrations from 5µg/ml to 160µg/ml. TNPs and TNTs were bath-sonicated under sterile conditions for 20min at room temperature prior to exposure. This step ensured a homogenous dispersion of the materials and was not required for TNT-P as the dispersion stability was considerably higher than TNPs and TNTs. All the experiments were performed after 24h of cellular exposure under incubation conditions of 5% CO_2 and 37°C.

3.6.2 CELLULAR PHENOTYPIC OBSERVATION BY PHASE CONTRAST MICROSCOPY

Cultured cells were observed under a phase contrast microscope for the identification of cellular phenotype. Morphologically developed cells in the T25 cell culture flask were directly viewed under a Leica DMIL microscope fitted with a camera.

3.6.3 CELLULAR UPTAKE STUDY USING IMAGING FLOW CYTOMETRY

Imaging Flow Cytometry was used to analyze the cellular uptake of TNPs into C6 cells after 24h exposure [Suzuki *et al*., 2007]. Forward scatter (FSC) and Side scatters (SSC) in flow cytometry represent cell size and granularity respectively. In principle, NP uptake increases cellular granularity and can be detected while inside the flow. Imaging Flowcyrometry has an additional advantage of imaging provision for the cells. An increase in SSC normally indicates an increase in cellular granularity and hence represents an increase in cellular uptake. For the present study, cells were seeded at an initial density of $1X10^5$ cells per well in a 6-well plate and exposed to three different concentrations of TNPs (5µg/ml, 40µg/ml, and 160µg/ml). These values denote the lowest, middle, and highest concentrations of TNPs. Cells without particle exposure represent the control cells. After 24h of exposure, cells were trypsinized and centrifuged for 5min at 12000rpm. The cell pellet collected was resuspended in 500µl PBS and analyzed using a flow cytometer (Amnis FlowSight® imaging flow cytometer), fitted with the Ideas Version 6.0 software.

3.6.4 EVALUATION OF CELL VIABILITY OR MITOCHONDRIAL ACTIVITY BY MTT ASSAY

The cell viability was assessed in terms of mitochondrial activity using an MTT assay. The assay relies on the activity of the NAD (P) H-dependent mitochondrial dehydrogenase enzyme to reduce the tetrazolium dye; MTT. In principle, the dehydrogenase enzyme reduces the MTT dye and forms an insoluble purple-colored formazan crystal. The color intensity of formazan crystal denotes the mitochondrial activity or metabolic status of the cells [Mosdam *et al*., 1983]. For the experiment, $1X10^4$ cells per wellwere seeded in two 96-well plates and were incubated overnight at 5% CO_2 and 37°C. Upon 80% confluence, culture media was removed and washed with PBS. Both TNPs and TNTs of various concentrations (5, 10, 20, 40, 80, and 160µg/ml) were exposed to cells in respective plates and incubated for another 24h at similar culture conditions. Cells without particle exposure served as the negative control and those cells treated with 0.1mM phenol were considered as a positive control. After incubation, media was removed, and added 100µl (50µg/well) of MTT reagent and incubated in dark for 3.5h at 37°C. Cells were then washed with PBS and insoluble formazan crystals were solubilized by

adding 100µl DMSO in each well. Plates were incubated for 20min in the dark and the purple color intensity was detected using an automated microplate reader (ELx 808, Bio-Tek Instruments, USA) at 540nm. The percentage (%) of cell viability was calculated using the formula:

$$\text{Cell viability (\%)} = \frac{\text{OD of treatment group}}{\text{OD of cell control group}} \text{ X } 100$$

3.6.5 MITOCHONDRIAL MEMBRANE POTENTIAL (MMP) EVALUATION BY JC1 STAINING

MMP of TNP and TNT exposed cells was evaluated using JC1 staining. JC1 denotes a cell-permeable fluorescent probe and has a strong affinity towards the mitochondrial compartment of cells. They form J- aggregates when binding with active mitochondria and emit red fluorescence. Perturbation in MMP results in the translocation of this probe towards the cytoplasm and exists as a monomer emitting green fluorescence. This denotes that, mitochondrial depolarization results in diminishing or loss of red fluorescence, and active mitochondria will be emitting reddish fluorescence [Shukla *et al*., 2015]. For the study, cells were seeded at a density of $1X10^5$ cells per well in two 6-well plates and incubated overnight. Media was replaced with three different concentrations of TNPs and TNTs (5, 40, and 160µg/ml) in respective plates and incubated for 24h at 5% CO_2 and 37°C. After media removal, cells were treated with 2µM JC1 in each well and incubated in dark for 30min at 37°C. Cells were later washed three times with PBS and observed under a fluorescence microscope (Axio Scope A1 microscope, Carl Zeiss (Germany).

3.6.6 EVALUATION OF LYSOSOMAL STABILITY USING NEUTRAL RED UPTAKE (NRU) ASSAY

Cell viability after NM exposure was further confirmed in terms of lysosomal stability using NRU assay. The theory of this assay is based on the selective uptake of supravital eurhodin dye; neutral red by the active lysosomes of healthy cells. Viable cells take up this dye via active

transport, whereas non-viable cells fail to incorporate neutral red as the lysosomes lose their integrity [Borenfreund *et al*., 1985]. $1X10^4$ cells were seeded per well in two 96-well plates and incubated overnight at 5% CO_2 and 37°C. Different concentrations of TNPs and TNTs were prepared in DMEM F12 (5, 10, 20, 40, 80, and 160µg/ml) and added to wells. Cells without particle treatment were kept as negative control and those treated with 0.1mM phenol were kept as a positive control. After 24h of exposure, media was removed and 100µl of 0.1% neutral red was added to each well of both of the plates. The plates were then incubated for 3h in dark at 37°C. Excess dye was removed by washing the wells with PBS. The cells were then de-stained by adding 100µl of a mixture of 50% ethanol, 49% D.I water, and 1% glacial acetic acid. Continuous shaking was provided using New Brunswick Innova 4080, (USA) for 30min at 60rpm in dark. Absorbance for the color developed was read using an automated microplate reader (ELx 808, Bio-Tek Instruments, USA) at 540nm.

3.6.7 ASSESSMENT OF LYSOSOMAL INTEGRITY USING ACRIDINE ORANGE STAINING

The lysosomal stability of treated cells was assessed using AO staining. AO is a fluorochromatic dye that has a strong affinity towards cellular compartments with low pH or highly acidic. It easily traverses the cell membrane because of weak basicity. Since lysosomes are highly acidic, AO selectively enters the lysosomes through an ATP-dependent proton pump on its membrane. While inside lysosomes, AO emits red fluorescence, and whenever the lysosomal integrity is lost or the membrane is damaged, the emission spectrum shifts towards the green region [Shi *et al*., 2010]. The level of lysosomal stability indicates the extent of cell viability. The cells were seeded in two 6-well plates at an initial density of $1X10^5$ cells per well and incubated overnight. Media was removed and exposed with three different concentrations of both TNPs and TNTs (5, 40, and 160µg/ml) in respective plates. After 24h of incubation, the media was removed and incubated with 5µg/ml of AO for 15min in dark at 37°C. Cells were then washed to get rid of the surplus stain with PBS (three times) and imaged under a fluorescence microscope [Axio Scope A1, Carl Zeiss (Germany)].

3.6.8 EVALUATION OF CELLULAR MORPHOLOGY USING NON-FLUORESCENT STAINING METHODS

3.6.8.1 Coomassie Brilliant Blue (CBB) staining for TNP exposure of C6 cells

Morphological evaluation of TNP-exposed cells was performed using CBB staining. CBB is considered as a widely employed non-fluorescent dye for the visualization of cellular proteins. It specifically binds the aromatic and basic amino acid side chains of proteins [Davoren *et al*., 2007]. Then cells were counted and seeded at a density of $1X10^5$ cells per well of a 6-well plate and incubated overnight at 5% CO_2 and 37°C. Media was replaced with various concentrations of TNPs prepared in DMEM F12 (5, 40, and 160µg/ml) and incubated for 24h. Cells were fixed using 4% formaldehyde for 3 min after washing with ice-cold PBS. 0.5% CBB (using methanol: acetic acid at 1:4 ratio) was added to each well and incubated for 15min at 37°C. After thorough washing with PBS (three times), cells were observed under a microscope (Olympus CX31, Japan).

3.6.8.2 Giemsa staining for TNT exposure of C6 cells

Giemsa staining is a gold-standard non-fluorescent staining technique for the evaluation of cellular morphology. It can profile the individual cellular components in which the nuclei will be stained dark blue and the cytoplasm blue to pink in color [Reshma *et al.*, 2017]. For the study, $1X10^5$ cells per well were seeded and incubated overnight. After cellular exposure of TNTs of three different concentrations (5, 40, and 160µg/ml) for 24h, media was removed and the cells were fixed using 4% formaldehyde for 3min at 37°C. 10% Giemsa stain was added to each well and incubated for 5min at room temperature. After washing with PBS three times, the stained cells were observed under a microscope (Olympus CX31, Japan).

3.6.9 EVALUATION OF CYTOSKELETAL INTEGRITY OR ACTIN FILAMENT ORGANIZATION BY RHODAMINE-PHALLOIDIN STAINING

Cytoskeletal integrity of the NM exposed C6 cells in terms of actin filament organization were evaluated using Rhodamine phalloidin staining. This is one of the widely used fluorescent phalloidin conjugates and possesses a strong binding capacity with filamentous actin. For the experiment, cells were seeded at an initial density of $1X10^5$ cells per well in two 6-well plates

and incubated overnight. Cells were exposed to varying concentrations of TNPs and TNTs (5, 40, and 160µg/ml) and incubated for 24h at 5% CO_2 and 37°C. After PBS washing, cells were fixed using 4% formaldehyde for 10min. Excess aldehyde was quenched by adding 0.1M Glycine prepared in PBS for 5min. 0.1% Triton-X 100 in PBS was used for the permeabilization of cells for 1min. Actin filaments were then stained with Rhodamine phalloidin in 1:200 ratio with PBS for 15min in dark. DAPI (5µg/ml) was used as the counterstain which selectively stains the nuclei blue. Cells were washed thrice with PBS and observed under a fluorescent microscope [(Axio Scope A1, Carl Zeiss (Germany)].

3.6.10 INVESTIGATION OF INTRACELLULAR OXIDATIVE STRESS

3.6.10.1 Evaluation of Reactive Oxygen Species (ROS) by DCFH-DA Assay

NM-induced generation of ROS was evaluated using DCFH-DA assay; a method proposed by Wan *et al*., 1993. DCFH-DA is a fluorogenic dye that detects the hydroxyl, peroxyl, and other minor ROS inside cells. This is a cell-permeable dye and esterase enzyme present in viable cells that converts DCFH-DA into DCFH. ROS generated inside the cells will hydrolyze this DCFH into a green fluorescent compound DCF (Dihydrofluorescein). The biochemical reaction involved in the assay is shown in Figure. 3.5.

.

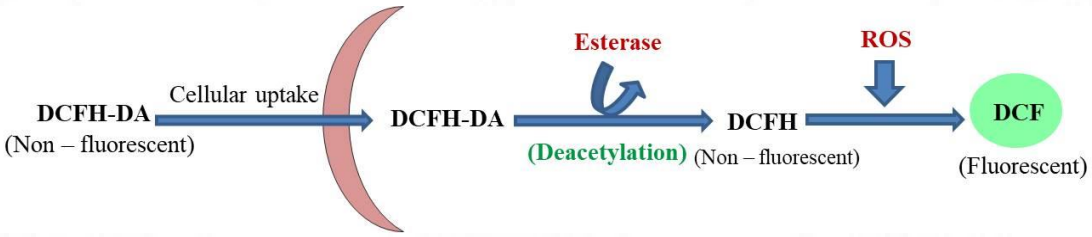

Figure 3.5 Biochemical reaction involved in DCFH-DA assay

For the experiment, $1X10^4$ cells per well were seeded in two 96-well plates and incubated overnight. Media was removed and 100µl of 1µM DCFHDA was added to each well and incubated for 45min in dark at 37°C. The reagent was then replaced with varying concentrations of TNPs and TNTs (5, 10, 20, 40, 80, and 160µg/ml) and incubated for 24h at

5% CO_2 and 37°C. Cells without particle exposure were kept as negative control and those treated with 0.09% H_2O_2 served as a positive control. Stress-induced ROS levels were then measured after incubation using a fluorescent microplate reader (Infinite F Nano + TECAM, Switzerland) at excitation/emission wavelengths of 495/530nm.

3.6.10.2. Evaluation of Reactive Nitrogen Species (RNS) by Griess reagent Assay

Stress-induced nitrile radical production was detected using the Griess reagent method as proposed by [Bryan *et al*., 2007]. The assay relies on a colorimetric chemical reaction between nitrite sulphanilamide and N-(1-naphthyl) ethylenediamine to generate a pinkish azo product. For the assay, cells were seeded at a density of $1X10^4$ cells per cell in two 96-well plates and incubated overnight. After media removal, cells were exposed to varying concentrations of TNPs and TNTs in respective plates (5, 10, 20, 40, 80, and 160µg/ml) for 24h. 50µl of the supernatant from each well of the plates was transferred to wells of another empty 96-well plate and mixed with 50µl of Griess reagent and incubated in dark for 10min at room temperature. The developed color was read at 540nm using an automated microplate reader (ELx 808, Bio-Tek Instruments, USA).

3.6.11 EVALUATION OF CELL MEMBRANE INTEGRITY USING LACTATE DEHYDROGENASE (LDH) RELEASE ASSAY

Cellular exposure to NMs can result in disruption of the cell membrane and subsequent release of LDH into the cytoplasm. LDH assay is a simple and reliable colorimetric assay for the determination of cytotoxicity based on this release. The morphological peculiarities of TNTs and TNPs can lead to varying responses in terms of cell membrane disruption and this concept is being evaluated through this assay (Bahadar *et al*., 2016). For the study, the quantification of cytosolic LDH was performed using a commercial LDH detection kit (CyQUANT^{TM}, Thermofisher Scientific). The principle includes an enzymatic coupling reaction in which cytosolic LDH catalyzes an oxidative conversion of lactate to pyruvate and the simultaneous release of NADH from NAD+. The NADH then reduces the tetrazolium salt (INT) in the system to form a yellow-colored product. The intensity of the formed yellow color is directly proportional to the level of LDH released. For the assay, $1X10^4$ cells per well were seeded in two 96-well plates and incubated overnight. Varying concentrations of TNPs and TNTs were

exposed (5, 10, 20, 40, 80, and 160µg/ml) and the plates were incubated for 24h. 100µl of cell supernatant from each well was transferred to another 96-well plate and the amount of LDH released was quantified as per the manufacturer's instruction.

3.6.12 LIVE/DEAD CELL STUDY FOR TNPS USING ACRIDINE ORANGE (AO) / ETHIDIUM BROMIDE (ETBR) DUAL STAINING METHOD

AO/EtBr dual staining method can be used to visualize cells in different stages of cell death pathways such as necrosis. The assay is a valuable tool to identify specific necrotic cell death changes occurring within the cell membrane via a fluorescence-based detection system. The principle includes, AO entering the viable cells through passive diffusion and emitting green fluorescence. EtBr is not capable of diffusing the cell membrane unless it loses its integrity or cell membrane damage occurs [Kasibhatla *et al*., 2006]. In brief, cells were seeded at $1X10^5$ cells per well in a 6-well plate and incubated overnight. Cells were exposed to three concentrations of TNPs (5, 40, and 160µg/ml) for 24h. After media removal, 5µg/ml of AO was added to each well and incubated for 15min in dark at 37°C. EtBr was also added (3µg/ml) 5min before the incubation ends and swirled gently. The fluorescence developed was then observed under a microscope [Axio Scope A1 fluorescence microscope, Carl Zeiss (Germany)].

3.6.13 LIVE/DEAD STUDY FOR TNTS USING CALCEIN AM/PI STAINING METHOD

Calcein AM is a highly efficient cell-permeable dye that can be used to predict cell viability. Calcein AM in bounded form is non-fluorescent. While inside the viable cells, cellular esterase hydrolyzes the acetoxymethyl ester in Calcein AM to release Calcein into the cytoplasm and it exhibits a green fluorescence. PI in contrast, is a non-cell permeable dye and it enters only when cell membrane integrity is lost. For the assay, $1X10^4$ cells per well were seeded in a 96-well plate and incubated overnight. Cells were exposed to different concentrations of TNTs (5, 10, 20, 40, 80, and 160µg/ml) and incubated for another 24h. The media was removed and washed with PBS. 100µl Calcein AM (1µg/ml) and PI (2.5µg/ml) mixture in DMEM F12 was added to each well and incubated for 30min in dark at 37°C. Relative fluorescence of the dyes was quantified using a fluorescent microplate reader (Infinite F Nano + TECAM, Switzerland)

at Excitation/Emission wavelengths of 485nm to 595nm. Corresponding fluorescence images of the cells treated with different concentrations of TNTs (5, 40, and 160 µg/ml) were also obtained using a similar procedure. Images were taken under a microscope [Axio Scope A1 fluorescence microscope, Carl Zeiss (Germany)] using green and red filters.

3.6.14 DNA LADDERING ASSAY FOR NUCLEAR INTEGRITY BY AGAROSE GEL ELECTROPHORESIS (AGE)

DNA laddering is one of the hallmarks of cytotoxicity in which specific DNA fragmentation can be confirmed by the aid of gel electrophoresis. The assay is considered as highly sensitive as it provides information regarding nuclear integrity during cytogenetic damage. For the experiment, cells were seeded at $1X10^5$ cells per well in a 6-well plate and incubated overnight. TNPs and TNTs prepared in varying concentrations (10 to 160µg/ml) were exposed the cells for 24h. Genomic DNA was isolated from each of the treated well using GenEluteTM mammalian genomic DNA Miniprep kit as per manufacture's instruction. Isolated DNA samples were then loaded and electrophoresed using 0.9% agarose gel containing EtBr for 2h at 80V. The size of the ladder was 1Kb and the positive control used was provided along with the kit.

3.6.15 EVALUATION OF NUCLEAR CONDENSATION BY DAPI STAINING

TNP induced nuclear condensation in C6 cells was evaluated using DAPI staining. Cells were seeded at an initial density of $1X10^5$ cells per well in a 6-well plate. After incubation overnight, cells were treated with varying concentrations of TNPs for 24h. After removing the culture media, cells were washed with PBS and fixed using 4% formaldehyde for 10min at room temperature. Staining was done using 1µg/ml of DAPI in each well and incubated for 5min in dark. PBS washing was provided for three times and observed under microscope [Axio Scope A1 fluorescence microscope, Carl Zeiss (Germany)].

3.6.16 IN VITRO TOXICITY STUDIES FOR TNT-P

After confirmation of surface coating of TNTs with P-F127 (as explained in section 3.5.1.3), basic cell viability assays and oxidative stress analysis was performed for TNT-P after 24h of exposure to C6 cells.

3.6.16.1 Evaluation of cell viability upon TNT-P exposure by MTT Assay

Cell viability of C6 cells after exposure with TNT-P was performed using MTT assay. For the assay, cells were seeded at an initial density of $1X10^4$ cells per well and incubated overnight. Cells were then exposed with various concentrations of TNT-P (5, 10, 20, 40, 80 and 160µg/ml) for 24h. After washing with PBS, MTT assay was perfomed as per the procedure mentioned in Section 3.6.4. Cell viability (%) was plotted against TNT-P concentrations used.

3.6.16.2 Study on effects of P-F127 polymer on C6 cell viability

Surface coating materials can contribute great to the cytotoxic response of NMs in *in vitro* studies. The cell viability rates in functionalized NM toxicity assays denote a cumulative toxic response of not only the material, but also the functionalizing compund. Hence, the nature of the functionalizing material can greatly influence the toxicity mechanisms elicited onto the cells and therefore the toxicity levels. Hence the present study requires to analyze the viability response of P-F127 alone on C6 cells and then to check the reliability of cytoxicity limits of TNT-P. For fulfilling the question, MTT assay was performed for C6 cells-P F127 interaction for 24h. Cells were added at a count of $1X10^4$ cells per well in a 96-well plate and incubated overnight. Cells treated with varying concentrations of P-F127 (5, 10, 20, 40, 80 and 160µg/ml) for 24h. MTT assay was done as per the procedure noted in section 3.6.4.

3.6.16.3 Lysosomal integrity study for TNT-P – C6 cells interaction

Viability rates observed for the glial cell interaction with TNT-P via MTT assay was confirmed using NRU assay in terms of lysosomal integrity. 1X104 cells per well were grown in a 96-well plate and exposed with different concentrations of TNT-P (5, 10, 20, 40, 80 and 160µg/ml) for 24h. NRU assay was peroformed as per the procedure mentioned in section 3.6.6.

3.6.16.4 Evaluation of ROS generation for C6 cells – TNT-P interaction

In general, among the various sub-cellular toxicity mechanisms idenfied so far, oxidative stress comprises the key toxicity pathway followed by NMs.The primary point of this experiment was

to compare the oxidative stress outcomes of TNTs before and after surface coating with P-F127 polymer. DCFH-DA assay was performed for the interaction of C6 cells with TNT-P using the procedure mentioned in Section 3.6.10.1.

3.7 INVESTIGATION OF ACUTE TOXICITY OF SURFACE COATED TiO_2 NANOTUBES USING WISTAR RAT

In vivo acute toxic response of TNT-P was investigated using Wistar rats. An overall work plan for the *in vivo* study is illustrated in Figure. 3.6.

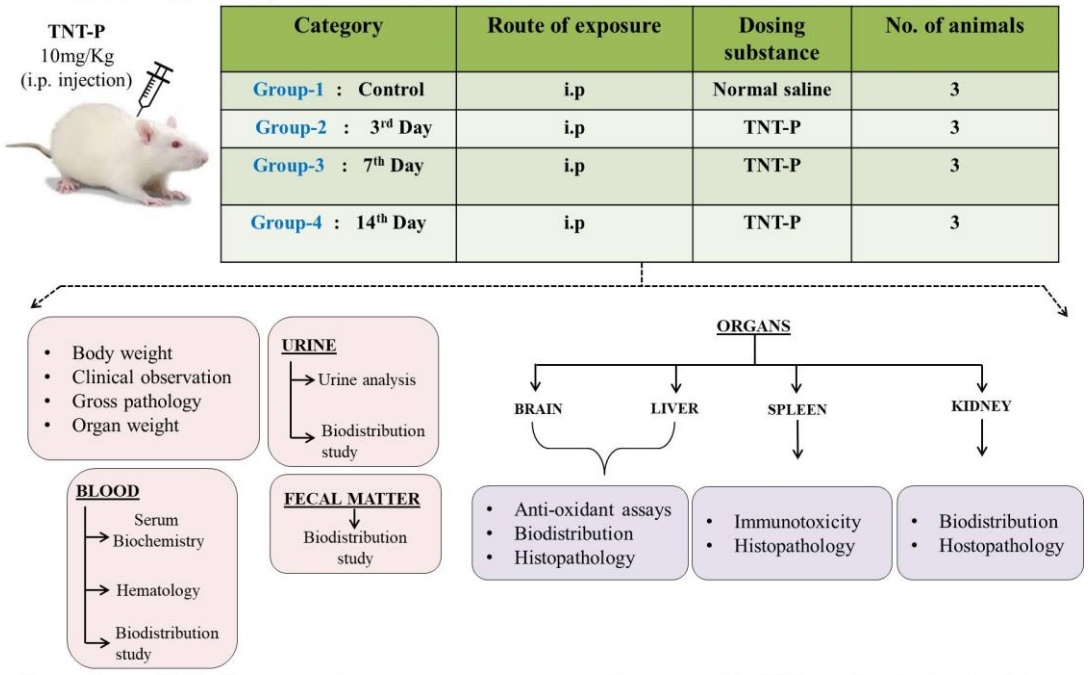

Figure 3.6 *In vivo* acute toxicity work plan using Wistar rat

3.7.1 EXPERIMENTAL DESIGN AND DOSAGE

A total 12 number of both male and female healthy Wistar rats weighing 200-250g were used for the study. They were divided into four different groups based on the day of sacrifice. Group-I of rats received only normal saline instead of TNT-P through the i.p. route and they were kept as the control group. The rest of the three groups were administered with a single dose of TNT-P (10mg/Kg body weight) via the i.p. route and were sacrificed on days 3, 7, and

14 respectively. TNT-P was prepared in D.I water at a concentration of 10mg/Kg body weight of the animal and the animals received 1-2 ml of the suspension.

3.7.2 VISUAL EXAMINATION FOR SIGNS OF BEHAVIORAL CHANGES

All of the experimental animals were observed for any type of signs related to behavioral changes. For this, a homecage examination was performed twice a day throughout the experimental period. Major signs for unusual changes scrutinized were; lacrimation, salivation, excretion, piloerection, motor activity, home cage posture, rearing, reduced food, and water consumption, *etc*.

3.7.3 BODY WEIGHT OF RATS

The body weight of all the animals was determined regularly on the 3rd, 7th, and 14th days of post-exposure and growth pattern was plotted for the values obtained.

3.7.4 EUTHANIZATION AND SAMPLE COLLECTION

At the end of each day of sacrifice, urine and fecal matter were collected in labeled collection tubes. Prior to euthanization, animals were anesthetized using choloroform, and blood was collected from the optical sinus of each animal using non-vacuum blood collection tubes. For hematological analyses, heparinized blood collection tubes were used. Appropriate volumes of blood were separated and kept for serum biochemistry and biodistribution studies. After sample collection, animals were euthanized by the cervical dislocation method.

3.7.5 GROSS PATHOLOGY ANALYSIS

After the euthanization of animals at the end of each observation period, their whole body and the key internal organs were subjected to postmortem examination. This step is crucial for the identification of any visible pathological lesions on the surface of the animal body or organs such as lumps, color change, edema, *etc*.

3.7.6 WET WEIGHT OF RAT ORGANS

Four key organs were isolated from euthanized animals at the end of each observation day and they include; Brain, Liver, Spleen, and Kidneys. The wet weight of all the organs was recorded immediately after euthanization.

3.7.7 HEMATOLOGY ANALYSIS

Blood samples collected in heparinized collection tubes were used for hematological evaluation. Various hematology parameters including Red Blood Cells (RBC), White Blood Cells (WBC), Hemoglobin (HGB), Hematocrit (HCT), Mean Corpuscular Volume (MCV), Mean Corpuscular Hemoglobin (MCH), Mean Corpuscular Hemoglobin Concentration (MCHC) and the platelet count were obtained with an automated hematology analyzer (Horiba Vet abc, Japan).

3.7.8 SERUM BIOCHEMISTRY ANALYSIS

Blood samples collected in non-heparinized collection tubes were allowed to form clots and serum was separated by centrifuging the clots at 3000rpm for 10min for serum biochemistry analysis. Major biochemistry parameters analyzed include; three key metabolic enzymes as Alanine transaminase (ALT), Aspartate transaminase (AST), and Alkaline phosphatase (ALP). The titer of certain other parameters such as glucose level, cholesterol, triglycerides, albumin, protein, and creatinine levels were also checked using an automated biochemical analyzer, Erba Mannheim XL300 (Germany).

3.7.9 DETERMINATION OF ANTIOXIDANT LEVELS IN THE BRAIN AND LIVER

The levels of major antioxidant levels in brain and liver samples such as total protein, GSH, and LPO was estimated using appropriate methods. Both of the organs were washed in normal saline immediately after isolation and transferred to a clean container kept in ice. Tissues were homogenized at 900rpm using a tissue homogenizer, Polytron P 3100 (10% homogenate using 0.1M phosphate buffer, pH=7.4). Samples were kept on ice completely during the experiment. The homogenate was centrifuged at 4°C, 3500rpm for 10min, and the supernatant was collected for antioxidant estimation.

3.7.9.1 Estimation of Total Protein by Lowry's method

The total protein contained in liver and brain homogenates was estimated by Lowry's method (Peterson *et al.*, 1977). The concept of the assay is based on the reaction between peptide nitrogen of protein with copper ions under an alkaline environment and changes the copper ion into a monovalent form. This monovalent copper ion along with the amino acid side chains of proteins (*e.g*. Tyrosine, Tryptophan, Cysteine, *etc*.) then reacts with Folin's reagent to form an

unstable purple-colored product. The color intensity developed is directly correlated to the quantity of protein present in the sample. The procedure for the assay is given in Figure. 3. 7. The amount of protein was detected using a spectrophotometer at 660nm [Lambda 25, UV/Vis spectrophotometer (Perkin Elmer, USA)] using BSA (Bovine Serum Albumin) standard graph.

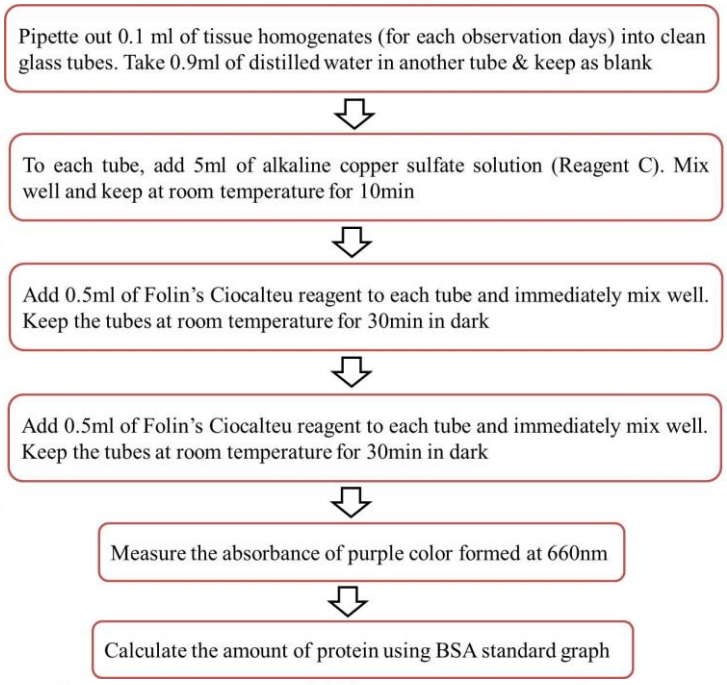

Figure 3.7 Procedure for estimation of total protein in brain and liver samples by Lowry's method.

3.7.9.2 Detection of Reduced Glutathione (GSH) by DTNB method

The levels of GSH in brain and liver tissue homogenates were detected using DTNB method (Moron *et al*., 1979). The assay is based on the selective oxidation of GSH by the sulfhydryl reagent, 5, 5'-dithio-bis (2-nitobenzoic acid) or DTNB to form 5'-thio-2-nitro benzoic acid (TNB). This compound is yellow in color and can be read spectrophotometrically at 412nm. The detailed procedure is shown in Table 3.1.

Table 3.1 Procedure for GSH estimation in brain and liver samples by DTNB method.

Content	**Sample** (Volume in ml)	**Blank** (Volume in ml)
Phosphate buffer (0.2M, pH=8)	4	4
Distilled water	-	0.5
Centrifuged tissue homogenate	0.5	-
5, 5'-dithio-bis (2-nitobenzoic acid) or DTNB	0.5	0.5
Mix the contents in each tube and place at room temperature for 30sec for the oxidation of GSH		
Record absorbance at 0, 1 and 2min at 412 nm & the concentration was calculated from GSH standard curve		

3.7.9.3 Detection of Lipid Peroxidation (LPO) by Thiobarbiturate Reaction

Lipid peroxidation denotes one of the key steps involved in ferroptosis which is driven by the antioxidant activity on lipids. In the present study, the level of lipid peroxidation was determined by thiobarbiturate (TBA) reaction. This method specifically detects the degradation products of lipids such as aldehydes and malondialdehydes (MDA) (Ohkawa *et al*., 1979). The procedure followed for the LPO assay is shown in Table. 3.2. The pink-colored product formed from the reaction between MDA and TBA was measured spectrophotometrically (Lambda 25, UV/Vis spectrophotometer, Perkin Elmer, USA) at 532m.

3.7.10 URINE ANALYSIS

Urine samples obtained in sterile collection tubes were analyzed for the presence of various components including leukocyte, nitrite, urobilinogen, protein, pH, blood, specific gravity, ketone bodies, bilirubin, and glucose. Analysis was done using urine analyser, Uro-dipchek 300 (Erba Mannheim, Germany).

Table. 3.2 Procedure for LPO assay

Content	**Sample** (Volume in ml)	**Blank** (Volume in ml)
Tissue homogenate	0.1	-
Distilled water	0.7	0.8
Sodium Dodecyl Sulfate (SDS) (8.1%)	0.2	0.2
Acetic acid (20%) (pH = 3 using NaOH)	1.5	1.5
Thiobarbituric acid (TBA) (0.8% aqueous solution)	1.5	1.5
Mix well and place in a water bath at 95°C for 60min		
Cool down the reaction mixture under tap water		
Distilled water	1	1
Mixture of n-butanol and pyridine (at v/v of 15:1)	5	5
Mix vigorously and centrifuge the mixture at 4000rpm for 10min		
Measure the absorbance of the upper organic layer at 532nm		

3.7.11 BIODISTRIBUTION STUDY USING INDUCTIVELY COUPLED PLASMA MASS SPECTROSCOPY (ICPMS)

ICPMS technique was used to assess the biodistribution pattern of TNT-P in isolated tissues (brain, liver, and kidney), urine, blood, and fecal matter samples of Wistar rats. The experiment was performed for the samples collected on all the days of observation (the 3rd, 7th, and 14th days). Inductively coupled plasma or ICP is a high-energy ionization source that is capable of decomposing materials into their constituent elements; followed by their transformation into individual ions. The ions are then detected with the aid of mass spectroscopy (MS) and the

spectra can be screened for the relative amount of elements contained in samples under examination. The emission of ions varies depending on the elemental composition of the material and hence the identified ions represent the type of the element(s) present. The MS part of the instrument is fitted with a quadrupole mass filter and a detector organized inside a vacuum chamber. The detection limit of ICPMS is generally <0.1 part per trillion (ppt) and can be employed for the detection of samples that are water or acid soluble or soluble in organic solvents.

3.7.11.1 Sample digestion

All the tissue samples were homogenized based on the procedure mentioned in section 3.7.9. These homogenized tissue samples along with blood, urine, and fecal matter samples were placed for vacuum drying. After ensuring the complete removal of water molecules from the surfaces, all the samples were subjected to microwave-assisted digestion (using The MARSXpress Microwave Digestion system (CEM, USA) before the analysis step. About 0.1g of each sample was weighed and mixed with 3ml of Nitric acid (HNO_3) and 2ml of Hydrogen peroxide (H_2O_2) in cleaned Teflon vessels. The digestion mixture was provided with the following conditions to reach desirable temperatures: The mixture was treated for, 15min (at 800watts) to reach 130˚C and 10min (at 800watts) to reach 185˚C. The temperature was then kept at 185˚C for 30min and allowed to cool down to room temperature. The digestion mixture was made up to 50ml in each tube using D.I water (Elix-EQ7000 Millipore water purification system) prior to analysis.

3.7.11.2 ICPMS Analysis

The digested samples were analyzed using an Inductively coupled plasma spectrometer iCAP RQ (Thermo Scientific, USA). The system included a quadrupole mass analyzer and an autosampler ASX-280 (Teledyne, CETAC Technologies, USA). The elemental analysis was performed using recommended operating conditions as mentioned in Table 3.3.

3.7.12 IMMUNOTOXICITY STUDY

Certain NPs are likely to be taken up by the immunoregulatory cells of the body and they will be modified in terms of their antigenicity. Subsequent alterations with the immune response can make the animal extremely immune-compromised. Upon invasion into animal body, NPs can stimulate antigen- presenting cells and other lymphocytes via lymphatic drainage into lymph

nodes. Here, the immunotoxic response of TNT-P was studied using splenocyte-proliferation assay after re-stimulating the isolated splenocytes *in vitro* and the measurement of their proliferative capacity. The proliferative capacity was measured on the basis of synthesis rate of new DNA strands in dividing splenocytes. The assay quantifies the incorporation of a radioactive nucleoside, tritiated (^{3}H- thymidine) into the developing DNA strands as a measure of splenic proliferation.

Table 3.3 Elemental analysis conditions for Inductively Coupled Plasma Mass spectroscopy (ICPMS).

Parameter	Value
Plasma power (RF)	1550 W
Nebulizer gas	1.06 Lmin-¹
Auxiliary gas	0.8 Lmin-¹
Cool gas flow (Argon)	14.0 Lmin-¹
CCT gas flow (He gas)	5.1 mLmin-¹
KED bias potential	3 V
Dwell time	0.05 s
Number of readings per sample	3 Main runs with 10 sweeps each

3.7.12.1 Splenocyte proliferation Assay by Tritiated (^{3}H) Thymidine incorporation

At the end of each observation day, spleens were aseptically collected from all the experimental animals into sterile collection tubes containing PBS and AB/AM solution. The sample tubes were kept immersed in ice for preserving the live splenocytes. Spleens were dissected using sterile scalpels and transferred to ice-cold RPMI 1640 medium (with 10% FBS) and the slices of spleen were placed on the surface of a sterile nylon mesh. The mesh was then placed above a 10mm petri dish containing media and the tissue was scrapped into the media as a single cell suspension. The suspension was carefully layered over histopaque contained in another tube and centrifuged at 1400rpm for 40min at 4°C. Splenocytes were separated as a buffy coat containing an opaque interface inside the suspension. The interface was collected carefully and

washed 2-3 times with PBS under a fume hood. After suspending into RPMI media, cells were counted and seeded at a density of $2X10^5$ cells/well in a 6-well plate. The plates were incubated for a period of 48h at 37°C and 5% CO_2. At the end of incubation, 0.5µCi of [^{3}H] - thymidine was added to each well and incubated for another 24h. Cells were scrutinized for contamination throughout the incubation period. Cell fixation was then performed using 5% trichloro acetic acid (TCA) and lysed using SDS/NaOH lysis buffer. Culture media containing cells were transferred to microcentrifuge tubes and centrifuged at 10,000g for 15min at 4°C. The cell button obtained was resuspended in 1ml scintillation fluid and radioactivity was measured using a scintillation counter (Hidex, Finland). The obtained values were expressed in counts per minute (CPM) (mean ± SD). An increase in radioactivity denotes increased incorporation of [^{3}H] – thymidine into newly formed splenocyte DNA strands and hence their proliferation level.

3.7.13 HISTOPATHOLOGY ANALYSIS

Histopathological evaluation of collected tissues (brain, liver, spleen, and kidney) was conducted using Hematoxylin and Eosin (H & E) staining after sacrificing at the end of each observation day. For preventing degradation, sliced tissues were washed in normal saline and transferred to 10% neutral buffered formaldehyde in individual collection bottles.

3.7.13.1 Tissue processing

Tissue samples were cut into appropriate sizes for fitting into cassettes. The tissues were then dehydrated using isopropanol (1h each for two times) and cleared in xylene (45min every three times). For easier sectioning, processed tissue slices were gently impregnated within paraffin wax (1h each for two times). The procedure for tissue processing is detailed in Table 3. 4.

3.7.13.2 Embedding

Tissues have to be embedded into molds before sectioning. For that, processed tissues as mentioned in section 3.7.13.1 were carefully taken out of the cassettes using pre-warmed clean forceps without any tissue breakage. The sections were then placed at the center of molten paraffin and pre-poured into molds. Proper labeling was provided for each mold which include;

the name of the tissue, the group of animals, and the date of sacrifice. Proper care was taken to place the sections partially immersed into the wax to minimize tissue breaks during sectioning. Also, it was made sure to place the tissues in proper alignment for getting good quality cross sections for staining.

Table 3.4 Embedding procedure for H & E staining.

Steps	Time of exposure
Isopropanol (I)	1h
Isopropanol (II)	1h
Xylene (I)	45min
Xylene (II)	45min
Paraffin wax (I)	1h
Paraffin wax (II)	1h

3.7.13.3 Preparation of glass slides

Slides for mounting the tissue sections were cleaned thoroughly before taking sections. The procedure for cleaning slides is given in Figure. 3.8. The surface of clean glass slides were coated with a thin layer of Meyer's egg albumin and kept aside for collecting the sliced tissue section. This part is crucial for obtaining good tissue section as it acts like glue between the glass slide and the tissue. This further prevents the section from shedding off during staining.

3.7.13.4 Sectioning of Paraffin blocks

Embedded paraffin blocks were trimmed and shaped carefully along the edges using a scalpel blade. Enough care was taken not to over-trim the blocks as it affects the proper fitting of the block into the machine. A rotary microtome (Leica RM 2125 RT) was used to section the blocks. The distance between the block and the microtome blade was maintained at 5µm to obtain the maximum thinner tissue sections possible. The surface of the paraffin blocks was cooled down in between using ice cubes by rubbing over it. This was for preventing the blocks from forming cracks. By rotating the knob at the side of the microtome, thin ribbons of wax

were obtained and continued until the tissue surface was fully exposed. The wax ribbon containing the tissue section was carefully transferred onto a tissue floating water bath maintained around 50-60°C (M.C. Dalal & Co., India). This helps to get rid of any undesirable folds on the surface of the wax ribbon. The sections were immediately picked up onto the pre-coated surface of a glass slide and dried at 37°C. Dried slides were kept at 4°C until the nextstep.

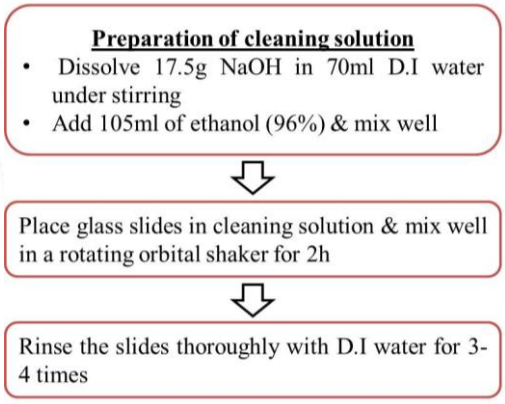

Figure 3.8 Procedure for cleaning glass slides for H&E staining.

3.7.13.5 Tissue staining using Hematoxylin and Eosin (H&E)

H&E staining is a gold standard method for the identification of cellular patterns, shapes, and morphological features in tissues. In this way, it helps to detect pathological lesions occurring in tissues. Hematoxylin is a basic dye and it specifically stains the basophilic compartments of the cell including nucleic acid moieties. Whereas, eosin is an acidophilic dye that strongly binds with moieties such as RBCs, cytoplasm, muscles, collagen, *etc*. Hematoxylin imparts a bluish-purple color and eosin provides a pink color to cellular compartments. The present study employed H&E staining for the examination of any possible pathological lesions including tissue edema, cellular infiltration, morphological changes, vacuolization, *etc*. The major steps involved in the staining procedure are illustrated in Table 3.5. Slides were kept at 50°C in an oven before staining. After the staining, slides were air dried and mounted using DPX mountant and imaged under microscope.

Table 3.5 Steps in Hematoxylin & Eosin (H&E) staining for tissue sections.

Steps	Time
Xylene I	10min
Xylene II	10min
Absolute alcohol	5 min
70% alcohol	5 min
Distilled water	5 min
Harris Hematoxylin	20min
Distilled water	Rinse
Acid alcohol	1-2dip
Distilled water	Rinse
Scott's tap water	3 min
Distilled water	Rinse
1% Eosin	1.5min
Distilled water	1 dip
70% Alcohol	2 min
Absolute alcohol	1 min
Xylene I	10min
Xylene II	10min

3.8 STATISTICAL ANALYSIS

All the experiments for the study were performed as triplicates and the results were expressed as mean ± Standard Deviation (SD). Statistical comparison of control groups and test groups was done using Student's t-test. For all the data analyzed, $p < 0.05$ was considered as significantly significant.

CHAPTER 4: RESULTS

4. RESULTS

4.1 SYNTHESIS OF TITANIUM DIOXIDE (TiO_2) NANOTUBES USING SOLVOTHERMAL ROUTE AND PHYSICO-CHEMICAL CHARACTERIZATION

4.1.1 SYNTHESIS OF TNTs AND POLYMER COATING

TNT synthesis for the study was achieved through a chemical reaction that included two broad phases. Phase I comprises the synthesis of TNPs via the urea precipitation method and synthesized TNPs were converted into TNTs in Phase II via solvo thermal method. $TiCl_4$ was used as the precursor molecule for the synthesis of TNPs since it offers a simpler synthesis approach via a single-step hydrolysis reaction. The precipitation method involved only a limited number of chemicals and did not demand highly sophisticated equipments. TNPs formed in Phase I exhibited a pale white-colored powdery consistency after the calcination step at 400°C for 1h. The solubility level of TNPs was analyzed in water and different solvents and it was observed to be insoluble in most of the mediums checked. The formation of TNTs, which is the Phase II involved solvothermal reaction of TNPs in a highly alkaline atmosphere. Higher alkalinity induced the formation of sodium titanate nanosheets, which further rolled around themselves to form the final nanotubular morphology under a slightly acidic environment. TNTs obtained after calcination exhibited pure white colored powdery consistency. The solubility was checked after Phase II and there was no observable change in the solubility level obtained. Both TNPs and TNTs showed slightly higher dispersity after bath sonication at 37°C for 20-30min.

Phase III involved the surface coating of TNTs with P-F127. It was observed that the dispersion stability of coated form of TNTs was far exceeding that of bare TNTs. Moreover, the sonication step was not required for this form of TNTs and they showed white color and powdery consistency similar to that of TNPs and TNTs.

4.1.2 PHYSICO-CHEMICAL CHARACTERIZATION

The physico-chemical characteristics of TNPs and TNTs were evaluated using different techniques and are detailed in the sections below.

4.1.2.1 Dynamic Light Scattering (DLS)

The hydrodynamic diameter (Z average dm) of TNPs in different dispersion media including distilled water and PBS was studied. This further pointed out the influence of media on the colloidal stability of the material in terms of the Poly Dispersity Index (PDI). The variation in Z average dm and corresponding PDI for TNPs in different dispersion media is shown in Table 4.1.

Table 4.1. Influence of dispersion media in terms of Z average dm and PDI for TNPs

Dispersion medium	DLS plot	Hydrodynamic diameter (nm)	Poly Dispersity Index (PDI)
Distilled Water	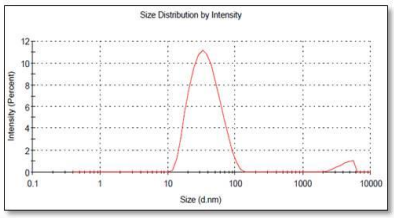	33.92 nm	0.241
Phosphate Buffered Saline (PBS)	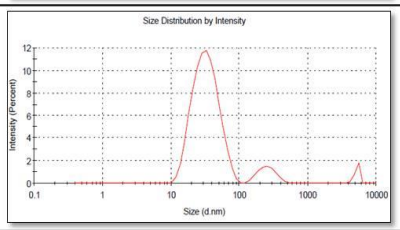	36.19 nm	0.352

4.1.2.2 Zeta potential Analysis

Surface charge or electrical potential difference between the outer and inner surface of TNPs was evaluated using zeta potential analysis. The material was observed to be positively charged with a magnitude of 12.9. The colloidal stability of the material was also confirmed in this way because the higher magnitude of ions around the surface confirmed the repulsive interaction of nearby particles and hence the homogeneity of TNPs (Figure 4.1).

4.1.2.3. Fourier Transform Infrared Spectroscopy (FT/IR)

Characteristic functional groups of the TNPs and TNPs were examined and compared using FT/IR spectroscopy. % transmittance corresponding to each material was detected over a range

of frequencies from 1000 to 4000 cm^{-1}. Major characteristic IR peaks obtained for TNPs were at the positions; 3415.6 cm-1, 1634.9 cm-1, and 587.4 cm^{-1}. These peaks correspond to the stretching and bending vibrations of hydroxyl bonds (O-H) and the stretching vibration of the Ti-O covalent bond respectively. Any other undesirable peaks indicating contamination were not observed, hence confirming the high purity of the material. To confirm chemical stability after phase transformation, FT/IR spectrum was achieved for TNTs also. Characteristic peaks obtained for TNTs were at the positions; 3429 cm^{-1}, 1631.9 cm^{-1}, and 481.9 cm^{-1} and all of the peaks were comparable to that of TNPs. Here also, observed peaks correspond to the stretching and bending vibration of O-H bonds and stretching vibration of Ti-O bonds respectively. No peaks for impurities were noted (Figure 4.2).

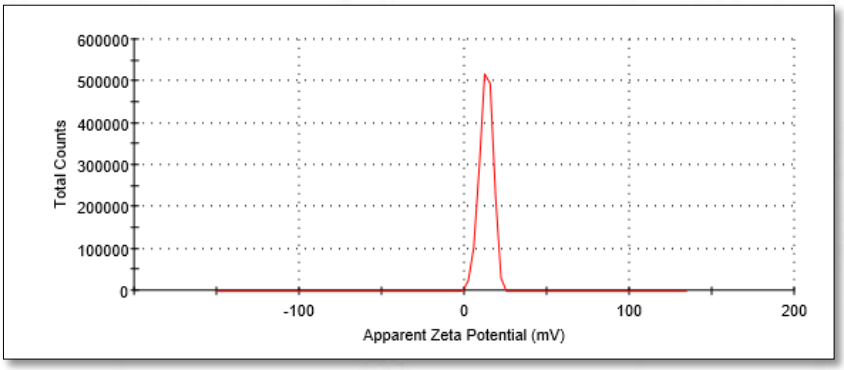

Figure 4.1 Zeta potential measurements of TNPs.

4.1.2.4 X-Ray Diffraction (XRD)

The crystalline structure and phasic nature of TNPs were studied using XRD (Figure 4.3). Definite diffraction peaks were obtained in accordance with each change in phasic information and were represented as diffraction angles (2θ). The crystal size of the material was calculated using the Debye-Scherer formula. The spacing between the lattice planes of atoms or ions was also noted (hkl indices). 2θ values of each peak and their corresponding hkl indices are shown in Table 4.2. From the calculated d-spacing information, the major population of the obtained peaks was identified to be anatase (for the 2θ values: 101, 103, 004, 200, 210, 204, and 215) and a minor population was also found which correspond to rutile phase (for the 2θ values: 110, 111 and 211). The nanosized distribution of the material was confirmed by the narrowing of the

diffraction peaks. The experimental XRD pattern of TNPs was comparable with the JCPDS card numbers 21-1272 and 21- 1276 for anatase and rutile phases respectively.

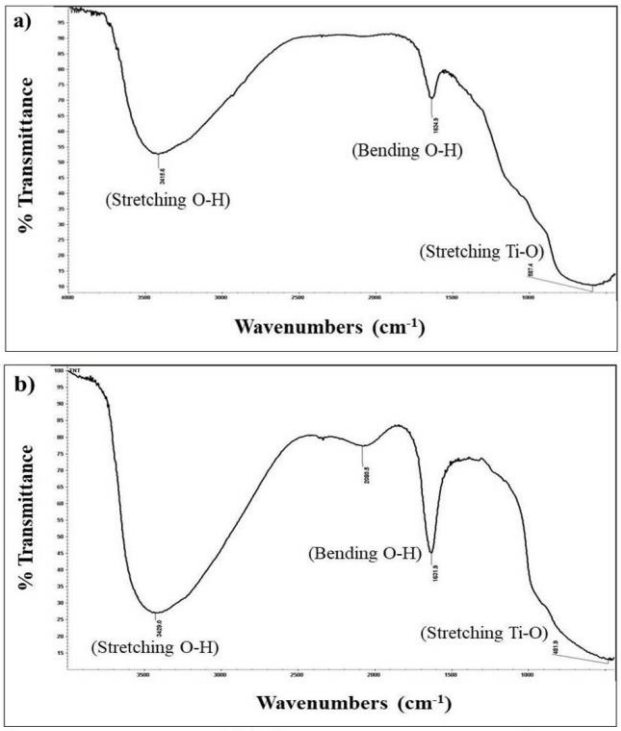

Figure 4.2. FT/IR spectroscopy: (a) TNPs and (b) TNTs

Table 4.2 Diffraction angles (2θ values) of each XRD peak and corresponding hkl indices.

Peak No.	2θ Value	h k l Value
1	25.26	1 0 1
2	27.38	1 1 0
3	36.00	1 0 3
4	37.67	0 0 4
5	41.18	1 1 1
6	47.98	2 0 0
7	55.01	2 1 1
8	62.04	2 1 0
9	68.66	2 0 4
10	74.82	2 1 5

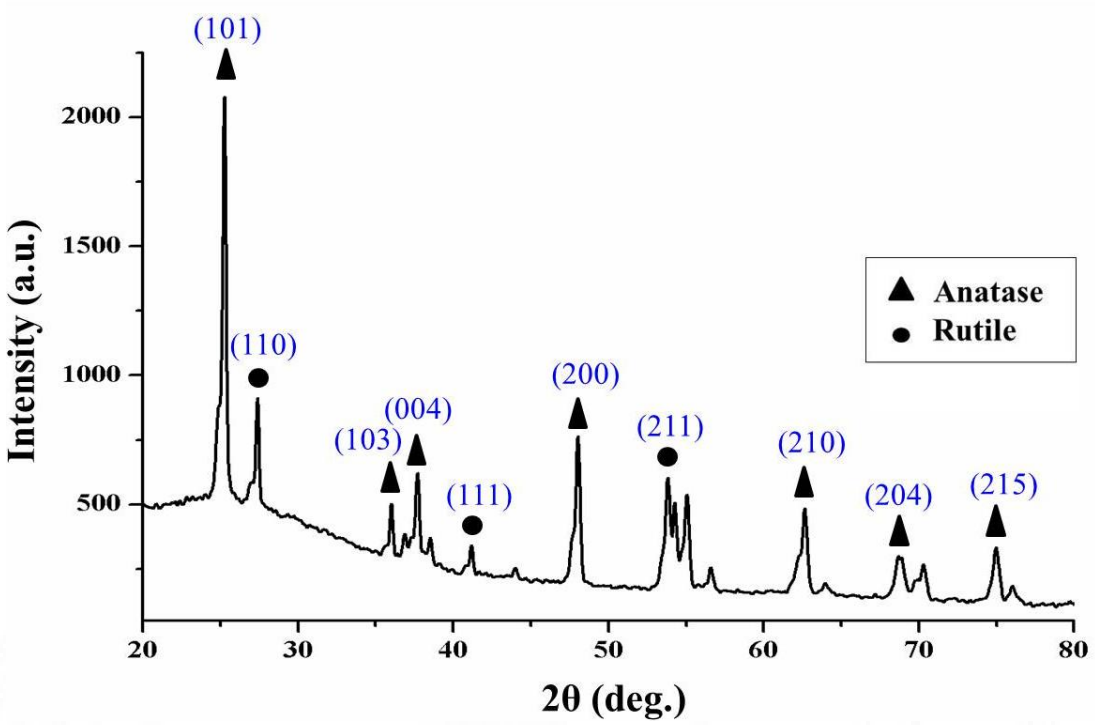

Figure 4.3 X-Ray diffraction pattern of TNPs. Peaks were compared with JCPDS database (Card No. 21-1272: Anatase and 21- 1276: Rutile).

4.1.2.5 Micro Raman Spectroscopy

The molecular distribution of TNPs and TNTs was examined using micro Raman spectroscopy in which Rayleigh scattering changes occurring with the incident light beam were recorded. Figure 4.4 represents the micro Raman spectroscopy spectra of TNPs and TNTs obtained. The first and major peak identified for TNPs was at the Raman shift position 146cm-1 and the following peaks were obtained at the positions, 194, 394, 514, 636, and 791cm^{-1}. Variations in peak positions and associated parameters were noted and compared. Table 4.3 illustrates Raman spectroscopic parameters of TNPs including; peak number, peak position, the intensity of light in pixels, the height of peaks, FWHM (full width and half maximum) as a reflection of structural distribution, and the identified symmetry. The parameters confirmed major population of the peaks obtained corresponds to the anatase phase. A similar observation was noted for the spectra of TNTs also, for which shift positions were observed at positions: 150, 246, 401, 512, and 631cm^{-1}. Raman spectroscopic parameters of TNTs are mentioned in Table

4.3. Phase transition of TNPs to TNTs was confirmed from the broadening of the peaks at identical Raman shift positions.

Table 4.3 Raman spectroscopic parameters for TNPs and TNTs.

Sample	Peak no.	Peak position (cm^{-1})	Intensity (Pixel)	Height (CCD cts)	FWHM (cm^{-1})	Symmetry
TNPs	1	146.169	48.628	70547.1	23.7661	1.00479
	2	194.313	59.212	1079.04	17.2542	0.121261
	3	394.004	103.724	9415.56	33.1661	1.12746
	4	513.617	130.868	7715.89	32.0521	1.00996
	5	636.138	159.056	16580	30.4961	0.973221
	6	791.5	195.375	323.176	43.4453	0.510411
TNTs	1	150.197	50.2105	1003.86	27.2206	0.98623
	2	246.344	71.4131	110.631	39.9544	1.1654
	3	401.136	106.03	272.502	38.3416	0.7532
	4	512.201	131.242	218.383	35.4131	0.744909
	5	631.075	158.582	466.056	66.8928	1.44695

4.1.2.6. Transmission Electron Microscopy (TEM)

The surface topography of the NMs before and after phase transformation was evaluated using TEM. TEM images obtained for TNPs exhibited a roughly spherical morphology and smooth surface with an average diameter of 22nm. Nano tubular morphology with an average length of 145nm and an average diameter of 24.6nm was obtained for TNTs. Both of the NMs showed a homogenous distribution under electron microscopic observation and the images obtained are shown in Figure 4.5.

4.1.2.7. Thermo Gravimetric Analysis (TGA)

Gradual weight loss of the materials in terms of thermal degradation was assessed using TGA analysis. Figure 4.6 represents the TGA curves of TNPs and TNTs over a temperature range of 0-700°C at a heating rate of 10°C/min under a nitrogen atmosphere. ~10% weight reduction was observed for TNPs during the initiation of the process at 83.22°C and can be attributed to the desorption of surface-bound water molecules. The second major weight loss (12.35%) was observed at 245.4°C. Final weight reduction was achieved at 583.21°C; wherein 82.41% of TNPs were retained. The plot attained a plateau level after this point. For TNTs, slightly different mass degradation was observed. The first weight loss point was marked at 128.85°C (5.28% loss) followed by 6.95% loss at 417.38°C. Final degradation was observed at 685.46°C (retained 92.66% of TNTs). Similar to TNPs, the plot reached a plateau value at this stage.

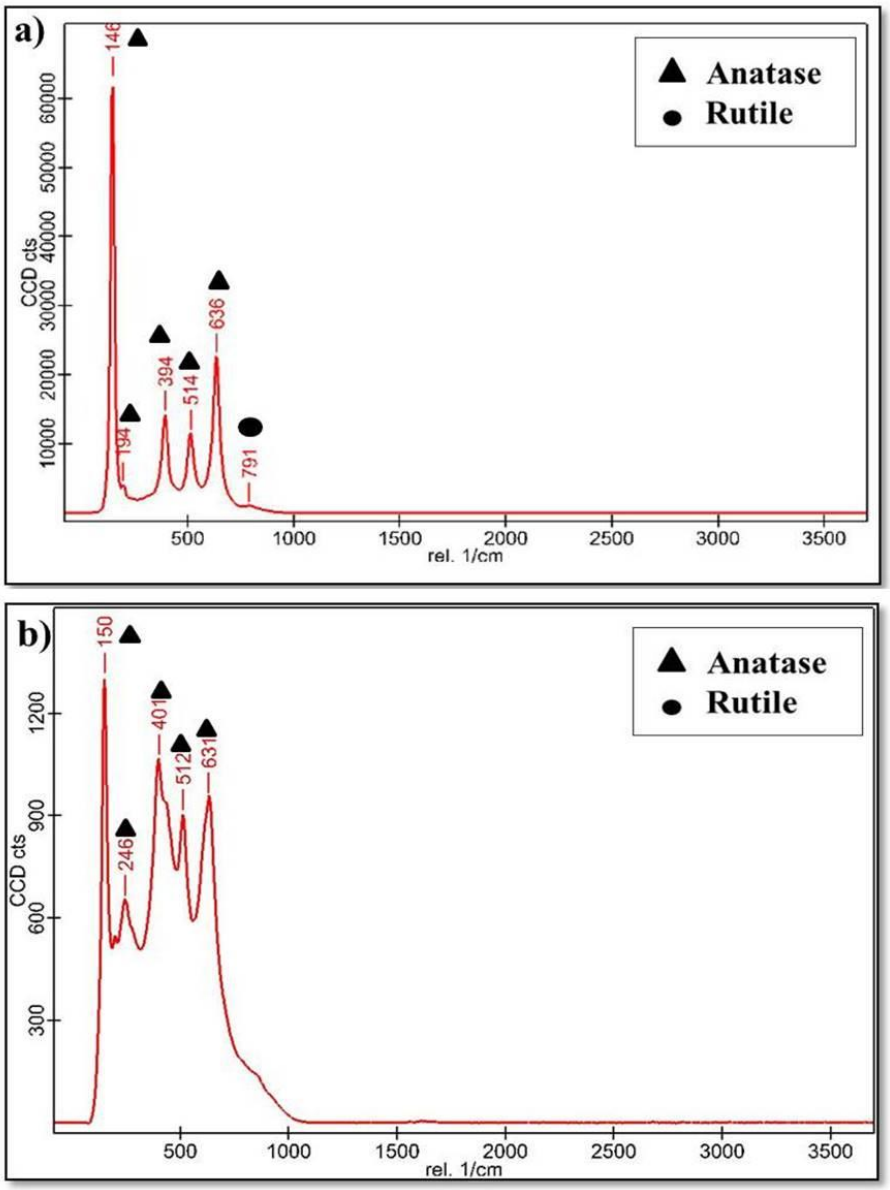

Figure 4.4 Micro Raman spectra of: a) TNPs and b) TNTs

4.1.2.8 Differential Thermal Analysis (DTA)

Temperature-assisted surface chemical reactions and phase transition were evaluated using DTA analysis. Figure 4.7 shows the DTA curve obtained for TNPs and TNTs. The first major peak for both TNPs and TNTs was obtained around 24°C, which

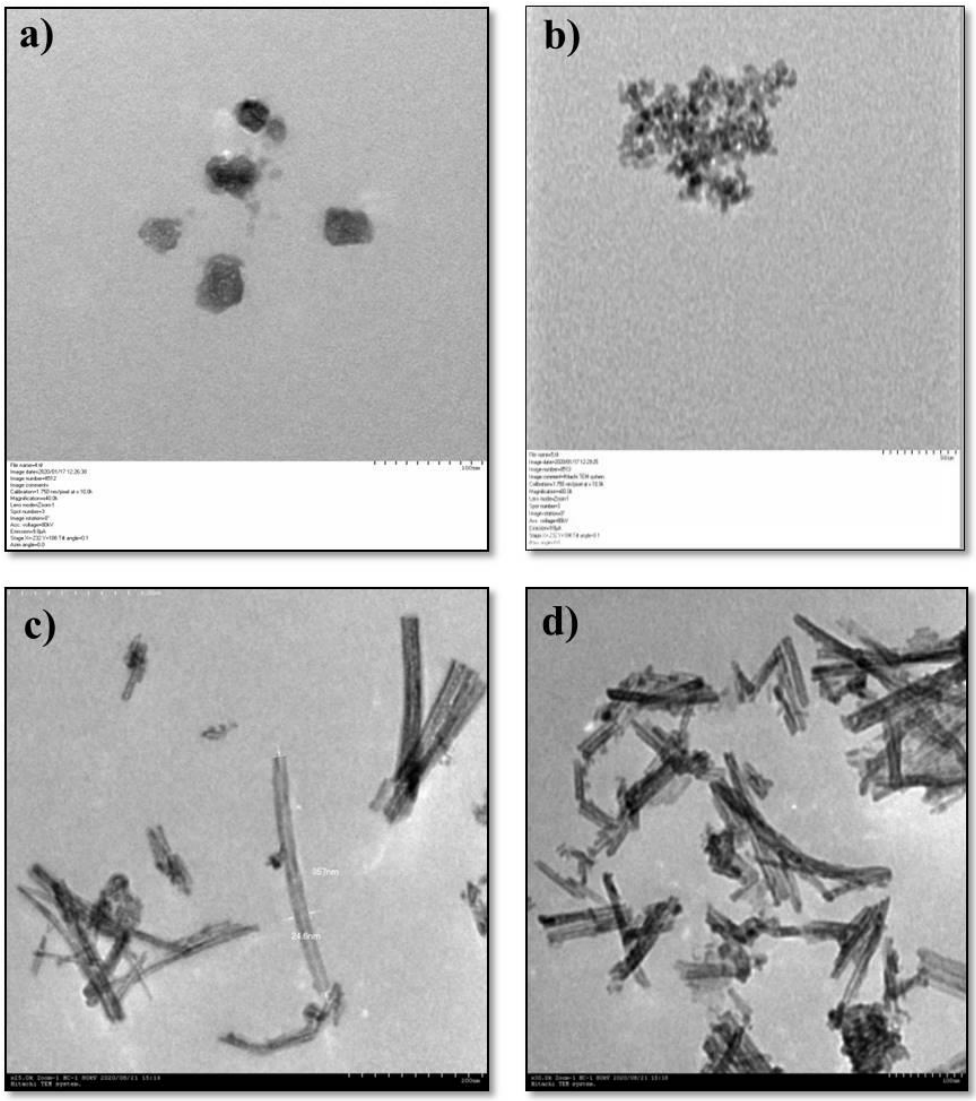

Figure 4.5 TEM images ofTNPs at different magnifications: a) 60,000X and b) 50,000X and that of TNTs at c) 60,000X and d) 50, 000X respectively. Scale bar: a) & d) 100nm, b) 50 nm and c) 200nm. Voltage: 80kV.

can be attributed to well defined endothermic peak for the desorption of water. The second endothermic peak was found for TNPs at 174.9°C which corresponds to decomposition or organic species or dehydroxylation processes. Second peak obtained for TNTs was at the position 67.61°C and it was found to be exothermic. This also corresponds to the removal of organic moieties. After this stage of organic decomposition, TNPs exhibited a defined exothermic peak at around 400°C which corresponds to phase transformation.

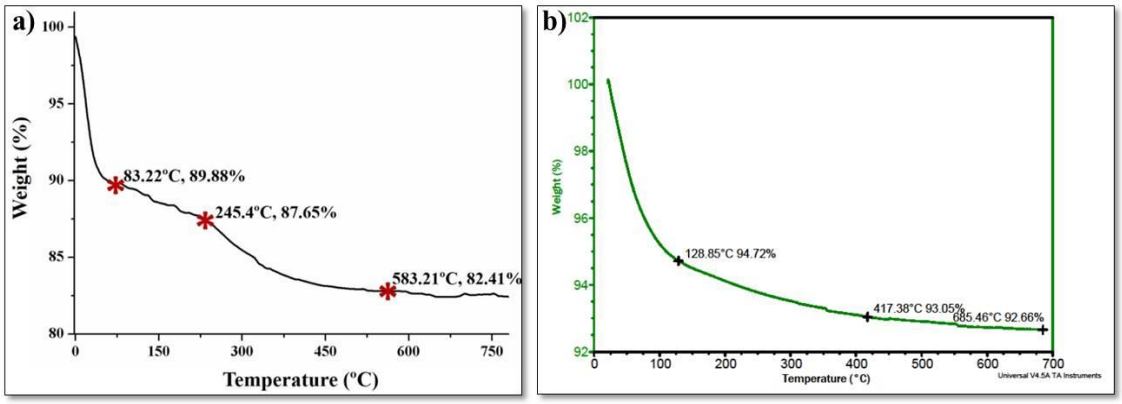

Figure 4.6 TGA analysis plots for, (a) TNPs and (b) TNTs.

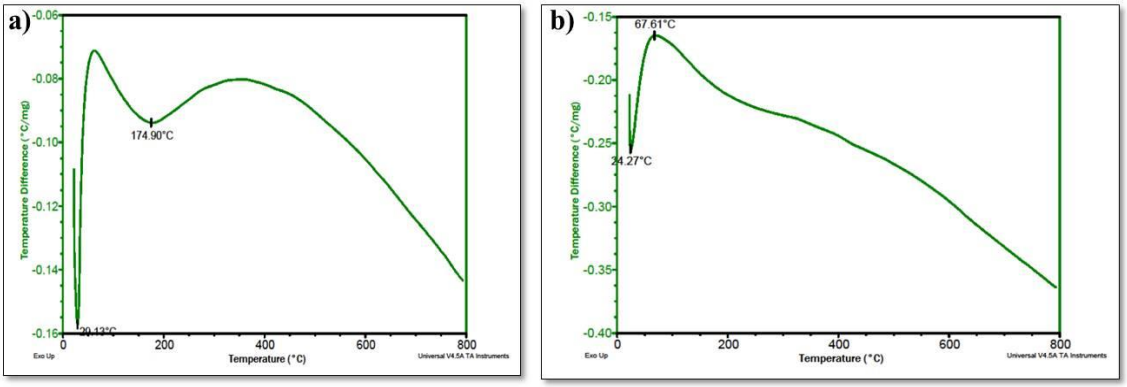

Figure 4.7 DTA analysis plots for, (a) TNPs and (b) TNTs.

4.1.2.9 FT/IR Spectroscopy for surface coating

Polymer coating of TNTs using P-F127 was characterized using FT/IR spectroscopy (Figure 4.8). Three individual spectra were recorded for bare TNTs, P-F127 and TNT-P.Characteristic peak of Ti-O bond was obtained for bare TNTs at around 435cm^{-1}. For P-F127, major peaks obtained were: 2883.58cm-1, 1342.46cm-1, 1060.85cm-1, 960.48cm-1 and 840.96cm-1. These correspond to stretching C-H bond, hydroxyl or O-H bending and bending vibrations of carbonyl or C=O and C-H respectively. The third and coated form of TNTs (TNT-P) possessed major characteristic peaks corresponding to both TNTs and P-F127. Major Ti-O bond was evident around 450cm^{-1}. Other peaks obtained for TNT-P were comparable to that of P-F127 at the positions 2883.58cm^{-1}, 1641cm^{-1}, 1342.46 cm^{-1}, 1060.85 cm$^{-1,}$ and 840.86cm^{-1}. P-F127 and TNT-P using frequency range between 400-4000cm^{-1}.

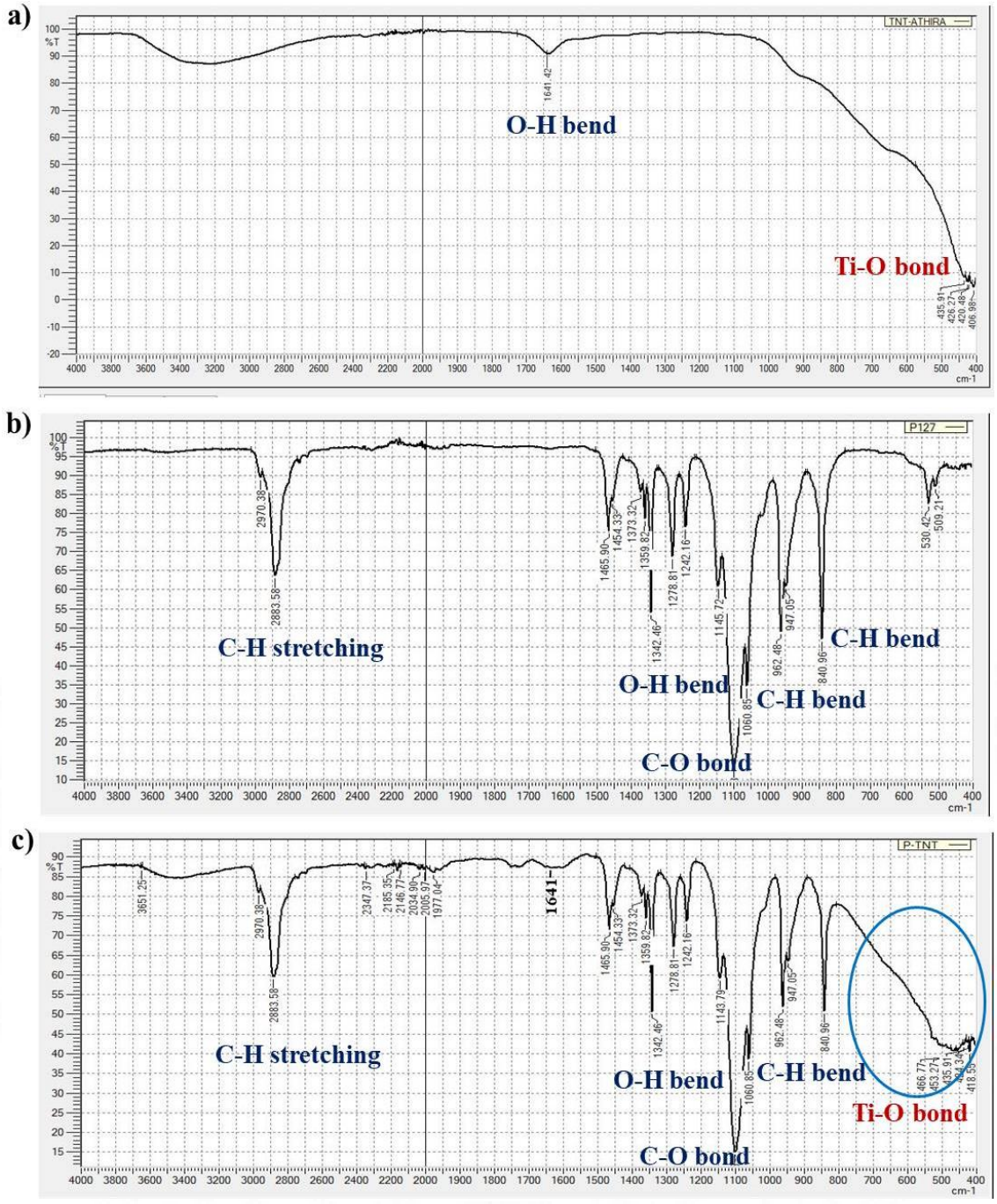

Figure 4.8. FT/IR spectroscopy for surface coating of TNTs: a) TNTs, b) P-F127 and c) TNT-P.

4.2 EVALUATION OF *IN VITRO* TOXICITY OF TiO_2 NANOTUBES USING C6 CELL LINE

4.2.1 C6 GLIAL CELL CULTURE AND NANOMATERIAL EXPOSURE

C6 glial cells were cultured in DMEM F12 medium under incubation conditions as mentioned in Chapter 3, Section 3.6.1. The cell exhibited characteristic spindle-shaped morphology with a pleomorphic pattern of organization and variably shaped nuclei. Cells showed completely developed neuronal distribution even at lower cell densities. The monolayer of readily proliferated cells was developed with well-defined neurites extending from both sides of the cell body. Nearby cells were observed to be forming networks using these early neurites. In completely matured forms, these neurites are provided with cell receptors for receiving growth-stimulating factors for developing into axons. More than 80% cell confluence was reached within 24h of incubation.

4.2.2. PHENOTYPIC OBSERVATION BY PHASE CONTRAST MICROSCOPY

Cultured C6 glial cells were observed under a phase contrast microscope for the examination of cellular phenotype after 24h of incubation. Characteristic spindle-shaped morphology was clearly visible with the outgrown neuritic network in a highly polarized manner. Images showing observed peculiar glial cell morphology under lower (10X) and higher (20X) magnifications are shown in Figure 4.9.

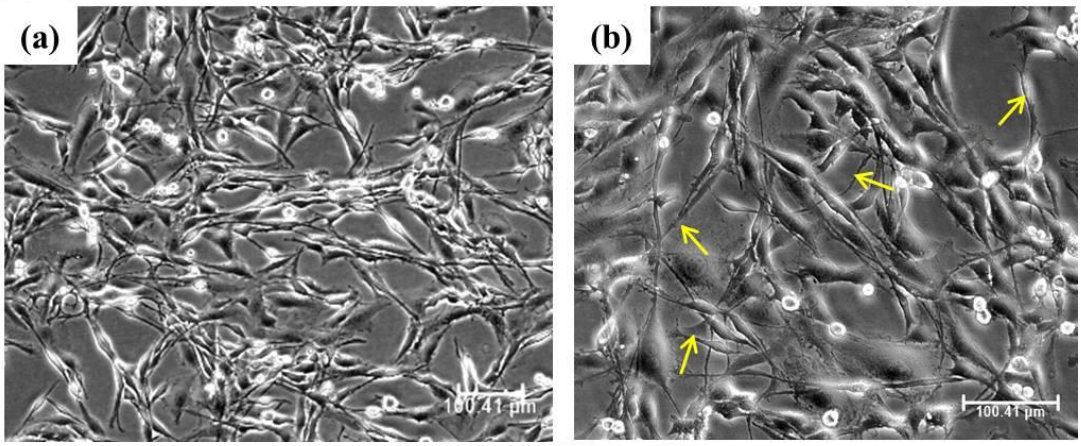

Figure 4.9 Phase contrast images of cultured C6 glial cells under, (a) 10X and (b) 20X magnifications. Early developed glial cell neurites are indicated by yellow arrows. Scale bar: 100.41µm.

4.2.3 CELLULAR UPTAKE STUDY USING IMAGING FLOW CYTOMETRY

Cellular uptake of TNPs was evaluated using Imaging flow cytometry, based on the change in cellular granularity. SSC was considered as the measure of granularity, whereas FSC was considered as the parameter for cell size. Cellular debris and doublet cells were gated out during analysis. At least 10,000 events per single cell in each sample were analyzed to get reliable data. The gating procedure was initiated by focusing single cells coming through the flow and identified using the gradient root mean square of the bright field image, bright field area, and the aspect ratio respectively. An increase in SSC pattern was noted during cellular flow inside the system in a concentration-dependent manner. This confirms the cellular uptake of TNPs (Figure 4.10).

4.2.4 CELL VIABILITY STUDY BY MTT ASSAY

TNPs and TNTs were evaluated for their capability to induce cytotoxicity in C6 cells using MTT assay. Figure 4.11 shows the results of MTT assay after 24h exposure of the materials with C6 cells. The mitochondrial activity or cell viability was not affected from 5µg/ml to 80µg/ml for both TNPs and TNTs. However, a significant decline in viability reduction or mitochondrial activity was observed for both the materials at 160µg/ml compared to negative control for 24h exposure. For TNPs and TNTs, the % viability at 160µg/ml was found to be 77.52±0.19 and 81.34±0.31 respectively.

4.2.5 MITOCHONDRIAL MEMBRANE POTENTIAL (MMP) ANALYSIS BY JC1 STAINING

JC1 staining was performed for assessing the MMP of TNP and TNT-exposed cells. JC1 generated J-aggregates where there was proper MMP existed or the dye exhibited bright red fluorescence when bound with active mitochondria. A clear shift in emission spectra was obtained when there was a drop in MMP and the dye showed green fluorescence. Figure 4.12 shows the fluorescence image of JC1 staining for both TNP and TNT-treated cells. For both cases, MMP was found to be retained for the lowest (5µg/ml) and middle concentrations (40µg/ml). Active mitochondria showed a red fluorescence compared to control cells up to

40µg/ml. For both TNPs and TNTs, a reduction in MMP was noted for the highest tested concentration (160µg/ml) and red fluorescence was reduced.

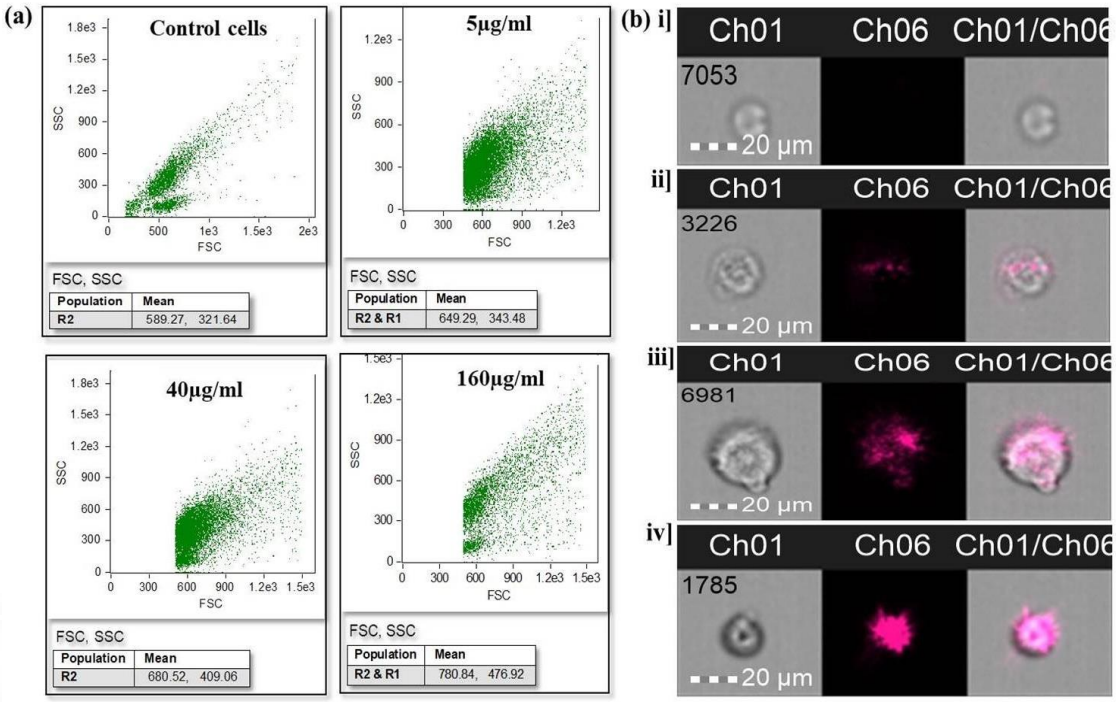

Figure 4.10 Imaging flow cytometry for identification of cellular uptake of TNPs into C6 cells upon 24h exposure. (a) Increasing SSC pattern of cells under treatment with different concentrations of TNPs, (b) representative images of cells detected in various channels of the system: i] Control cells, ii] 5µg/ml, iii] 40µg/ml and iv] 160µg/ml. Ch01- Channel 1 (Bright field), Ch01/Ch06- merged image for Ch01 and Ch06. Analysis was done using Amnis FlowSight®, Scale bar: 20µm.

4.2.6 LYSOSOMAL INTEGRITY STUDY USING NRU ASSAY

Figure 4.13 shows the cell viability or lysosomal integrity of TNP and TNT exposed cells analyzed using NRU assay. C6 cells were exposed to various concentrations of both of the materials for 24h. For TNP exposed cells, the viability was not affected until 80µg/ml, and a non-significant reduction in viability was observed for 160µg/ml compared to negative control. Whereas, TNT exposure resulted in a decline in lysosomal integrity from 40µg/ml to 160µg/ml in a non-significant manner.

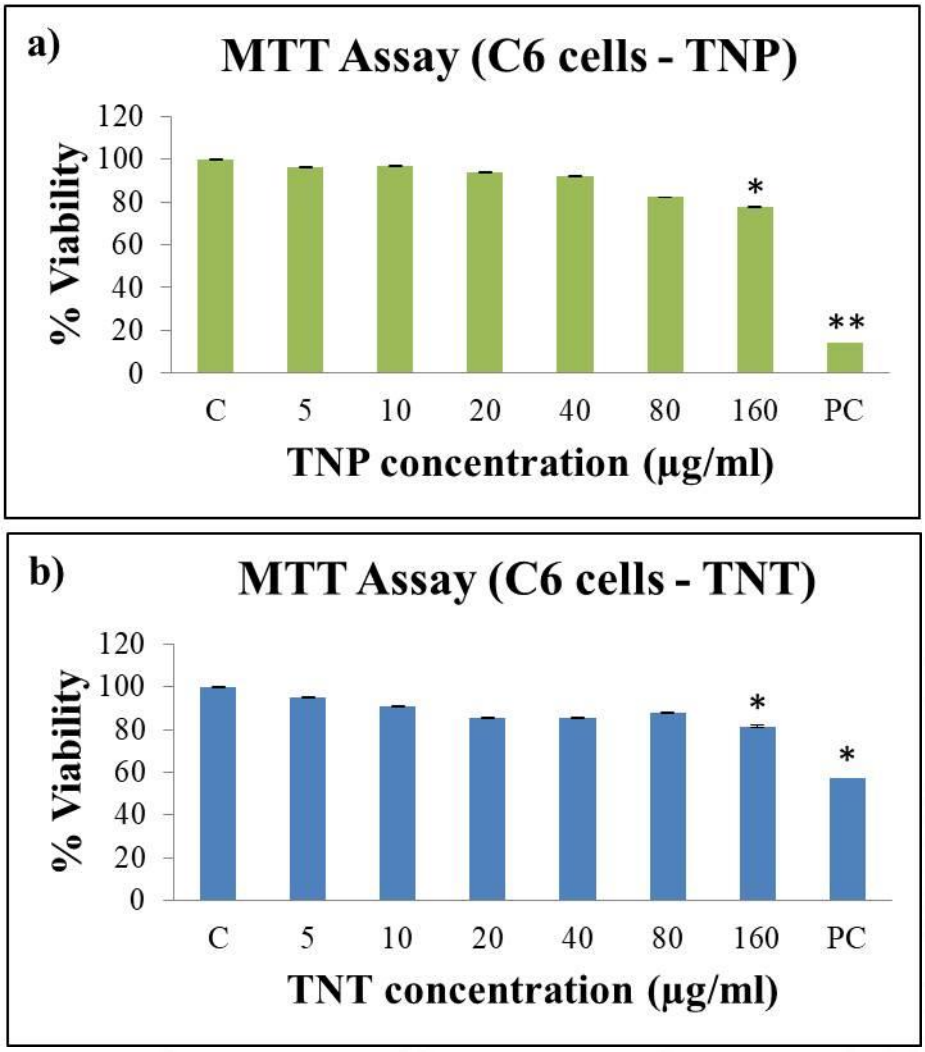

Figure 4.11 MTT Assay of C6 cells after 24h exposure with, a) TNPs and b) TNTs. % viability values obtained for each concentration of nanomaterials were compared with control values. C- Negative control, Positive control (PC): Phenol. The data represent mean ± SD of three independent experiments (N=3).Asterisks denote statistically significant deviation from negative control (* $p<0.05$, ** $p< 0.01$ and *** $p<0.001$).

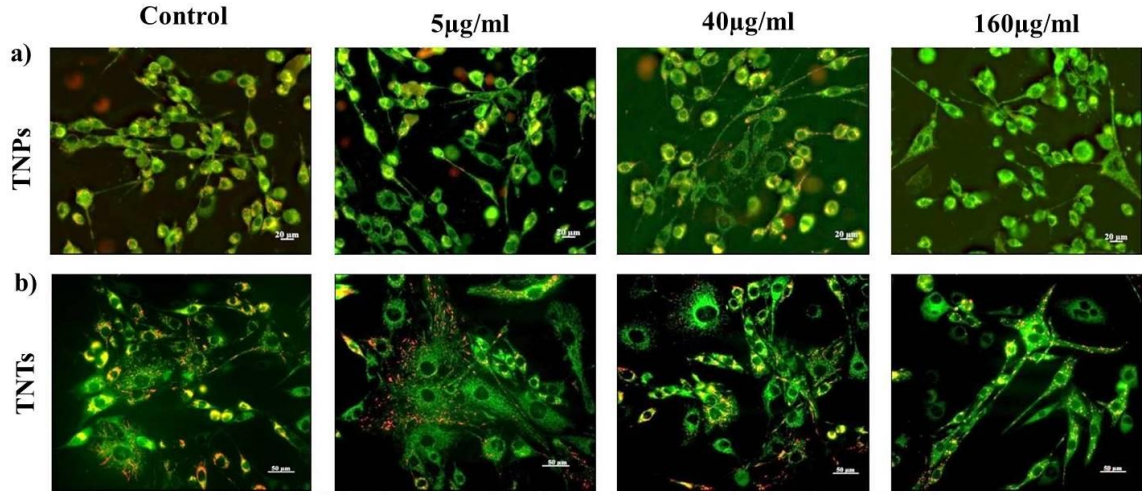

Figure 4.12 Mitochondrial membrane potential (MMP) analysis using JC1 staining for C6 cells treated with, a) TNPs and b) TNTs for 24h. Reddish orange fluorescence denotes JC1 aggregates in active mitochondria. Shift in spectrum to green fluorescence denotes JC1 monomer in cytoplasm & loss of membrane potential.Magnification: (a) & (b) 20X, Scale bar: (a) 20µm & (b) 50µm.

4.2.7 ACRIDINE ORANGE (AO) STAINING

Lysosomal integrity of TNP and TNT-exposed cells was confirmed using AO staining. Fluorescent microscopic observation was used to evaluate the NM-induced lysosomal membrane destabilization. The qualitative study was performed after 24h exposure of the cells to TNPs and TNTs. Both of the materials were compared for their toxic outcomes in the lysosomal compartment using three different concentrations as representatives of the lowest, middle, and highest concentrations (5, 40, and 160µg/ml). The study indicated that none of the materials is inducing a discernable alteration in lysosomal integrity at any of the tested concentrations used. In both control and treated cells, AO was observed to be internalized to the cells and imparted a reddish fluorescence to the active lysosomes. A noticeable loss of red fluorescence was not obtained until the highest concentration of both of the materials (Figure 4.14). This result suggests that TNPs and TNTs do not significantly affect the lysosomal stability of exposed cells.

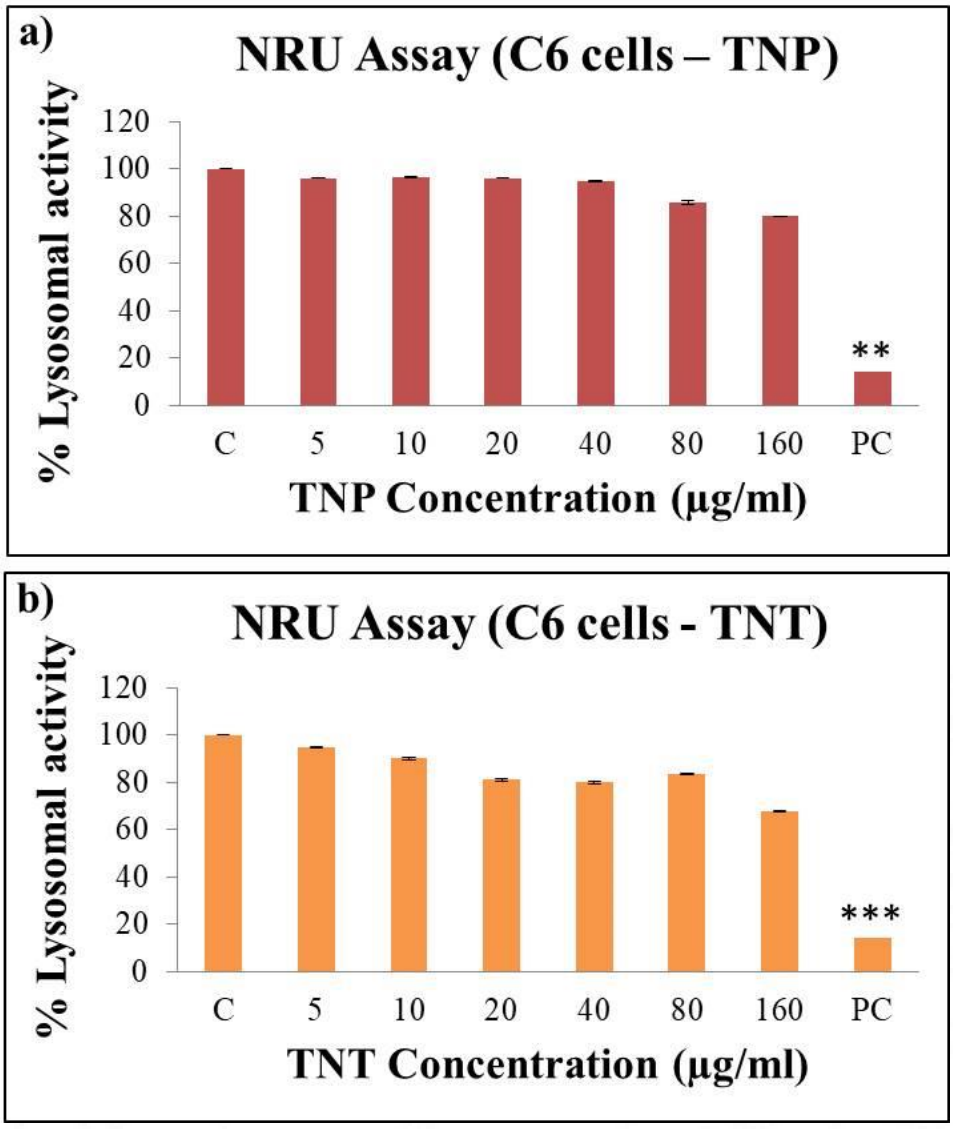

Figure 4.13 Cell viability or lysosomal integrity study by Neutral red uptake assay for cells exposed with, a) TNPs and b) TNTs. Red color intensity corresponding to the level of neutral red uptake by healthy lysosomes was quantified and compared with that of control cells. C-Negative control, Positive control (PC): Phenol. The data represent mean ± SD of three independent experiments (N=3). Asterisks denote statistically significant deviation from negative control (* $p<0.05$, ** $p< 0.01$ and *** $p<0.001$).

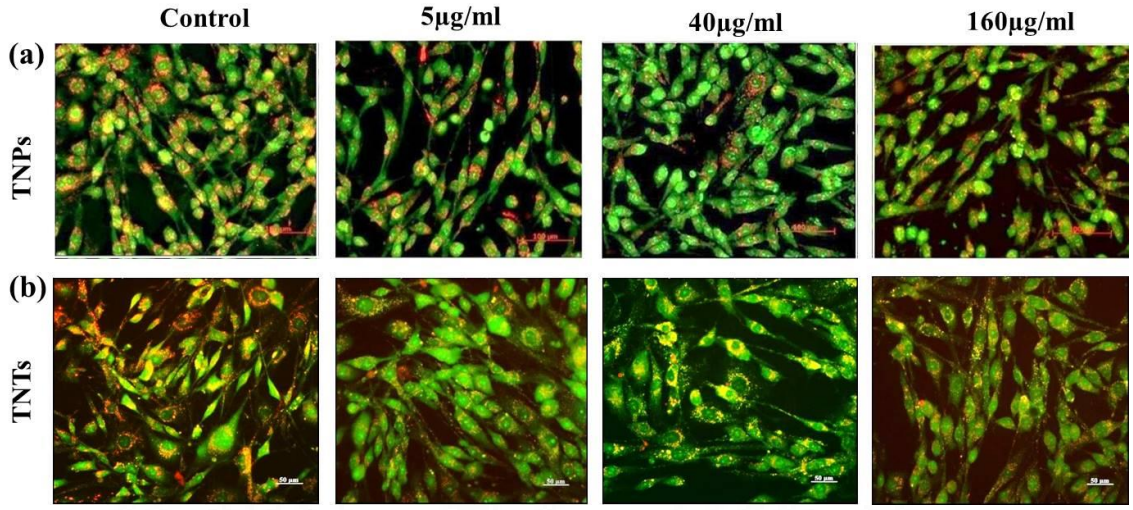

Figure 4.14 Lysosomal integrity study using AO stainingfor cellular exposure with, a) TNPs and b) TNTs for 24h.Reddish orange fluorescence denotes active lysosomes and shift in absorption spectrum to green fluorescence denotes loss of lysosomal integrity. Magnification: (a) & (b) 20X, Scale bar: (a) 100µm & (b) 50µm.

4.2.8 EVALUATION OF CELLULAR MORPHOLOGY

4.2.8.1 Coomassie Brilliant Blue (CBB) Staining

Basic morphological changes in cells after TNP exposure for 24h were assessed using CBB staining. The cells did not show noticeable deviation in morphology and were comparable with that of control cells up to 40µg/ml. However, 160µg/ml of TNPs induced slight cytoplasmic shrinkage, which affected the normal spindle, shaped morphology of glial cells (Figure 4. 15).

4.2.8.2 Giemsa Staining

Morphological alterations associated with cellular exposure of TNTs were analyzed using Giemsa staining. In contrast to TNP exposure, TNTs did not induce any discernable alterations to cellular morphology compared to control cells. 160µg/ml exhibited no visible signs of cytoplasmic shrinkage, except a slight reduction in cell number. Figure 4.16 shows Giemsa staining of C6 cells after TNT exposure.

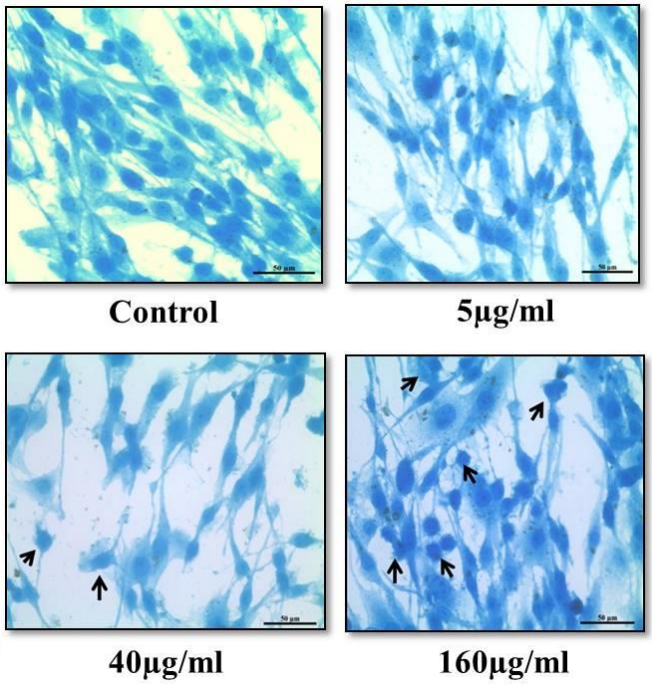

Figure 4.15 Morphological evaluation of C6 cells using non-fluorescent CBB staining method for 24h cellular exposure with TNPs. Black arrows in 160µg/ml indicate cytoplasmic shrinkage in cells. Magnification: 20X, Scale bar: 50µm

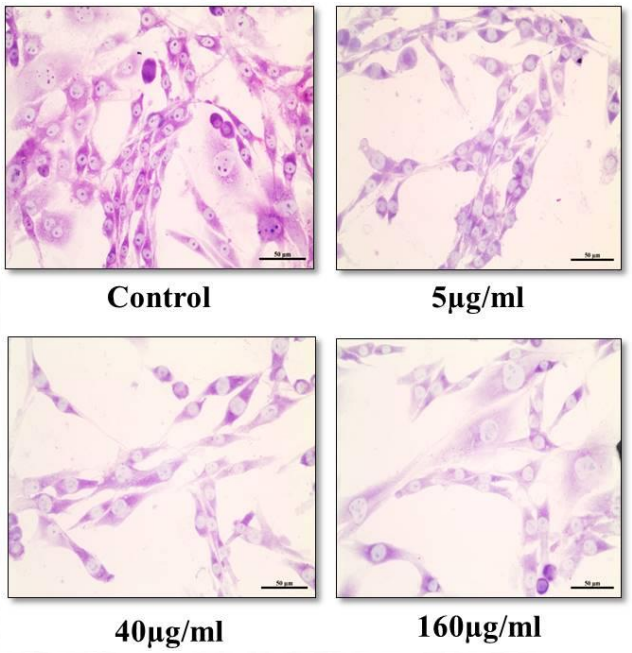

Figure 4.16 Giemsa staining of C6 cells after TNT exposure for 24h. Cells were observed to be retaining normal spindle shaped morphology up to 160µg/ml. No signs of cytoplasmic changes were noted. Magnification: 20X, Scale bar: 50µm.

4.2.9 ACTIN FILAMENT STAINING USING RHODAMINE PHALLOIDIN

Actin filament organization after 24h cellular exposure of TNPs and TNTs was studied using Rhodamine phalloidin staining. The cytoskeleton or actin filaments exhibited red fluorescence and nuclei were found to be blue stained using the counter stain, DAPI. Extended neurites from lateral ends of cells were clearly visible in red color and the nuclei were round to oval in shape. Comparable to CBB staining, TNP exposure resulted in mild cytoplasmic shrinkage at 160µg/ml concentration without affecting cytoskeletal integrity at lower concentrations. Similarly, TNT exposure caused only a negligible level of actin filament disorganization at the highest tested concentration of 160µg/ml (Figure 4.17).

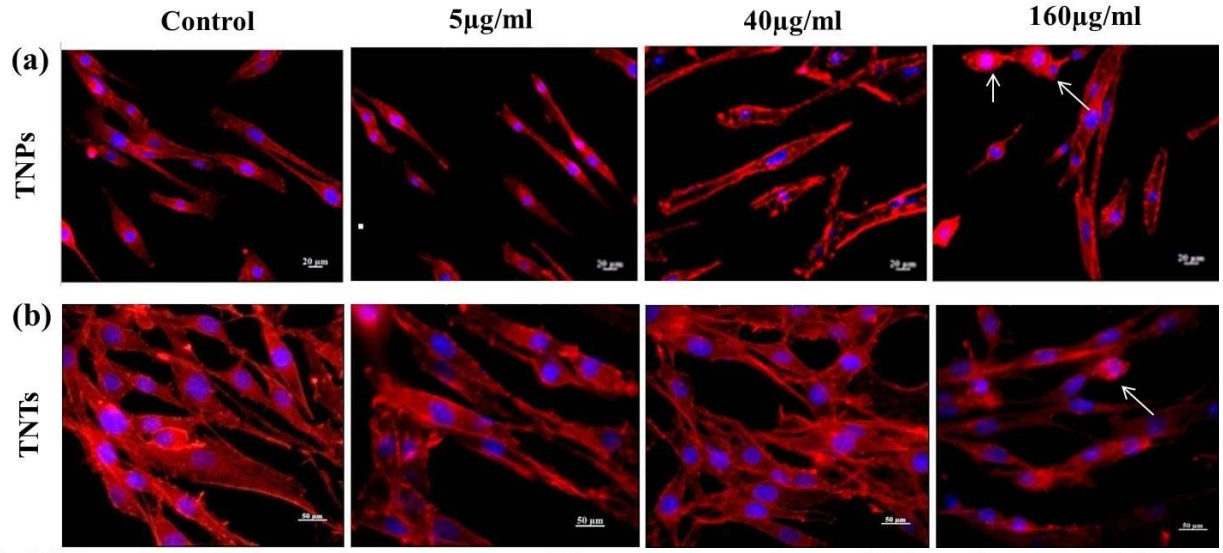

Figure 4.17 Actin filament organization study using Rhodamine phalloidin staining. (a) C6 cells were exposed to different concentrations of TNPs for 24h. White arrows represent cytoplasmic shrinkagein cells. Magnification: 20X, Scale bar: 20µm. (b) Cells exposed with different concentrations of TNTs for 24h. Magnification: 20X, Scale bar: 50µm. Counterstain used: DAPI (5µg/ml).

4.2.10 INVESTIGATION OF INTRACELLULAR OXIDATIVE STRESS

4.2.10.1 Detection of ROS by DCFH-DA Assay

Induced intracellular oxidative stress after TNP and TNT exposure was evaluated by quantifying the level of ROS inside cells by DCFH-DA assay. The values obtained were expressed in the Relative Fluorescence Unit (RFU). A significant amount of ROS was detected

in TNP-treated cells at 80µg/ml (29155.4 ± 1613.4) and 160µg/ml (28147.6 ± 758.85) after 24h of exposure. Rest of the lower concentrations did not produce significant ROS in cells (5µg/ml: 22555 ± 1685.6, 10µg/ml: 27210.6 ± 4976.9, 20µg/ml: 28560 ± 4151.1). For TNT exposure, cells generated significant ROS at 160µg/ml alone compared to control cells (39398.33 ± 3097.86). None of the other lower concentrations of TNTs were found to be producing a significant amount of ROS after 24h exposure (5µg/ml: 34732.67 ± 4044.538, 10µg/ml: 36756 ± 3189.796, 20µg/ml: 37261 ± 434.3835, 40µg/ml: 37174.67 ± 2766.794, 80µg/ml: 36592.67 ± 2440.476). The results of DCFH-DA assay are shown in Figure 4.18.

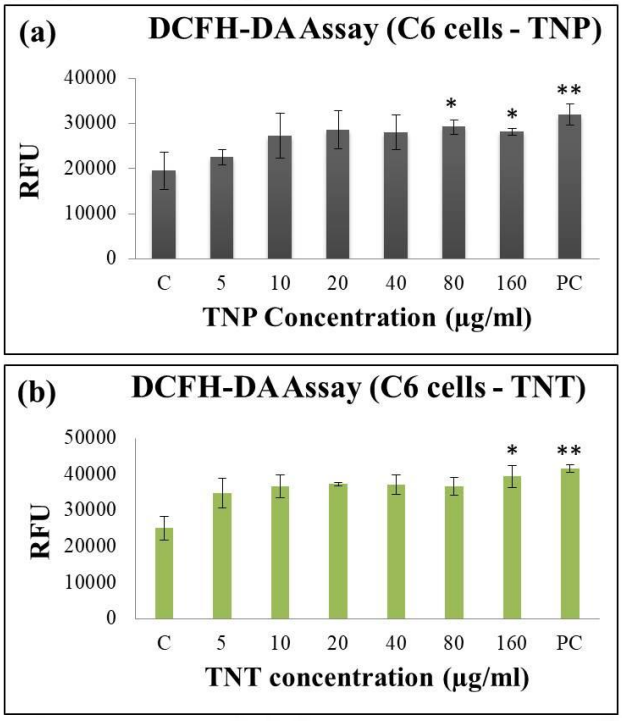

Figure 4.18 DCFH-DA assay for ROS detection after 24h cellular exposure with, **(a)** TNPs and **(b)** TNTs. Results are expressed in Relative Fluorescence Unit (RFU). C- Negative control, Positive control (PC): 0.09% H_2O_2. The data represent mean ± SD of three independent experiments (N=3). Asterisks denote statistically significant deviation from negative control (* $p<0.05$, ** $p< 0.01$ and *** $p<0.001$).

4.2.10.2 Detection of RNS by Griess reagent Assay

Generation of nitrogen species is considered as one of the hallmarks of nanomaterial associated toxicity in cells. TNP and TNT induced RNS production in C6 cells was evaluated using Griess

reagent assay. For both of the materials, there was no statistically significant generation of ROS and RNS occurred up to the highest tested concentration of 160µg/ml. Only the positive control for both the systems produced significant levels of RNS (For TNPs: 0.156667 ± 0.038 & for TNTs: 0.291 ± 0.05). Figure 4.19 displays results of Griess reagent assay for RNS production.

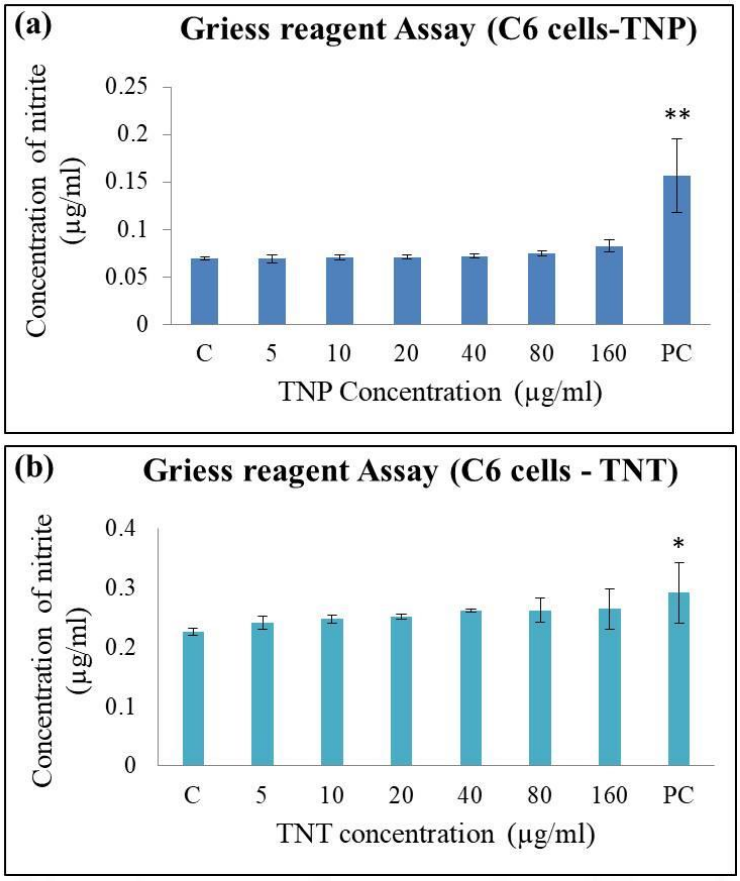

Figure 4.19 Griess reagent assay for the detection of intracellular reactive nitrogen species (RNS) after exposure with, **(a)** TNPs and **(b)** TNTs. C- Negative control, Positive control (PC): 0.09% H_2O_2. The data represent mean ± SD of three independent experiments (N=3). Asterisks denote statistically significant deviation from negative control (* $p<0.05$, **$p< 0.01$ and ***$p<0.001$).

4.2.11 CELL MEMBRANE INTEGRITY BY LDH RELEASE ASSAY

Cell membrane damage associated with TNP and TNT exposure for 24h was evaluated using LDH release assay. The cytosolic release of LDH upon membrane damage was quantified using a commercial LDH detection kit. For both TNP and TNT exposure, there were no statistically significant levels of LDH release were obtained compared to control cells even at

the highest tested concentrations of 160µg/ml. Figure 4.20 shows the plots obtained for the LDH release study.

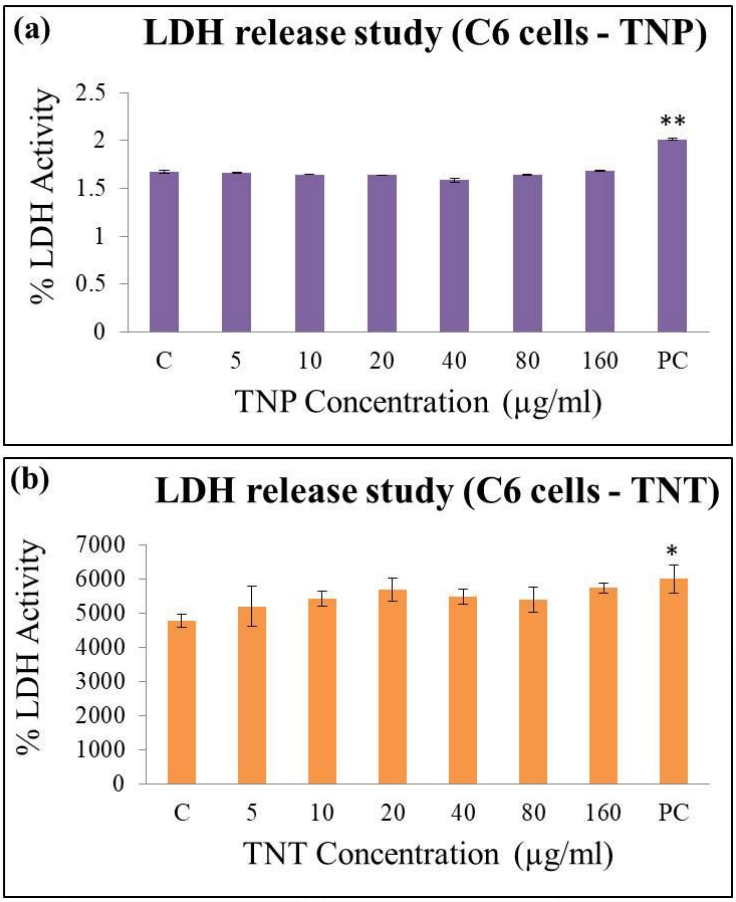

Figure 4.20 Cell membrane damage study using LDH release assay for cells treated with, (a) TNPs and (b) TNTs. C- Negative control, Positive control (PC): 0.09% H_2O_2. The data represent mean ± SD of three independent experiments (N=3). Asterisks denote statistically significant deviation from negative control (* $p<0.05$, ** $p< 0.01$ and *** $p<0.001$).

4.2.12 LIVE/DEAD CELL STUDY FOR TNPs

Different stages of the cell death pathway in TNP-exposed cells were detected using AO/EtBr dual staining method. Fluorescence images of cells under different cell death events were captured and are illustrated in Figure 4.21. It was observed that the lowest concentration of TNPs (5µg/ml) did not induce any cell death events in C6 cells and was comparable with that of control cells. As the concentration was increased to 40µg/ml, a minor population of cells was found to be entering the necrotic cell death pathway and those cells were noted to possess

necrotic injury over the core of the cell body. Injured areas of cells were identified by reddish-orange fluorescence and healthy areas were showing green fluorescence. At 160µg/ml, a major population of cells was observed to be undergoing a necrotic cell death pathway and were discernible from other cells by the emission of reddish-orange fluorescence. The emission of reddish-orange fluorescence was originated from the passive diffusion of EtBr upon necrotic cell death at 160µg/ml.

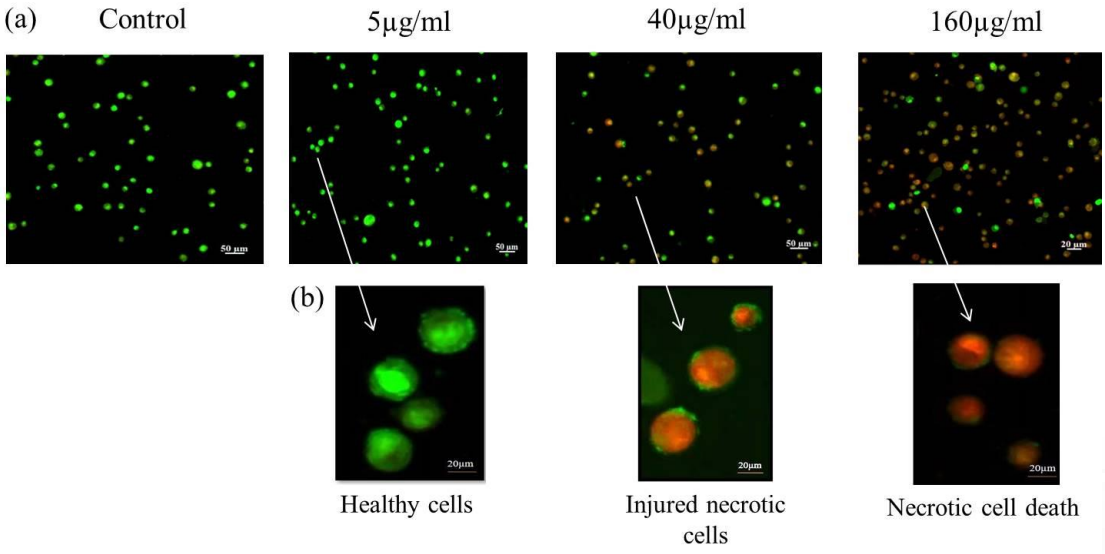

Figure 4.21 Live/dead study by AO/EtBr dual staining for cells exposed with TNPs for 24h. Green fluorescence denotes healthy cells stained by AO & reddish orange fluorescence denotes unhealthy cells or necrotic cell death events stained with EtBr.(a) Cells imaged under lower magnification (10X). Scale bar: 50µm. (b) Cells imaged under higher magnification of 100X by oil immersion. Scale bar: 20µm.

4.2.13 LIVE/DEAD CELL STUDY FOR TNTs

Quantitative evaluation of cell death pathway in TNT exposed cells was performed using Calcein AM/PI staining. Relative ratio of green and red fluorescence were calculated and plotted against corresponding TNT concentration. Values obtained for treated groups were compared with negative control. From 5µg/ml to 80µg/ml, cells did not deviate significantly from control values (5µg/ml: 39497 ± 1497, 10µg/ml: 39393 ± 3114.714, 20µg/ml: 39495.5 ± 1226.593, 40µg/ml: 39371.5 ± 2130.5, 80µg/ml: 39348 ± 2050.6). However, 160µg/ml TNPs

caused significant reduction in fluorescence ratio (38892 ± 1061.18) compared to control. Figure 4.22 (a) shows the quantitative evaluation of Calcein AM/PI staining (485/520nm). Corresponding fluorescence images of Calcein AM/PI staining is shown in Figure 4.22 (b). Only 160µg/ml exhibited red fluorescence by the dead population of cells.

4.2.14 DNA LADDERING BY AGAROSE GEL ELECTROPHORESIS (AGE)

NM-induced DNA fragmentation was studied using DNA laddering assay by gel electrophoresis. Genomic DNA from TNP and TNT exposed cells was isolated as per the manufacture's instruction. Gel documentation study revealed that there were no fragmented DNA bands identified and the loaded genomic DNA remained intact with a size of above 10,000bp for all the tested concentrations of both of the materials. Only the positive control showed fragmented bands with a lowest band size of below 300bp (Figure 4.23). Absence of DNA laddering further justifies the fact that the tested materials do not cause any deleterious effect on the nuclear integrity of C6 cells.

4.2.15 NUCLEAR CONDENSATION BY DAPI STAINING

TNP induced nuclear condensation was evaluated using DAPI staining via fluorescent imaging. As shown in Figure 4.24, TNPs did not induce any chromatin condensation at the lowest concentration of 5µg/ml. However, mild levels of nuclear condensation were observed for the middle (40µg/ml) and the highest tested concentration (160µg/ml) of TNPs after 24h of exposure. DAPI exhibited increased emission of blue fluorescence at condensed nuclear loci.

4.3 IN VITRO TOXICITY STUDIES FOR TNT-P

4.3.1 CELL VIABILITY STUDY BY MTT ASSAY

Cell viability or mitochondrial activity after cellular exposure with different concentrations of TNT-P was studied by MTT assay. In contrast to both TNPs and TNTs as represented in section 4.3.4, surface coated TNTs did not cause any statistically significant reduction in cell viability up to 160µg/ml compared to control (5µg/ml: 99.21±0.36, 10µg/ml: 97.92±0.25, 20µg/ml: 99.58±0.55, 40µg/ml: 99.51±0.31, 80µg/ml: 0.66 & 160µg/ml: 95.53±0.57). The

observation clearly suggests surface coating with P-F127 could effectively mask the inherent toxicity exhibited by TNTs in neuronal cells (Figure 4.25).

4.3.2 EFFECTS OF P-F127 ON C6 CELL VIABILITY

The interference of P-F127 polymer on C6 cells was studied by MTT assay after cellular exposure of the polymer at different concentrations for 24h. From the cell viability plot it was observed that, the mitochondrial activity or % viability of cells was significantly increasing from 5µg/ml P-F127 onwards compared to the control value (5µg/ml: 116.22±0.19, 10µg/ml: 130.77±0.14, 20µg/ml: 154.52±0.016, 40µg/ml: 154.95±0.069, 80µg/ml: 139.07±0.22 & 160µg/ml: 141.21±0.13). The values showed statistical significance from 10µg/ml onwards and the pattern of viability increment continued up to 40µg/ml and then slightly reduced for 80 and 160µg/ml. All of the treatment groups showed higher viability value than the negative control (Figure 4.26). This highlights high neuronal compatibility of P-F127 and its role as a cell proliferation promoter.

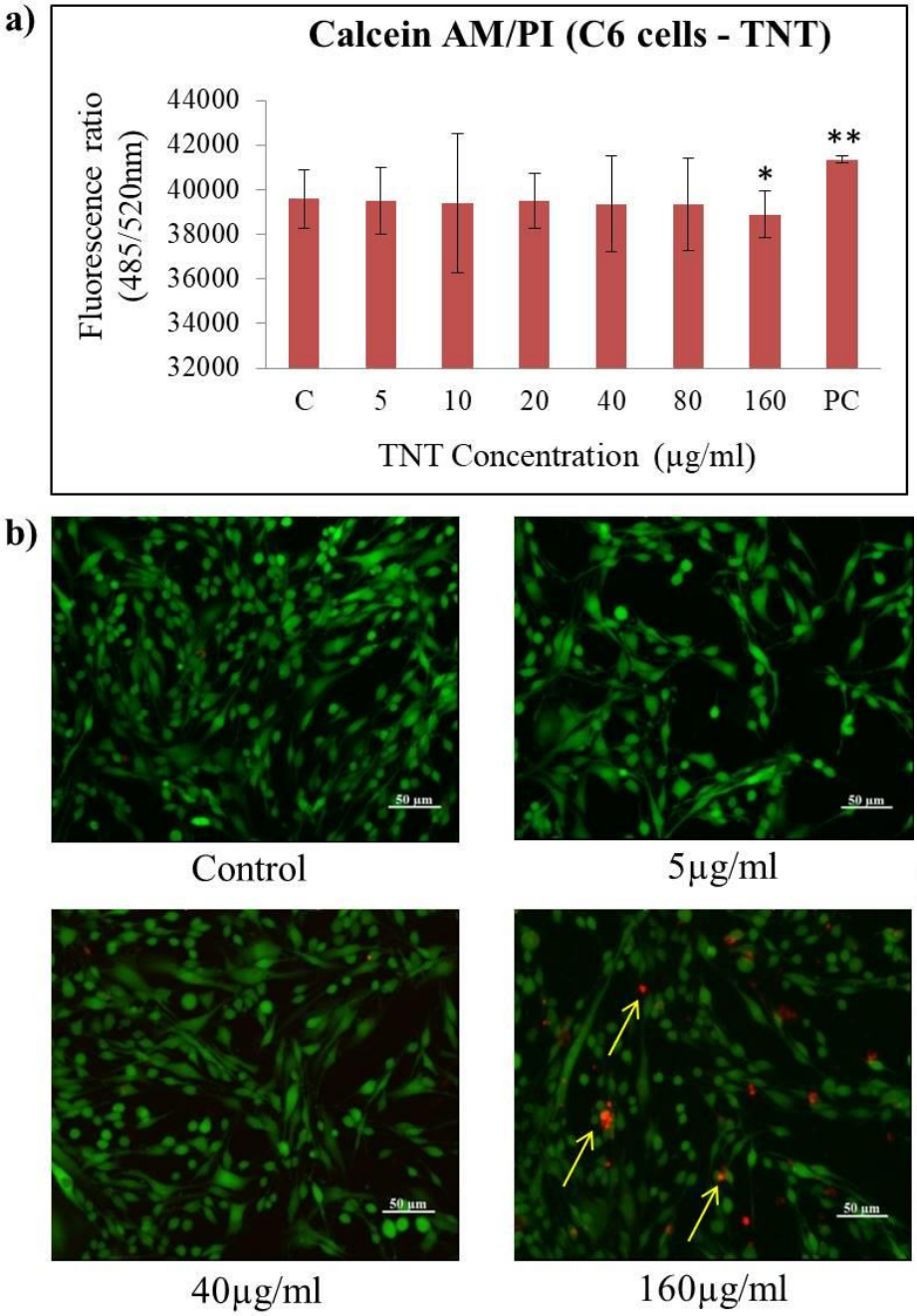

Figure 4.22 Live/dead study by Calcein AM/PI staining for cells treated with TNTs for 24h. a) Quantitative evaluation showing ratio of green and red fluorescence (485/520nm). C- Negative control, Positive control (PC): Phenol. The data represent mean ± SD of three independent experiments (N=3). Asterisks denote statistically significant deviation from negative control (* $p<0.05$, ** $p< 0.01$ and *** $p<0.001$). b) Fluorescence images of control and TNT treated cells after Calcein AM/PI staining. Green signal denotes Calcein entrapped cells & red signal denotes cells stained with PI. Yellow arrows indicate dead cells and are stained red with PI. Magnification: 10X, Scale bar: 50µm.

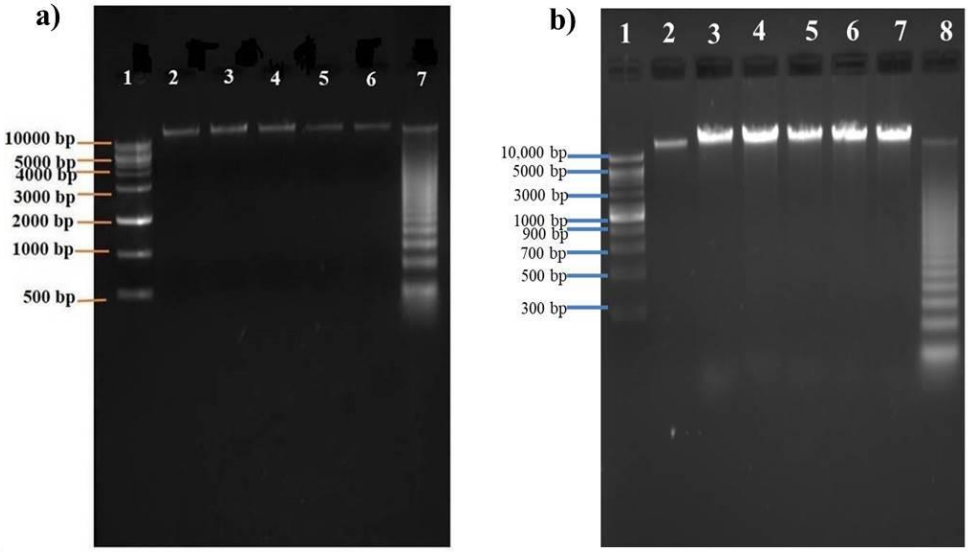

Figure 4.23 DNA laddering assay by Agarose gel electrophoresis. (a) Gel image of DNA isolated from cells exposed with TNPs at various concentrations. Lane 1: 1Kb DNA ladder, Lane 2: Control, Lane 3: 10µg/ml, Lane 4: 40µg/ml, Lane 5:80µg/ml, Lane 6: 160µg/ml & Lane 7: Positive control (provided with the ladder kit). (b) Gel image of DNA isolated from cells exposed with TNTs at various concentrations. Lane 1: 1Kb DNA ladder, Lane 2: Control, Lane 3: 10µg/ml, Lane 4: 20µg/ml, Lane 5: 40µg/ml, Lane 6: 80µg/ml, Lane 7: 160µg/ml & Lane 8: Positive control (provided with the ladder kit). Base size of the 1Kb DNA ladder is indicated along the left side of each gel image.

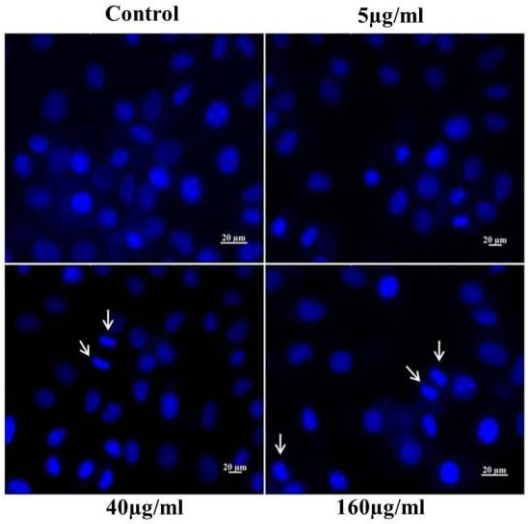

Figure 4.24 Nuclear condensation study by DAPI staining for cells exposed to TNPs at various concentrations. White arrows indicate nuclear condensation at 40 & 160µg/ml of TNPs. Magnification: 20X, Scale bar: 20µm.

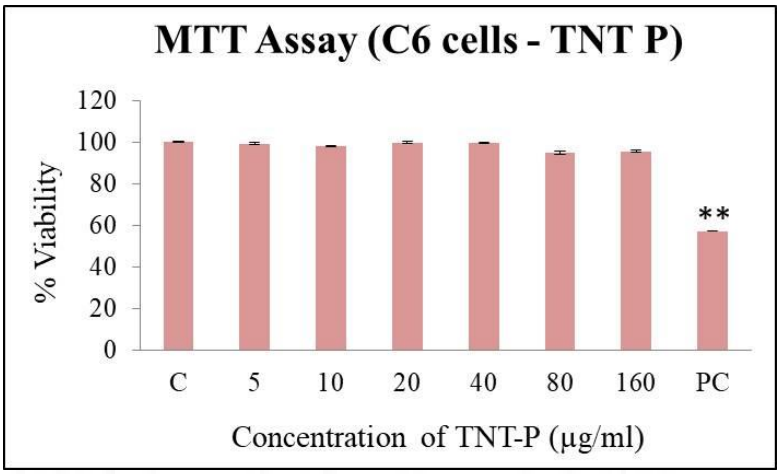

Figure 4.25 MTT assay for cellular interaction with TNT-P.C- Negative control, Positive control (PC): Phenol. The data represent mean ± SD of three independent experiments (N=3).Asterisks denote statistically significant deviation from negative control (* p<0.05, **p< 0.01 and ***p<0.001).

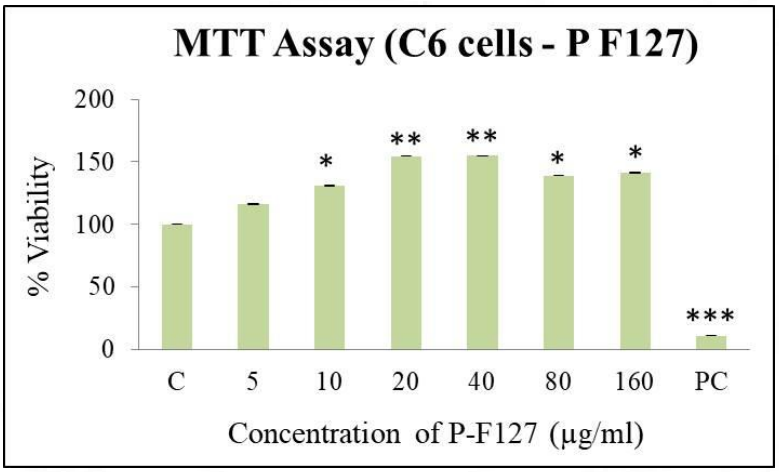

Figure 4.26 Effect of P-F127 on cell viability by MTT assay.C- Negative control, Positive control (PC): Phenol. The data represent mean ± SD of three independent experiments (N=3).Asterisks denote statistically significant deviation from negative control (* p<0.05, **p< 0.01 and ***p<0.001).

4.3.3 LYSOSOMAL INTEGRITY BY NRU ASSAY

Cell proliferating capacity of TNT-P was confirmed further using NRU assay after cellular exposure for 24h. None of the tested concentrations of TNT-P was observed to be showing alteration in lysosomal integrity compared to the control value (5µg/ml: 99.59±0.014, 10µg/ml: 99.43±0.08, 20µg/ml: 99.39±0.005, 40µg/ml: 98.93±0.09, 80µg/ml: 97.82±0.22 & 160µg/ml:

98.23±0.03). This confirms higher viability rate after polymer coating of P-F127. Figure 4.27 shows NRU assay for TNT-P after cellular exposure.

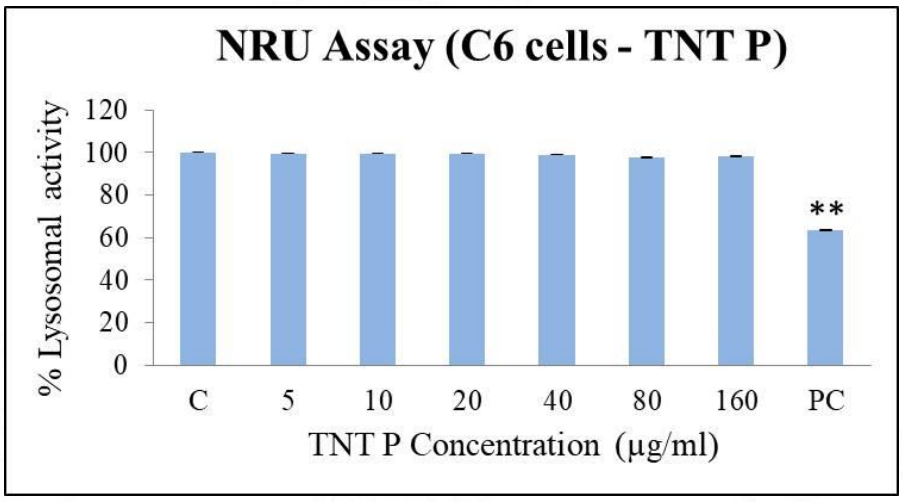

Figure 4.27 Lysosomal integrity study for TNT-P after 24h exposure.C- Negative control, Positive control (PC): Phenol. The data includes mean ± SD of three independent experiments (N=3).Asterisks denote statistically significant deviation from negative control (* $p<0.05$, ** $p<0.01$ and *** $p<0.001$).

4.3.4 ROS GENERATION BY DCFH-DA ASSAY

A comparative evaluation on induced ROS generation by TNT-P was performed by DCFH-DA assay. Compared to bare TNTs as mentioned in section 4.3.10.1, polymer coated form resulted in a slight reduction in intracellular ROS levels at the highest concentration of 160µg/ml.

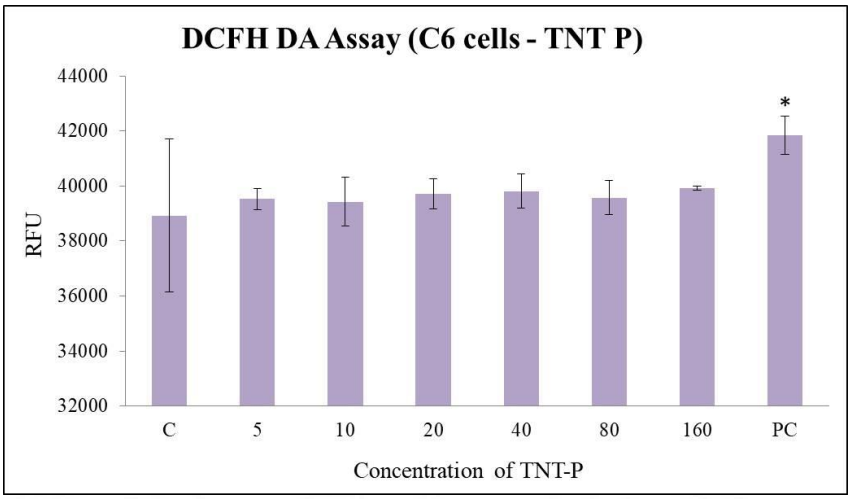

Figure 4.28 Oxidative stress evaluation for TNT-P by DCFH-DA assay. Results are expressed in Relative Fluorescence Unit (RFU). C- Negative control, Positive control (PC): 0.09% H_2O_2. The data represent mean ± SD of three independent experiments (N=3). Asterisks denote statistically significant deviation from negative control (* $p<0.05$, ** $p< 0.01$ and *** $p<0.001$).

Rest of the lower concentrations did not show a noticeable deviation from the control value (5µg/ml: 39530.3±384.39, 10µg/ml: 39428.6±878, 20µg/ml: 39717.6±545, 40µg/ml: 39811.6±628, 80µg/ml: 39572±623 & 160µg/ml: 39921.6±64.2). This denotes anti-oxidant effect elicited by TNT after P-F127 coating (Figure 4.28).

4.4 INVESTIGATION OF ACUTE TOXICITY OF SURFACE COATED TiO_2 NANOTUBES USING WISTAR RAT

4.4.1 VISUAL EXAMINATION OF BEHAVIORAL CHANGES

A single dose of TNT-P (10mg/Kg body weight) was administered to Wistar rats weighing 200-450g. Animals were allotted into four different groups based on the day of observation and were sacrificed on the 3rd, 7th and 14th days from the day of administration. Visual examination for various signs of behavioral changes was performed on all the observation days and is illustrated in Table 4.4. None of the animal groups showed any signs of behavioral changes or lethal symptoms of death compared to the control group up to 14 days of study.

4.4.2 BODY WEIGHTS OF RATS

Body weights of Wistar rats were recorded prior to sacrifice on all the observation periods. There occurred a normal increment in growth of rats over the period of 14 days compared to the control animals (Figure 4.29).

Table 4.4 Visual examination of Wistar rats for behavioral changes (n=3).

Clinical signs and behavioural changes	**Control**	**Tests**
Lacrimation	Normal	Normal
Salivation	Normal	Normal
Excretion	Normal	Normal
Piloerection	Normal	Normal
Motor activity	Normal	Normal
Home cage posture	Normal	Normal
Rearing	Normal	Normal

4.4.3 GROSS PATHOLOGY EVALUATION

Euthanized animals were subjected to gross pathology evaluation prior to organ isolation. There were no pathological signs like lesions on body or organ surface such as color change, lumps or edema *etc*. were observed. All the organs exhibited normal consistency and shape (Figure 4.30).

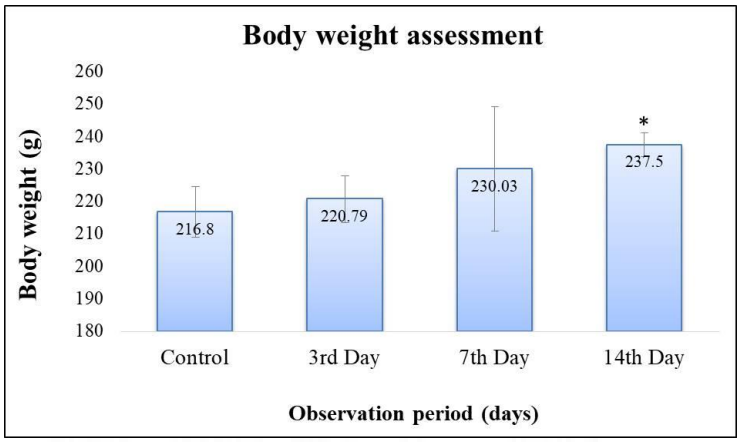

Figure 4.29 Body weight assessment of Wistar rats.The data includes mean ± SD of three independent experiments (N=3).

Figure 4.30 Gross pathology evaluation for Wistar rat treated with TNT-P.

4.4.4 WET WEIGHT OF ORGANS

Four key organs such as the brain, liver, spleen, and kidneys were isolated from each experimental animal on all the observation days. Wet weight of all of the organs was recorded

and is indicated in Table 4.5. A plot was drawn for organ weight against observation period and is shown in Figure 4.31**.** Wet weight of organs such as brain, spleen and kidney on 3rd, 7th and 14th day did not alter noticeably from that of the control group. However, liver showed a non-significant increase in wet weight compared to control in a time dependent manner.

Table 4.5 Wet organ weight of Wistar rats exposed with TNT-P (n=3, Mean±SD).

Sample & route of administration	**Animal group**	**Organ weight (g)**			
		Brain	Liver	Spleen	Kidney
TNT-P (i.p.)	Control	1.67±0.04	9.29±4.47	0.54±0.11	1.68±0.72
	3rd Day	1.69±0.15	11.28±3.01	0.576±0.05	1.83±0.66
	7th Day	1.71±0.07	11.29±4.44	0.58±0.19	1.86±0.41
	14th Day	1.73±0.13	12.1±1.85	0.582±0.03	1.76±0.13

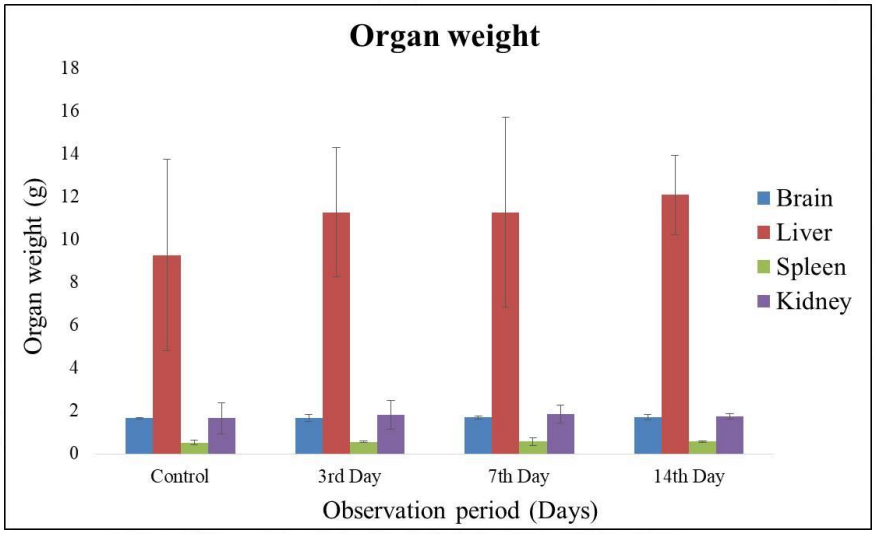

Figure 4.31.Wet weight of organs isolated from Wistar rats after TNT-P administration. The data repre mean ± SD of three independent experiments (n=3).

4.4.5 HEMATOLOGY ANALYSIS

Blood samples were collected from TNT-P treated rats and subjected to hematological analysis for various parameters. The values obtained for each parameter are shown in Table 4.6. The result of the analysis indicated that, there were no remarkable alterations occurred for any of the parameters checked (RBC, WBC, HGB, HCT, MCV, MCH & MCHC) for control and 3rd day after TNT-P administration. However, 7th day showed a change in values for hemoglobin count, hematocrit, cell volume and average amount of hemoglobin. Hematocrit value on 7th day showed a statistically significant reduction and an increment for blood cell volume. MCH and MCHC values for 7th day showed a non-significant increment compared to control group. 14th day of observation showed an increase in hemoglobin and HCT and a reduction in MCV without any statistical significance Figure 4.32 (a). The platelet count for all the observation days remained within the normal range compared to the control group [Figure 4.32 (b)].

4.4.6 SERUM BIOCHEMISTRY

Liver and kidney functionality was assessed using serum biochemistry evaluation after administration of TNT-P into Wistar rats. Both ALT and AST exhibited a time-dependent increase in values up to the 7th day compared to the control group. On the 7th day of observation, ALT and AST showed a statistically significant increase in their levels (82.53±2.05 & 351.36±41.67 respectively). By day 14, the level was decreased for both ALT and AST non-significantly. ALP showed a sharp time-dependent increase in level compared to the control group with a statistical significance on the 14th day (424±180.83) Level of glucose also significantly increased on the 7th day and normalized on the 14th day.

Triglyceride and creatine levels also showed a slight non-significant increase on the 7th day and reached a normal level on the 14th day. The rest of the tested biochemical parameters like cholesterol, albumin, and protein did not alter significantly at any of the observation periods compared to the control group. Table 4.7 shows the values obtained for biochemistry parameters and the corresponding graphs for ALT, AST & ALP are given in Figure 4.33(i). Other parameter graphs are illustrated in Figure 4.33 (ii).

Table 4.6 Hematology parameters count for Wistar rats exposed with TNT-P. RBC: Red blood cells, WBC: White blood cells, HGB: Hemoglobin, HCT: Hematocrit, MCV: Mean corpuscular volume, MCH: Mean corpuscular hemoglobin, MCHC: Mean corpuscular hemoglobin concentration. Data denotes mean±SD of three independent experiments.

Parameters	**Animal group**			
	Control	**3rd Day**	**7th Day**	**14th Day**
RBC (10^6/mm^3)	7.85±0.29	7.85±0.29	4.65±0.14	8.83±0.41
WBC (10^3/mm^3)	12.93±1.40	12.93±1.40	12.36±0.75	8.40±2.21
HGB (g/dl)	15.60±1.30	15.60±1.30	15.20±0.52	17.66±0.55
HCT (%)	39.20±1.38	39.20±1.38	30.80±1.35*	44.5±2.05
MCV (µm^3)	49.93±1.35	49.93±1.35	66.33±1.52*	50.40±2.30
MCH (pg)	19.83±1.05	19.83±1.05	32.73±0.81	20.03±0.58
MCHC (g/dl)	39.73±1.87	39.73±1.87	49.43±0.66	39.73±0.83
Platelet (10^3/mm^3)	846.66±270	846.66±270	786±52.84	723±132

4.4.7. ANTIOXIDANTS IN BRAIN AND LIVER

Antioxidant titers in brain and liver samples were studied using different estimation methods. Total protein estimation by Lowry's method indicated that protein levels in both brain and liver homogenates were increased on 3rd day compared to the control. The protein level then declined on subsequent observation days (3rd Day brain: 0.20±0.03, 7th Day brain: 0.17±0.02, 14th Day brain: 0.16±0.01, 3rd Day liver: 0.46±0.04, 7th Day liver: 0.3±0.04 & 14th Day liver: 0.29±0.04*) [Figure 4.34 (a)]. Considering reduced glutathione or GSH, the levels in both the brain and liver were increased in a time-dependent manner compared to the control group, with a statistical significance on the 14th day (3rd Day brain: 0.90±0.03, 7th Day brain: 0.93±0.03, 14th Day brain: 0.97±0.08*, 3rd Day liver: 0.94±0.03, 7th Day liver: 0.95±0.06 & 14th Day

liver: 0.99±0.01*) [Figure 4.34 (b)]. Both of the tissues did not reveal any alterations with lipid peroxidation levels compared to control group on any of the observation periods (3rd Day brain: 0.10±0.02, 7th Day brain: 0.1±0.008, 14th Day brain: 0.11±0.007. 3rd Day liver: 0.12±0.01, 7th Day liver: 0.11±0.01 & 14th Day liver: 0.11±0.02) [Figure 4.33 (c)].

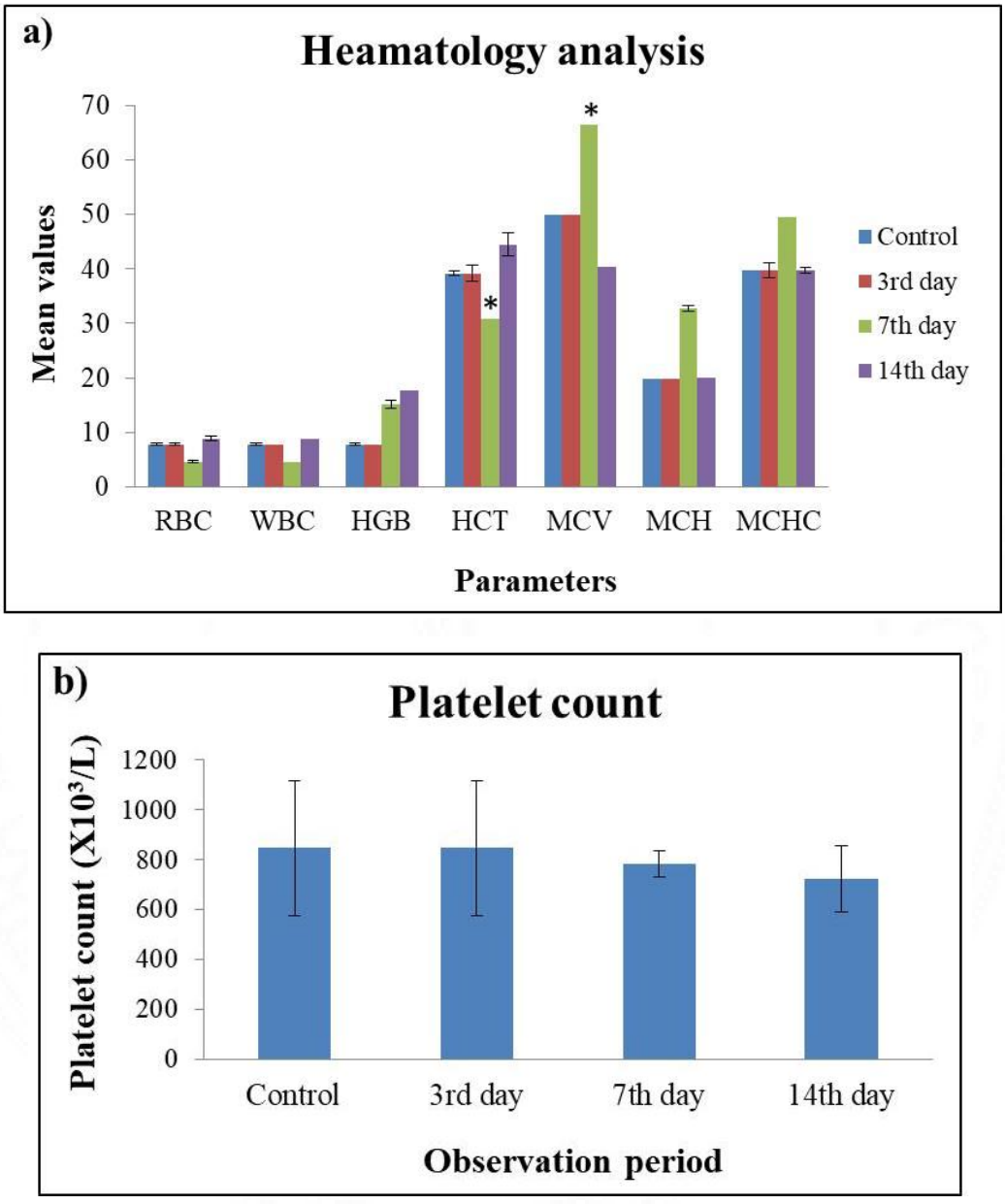

Figure 4.32 (a) Plot showing hematology parameters mean value for Wistar rats treated with TNT-P (b) Platelet count for blood samples from Wistar rats.The data include mean ± SD of three independent experiments (N=3). Asterisks denote statistically significant deviation from negative control (* $p<0.05$, ** $p< 0.01$ and *** $p<0.001$).

Table 4.7 Serum biochemistry analysis for Wistar rats treated with TNT-P. ALT: Alanine transaminase, AST: Aspartate transaminase and ALP: Alkaline phosphatase. Data depict mean±SD of three independent experiments.

Parameters	**Animal group**			
	Control	**3rd Day**	**7th Day**	**14th Day**
ALT (IU/L)	31.86±19.50	62.16±2.57	82.53±2.05*	71.13±26.8
AST (IU/L)	207.86±27.34	230.4±19.92	351.36±41.67*	180.80±36.3
ALP (IU/L)	163.33±34.12	241.66±59.50	382.66±52.54	424±180.8*
Glucose (mg/dl)	65.33±11.60	65.36±14.25	89.80±28.28*	72.66±15.21
Cholesterol (mg/dl)	82.0±7.25	84.0±21.07	77.33±13.05	93.60±9.71
Triglycerides (mg/dl)	136.0±85.84	112.33±5.68	171.66±36.29	51.73±0.53
Albumin (g/dl)	4.83±0.45	4.90±0.30	5.13±0.80	5.3±0.50
Protein (g/dl)	10.33±1.11	11.33±0.92	10.23±1.53	10.66±1.36
Creatinine (mg/dl)	0.88±0.07	0.95±0.06	1.04±0.11	0.88±0.05

4.4.8 URINE ANALYSIS

Kidney functions were examined by checking various urinary parameters from TNT-P treated Wistar rats before sacrifice on each observation day. The results are illustrated in Table 4.8. It was observed that the levels of leukocytes, nitrite, urobilinogen, and protein did not show alterations when compared to the control group. The pH was slightly increased on 3rd Day & 7th Day and then normalized on 14th Day. There was no detectable level of blood and ketones

present and the urine showed a specific gravity within normal range. The glucose level was also found to be normal compared to control.

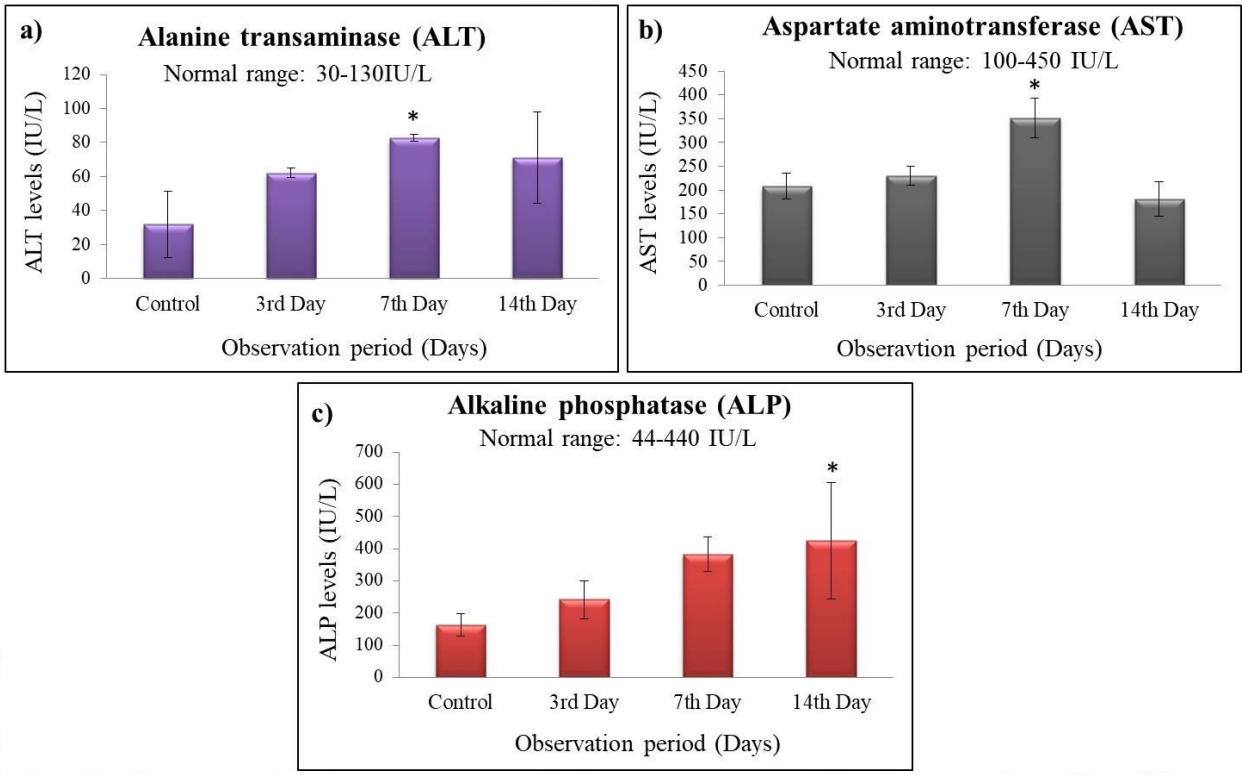

Figure 4.33 (i) Biochemistry evaluation for metabolic enzymes from Wistar rats exposed with TNT-P**.** (a) ALT: Alanine transaminase**,** (b) AST: Aspartate transaminase, (c) ALP: Alkaline phosphatase. The data includes mean ± SD of three independent experiments (N=3). Asterisks denote statistically significant deviation from negative control (* $p<0.05$, ** $p< 0.01$ and *** $p<0.001$).

4.4.9. BIODISTRIBUTION STUDY

Biodistribution of TNT-P in isolated tissues samples (brain, liver and kidney), urine, blood and fecal matter from Wistar rats was studied for 3rd, 7th and 14th days of exposure using ICPMS technique. As per the results of tissue samples, TNT-P was detected at highest level in brain and liver on 7th day compared to 3rd day of observation (3rd Day brain: 0.43±0.04, 7th Day brain: 0.19±0.23, 3rd Day liver: 7.9±5.4, 7th Day liver: 9.3±6.4) [Figure 4.35 (a) & (b)]. The level was non-significantly declined on 14th day for both the tissues (14th Day brain: 0.30±0.15 & 14th Day liver: 1.5±0.98). Kidney showed a time dependent decrease in TNT-P level with the lowest value on the 14th day (3rd Day: 0.45±0.02, 7th Day: 0.33±0.05 & 14th Day:

0.24±0.11) [Figure 4.35 (c)]. Excretory removal of TNT-P was evident from the levels of TNT-P in blood (3rd Day: 0.16±0.05, 7th Day: 0.19±0.01 & 14th Day: 0.17±0.003), urine (3rd Day: 0.32±0.21, 7th Day: 0.33±0.13 & 14th Day: 0.14±0.08) and fecal matter (3rd Day: 5.5±2.5, 7th Day: 14.2±5.2 & 14th Day: 24.8±1.9) [Figure 4.35 (d), (e) & (f)]. Results indicated that TNT-P was effectively removed from the rat body without considerable accumulation over a period of 14 days.

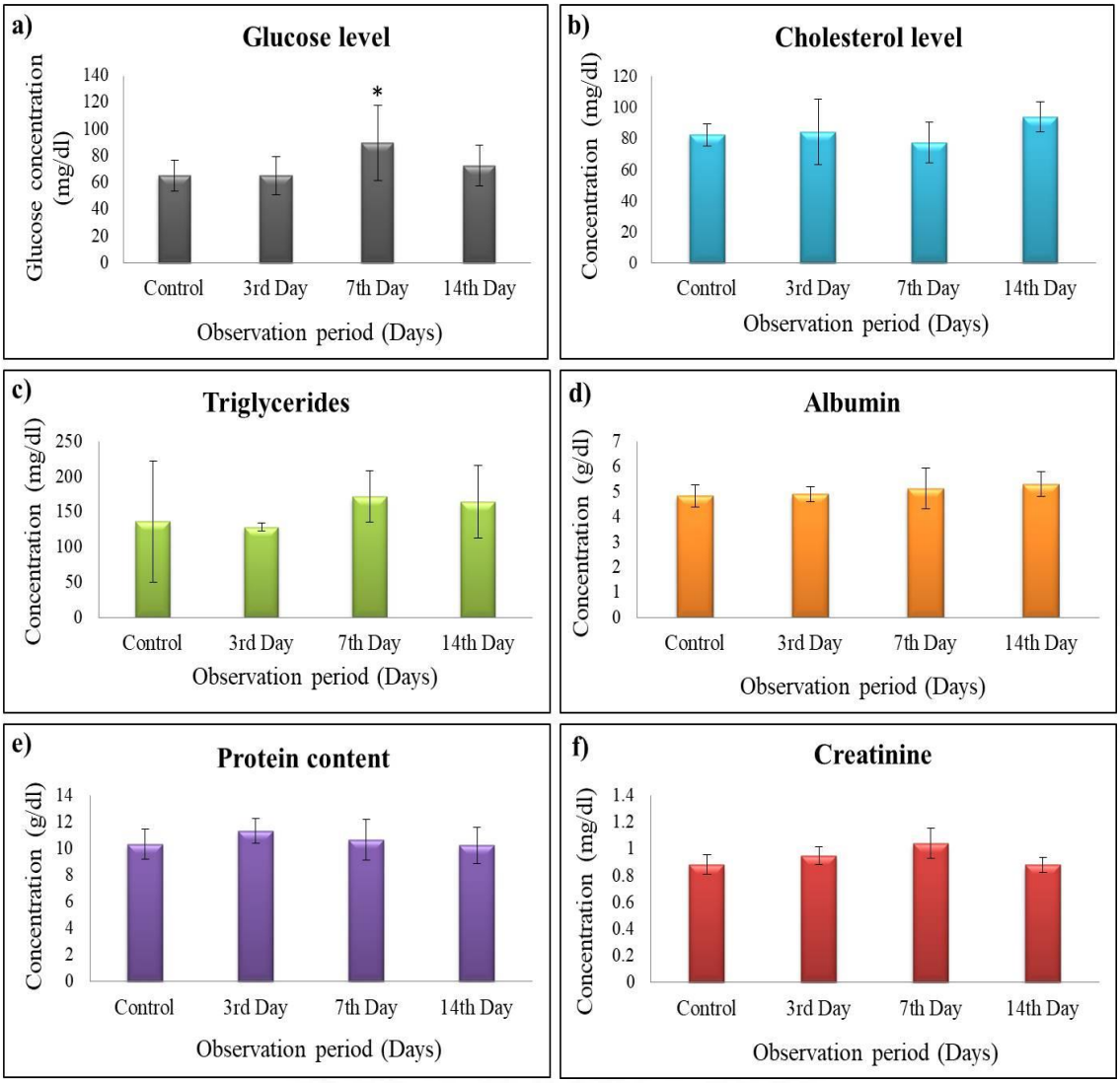

Figure 4.33 (ii) Analysis for biochemical parameters of Wistar rats after exposure with TNT-P: (a) Glucose level, (b) Cholesterol level, (c) Triglycerides, (d) Albumin, (e) Protein content, (f) Creatinine. The data depicts the mean ± SD of three independent experiments (N=3). Asterisks

denote statistically significant deviation from negative control (* p<0.05, **p< 0.01 and ***p<0.001).

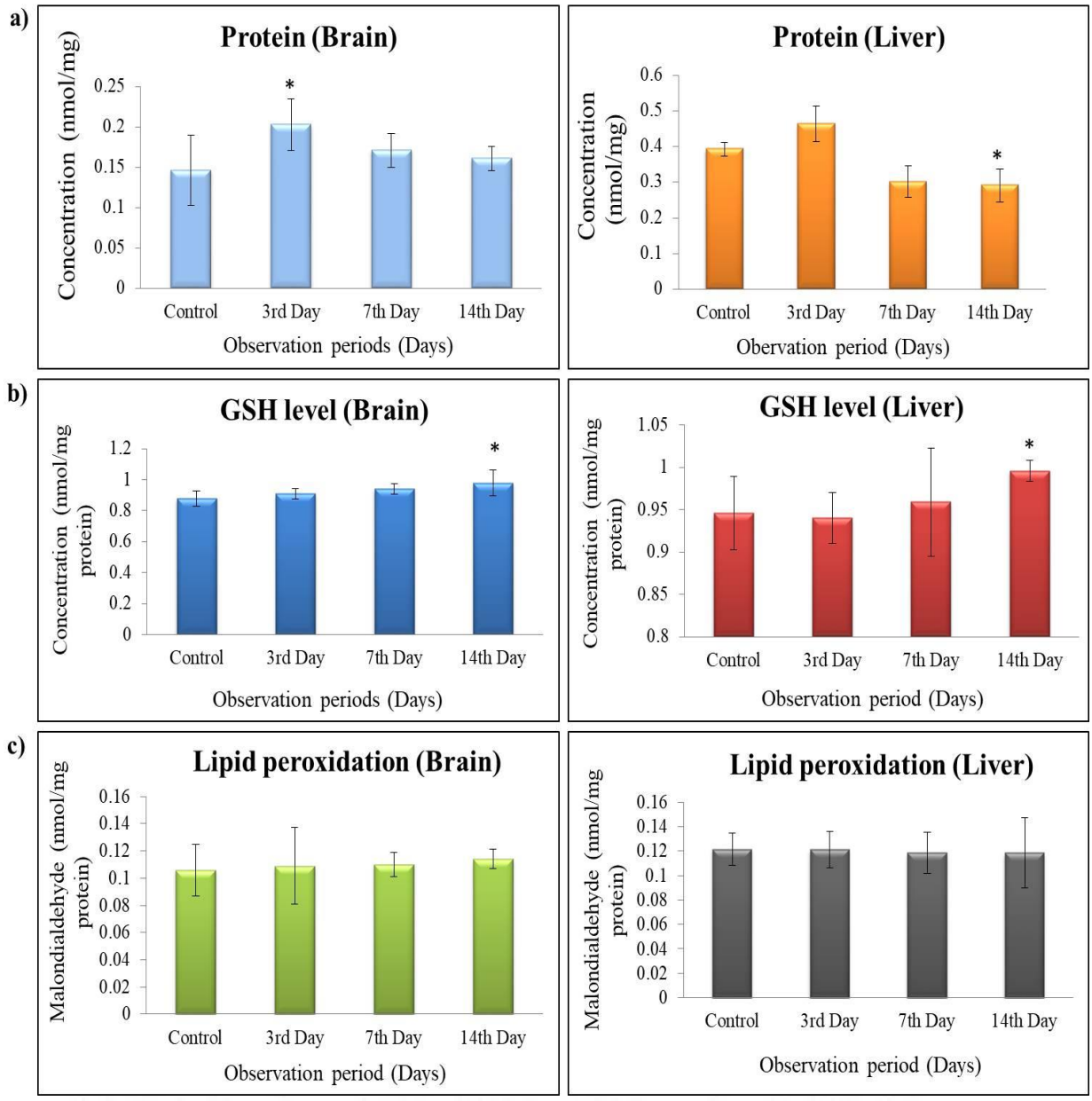

Figure 4.34 Evaluation of antioxidant levels in brain and liver from Wistar rats exposed with TNT-P. (a) Protein level in brain and liver, (b) GSH (Reduced glutathione) in brain and liver, (c) Lipid peroxidation levels in brain and liver.The data includes mean ± SD of three independent experiments (N=3). Asterisks denote statistically significant deviation from negative control (* p<0.05, **p< 0.01 and ***p<0.001).

Table 4.8 Urine analysis of Wistar rats exposed with TNT-P. Data stands for mean±SD of three independent experiments.

Parameters	**Control**	**3rd Day**	**7th Day**	**14th Day**
Leukocyte	Negative	Negative	Negative	Negative
Nitrite	Positive	Positive	Positive	Positive
Urobilinogen (mg/dl)	0.1±0.0	0.1±0.00	0.11±0.01	0.1±0.1
Protein (mg/dl)	14.66±1.53	14.00±1.41	14.33±1.15	14.11±1.3
pH	7.5±0.0	8.00±0.0	8.00±0.0	7.33±0.28
Blood	Negative	Negative	Negative	Negative
Specific gravity	1.021±0.005	1.015±0.0	1.015±0.0	1.02±0.002
Ketones (mg/dl)	Negative	Negative	Negative	Negative
Bilirubin	Small	Small	Small	Small
Glucose (mg/dl)	Normal	Normal	Normal	Normal

4.4.10 IMMUNOTOXICITY

Immunotoxic response of TNT-P was studied using splenocyte proliferation assay using [^{3}H]-thymidine incorporation. The proliferation capacity of splenocytes was observed to be increasing for all the treatment groups compared to the control in a time dependent manner. Maximum proliferation was obtained on 7th day of observation and showed a statistically significant value (Control: 100.3±13.2, 3rd Day: 125.6±12.3, 7th Day: 14.2±5.2 & 14th Day: 24.8±1.9). Result of the assay suggests TNT-P induced an immunological response in the rat body Figure 4.36.

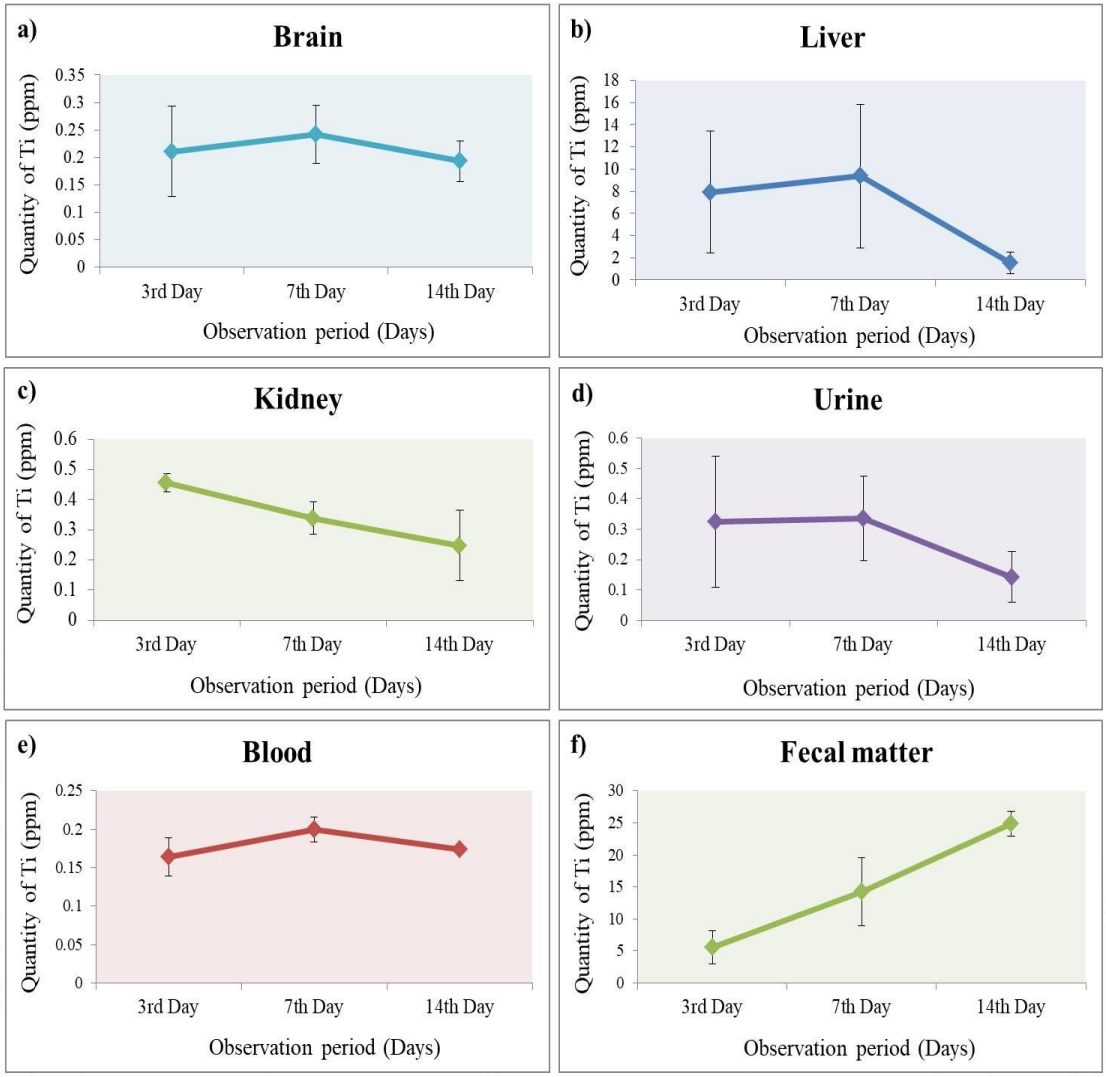

Figure 4.35 Biodistribution study of samples isolated & collected from Wistar rats after TNT-P administration. (a) Brain, (b) Liver, (c) Kidney, (d) Urine, (e) Blood and (f) Fecal matter. The data represents mean ± SD with N=3. Asterisks denote statistically significant deviation from negative control (* $p<0.05$, ** $p< 0.01$ and *** $p<0.001$).

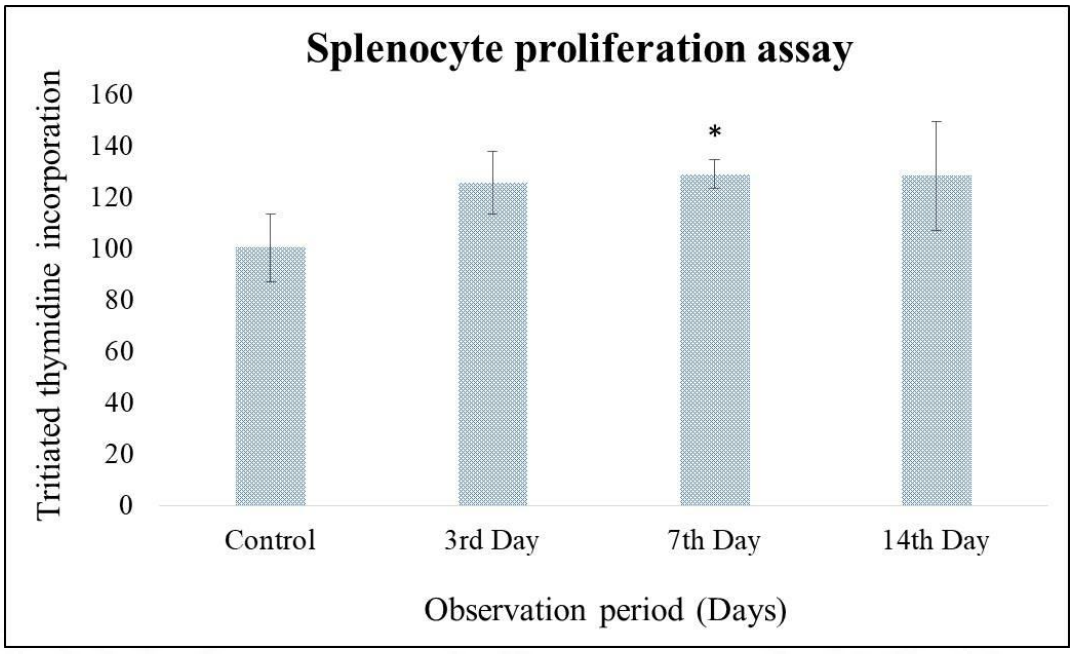

Figure 4.36 Immunotoxicity study by splenocyte proliferation assay for Wistar rats after TNT-P exposure.The data represents mean ± SD from three independent experiments (N=3). Asterisks denote statistically significant deviation from negative control (* $p<0.05$, ** $p< 0.01$ and *** $p<0.001$).

4.4.11 HISTOPATHOLOGY

Histopathological examination of isolated tissue samples was performed using H&E staining. Results indicated that over a period of 14 days, TNT-P did not cause any pathological signs in the brain compared to the control image. However, a certain level of pathological lesions including cellular infiltration was observed in the liver from 3rd day onwards. This indicates TNT-P-induced hepatocellular damage. Figure 4.37 (a) & (b) represents histopathology results of brain and liver samples respectively. The histopathological examination of spleen and kidney samples could not identify any pathological lesions compared to the control group. These tissues retained their characteristic cellular morphology and characteristic features up to 14 days of observation [Figure 4.38 (a) & (b)].

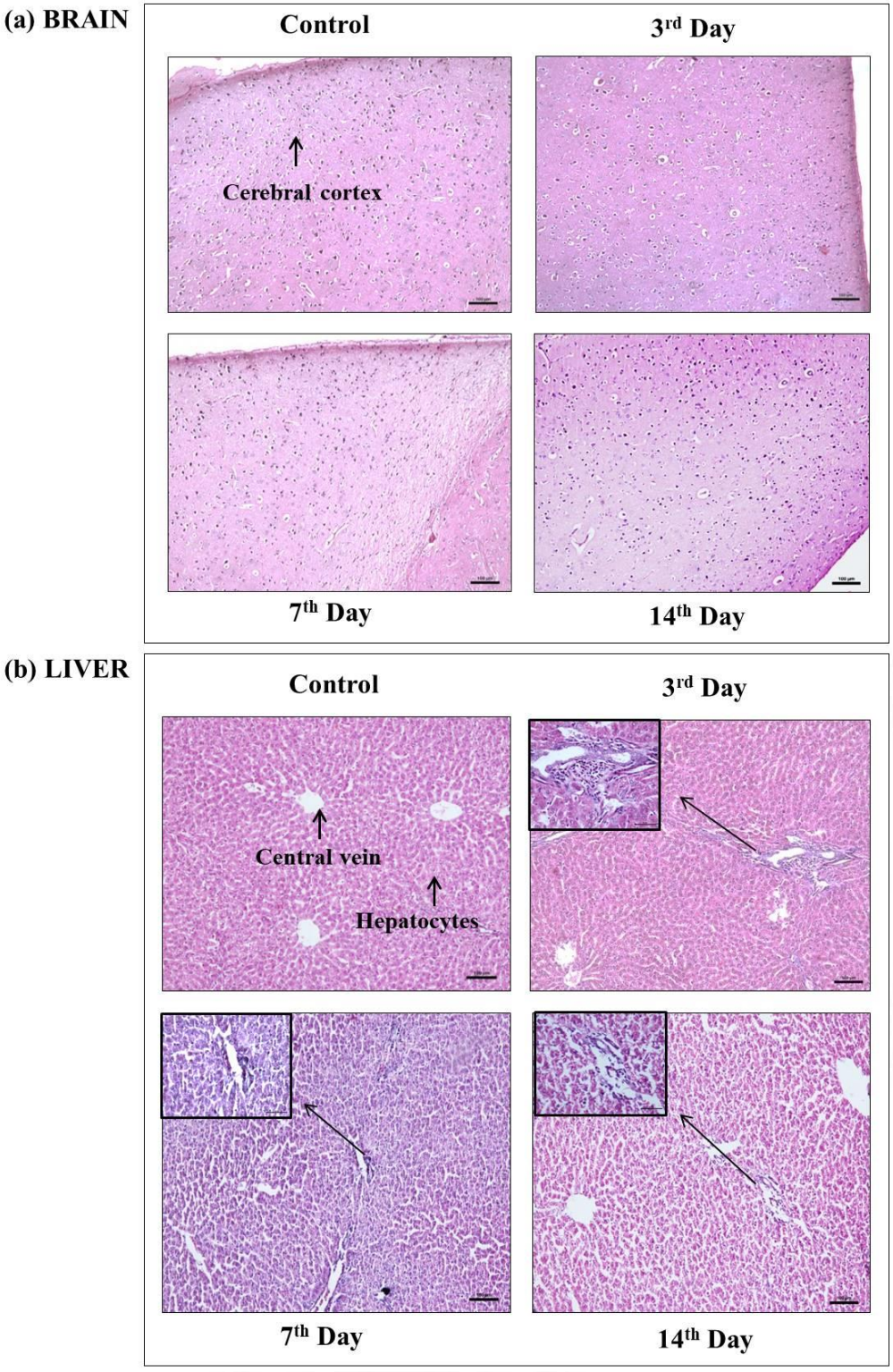

Figure 4.37 Histopathology evaluation of tissue samples from Wistar rats exposed with TNT-P using H&E staining. (a) Brain, (b) Liver. Magnification: 10X, Scale bar: 100µm. Insets

highlighted at the top left corner of liver images represent pathological lesions showing cellular infiltration (Magnification: 40X, Scale bar: 50µm).

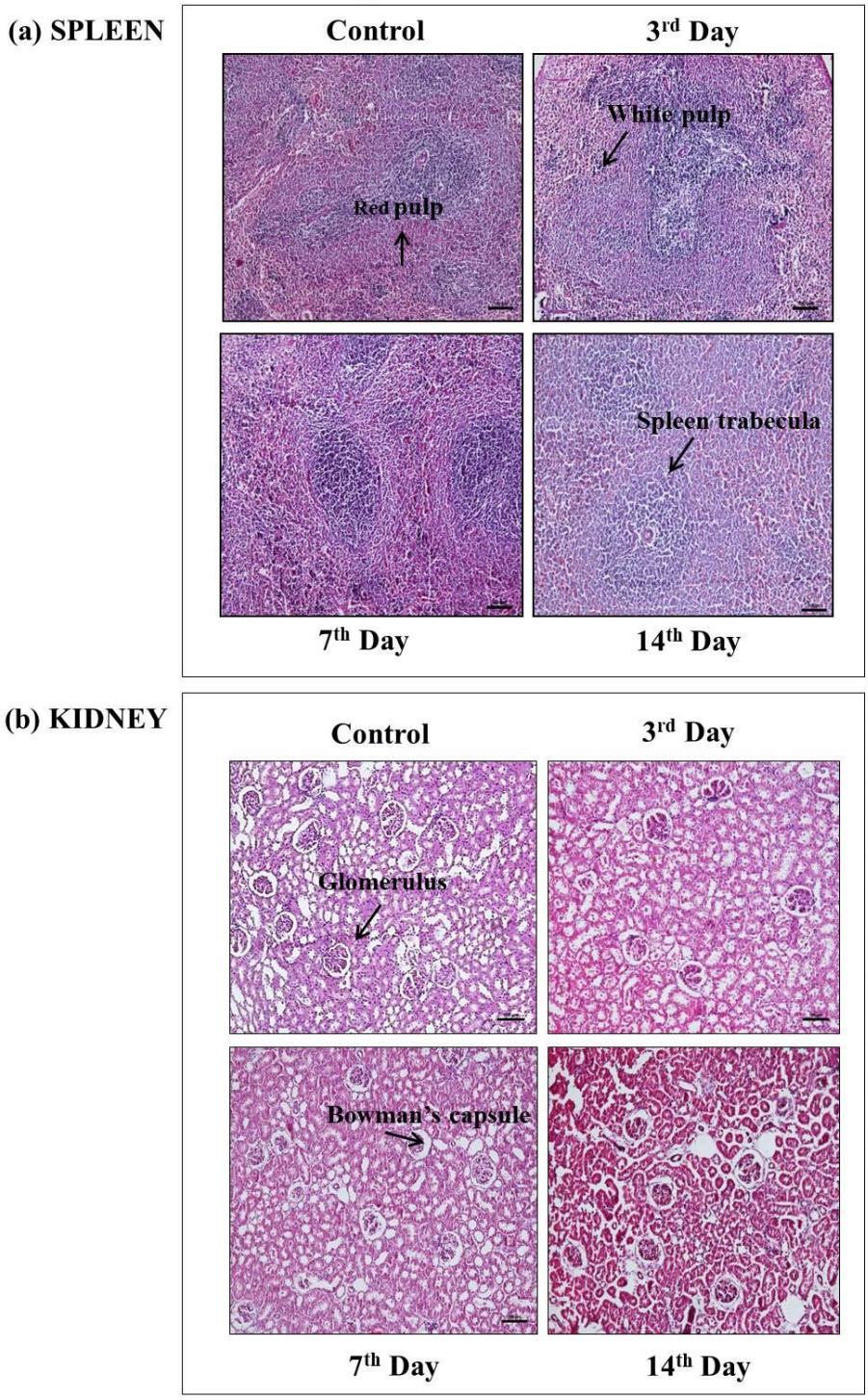

Figure 4.38 Histopathological evaluation for tissue samples from Wistar rats exposed with TNT-P. (a) Spleen, (b) Kidney. Magnification: 10X, Scale bar: 100µm.

CHAPTER 5. DISCUSSION

5. DISCUSSION

5.1 SYNTHESIS AND PHYSICO – CHEMICAL CHARACTERIZATION OF TiO_2 NANOTUBES

5.1.1 SYNTHESIS OF TNTs AND BIO-POLYMER COATING

TNTs were synthesized via two-phase chemical reactions in which TNPs were synthesized in Phase-1 via the urea precipitation method and TNTs were synthesized by the solvo thermal route. Urea precipitation is considered one of the appropriate synthesis methods since it allows the formation of homogenously dispersed nanoparticles of TiO_2. Also, it provides the advantages of nominal involvement of hazardous chemicals and does not require sophisticated fabrication equipments (Di Paola *et al*., 2008). Moreover, the precipitation method surpasses other synthesis methods which all involve certain drawbacks such as expensive precursors, longer processing time, presence of impurities like carbon, *etc*. The process hence promises highly controlled synthesis of TNPs through a simple bottom-up approach (Gupta *et al*., 2012). Phase-II involved the phase transformation of TNPs into nanotubes through a modest route of synthesis based on the pH of the reaction system. Solvo thermal treatment of precursor TNPs under an alkaline atmosphere and subsequent acid washing underlies the formation of characteristic nanotubular morphology followed by nanosheet formation. Acid washing is a crucial step as it determines the phase transformation by the replacement of Na+ ions from the nanosheets. The present study employed this very efficient synthesis method for TNTs and annealed the material at an optimum temperature of 400°C for obtaining highly suitable tubular morphology (Zavala *et al*., 2017).

Based on the available literature, TNTs synthesized via solvothermal route are considered the most reproducible approach in the context of biomedical application procedures. Nevertheless, contradictory research outputs are still coming up regarding the crystallinity of TNTs raised by solvothermal route and the influence of annealing temperature. Some reports suggest that a temperature range of above 400-500°C compromises the nanotubular stoichiometry of TNTs. In addition, precise control over the concentration of H+ ions in the reaction system also plays a crucial role and requires high throughput screening (Mostafa *et al*., 2015). To ensure increased dispersion stability and application potential of TNTs, the present study evaluated the

efficiency of P-F127 as a surface coating agent for TNTs in both *in vitro* and *in vivo* levels. Enhanced performance of TNTs after surface modifications using other components have also been reported. For example, modified surface of TNTs elicited enhanced performance in solid state dye-sensitized solar cells and improved photocatalytic removal of perfluorooctanoic acid (PFOA) after silver coating (Tian *et al*., 2017). Studies have proved the capability of P-F127 as a safe, biodegradable drug carrier for several therapeutic strategies with high potential. Enhanced biocompatibility and protection against particle aggregation make it an excellent coating agent for nanomaterial for various biomedical application strategies (Horváti *et al*., 2018). Toxicity evaluation of TNT-P in the present study is considered a valid piece of information to be noted before performing any biomedical procedures.

5.1.2 PHYSICO-CHEMICAL CHARACTERIZATION

TNPs and TNTs were physico-chemically characterized in terms of hydrodynamic diameter, surface charge, surface morphology and size, functional groups, crystallinity, thermal stability and molecular organization using various techniques. Surface coating of TNTs was characterized using FT/IR spectroscopy for the presence of P-F127.

5.1.2.1 Dynamic Light Scattering (DLS)

The hydrodynamic size and respective polydispersity index (PDI) of TNPs were estimated using the DLS method. Both of these parameters were obtained in two different dispersion media including distilled water and PBS. The change in hydrodynamic size in each of these dispersion media can be attributed to the varying ionic composition and hence the type of adhering molecules on the surface of the nanoparticles. With increasing ionic composition, the colloidal medium tends to form a network of repulsive particles and this repulsive force will induce the NPs to center inside a cage formed by neighbouring NPs. This contributes to an elevation in DLS size (Suttiponparnit *et al*., 2011). Here, PBS possesses higher media concentration than distilled water. This caused an increasing hydrodynamic diameter for TNPs in the order PBS > Distilled water. Correspondingly, an increase in heterogeneity of the media resulted in high PDI values in a similar order. DLS measurement for TNTs produces a challenge as the agglomeration tendency of the NTs is higher than TNPs due to the characteristic morphology and this creates difficulty in achieving single NT suspension.

Moreover, most of the therapeutic procedures employing TNTs require them to be in a stable suspension rather than in powder form (Yamamoto *et al*., 2009). Therefore the study preferred size estimation of nanotubes using TEM over DLS in order to obtain measurements in dry form.

5.1.2.2 Zeta potential Analysis

The surface charge of TNPs was determined by zeta potential analysis. The potential measurement is directly proportional to the stability of the prepared NPs in suspension. The net surface charge of TNPs was observed to be +12.9 mV and hence indicates heightened internalization potential across biological membranes. Studies have proved passive diffusion of cationic NPs through the lipid bilayer of cell membranes and thereby achieving enhanced *in vivo* responses. In addition, the cationic surface charge of NPs induces their rapid clearance from circulation. A potential magnitude of above 10mV denotes the considerable level of dispersion stability of NPs. (Blanco *et al*., 2015).

5.1.2.3 Fourier Transform Infrared Spectroscopy (FT/IR)

Functional groups of TNPs after urea precipitation were analyzed using FT/IR technique. Consistency in those functional groups after phase transformation into TNTs was also monitored. Characteristic peaks for TNPs were identified from the FT/IR peaks at 3415.6 cm^{-1}, 1634.9 cm^{-1}, and 587.4 cm^{-1}. These peaks correspond to various functionalization of oxygen present in TNPs. The first peak at 3415.6 cm^{-1} can be assigned to the O-H stretching mode contributed by the H-bonded surface water molecule (Yuan *et al.*, 2004). The peak at 1634.9 cm^{-1} corresponds to the bending vibration of O-H bonds from water molecules on the surface of titania. The final major peak at 587.4 cm^{-1} can be ascribed to the stretching mode of the Ti-O covalent bond. This step further confirmed the clear formation of TiO_2 and was found to be stable up to the final processing of the material (Gao *et al*., 2009). The third major peak was of high intensity and suggested a defined double bonding between Ti and oxygen in the TiO_2 lattice. The IR peaks of TNTs confirmed consistency in the parent functional groups identified for TNPs even after phase transformation. Peaks were identified at comparable positions to that of TNPs. The absence of any peaks contributed by NaOH or HCl used during TNT synthesis justifies the excellent purity of the material via repeated washing after synthesis (He *et al*., 2013).

5.1.2.4 X-Ray Diffraction (XRD)

The crystallographic phases of TNPs were evaluated by the XRD technique. Diffraction angle (2θ) values for each peak were noted and respective crystalline phases were identified. X-ray measurements at angles 25.26°, 36°, 37.67°, 47.98°, 62.04°, 68.66°, and 74.82° corresponded to the anatase phase of TNPs and were confirmed to be dominated over remaining peaks for the rutile phase. The sharp Bragg's peaks obtained for the analysis can be attributed to the distinct crystallinity of the material rather than its amorphous nature. This confirms the effectiveness of the calcination step at 400°C conducted after the synthesis of TNPs (Yan *et al*., 2015). From the XRD pattern, the material was confirmed to be a heterogeneous mixture of anatase and rutile phases. High-temperature calcination favours the crystalline growth of NMs and this explains the minor transformation of TNPs from one phase to another. Also, the high purity of the material was confirmed by a negligible range of background noise in the XRD plot. Pronounced dehydration will occur on the surface of TNPs at high-temperature calcination, which will assist more active sites in getting exposed. Comparison with JCPDS XRD peaks confirmed the purity and accuracy of the crystalline phases (Saikumari *et al*., 2021). Phase transition was checked using Micro Raman spectroscopy as it provides more reliable information than XRD in this context.

5.1.2.5 Micro Raman Spectroscopy

Raman spectra are considered one of the reliable techniques for the evaluation of material purity and molecular structural identification of metal oxide NMs like TiO_2 (Banfield *et al.,* 1991). This explains the phase identity and phase transitions of nanostructured materials. For the present study, a Raman spectrum was used as a significant tool for the identification of phase transition from TNPs to TNTs. For TNPs, peaks at 146 (Eg), 194 (Eg), 394 (Eg), 514 (Eg), and 636 (Eg) reveal the anatase phase of TiO_2. A single peak at position 791 (Eg) corresponds to the rutile phase. This observation can be correlated well with the information from XRD analysis. The sharp edges of the peaks and their pattern of distribution explain the precision of the molecular arrangement. The absence of objectionable peaks confirms the chemical purity of the material. Raman spectrum of TNTs was found to be comparable to that of TNPs and a slight broadening of the peaks is generally possible due to the alteration of material morphology from one form to another. Ramakrishnan *et al*., in 2020 have proposed

that such a shift in diffraction spectra towards higher wavelength can be strongly attributed to the photon confinement effect. Consistency of the material crystallinity after phase transformation from TNPs to TNTs was hence confirmed from Micro Raman spectroscopy [Ramakrishnan *et al*., 2020].

5.1.2.6 Transmission Electron Microscopy (TEM)

Surface topography, morphology, and the size of TNPs and TNTs were analyzed using the TEM method. The surface of TNPs was observed to be roughly spherical and possessed an average diameter of 22nm. A comparable size range was obtained for TNTs (24.6nm), which explains the precise control over the rolling up of individual nanosheets formed in the alkaline phase to tubes after acid wash (Arruda *et al*., 2015). The formation of tube geometry is based on the exfoliation of the TiO_2 crystalline phase in a highly alkaline environment and stabilized Ti-O-Na+ bonds. Heterogeneously distributed hollow nanotubular structures were noted for TNTs under high magnification of TEM. Excellent uniformity in terms of tubular diameter was noticed for TNTs irrespective of the heterogenous distribution. Alteration in material size from DLS measurement to TEM imaging justifies the fact that TEM size accounts for the actual size of the NM core; whereas DLS size depicts a cumulative measure of the water layer and the material together (Yoshida *et al*., 2005).

5.1.2.7 Thermo Gravimetric Analysis (TGA)

Thermal stability and associated weight loss of TNPs and TNTs were determined using the TGA technique. Both of the materials showed high thermal stability up to the maximum given temperature of 700°C. As per the literature, a temperature beyond this range can elicit a significant loss of material properties, including crystalline destruction (Elgh *et al*., 2014). Initially, a negligible amount of weight loss was noticed for both of the TiO_2 nanostructures below 130°C and can be attributed to the loss of moisture content absorbed during synthesis. The second point of weight loss was obtained at 245.4°C and 417.38°C for TNPs and TNTs respectively. These points correspond to the dehydroxylation step in which H^+ ions were added to –OH groups on the respective material surface. Therefore it indicates progressive dehydration of hydroxyl groups over a range of temperatures (Chakraborty *et al*., 2014). Final weight loss was obtained at 583.21°C for TNPs and 685.46°C for TNTs, suggesting phase transformation from anatase to rutile. A comparatively heightened thermal stability was noted

for TNTs than TNPs in which a final non-degraded amount of TNPs and TNTs were 82.41°C and 92.66°C respectively. This can be assigned to the varying reaction conditions, precursors and the type of chemical reaction followed for the synthesis. For TNTs, synthesis was started from purely crystalline anatase TNPs under a highly alkaline atmosphere. Stronger ionic interaction with Na^+ ions during this stage contributed well to the strengthening of the TNT crystalline lattice. This has caused the generation of a highly stable hollow nano-tubular structure. TNPs in contrast, were synthesized from an inorganic precursor under mild reaction conditions and exhibited relatively lower thermal stability (Zhu *et al*., 2018).

5.1.2.8 Differential Thermal Analysis (DTA)

Specific chemical reactions associated with temperature fluctuations were analyzed using the DTA method for TNPs and TNTs. A major exothermic peak was noticed for both of the materials below 100°C immediately after the beginning of the procedure. According to the literature, this point corresponds to an exothermic reaction associated with the loss of organic matter remaining on the material surface (Zoccal *et al*., 2010). This thermal reaction aligns well with the first thermal degradation obtained for TGA. For TNPs, a clear endothermic reaction occurred at 174.90°C and this suggests the removal of physisorbed water molecules from their surface (Ying *et al*., 2003). A noticeable thermal reaction was then not obtained after this time point for both TNPs and TNTs and hence can be attributed to the chemical stability of the materials.

5.1.2.9 FT/IR Spectroscopy for surface coating

FT/IR is an effective technique for the analysis of the surface coating of nanomaterials. This technique counts for the basic functional group changes occurring after events of chemical transformations (Poliskie *et al*., 2008). For the present study, the surface coating of TNTs using P-F127 was evaluated using FT/IR spectroscopy. The IR spectra of bare TNTs, P-F127, and TNT-P were compared for the identification of surface coating. TNTs possessed characteristic peaks at positions; 1641 cm^{-1} (O-H bending) and around 435cm^{-1} (Ti-O covalent bond). P-F127 is a non-ionic biopolymer that has been reported to promote the solubilization of insoluble compounds in physiological media (Wu *et al*., 2012). Major peaks identified for P-F127 were; 2883.58cm-1 (C-H bond), 1342.46cm-1 (O-H bending), 1060.85cm-1 (bending C=O) and 960.48cm-1 (bending C=H). Effective surface coating of TNTs was confirmed from the

presence of major characteristic peaks from TNTs (at 450cm^{-1} corresponding to Ti-O covalent bond) and P-F127 (at 2883.58cm-1 for C-H bond, 1641cm-1 for O-H bending, 1342.46 cm-1 for O-H bending, 1060.85 cm-1 for C=O bending, and 840.86 cm-1 for C=H bending). The broadness of the Ti-O bond in TNT-P demonstrated the strong chemical interaction between TNTs and P-F127. Such a novel approach by the present study agrees with the observation by Ali-Boucetta *et al.*, (2011) in a cytotoxicity study involving the surface coating of carbon nanotubes (CNTs) by P-F127 [Ali-Boucetta *et al*., 2011].

5.2 *IN VITRO* TOXICITY OF TiO_2 NANOTUBES USING C6 GLIAL CELLS

Glial cells are a heterogeneous group of immune regulatory cells in the nervous system and hence represent an ideal *in vitro* model for neurotoxicity studies. Toxic anomalies of an agent can be addressed well with this large population of cells with extreme reliability (Jäkel *et al*., 2017). Physico-chemical properties of such agents, including NMs play an inevitable role in determining the extent of toxicity. Many recent studies have shown that morphology and surface-modifying agents can be of extreme importance in this context (Favi *et al*., 2015). In objective 2 of the present study, *in vitro* toxic response of nanostructured TiO_2 was evaluated using C6 glial cells. The influence of nano TiO_2 morphology and an innovative concept of P-F127 coating on NTs were scrutinized in terms of toxicity after short-term cellular exposure. The results of *in vitro* toxicity evaluation of the study are mainly discussed in the following sections. Major emphasis is given to the effects of TNPs and TNTs followed by a basic compatibility study of TNT-P in glial cells.

5.2.1. C6 GLIAL CELL CULTURE AND NANOMATERIAL EXPOSURE

C6 cells were grown in a T25 cell culture flask using DMEM F12 medium under proper incubation conditions. Complete neurite growth and a spindle-shaped morphology were obtained within 24h of incubation. This represents monolayer formation by C6 cells and it requires a prolonged time period for transforming into tumor cells. Studies have reported three distinct tumor growth phases of C6 cells related to their vascularization status: lag phase,

proliferative phase, and exponential phase. Glial cells have to be provided with proper growth factors in addition to a longer period of growth for attaining this tumor stage (Gross *et al*., 1990). In general, monolayers of immortal cell lines are regarded as suitable for examining NM toxicity as they retain the characteristics of the original tissue line during early passages (Panessa-Warren *et al*., 2006). For this reason, nanostructured TiO_2 was studied using a monolayer of C6 cells once it reached ~80% confluence. Nano TiO_2 was prepared in a range of concentrations in accordance with the information from certain major implant studies (Banaszkiewicz *et al*., 2014, Vamanu *et al*., 2008).

5.2.2 PHASE CONTRAST MICROSCOPY

Characteristic morphology of C6 cells before nano TiO_2 exposure was studied using phase contrast microscopy. The key benefit of this microscopy is that it makes possible the examination of live cell dynamics using high-contrast imaging and minute details of the specimen can be examined (Jaccard *et al*., 2014). Here, spindle-shaped morphology as well as the developed neurites was visible for the glial cell network under observation. This indicated the neuritic growth stage suitable for nanomaterial exposure.

5.2.3 IMAGING FLOW CYTOMETRY

The cellular uptake of TNPs was analyzed using imaging flow cytometry. The degree of SSC changes was monitored for each concentration of TNP exposed and compared with that of untreated control cells. Light scattering properties of TiO_2 aid their identification in cells via flow cytometry (Hewitt *et al*., 2017). A dose-dependent increase in particle uptake was evident from SSC pattern and can be attributed to the alteration in the distribution of TNPs as small individual aggregates in control cells and fine coarse aggregates in treated samples. A similar observation was obtained by [Zucker *et al*., in 2012]; for which dose-dependent selective uptake of TNPs was evident inside the perinuclear space, endoplasmic reticulum, and the Golgi apparatus of retinal epithelial cells. Studies suggest that an increase in the SSC can be well correlated with increased granularity in cells and hence can be a measure of the degree of granulation. For instance, [Salzman *et al*., 1999] have used elevated granularity as an indication

of WBCs (granulocytes) and detected them using flow cytometry. Despite of NP's size, the type of source material also determines the degree of light scattering and identification in flow cytometry. For example, metallic NPs like gold, silver, titanium, *etc*. possess exceptionally high light scattering properties and thereby can be easily identified. This can be associated with the surface plasmon resonance property of these NMs (Aaron *et al*., 2007). The conceivable explanation for the increase in SSC or decrease in FSC can be either reflection or absorption of incident laser light by TNPs and subsequent reduction in the quantum of light recorded at the forward scatter detector. The current study observed a fourfold increase in SSC for 160µg/ml than control cells. Comparable observation has previously been reported by [Suzuki *et al*., (2007)]; in which cells exhibited a fourfold increase in SSC for TNP concentrations around 200µg/ml than control cells. However, a satisfactory comparison between uptake studies cannot be made since the aggregation property of NPs including TNPs changes in accordance with the cell line, duration of exposure as well as instrument specifications.

5.2.4 MTT ASSAY

MTT assay has been accepted as one of the simplest and most highly reliable viability assays which rely on the mitochondrial metabolism of the cells. Colorimetric quantification of this assay product allows the determination of nanomaterial toxicity limits (Makino *et al*., 2008). Cytotoxicity and carcinogenicity of TNPs have previously been investigated based on MTT assay with consistent results in many cell lines (Zhao *et al*., 2009). Current study results have shown that TNPs and TNTs were inducing a significant toxicity in C6 cells ≥160µg/ml within 24h. However, [Coccini *et al*., (2015)] have reported a comparatively higher cytotoxic response of anatase TiO_2 nanopowder (15nm) in human astroma cells (D384). For the study mentioned, a 25% reduction in viability was observed from 31µg/ml dose onwards and reached a 60% reduction for 250µg/ml. This can be attributed to the method of synthesis and the chemicals used. The pronounced cytotoxic response of TNPs in PC12 neuronal cells was reported recently by [Punitha *et al*., (2020)] for which 50% viability reduction was observed at 31.2-62.5µg/ml. Considering TNTs, the present study observed 81.34% viability at 160µg/ml and agreed with the result by [Hong *et al*., (2012)]; wherein 85.73% viability was retained by TNTs in colon cancer cell line (CT-26).

5.2.5 JC1 STAINING

Owing to the perturbed mitochondrial enzyme activity observed in the MTT assay, JC1 staining was performed for the confirmation of TNP and TNT-induced MMP damage. Recognition of mitochondrion as a 'target' of NM toxicity is a recent development which requires special attention. In agreement with the MTT assay, higher concentrations of TNPs and TNTs induced a drop in MMP and hence indicated mitochondrial damage. Similar results were shown by [Yu *et al*., (2017)] in a study evaluating the toxicity of anatase TNPs in macrophages and they proposed that the crystallinity of TNPs has a significant impact on their toxicity. This general concept of variation in MMP loss in accordance with TNP crystallinity was studied by De [Matteis *et al*., (2016)]. The current study aligns with this observation because the predominant crystalline phase identified from XRD analysis was anatase and this can be the underlying reason for the induced loss of MMP at higher concentrations. However, the mechanism of mitochondrial membrane damage by anatase TNPs is yet to be elucidated.

5.2.6 NRU ASSAY

Convergence of NMs upon endocytosis into selective intracellular loci including lysosomes leads to abruption of subcellular functionalities. Lysosomes are regarded as the most prominent cytoplasmic compartment of TNP sequestration and degradation. Such bio-persistence of nanomaterials can further stimulate autophagy and lysosomal dysfunctions; leading to cell death. The present study evaluated the lysosomal destructive effect of TNPs and TNTs within 24h and it was noticed that none of the materials were compromising lysosomal stability up to 160µg/ml. The varying lysosomal stability in the present study and the aforementioned study can be due to the difference in the size of TNPs and the type of cells under investigation. The higher size of TNPs can certainly lead to mechanical damage to lysosomes and loss of activity. In the meantime, the non-toxic response of TNPs in terms of lysosomal integrity has recently been reported by [Bermejo-Nogales *et al*., (2017)]. The study demonstrated that TNPs acted to preserve the lysosomal integrity of the hepatocellular carcinoma cell line (PLHC -1). These facts stipulate that TNPs can compromise lysosomal activity depending on their size, type of

cell, and dosage. Morphology-dependent change in lysosomal activity was not observed as both TNPs and TNTs exhibited comparable effects in C6 cells.

5.2.7 ACRIDINE ORANGE (AO) STAINING

The usefulness of AO as a marker to detect acidic compartments of cells has been justified by the emission of reddish fluorescence upon selective binding. Potential risk assessment of NMs has proved that lysosomes constitute the most vulnerable cellular organelle for NM toxicity and has already been discussed in detail in previous sections. In order to confirm the adequacy of the NRU assay result, the present study employed a fluorescent staining method using AO for lysosomal stability screening. In conformity with the NRU assay, AO staining also proved consistent lysosomal integrity and stability after TNP and TNT treatment for 24h. This observation further confirms that cell viability loss obtained for the highest nano TiO_2 dose cannot be stated as lysosome driven, instead due to other cytotoxic events that occurred. Retention of red fluorescence up to 160µg/ml justifies this fact and is observed to be not affected by a change in the morphology of the material. A proportional increase in green fluorescence was not observed with an increase in TiO_2 concentration, which could otherwise have been regarded as a reduction in lysosomal stability (Verma *et al*., 2018). The lysosomal protective effect of TNPs was reported earlier by [Vevers *et al*., (2008)]; in which TNPs exhibited only negligible toxicity in the lysosome of goldfish skin cells. The retention of lysosomal activity after nano TiO_2 exposure denotes a minor probability of induced apoptosis caused by leakage of hydrolyzing enzymes from lysosomes.

5.2.8 CELLULAR MORPHOLOGY

5.2.8.1 Coomassie Brilliant Blue (CBB) Staining

Morphological changes associated with NM exposure are measured as one of the hallmark mechanisms of cytotoxicity. In general, these materials interact with specific plasma membrane components and gain entry into the cells mainly via endocytosis. Further intracellular fate of NMs depends on many factors such as; size and shape, surface charge, hydrophobicity, surface functionality, *etc*. (Behzadi et *al*., 2017). The present study evaluated the influence of TNPs on

glial cell morphology by the non-fluorescent CBB staining method. Signs of cytoplasmic shrinkage were evident at 160µg/ml TNPs whereas lower concentrations did not cause any observable change in morphology. The result agrees with the report by [Pandurangan *et al*., (2016)]; which investigated the therapeutic efficiency of TNPs against human cervical carcinoma cells. Necrotic cell death associated with condensed cellular cytoplasm was observed in another study evaluating TNP toxicity in phagocytic cells (Geiser *et al*., 2005). Studies suggest that this can arise from an irreversible alteration occurring in the cytoskeleton of cells after TNP exposure.

5.2.8.2 Giemsa Staining

Alteration in cellular structure with change in TNP morphology was assessed using Giemsa staining. The result indicates that, detectable levels of cytoplasmic shrinkage or any other morphological deviations were not observed at any of the TNT concentrations. Similar observation pointing non-interfering nature of TNTs has previously been reported by Magrez *et al*., in 2009. The study highlights the point that, NM morphology has a lesser impact on cellular morphology than other characteristic features.

5.2.9 RHODAMINE PHALLOIDIN STAINING

Fluorescent microscopy has several advantages over non-fluorescent techniques since it offers cellular imaging with multifold sensitivity, an occasion to stain specific cellular structures of interest. Moreover, it allows imaging of cells in both live and dead states. The present study used rRhodamine phalloidin fluorescent staining method to evaluate the magnitudes of TNP and TNT interaction with C6 cells. Comparable results with CBB and Giemsa stainings indicate that, 160µg/ml of TiO_2 in NP form elicit more structural changes with cytoskeleton including reduction in cytoplasmic volume than TNTs. Cellular nuclei at this concentration were visible as condensed and the organelle as tightly packed. Studies suggest that cytoplasmic shrinkage can be attributed to these nuclear condensation events which results in the spatial organization of highly ordered structures (Pandurangan *et al*., 2016).

In general, cytoplasmic shrinkage accompanies loss of metabolic contents, irregularity in mitochondrial organization and other organelle, high density of matrix, vacuolization as well as

accumulation of calcium salts *etc*. Metallic NPs like TNPs at higher concentrations can generate such cytotoxic signals and are regarded as signs of necrotic cell death (Mohammadinejad *et al*., 2019). Conversely, TNTs did not induce any morphology change with C6 cells and the actin filaments retained their normal structural organization. Such unidirectional cytoskeleton formation by actin filaments and proper lamellipodial growth was observed on TNT surface in a study by Brammer *et al*., (2008).

5.2.10 INTRACELLULAR OXIDATIVE STRESS

5.2.10.1 DCFH-DA Assay

Acellular factors such as size, shape, surface charge, and functionalization of NPs can lead to intracellular oxidative stress, whereas cellular responses such as mitochondrial respiration, activation of immune cells *etc.* can generate oxidative damage to cells. The present study evaluated the potential of TNPs and TNTs in terms of ROS generation using DCFH-DA assay. Results confirmed induced ROS production after TNP exposure with a slightly higher magnitude than TNTs. As per literature, NMs originating from metallic precursors tend to lodge on cellular surfaces or sub-cellular organelle and stimulate oxidative stress signaling cascades. TNPs have proven to induce ROS generation in cells primarily via metal ion-catalyzed Fenton-type reactions (Buzea *et al*., 2007). Key aspects driving NP-induced ROS generations include; the presence of pro-oxidant functional groups on the reactive surface of NMs, redox cycling mechanisms by metal oxide NPs and direct cellular interactions. High bandgap possessed by TNPs (~3.2 eV) turns it to be a potent agent for photodynamic therapy (PDT) for cancers based on ROS generation (You DG *et al*., 2016). NP induced ROS generation is likely to be the contributing agent for mitochondrial damage via perturbation of electron transport chain (ETC), structural changes and activation of NAD(P)H enzyme system *etc*. Hence, ROS generation at higher doses of TNPs and TNTs can be the route of imbalanced MMP as observed in JC1 staining. The result aligns in proximity with the observation by Shukla *et al*., (2013). In addition to ROS generation, NPs are capable of causing RNS production based on many cellular and material characteristics.

5.2.10.2 Griess reagent Assay

Cell-based toxicity studies have revealed that, the determination of free radical generation such as ROS and RNS is relatively tedious since the half-life of such reactive entities is very short. The present study employed Griess reagent assay for the detection of RNS and results showed no evident production of RNS for both TNP and TNT exposure. However, a whole lack of RNS cannot be expected since there was a sign of oxidative stress via ROS generation as evident from the DCFH-DA assay. A probable intepretation for this observation is that, both anatase and rutile phases of TNPs exhibit Ti^{3+} substitution sites on their surface which can effectively scavenge nitrogen species such as Nitrogen dioxide ($\cdot NO_2$), nitrosoperoxycarbonate ($ONOOCO^{2-}$), dinitrogen trioxide (N_2O_3) *etc*. Moreover, the persistence of such scavenging action of TNPs was confirmed from the current study even after the phase transformation into TNTs (Fu *et al*., 2014). Nevertheless, TNP-induced RNS generation in small amounts has recently been reported by Feng *et al*., (2020).

5.2.11 LDH RELEASE ASSAY

LDH release is associated with cell membrane damage and subsequent cell death. Nanotoxicity studies rely on cytoplasmic release of LDH into extracellular matrix as a measure of cell death. Owing to the strong relationship between NP accumulation and cell damage, studies propose that, the phenomenon can be justified by a theory termed as 'proton sponge hypothesis. According to this theory, the cationic nature of a NP can impose a buffering action on cell membrane proton transport chains and can further results in unimpeded water influx into phagosomes. This develops an unusual pressure inside endosomes and ends up in rupture. Free-floating of cellular components as a result of endosomal rupture will cause structural damage to the cell membrane; through which LDH escapes (Boussif *et al*., 1995). However, this is not necessarily possible always like the present study reports. Herein, neither TNPs nor TNTs are capable of causing LDH efflux via the damaged cell membrane. This can be related with the fact that NPs possessing cationic surface charge with magnitudes of <20mV may not be capable of eliciting such a phenomenon and thus does not result in LDH release (Hussain *et al*., 1998). In another study, Jeng *et al*., (2006) reported a comparable observation of TNP toxicity

in which a detectable level of LDH release was not obtained up to the concentration of >200µg/ml.

5.2.12 AO/EtBR DUAL STAINING

Necrotic cell death by NMs can easily be identified by AO/EtBr method as it is extremely reliable and simply measurable. Here, the relative amount of live/dead cells after TNP exposure was measured via AO/EtBr staining and evidence of a progressive increase in cell death was noticed at higher concentration of TNPs. Live cells were stained green, whereas damaged or dead cells have selectively taken up PI and emitted red fluorescence. This observation aligns well with the cell viability results of TNPs as mentioned earlier in this chapter (Section 5.2.4). Injured or dead cells showed evidence of chromatin condensation from the high intensity region of PI and agree with the results of CBB and actin staining.

5.2.13 CALCEIN AM/PI STAINING

Relative amounts of live and dead cells in TNT-exposed cells were analyzed using Calcein AM/PI staining. Viability was indicated as the ratio of Calcein (green) and PI (red) fluorescence from live and dead cells respectively. Comparable with cell viability assays and other toxicity assays mentioned earlier in this chapter, induced cell death at higher concentrations of TNTs was noticed in Calcein AM/PI staining. A similar observation of induced cell death was identified for TiO_2 nanofibers in an implant study by Wang *et al*., (2020).

5.2.14 DNA LADDERING ASSAY

The absence of bands for genetic DNA isolated from TNP and TNT-exposed cells indicated non-interference of the materials with cellular DNA in terms of fragmentation. The characteristic band size of the DNA strands was retained (10,000bp) in both cases. This indicates that, neither TNPs nor TNTs are capable of inducing pro-apoptotic signals including genomic DNA disintegration. Also, the observation confirms the inactivity of intracellular ROS produced upon post TiO_2 exposure on nuclear integrity. In other words, this can be justified by the high efficiency of DNA repair mechanisms in glial cells (Punitha *et al*., 2020).

5.2.15 DAPI STAINING

The consequences of TNP exposure on the entire nuclear compartment were analyzed using DAPI staining. As per the result obtained, TNPs caused chromosome condensation at middle and highest tested concentrations compared to the control. Current study does not have a straight indication on direct interaction of TNPs with chromatin as a cause of condensation, instead it can be considered as evidence of genotoxicity resulting from TNPs. Reports are available on similar observations in which TNPs strictly compromise nuclear stability with the execution of micronuclei, chromatin condensation *etc*. (Wang *et al*., 2015). Such an appearance of condensed chromatin toward the nuclear periphery suggests apoptotic cell death, which may accompany cell shrinkage and translocation of membrane phospholipids towards cell membrane outer leaflet.

5.2.16 IN VITRO TOXICITY STUDIES FOR TNT-P

5.2.16.1 MTT Assay

MTT assay was used for the cell viability evaluation of C6 cells post TNT-P exposure. The cytotoxicity limit of bare TNTs was found to be significantly lowered compared to control values. Facilitated non-covalent conjugation with polymers and subsequent reduction in cytotoxicity by nanotubes has previously been reported by Vardharajula *et al*., (2020). Moreover, polymer functionalization can markedly improve the dispersion stability and improved biocompatibility of nanotubes such as CNTs, TNT *etc*. Improved cell viability for TNT-P can be attributed to the synergistic effect of P-1F127 and TNTs in flaunting more active sites for selective binding and thereby improved proliferation of glial cells. This modified surface of TNTs can effectively immobilize certain biomolecules including enzymes which can remarkably nourish cell growth and differentiation (Smolinske *et al*., 1990).

The surface coating method adopted for the present study falls in the category of dipping method for nanomaterial functionalization. Upon mixing of TNTs and P-F127 under a suitable atmosphere, there would be an electrostatic interaction between negatively charged surface of P-F127 and oppositely charged TiO_2 surface. This further aids the formation of a uniform layer of P-F127 around TNTs. Moreover, being less expensive and a simpler approach, dip coating allows surface coating of nanomaterials without requiring sophisticated equipments (Oliveira *et*

al., 2017). Considering improved dispersion stability and significantly improved cell viability, TNT-P is likely to be a recommendable material for neurotherapeutic applications.

5.2.16.2 Effects of P-F127 on C6 cell viability

Interference of P-F127 with the assay reagents and the compatibility on C6 cells were evaluated using MTT assay after direct cellular exposure with the polymer. The assay mimicked all the experimental conditions of cytotoxicity study for bare as well as coated TNTs. Significant improvement in cell proliferation was noted compared to control cells. This can be a reflection of modified mitochondrial enzymatic activity including the action of oxidoreductase. This way, polymer exposure significantly activated oxidoreductase enzyme and thus caused high colorimetric readings than the control. Moreover, lower to middle concentrations of P-F127 mimicked the action of a growth factor that binds with cell surface receptors and stimulated cellular proliferation rate. Relatively lower cell viability at higher concentrations of P-F127 can be possible by the interference of this polymer with cell signaling pathways and consequent reduction in viability. However, every selected concentrations of P-F127 caused significantly higher viability than the control value (Jeng *et al*., 2006).

5.2.16.3 NRU Assay

Cell viability for TNT-P with C6 cells was confirmed using NRU assay. In comparison with cytotoxicity results of bare TNTs, cell viability was markedly improved up to the highest concentration. This agrees with the observation of MTT assay aforementioned in section 5.2.16.1 and can be attributed to the enhanced showcasing of bioactive receptor sites for the binding of cellular neuritic outgrowths. By merging this observation and the improved cell proliferation upon P-F127 exposure, it is well obvious that, improved cell viability at higher concentrations of TNT-P is resulting from modified enzymatic activity by P-F127 and availability of more active sites on nanomaterial surface (Hall *et al*., 1986).

5.2.16.4 DCFH-DA Assay

Reactive radical generation is one of the most important hallmarks of NM toxicity. Implant technology experiences oxidative stress related impairment of tissue homeostasis and hence requires functionalized nanomaterials with anti-oxidant activity. Upon confirmation of reduced cytotoxicity, the present study evaluated ROS generation limits of TNT-P using DCFH-DA assay. According to the results, TNT-P possesses remarkable free radical scavenging action

within 24h of exposure. Anti-oxidant activity of functionalized TNTs have previously been reported by Chen *et al*., (2020); wherein silver functionalized TNTs could significantly reduce ROS generation in macrophages. This can be explained by the modified anti-oxidant enzymatic pool in C6 cells after TNT-P exposure. Similar ROS scavenging activity of drug loaded TNTs was reported by Gao *et al*., 2019.

5.3 *IN VIVO* EXPERIMENTS FOR ACUTE TOXICITY RESPONSE OF TNT-P

Acute toxic response of TNT-P was assessed using Wistar rats over a period of 14 days from the day of administration. Wistar rats were used for the study since they offer smaller size and high survival rate. They share approximately $1/4^{th}$ of the genetic constitution of humans and hence the study results can be correlated well with human counterparts in every aspect. Rats were intraperitoneally administered with 10mg/Kg of TNT-P as it represents the recommended dose for most of the clinical applications. Studies have identified that nano forms of TiO_2 should be administered with a dose of ≤10mg/Kg in order to minimize metabolic changes or tissue damage in animals. Dose beyond this level can elicit histopathological changes with many more adverse physiological effects in Wistar rats (Smital *et al*., 2020).

5.3.1 BEHAVIORAL CHANGES

All of the experimental animals were checked for any altered behavioral changes after TNT-P administration and none of them showed any noticeable changes during visual examination. Clinical signs including lacrimation, salivation, excretion, piloerection, motor activity, home cage posture and rearing were the major parameters checked and all of them were found to be comparable with that of control group. The result suggests that, a single dosage of TNT-P did not elicit any toxic effects on animal behavior within a 14 days window period. However, reports are available on induced emotional behavior changes including increased anxious index in rats post TNP exposure and attributed to the oxidative damage occurring in rat CNS (Younes *et al*., 2015).

5.3.2 BODY WEIGHT

Body weight of TNT-P treated Wistar rat was evaluated prior to sacrifice on all observation days. A time-dependent increase in body weight was noticed until the 14^{th} day and a significant value was also noted compared to control on final day of observation. The result can either be correlated with normal body growth with time or it can be a characteristic feature of single or multiple organ damage. For example, Heinrich *et al*., in 1995 has witnessed a significant increase in rat lung weight after respiratory exposure with ultrafine TNPs. This can be related to severe metabolic changes in animal tissues and concomitant decline in intestinal absorption. However, in the present study, a conclusive statement on such a time-dependent body weight increase cannot be drawn at this time. As a justification, additional experiments have been performed and are discussed in detail in the rest of the chapter.

5.3.3 ORGAN WEIGHT

Wet weight of four organs (brain, liver, spleen & kidneys) from sacrificed animals were obtained and plotted. It was observed that, the liver showed a time-dependent increase in weight compared to control. This point can be related to body weight increment as mentioned in the previous section. Since all of the tested organs except the liver did not show a noticeable change in terms of weight, whole body weight increment can probably resulted from liver weight gain. As per reports, significant liver weight change is possible with altered expression of oxidative stress markers as well as pro-inflammatory cytokine production in response to TiO_2 exposure. Inflammatory response outweighs in this context and contributes to the generation of reactive lymphocytes and other inflammatory markers (Interleukin-1α or IL-1α, Interleukin-4 or IL-4, Tumour Necrosis Factor or TNF *etc*.) [Chen *et al*., (2019)]. In order to confirm an induced hepatic toxicity, several other assays were also performed and are discussed in the following sections.

5.3.4 HEMATOLOGY

Hematology analysisis generally considered as the most sensitive and reliable measure of pathological anomalies in animals as well as humans. Here, **s**acrificed animals were subjected to hematology analysis using blood collected from optical sinus. Main parameters analyzed were; RBC, WBC, HGB, HCT, MCV, MCH, MCHC& platelet count. Toxic consequences of nano forms of TiO_2 have not systematically been elucidated yet. However, evidence for TiO_2-induced hematological changes are available after intragastric administration in mice (Duan *et al*., 2010). Current study noted a significant change in HCT & MCV values compared to control on 7^{th} day of observation. This situation reverted back to normal on 14^{th} day of study. Reduction in HCT suggests disturbed erythropoiesis or inhibition of heme synthesis in rat body. Another probable route for lower HCT can be due to unusual destruction of erythrocytes in circulation or respective organs of origin. Such destruction can be possible from the free radical generation caused by TNT-P. Simultaneous increase in MCV on 7^{th} day denotes TNT-P induced swelling of erythrocytes or macrocytic anemia; both are the mostly identified validation for opposite trends in HCT & MCV measures in challenged rats (Grissa *et al*., 2015). Absence of any toxic signs in platelet count denotes non-interference of TNT-P with blood cloating phenomenon for 14 days of study. Hence the experiment confirms significant alteration in certain hematology parameters on 7^{th} day of observation after i.p administration of TNT-P to Wistar rats.

5.3.5 SERUM BIOCHEMISTRY

Biochemical indices are considered as one of the relevant clinical toxicity indications. Alteration of biochemical parameters, hepatic and renal toxicity in Wistar rats was evaluated using serum biochemistry study. Metabolic enzymes such as ALT, AST and ALP are regarded nowadays as the key markers of hepatotoxicity. These enzymes are originated mainly from liver, heart, RBC, pancreas, kidneys, biliary ducts and some other minor bodily tissues. Plasmatic levels of these enzymes elevate once there is a liver or cardiac tissue damage occurs. In the current study, a significant increase in ALT and AST values on 7^{th} day of observation can be attributed to TNT-P induced hepatic damage. Orazizadeh *et al*., (2014) reported similar hepatic damage in male Wistar rats after mixed exposure of rutile and anatase phases of TNPs.

Similarly, increased ALP levels represent possibilities of biliary duct obstructions, intrahepatic cholestasis, infiltrative hepatic disorders or bone diseases. Thus, the simultaneous increase in ALT, AST and ALP levels here clearly indicate hepatocellular injury within 7 days of TNT-P exposure. Kidney functions were scrutinized from serum uric acid and creatine levels and did not show any noticeable evidence of nephrotoxicity up to 14th day of exposure.

5.*3.6 ANTIOXIDANTS IN BRAIN AND LIVER*

NM exposure can induce selective inhibition of anti-oxidant enzymes and hence elicit oxidative stress in animal tissue. Considering total protein in tissues, free radicals including ROS generation can lead to oxidation of free amino acid and thereby release of mitochondrial oxygen radicals in an uncontrollable manner. This oxygen radical surge can cause oxidative damage in respective tissues. The present study demonstrated an increase in total protein levels in both brain and liver on 3rd day after TNT-P administration. This can arise from acute inflammatory or inflammation reaction induced by the nanomaterial (Adeyanju *et al*., 2022). NMs have been identified to be an inducer of redox state misbalancing in cells; either through accelerated generation of ROS or direct enzymatic damage to anti-oxidant pool in tissues. GSH represents one of the major antioxidant enzymes in almost every cell in the animal body and plays a key role in maintaining a balanced redox state in cells. In the current study, the level of GSH increased in a time dependent manner and reached a significantly higher value on 14th day than the control group. This indicates that cells exhibited a defense mechanism against oxidative stress induced by TNT-P, so as to protect the cellular components from deterioration (Sies *et al*., 1984).

LPO is one of the hallmark features of NM- induced oxidative damage in cells. It has been reported that TNPs can result in cytotoxic as well as genotoxic effects in male Wistar rats; for which oxidative stress was identified to be the root cause of the phenomenon. Levels of lipid peroxidase in the mentioned study was increased and resulted in fertilizing potential of the spermatozoa (Meena *et al*., 2015). However, present study did not observe a remarkable change in levels of lipid peroxidation neither in brain, nor in the liver. This can possibly be attributed to the protective effect of P-F127 on the surface of TNTs; which could effectively prevent the oxidative damage of lipid chains.

5.3.7 URINE ANALYSIS

The present study evaluated the effect of TNT-P exposure on various urine parameters in Wistar rats. Almost every evaluated parameter remained unaltered for all the observation days compared to the control group. The urine did not have any traces of blood or any other relevant components. Slight increase in urine pH was noted on 3rd and 7th days; which may occur from the renal capture of circulating TNT-P during the initial days following i.p. administration. Comparable observation has previously been reported by Escárcega *et al*., (2015). Hence, urine analysis for the present study confirms that, TNT-P did not elicit a toxic effect with major urinary parameters and hence the primary renal functions of Wistar rats.

5.3.8 BIODISTRIBUTION BY ICP-MS

ICP-MS comprises one of the reliable quantitative methods for the study of the biodistribution of NMs. It offers a high level of sensitivity, selectivity and a high degree of precision in determining the amount of various elements in tissue samples. In the present study, biodistribution pattern and relative amounts of TNT-P in major organs (brain, liver and kidney), blood, urine and fecal matter of Wistar rats was evaluated using ICP-MS on 3rd, 7th and 14th day of observation. The results revealed that, increased distribution of TNT-P was observed in liver and brain on the 3rd and 7th days. This signifies that, the liver constitutes the first line of defense against any nanomaterial invasion; similar to the entry of any other xenobiotics or foreign entities. Fastened hepatic uptake of TNT-P can be due to the presence of specific sub-population of mononuclear phagocytic cells in the liver; which fall under the category of reticulo-endothelial system (RES). Foremost member of this RES in liver includes Kupffer cells which selectively sequester NPs from circulation (Johnston *et al*., 2010). Another justification for hepatic distribution of TNT-P can be due the specific activation of metallothioneins; which plays a key role in detoxification of heavy metal oxide NPs.

The higher distribution of TNT-P in brain regions clearly highlights the conserved ability of TNPs to cross BBB even after phase transformation. Reports are available on specific upregulation of structural and functional genes in the brain including claudin 5, ocluudin *etc*.,

and following modification of BBB to bypass TNPs (Brun *et al*., 2012). Moreover, a reduction in TNT-P levels in both brain and liver on 14^{th} day of observation and concomitant increase in urine and fecal matter suggests gradual removal from each tissue without long term accumulation. Amount of TNT-P from kidneys also supports this fact of time-dependent elimination of the material from rat body. Thus from a kinetic point of view, TNT-P exhibited suitable translocation property from major tissues and well-framed elimination through body fluids within 14 days of exposure.

5.3.9 IMMUNOTOXICITY

Splenocyte proliferation assay demonstrates NM-induced, cell-mediated immune response in animal body based on lymphocyte activation. Splenocytes include a mixed population of WBCs situated in the spleen; which primarily perform defensive action against invading pathogen or nanomaterial. Mainly such splenic cells include; T lymphocytes, B lymphocytes, macrophages, dendritic cells *etc*. Upon association with foreign antigens, splenic concentration or proliferation rate of such cells will shoot up unusually and hence can be considered like a marker of immune response. The present study reports a time-dependent increase in proliferation of splenocyte, which was evident from the incorporation of [^{3}H] - thymidine into naïve DNA strands of proliferating cells. The rate of clonal expansion was directly proportional to the amount of radiolabelled nucleotide incorporation. Overall assay indicates that, time-dependent activation of rat immune system for the effective elimination of TNT-P from animal body. A comparable observation was obtained in another study in which immune activation of *in vivo* animal were observed after nano TiO_2 administration (Moon *et al*., 2011).

5.3.10 HISTOPATHOLOGY

Acute toxic response upon TNT-P exposure to Wistar rats was assessed in terms of histopathological changes after staining of isolated organs such as brain, liver, spleen and kidney using H&E method. According to the results obtained, relatively higher level of pathological lesions, portal and lobular infiltration with inflammatory cells and granulation was observed in the liver than in other tissues. This observation aligns in proximity with the results

of increased serum levels of ALT and AST as well as antioxidant amounts in the liver. As mentioned in section 5.3.3., time-dependent increase in wet weight of liver during the very initial stage of the study can be correlated well with these pathological changes. Comparable reports are available and justify such pathological changes with hydropic degeneration, cloudy swelling in response to exposed nanomaterial with time (Alarifi *et al*., 2013). None of the other tissues, including brain, spleen, and kidney showed any alterations with innate architecture even up to 14 days of exposure.

CHAPTER 6. SUMMARY AND CONCLUSION

6. SUMMARY AND CONCLUSION

6.1 SUMMARY

Metal and metal oxide NPs are gaining immense attention among researchers because of their potential applications in various therapeutic procedures. TiO_2 comprises one among the leading members of this category owing to their unique characteristic features to be applied in innumerable medical and non-medical scenarios. Wider applications in food industry, cosmetic industry, solar cells, paper, plastic and rubber industries, wastewater treatment, construction, agriculture and sericulture *etc*. have turn them to be an obligatory NM in public sector. Considering different one dimensional forms, nanotubular forms of TiO_2 (TNTs) are of extreme significance in healthcare applications. TNTs possess unique level of (photo)-electrochemical and photocatalytic properties, low cost and wide-ranging fabrication procedures. Some attractive medical applications of TNTs can be itemized as in bone implants, cardiovascular stents, biosensors, brain tumors, dental implants; to name a few. Despite of such long list of advantageous therapeutic applications, safety limits or toxicity range of TNTs should also be addressed. Although toxicity reports are being flourished for TNPs, a comprehensive report on that of TNTs is currently underway. In view of such a scenario, the present study addressed a detailed evaluation of *in vitro* as well as acute *in vivo* toxic consequences of TNTs. The study delivers a worthwhile toxicity report which can be taken into consideration before medial application procedures involving TNTs.

Nanosafety evaluations decisively rely on the cell type opted for *in vitro* studies; in which most of them involve cancerous cell lines because of the prevailing advantages in many aspects. As per scientific indications, neuronal tissue encompasses the principal regulatory unit of a living body and also regarded as greatly vulnerable to nanomaterial exposure and toxicity. Owing to the specific neuronal applications of TNTs in brain tissue (for *e.g*. as intravascular stent) and the influence of NM morphology on toxicity profile, the present study aimed to address *in vitro* toxicity of nanoparticle and nanotubular forms of TiO_2 in C6 glial cells. The study was initiated with the synthesis of TNPs via urea precipitation method (Phase I) followed by their conversion into TNTs via solvo thermal route. Both morphological forms of nano TiO_2 were physico-chemically characterized using different sophisticated techniques such as DLS, TEM,

FT/IR, XRD, Micro Raman spectroscopy, TEM, TGA and DTA. As an intention to improve the dispersion stability and thereby the application potential of TNTs, surface coating approach was taken for TNTs using a biopolymer Pluronic-F127 (P-F127) using a suitable coating method. The surface coating efficiency was evaluated using FT/IR technique and was confirmed from the presence of characteristic peaks in coated form of TNTs (TNT-P).

A comparative *in vitro* toxicity profiling was performed for TNPs and TNTs using cultured C6 glial cells after 24h exposure. Characteristic glial cell morphology was checked for the cultured cells using phase contrast microscopy. A plethora of *in vitro* experiments were conducted based on various cellular functions as toxicity markers. Prior to the experiments, cellular uptake of TNPs was confirmed using imaging flow cytometry; for which increase in side scatter was observed depending on TNP concentration indicated dose dependent internalization of TNPs. Cell viability evaluation was initially performed using MTT assay based on mitochondrial enzymatic activity. Cell viability was observed to be reduced for both TNPs and TNTs at 160µg/ml compared to the control. The viability response was confirmed using fluorescent imaging technique using JC1 probe and reduction in viability was seen for the highest tested concentration. Viability in terms of lysosomal integrity was then evaluated using neutral red uptake (NRU) assay and similar observation was seen in which; 160µg/ml induced cell death for both TNPs and TNTs. AO staining was done for ensuring the NRU assay result and a significant loss of lysosomal instability was not observed even at the highest concentration.

Alteration in cellular morphology after TNP and TNT exposure was evaluated using Coomassie brilliant blue (CBB) and Giemsa stainings respectively. TNP treated cells showed signs of cytoplasmic shrinkage in a concentration-dependent manner, which was absent in the case of TNTs. Cytoskeletal stability or actin filament organization was then confirmed using Rhodamine phalloidin staining. Similar signs of cytoplasmic shrinkage were observed for TNP treated cells and hence indicated structural damage at higher concentration of 160µg/ml. Intracellular oxidative stress upon TNP and TNT exposure of glial cells was analyzed using DCFH-DA and Griess reagent assays which account for the generation of ROS and RNS species respectively. Results revealed that TNP exposure results in a significant increase in ROS levels at higher concentrations of 80 &160µg/ml. TNT induced significantly higher ROS levels for 160µg/ml concentration alone. Meanwhile, both of the materials were not found to be

causing intracellular RNS generation up to the concentration of 160µg/ml. Intact glial cell membrane integrity was confirmed post treatment of both TNPs and TNTs for every dose using LDH release study.

Necrotic cell death pathway for TNP exposed cells was evaluated by means of the AO/EtBr dual staining method. According to the results, TNPs were found to be inducing necrotic cell death at the highest concentration; which was evident from the higher red fluorescence emitted by PI from damaged cells. For TNT exposure, live/dead cell count was obtained both quantitatively and qualitatively using calcein AM/PI staining. Similar to cell viability outcomes, TNTs were found to be inducing cell death at the highest concentration, as evident from the increasing PI fluorescence obtained. Interference of TNPs and TNTs with nuclear integrity of glial cell population was analyzed using DNA laddering assay by agarose gel electrophoresis. Interestingly, no laddering was obtained for any of the treated concentrations for either of the materials; hence confirming unbroken DNA strand without any fragmentation. Nevertheless, signs of chromatin condensation were observed for higher concentration of TNPs, as apparent from higher intensity of DAPI in aforementioned condensed areas.

Dispersion stability of TNTs was markedly improved after P-F127 exposure and did require bath sonication before cellular exposure and hence represents a stable suspension for medical applications. Cytotoxic levels of TNT-P was evaluated initially by MTT assay and compared with that of unmodified TNT exposure. Cytocompatibility of TNTs was observed to be remarkably improving after P-F127 coating than unmodified TNTs under similar exposure conditions. Such a condition can be attributed to the synergistic effect of the polymer and TNT surface in presenting more active sites for better cell proliferation and growth. This was further supported by the cell growth promoting nature of P-F127 through MTT assay for glial cell exposure with polymer alone. Cell viability response for TNT-P was then confirmed through NRU assay and obtained similar results. Induced oxidative stress via intracellular ROS generation after TNT exposure was observed to be diminishing via DCFH-DA assay after P-F127 coating. This further confirmed improved cytocompatibility of the NM than its bare form.

An *in vivo* acute biocompatibility study for TNT-P was evaluated using Wistar rats after intraperitoneal exposure (10mg/Kg body weight) for 14 days. Animals were sacrificed on the 3rd, 7th and 14th day after TNT-P administration and various *in vivo* toxicity experiments were performed. Experimental animals were routinely screened for any signs of behavioral changes by home cage observation. No signs of behavioral changes were observed including lacrimation, salivation, excretion, piloerection, motor activity, home cage posture and rearing compared to the unexposed control group. Body weight of all animals was noted before sacrifice and time dependent normal body growth was observed. Wet weight of major organs such as the brain, liver, spleen and kidneys were noted. All the organs except the liver did not show any significant deviation in weight compared to the control group. Blood samples collected from optical sinus from every animal were used for hematology analysis for different parameters like RBC, WBC, HGB, HCT, MCV, MCH, MCHC & platelet count. Significant deviation in HCT and MCV values were noted on the 7th day, without any change for any other parameters.

Biochemical indices were evaluated as a marker of hepatic and renal toxicity in Wistar rats. Serum was collected from blood samples and analyzed for ALT, AST and ALP levels. Significant elevation in values of ALT, AST and ALP was noticed on the 7th day of observation and indicates TNT-P induced hepatic damage. Renal toxicity was checked by taking measures of creatinine and uric acid levels, and both of them did not show a noticeable change and hence indicates intact kidney functioning. Antioxidant titer of brain and liver tissues was studied from the levels of relevant oxidative stress markers such as total protein, GSH and LPO levels. Significant increase in protein and GSH measures was noted in a time-dependent manner; without any change in LPO levels. The results were found to be similar for both brain and liver. Urine analysis was conducted by checking the values of various parameters such as leukocyte, nitrite, urobilinogen, protein, pH, blood, specific gravity, ketone bodies, bilirubin and glucose. All of the parameters showed stable values for all the observation days, with a slight increase in pH for 3rd and 7th days.

The biodistribution pattern of TNT-P was studied using ICP-MS in major organs like the brain, liver, and kidneys; in addition to urine, blood and fecal matter. Major distribution of the material was observed for brain and liver on the 3rd and 7th days. 14th day showed a declined

value and concomitant increase in the level of the material in urine and fecal matter. This points out to the effective clearance of TNT-P from tissues and circulation without long terms accumulation. Apart from this, immune activation of rat body in response to TNT-P exposure was evaluated from splenocyte proliferation assay. Time-dependent increase in splenocyte activation clearly indicates induced activation of splenic cells including lymphocytes. Finally, histopathological signs in major tissues such as brain, liver, spleen and kidneys were studied using H&E staining. According to the observation, no marked pathological lesions were obtained for all tissues except liver. Liver showed significant pathological indications such as portal and lobular infiltration with inflammatory cells and granulation. This observation agrees with the acute toxic signs obtained in previous assays conducted. Hepatic damage from the 3rd day of observation was the only pathological feature evident from H&E staining.

6.2 METHODOLOGY ADAPTED FOR THE STUDY

- Synthesis of two different morphological forms of nano TiO_2 via two phase procedures. First phase includes synthesis of TNPs using urea precipitation method and second phase includes solvothermal synthesis of TNTs.
- In Phase-1, TNPs were synthesized from a metal halogenic precursor ($TiCl_4$) without using many hazardous chemicals. Dried and calcined TNPs were physico-chemically characterized before converting into TNTs.
- Major characterization techniques used for TNPs were: DLS, Zeta potential analysis, FT/IR, TEM, XRD, Micro Raman spectroscopy, TGA and DTA.
- TNTs after solvothermal synthesis were also characterized properly using required techniques like TEM, FT/IR, Micro Raman spectroscopy, TGA and DTA.
- Surface coating was provided for TNTs for improving their dispersion stability and compatibility using a bio-polymer (P-F127) via a suitable coating procedure.
- Polymer coating efficiency on TNTs was evaluated using FT/IR technique.
- *In vitro* toxicity studies were conducted in C6 glial cells. For that, cells were cultured in DMEM F12 medium supplied with 10% FBS.
- Cellular uptake of TNPs into glial cells was confirmed using imaging flow cytometry.

- Cytotoxicity of TNPs and TNTs were evaluated initially by treating the cells with varying concentrations of each material prepared in DMEMF12 (for 24h), after bath sonication for around 20min at RT.
- Cell viability was analyzed in terms of mitochondrial enzyme activity using MTT assay.
- Mitochondrial integrity after nanomaterial treatment was then confirmed using JC1 staining.
- Lysosomal activity analysis and thereby cell viability was checked using NRU assay and was confirmed by Acridine orange staining for both TNPs and TNTs.
- Cellular morphology changes were analyzed for TNP treated cells using CBB staining and those for TNT treated cells via Giemsa staining.
- Cytoskeletal integrity or actin filament organization was analyzed using Rhodamine phalloidin staining.
- Intracellular oxidative stress after TNP and TNT exposure was evaluated in terms of ROS and RNS production via DCFH-DA and Griess reagent assays respectively.
- Glial cell membrane integrity after cellular exposure with TNPs and TNTs was checked using LDH release assay.
- Live/dead cell levels or necrotic cell death were qualitatively estimated for TNP treated cells via AO/EtBr dual staining using fluorescence microscope.
- TNT exposed cells were subjected to live/dead cell count using Calcein AM/PI staining.
- Nuclear integrity of both TNP and TNT exposed cells was evaluated using DNA laddering assay via agarose gel electrophoresis method. Nuclear integrity was also confirmed using DAPI staining.
- Cell viability after exposure with surface coated TNTs (TNT-P) was detected using MTT assay. Similar procedure was repeated for cellular interaction of P-F127 alone under the same treatment conditions.
- Viability results for TNT-P was confirmed using NRU assay
- Intra cellular oxidative stress was performed for TNT-P interaction with glial cells using DCFH-DA assay.
- Acute toxicity of TNT-P was investigated in Wistar rats after exposing intraperitoneally for a period of 14 days (10mg/Kg body weight).

- Experimental animals were sacrificed on the 3rd, 7th and 14th days after administration and various toxicity studies were conducted. Control group of animals were injected with normal saline.
- Home cage observation of the animals was performed on each observation day prior to sacrifice for various clinical signs of behavioral changes.
- Body weight of all animals was noted prior to sacrifice for all animal groups on respective days.
- At the end of each observation day, urine, fecal matter, blood and major tissues (brain, liver, spleen and kidneys) were collected for further experiments.
- Blood samples were used for hematology and serum biochemistry evaluation
- Appropriately weighed brain and liver samples were used for anti-oxidant estimations.
- Urine samples were subjected to counting for various parameters using an automated counter.
- Immunotoxic response towards TNT-P was studied using splenocyte proliferation via [3H]-thymidine incorporation assay.
- Biodistribution of TNT-P in major organs (brain. Liver and kidneys), urine, blood and fecal matter samples was evaluated using ICP-MS technique.
- Histopathology analysis of collected organs (brain, liver, spleen and kidneys) was conducted using H&E staining.

6.3 MAJOR FINDINGS OF THE STUDY

- Two morphological forms of nano TiO_2 were synthesized via two-phase procedure.
- Nano-sized, homogenously dispersed TNPs and TNPs were synthesized using urea precipitation and solvo thermal methods respectively.
- Hydrodynamic diameter of TNPs showed an increasing trend depending on the dispersion medium used. Surface charge of TNPs was found to be +12.9.
- In FT/IR spectrum, both TNPs and TNTs exhibited major characteristic peak at positions 587.4cm^{-1}; which corresponds to the Ti-O bond.
- XRD indicated the presence of a mixture of two phases of TiO_2 (anatase & rutile); wherein, anatase dominated. Peaks were comparable with JCPDS database.

- Micro Raman spectroscopy indicated similar chemical composition for both TNPs and TNTs with comparable peaks corresponding to molecular system.
- Average diameter of below 25nm was confirmed for both TNPs and TNTs using TEM imaging. Nanoparticular and nanotubular morphology was also confirmed for each of the materials.
- Surface coating efficiency of TNTs using P-F127 was confirmed using FT/IR technique; in which TNT-P contained peaks from both TNTs and P-F127.
- Cellular uptake of TNPs was confirmed using imaging flow cytometry. Increase in side scatter indicated an increase in particle uptake in a dose dependent manner.
- MTT & NRU assays showed a slight reduction in cell viability for TNTs compared to TNPs. 160µg/ml induced a significant drop in cell viability for both TNPs & TNTs.
- MMP was negatively affected at 160µg/ml alone for both TNPs & TNTs.
- Lysosomal integrity was maintained for all the concentrations for both TNP & TNTs as evident from AO staining.
- Slight cytoplasmic shrinkage was observed for TNP exposed cells, whereas it was slightly seen in TNT exposed cells.
- Significant increase in ROS induced oxidative stress was observed for TNT exposed cells at 160µg/ml. TNP showed a reduction in ROS level at 160µg/ml.
- Cell membrane integrity was intact for both TNP & TNT treated cells as evident from LDH release study.
- Nuclear integrity was not at all affected for both TNPs & TNTs.
- Cell viability was increased markedly when TNTs were surface coated with P-F127.
- *In vivo* acute bio-nano interaction of TNT-P was carried out using Wistar rats at a dose of 10mg/Kg via i.p injection.
- All the animals were euthanized after 3rd, 7th & 14th days of observation period & various toxicity studies were performed.
- No alterations were seen in clinical / behavioral signs throughout the observation periods.
- Gross pathology was found to be normal & a non-significant increase in body weight was noted in a time dependent manner.
- Hematology parameters were normal except HCT showed significant reduction & MCV showed elevation on 7th day.

- Regarding antioxidant levels, protein level decreased on 14th day & GSH level increased. Lipid peroxidation did not alter significantly (liver & brain).
- Serum biochemistry confirmed increased ALT & AST levels on 7th day & increased ALP on 14th day.
- Urine parameters were normal for all the observation periods; except for a slight increase in pH on 3rd and 7th days.
- ICP-MS indicated higher biodistribution of TNT-P occurred mainly in liver and brain. Concomitant removal of the material was also confirmed from increased values on 14th day in excretory samples (urine & fecal matter).
- Increase in splenocyte proliferation was noted on 7th day.
- Pathological lesions were observed in liver on 3rd, 7th & 14th days.

6.4 CONCLUSION

Two morphological forms of nano sized TiO_2 were synthesized through appropriate methods. As first phase of synthesis, roughly round shaped TiO_2 (TNPs) NPs were synthesized via urea precipitation method and physico-chemically characterized using various sophisticated techniques such as DLS, Zeta potential analysis, FT/IR, TEM, XRD, Micro Raman spectroscopy, TGA and DTA. Second phase involved conversion of these TNPs into nanotubular TiO_2 via solvo thermal route and were properly characterized using FT/IR, TEM, Micro Raman spectroscopy, TGA and DTA. As an approach to improve the dispersion stability and to compare the increased biocompatibility, surface of TNTs was coated using a biopolymer, P-F127. *In vitro* neurotoxicity of TNPs and TNTs was evaluated in terms of cell viability, oxidative stress, morphology, organelle toxicity, enzymatic activity and nuclear integrity. As per the results, TNTs were found to be inducing slightly higher toxicity in glial cells without significantly affecting cellular functionalities. TNTs generated relatively higher intracellular ROS than TNPs at 160µg/ml. From the cell viability study conducted for TNT-P, it was evident that, surface coating of TNTs helps to disguise the toxic impacts displayed by TNTs in glial cells. Owing to the improved cytocompatibility, a detailed *in vivo* acute toxicity study was designed for TNT-P in Wistar rats. No alteration in clinical signs of behavioral changes was noted throughout the 14 days of observation. Hematology evaluation suggests signs of toxicity on the 7th day which caused deviations in values of HCT and MCV. Anti-

oxidant studies showed evidence of slight hepatic toxicity in a time-dependent manner. Serum biochemistry also supports time-dependent onset of slight hepatic damage. Biodistribution pattern from ICPMS shown that, the material was effectively removed from the rat body without undesirable accumulation. Histopathology analysis has shown signs of hepatic injury in a time-dependent manner; without affecting other tested organs (brain, spleen, and kidney). In a nutshell, the study presents a novel pluronic surface coating approach for TNTs and showed evidence for improved cytocompatibility in neuronal cells than their bare form. However, further repeated dose toxicity study would be required to declare TNT-P as a safe validated material for medical/clinical applications.

6.5 FUTURE DIRECTIONS

- Identification of cellular uptake routes for TNPs/TNTs/TNT-P.
- Identification of cell death pathway for the cellular interaction of TNPs/TNTs/TNT-P with neuronal cell line.
- Gene expression studies for polymer-coated TNTs for confirming non-toxic response.
- A comprehensive *In vivo* toxicity evaluation using repeated dose of TNT-P and associated target organ toxicity.
- Research on finding more compatible surface modification strategies for TNTs

REFERENCES

Aaron, Jesse S, Nitin N, Kort Travis, Sonia Kumar, Thomas G Collier, Park, Sun Yong Park, Yacaman, M.J., Coghlan, L., et al. (2007). Plasmon resonance coupling of metal nanoparticles for molecular imaging of carcinogenesis in vivo. *Journal of biomedical optics* 12(3): 034007.

Adeyanju, Anne A, Asejeje, F.O., Molehin, O.R., Owoeye, O., Olatoye, E.O. and Ekpo, E.N., (2022). Protective role of protocatechuic acid in carbon tetrachloride-induced oxidative stress via modulation of proinflammatory cytokines levels in brain and liver of Wistar rats. *Journal of Basic and Clinical Physiology and Pharmacology* 33(2): 143-154.

Alarifi, S., Ali, D., Al-Doaiss, A.A., Ali, B.A., Ahmed, M. and Al-Khedhairy, A.A., (2013). Histologic and apoptotic changes induced by titanium dioxide nanoparticles in the livers of rats. *International journal of nanomedicine* 8: 3937.

Albu, S.P., Ghicov, A., Macak, J.M., Hahn, R. and Schmuki, P., (2007). Self-organized, free-standing TiO_2 nanotube membrane for flow-through photocatalytic applications. *Nano letters* 7(5): 1286-1289.

Ali-Boucetta, H., Al-Jamal, K.T., Müller, K.H., Li, S., Porter, A.E., Eddaoudi, A., Prato, M., Bianco, A. and Kostarelos, K., (2011). Cellular Uptake and Cytotoxic Impact of Chemically Functionalized and Polymer-Coated Carbon Nanotubes. *Small* 7(22): 3230-3238.

An, Y., Tang, L., Jiang, X., Chen, H., Yang, M., Jin, L., Zhang, S., Wang, C. and Zhang, W., (2010). A photoelectrochemical immunosensor based on Au-doped TiO_2 nanotube arrays for the detection of α-synuclein. *Chemistry–A European Journal* 16(48): 14439-14446.

Arruda, L.B., Santos, C.M., Orlandi, M.O., Schreiner, W.H. and Lisboa-Filho, P.N., (2015).Formation and evolution of TiO_2 nanotubes in alkaline synthesis. *Ceramics International* 41(2): 2884-2891.

Athira SS, Prajitha N, Mohanan PV, (2018). Interaction of nanoparticles with central nervous system and its consequences.*American Journal of Research In Medical Sciences* 4(1) 1-32.

Bahadar, H., Maqbool, F., Niaz, K. and Abdollahi, M., (2016).Toxicity of nanoparticles and an overview of current experimental models. *Iranian biomedical journal* 20(1):1.

Banaszkiewicz, P.A., (2014). Metallic wear in failed titanium-alloy total hip replacements: A histological and quantitative analysis. *Classic Papers in Orthopaedics* 97:100.

Banerjee, S., Adhikari, E., Sapkota, P., Sebastian, A. and Ptasinska, S., (2020). Atmospheric Pressure Plasma Deposition of TiO_2: A Review. *Materials* 13(13): 2931.

Banfield, J.F., Veblen, D.R. and Smith, D.J., (1991). The identification of naturally occurring TiO_2 (B) by structure determination using high-resolution electron microscopy, image simulation, and distance-least-squares refinement. *American Mineralogist* 76(3-4): 343-353.

Bauer, S., Park, J., Faltenbacher, J., Berger, S., von der Mark, K. and Schmuki, P., (2009). Size selective behavior of mesenchymal stem cells on ZrO_2 and TiO_2 nanotube arrays. *Integrative Biology* 1(8-9): 525-532.

Behzadi, S., Serpooshan, V., Tao, W., Hamaly, M.A., Alkawareek, M.Y., Dreaden, E.C., Brown, D., Alkilany, A.M., Farokhzad, O.C. and Mahmoudi, M., (2017). Cellular uptake of nanoparticles: journey inside the cell. *Chemical Society Reviews* 46(14): 4218-4244.

Bermejo-Nogales, A., Connolly, M., Rosenkranz, P., Fernández-Cruz, M.L. and Navas, J.M., (2017). Negligible cytotoxicity induced by different titanium dioxide nanoparticles in fish cell lines. *Ecotoxicology and environmental safety* 138: 309-319.

Bernaerts, D., Amelinckx, S., Lambin, P. and Lucas, A.A., (1998).The diffraction space of circular and polygonized multishell nanotubules. *Applied Physics A: Materials Science & Processing 67*(1).

Blanco, E., Shen, H. and Ferrari, M., (2015). Principles of nanoparticle design for overcoming biological barriers to drug delivery. *Nature biotechnology 33*(9): 941-951.

Borenfreund, E. and Puerner, J.A., (1985). Toxicity determined in vitro by morphological alterations and neutral red absorption. *Toxicology letters*, 24(2-3): 119-124.

Boussif, O., Lezoualc'h, F., Zanta, M.A., Mergny, M.D., Scherman, D., Demeneix, B. and Behr, J.P., (1995). A versatile vector for gene and oligonucleotide transfer into cells in culture and in vivo: polyethylenimine. *Proceedings of the National Academy of Sciences* 92(16): 7297-7301.

Brammer, K.S., Oh, S., Gallagher, J.O. and Jin, S., (2008). Enhanced cellular mobility guided by TiO_2 nanotube surfaces. *Nano letters* 8(3): 786-793.

Bromley, S.T., de PR Moreira, I., Neyman, K.M. and Illas, F., (2009). Approaching nanoscale oxides: models and theoretical methods. *Chemical Society Reviews* 38(9): 2657-2670.

Brun, E., Carrière, M. and Mabondzo, A., (2012). In vitro evidence of dysregulation of blood–brain barrier function after acute and repeated/long-term exposure to TiO_2 nanoparticles. *Biomaterials* 33(3): 886-896.

Bryan, N.S. and Grisham, M.B., (2007). Methods to detect nitric oxide and its metabolites in biological samples. *Free radical biology and medicine* 43(5): 645-657.

Butler, W.L. and Wadleigh, C.H., (1987). Sterling Brown Hendricks. *Biographical Memoirs* 56:*56*.

Buzea, C., Pacheco, I.I. and Robbie, K., (2007). Nanomaterials and nanoparticles: sources and toxicity. *Biointerphases* 2(4):17-71.

Camilli, L., Pisani, C., Gautron, E., Scarselli, M., Castrucci, P., D'Orazio, F., Passacantando, M., Moscone, D. and De Crescenzi, M., (2014). A three-dimensional carbon nanotube network for water treatment. *Nanotechnology* 25(6): 065701.

Cartaxo, A.L.P., (2018). Nanoparticles types and properties–understanding these promising devices in the biomedical area. *International Journal of Nanomedicine* 1-8.

Chakraborty, A.K., (2014). Dehydroxylation Mechanism. In *Phase Transformation of Kaolinite Clay*, Springer, New Delhi. pp. 313-322. DOI: 10.1007/978-81-322-1154-9-25.

Chapman, R., Danial, M., Koh, M.L., Jolliffe, K.A. and Perrier, S., (2012). Design and properties of functional nanotubes from the self-assembly of cyclic peptide templates. *Chemical Society Reviews* 41(18): 6023-6041.

Chen, J., Dong, X., Xin, Y. and Zhao, M., (2011). Effects of titanium dioxide nano-particles on growth and some histological parameters of zebrafish (Danio rerio) after a long-term exposure. *Aquatic Toxicology* 101(3-4): 493-499.

Chen, Y., Crittenden, J.C., Hackney, S., Sutter, L. and Hand, D.W., (2005). Preparation of a novel TiO_2-based p− n junction nanotube photocatalyst.*Environmental science & technology* 39(5): 1201-1208.

Chen, Y., Guan, M., Ren, R., Gao, C., Cheng, H., Li, Y., Gao, B., Wei, Y., Fu, J., Sun, J. and Xiong, W., (2020). Improved immunoregulation of ultra-low-dose silver nanoparticle-loaded TiO_2 nanotubes via M2 macrophage polarization by regulating GLUT1 and autophagy. *International Journal of Nanomedicine* 15: 2011.

Chen, Z., Zhou, D., Han, S., Zhou, S. and Jia, G., (2019). Hepatotoxicity and the role of the gut-liver axis in rats after oral administration of titanium dioxide nanoparticles. *Particle and fibre toxicology* 16(1): 1-17.

Coccini, T., Grandi, S., Lonati, D., Locatelli, C. and De Simone, U., (2015). Comparative cellular toxicity of titanium dioxide nanoparticles on human astrocyte and neuronal cells after acute and prolonged exposure. *Neurotoxicology* 48: 77-89.

Cronemeyer, D.C., (1959). Infrared absorption of reduced rutile TiO_2 single crystals. *Physical review* 113(5): 1222.

Davoren, M., Herzog, E., Casey, A., Cottineau, B., Chambers, G., Byrne, H.J. and Lyng, F.M., (2007). In vitro toxicity evaluation of single walled carbon nanotubes on human A549 lung cells. *Toxicology in vitro* 21(3): 438-448.

De Gusseme, B., Sintubin, L., Baert, L., Thibo, E., Hennebel, T., Vermeulen, G., Uyttendaele, M., Verstraete, W. and Boon, N., (2010). Biogenic silver for disinfection of water contaminated with viruses. *Applied and Environmental Microbiology* 76(4): 1082-1087.

De Matteis, V., Cascione, M., Brunetti, V., Toma, C.C. and Rinaldi, R., (2016). Toxicity assessment of anatase and rutile titanium dioxide nanoparticles: The role of degradation in different pH conditions and light exposure. *Toxicology in vitro* 37: 201-210.

Di Giorgio, M.L., Di Bucchianico, S., Ragnelli, A.M., Aimola, P., Santucci, S. and Poma, A., (2011). Effects of single and multi-walled carbon nanotubes on macrophages: cyto and genotoxicity and electron microscopy. *Mutation Research/Genetic Toxicology and Environmental Mutagenesis* 722(1): 20-31.

Di Paola, A., Cufalo, G., Addamo, M., Bellardita, M., Campostrini, R., Ischia, M., Ceccato, R. and Palmisano, L., (2008). Photocatalytic activity of nanocrystalline TiO_2 (brookite, rutile and brookite-based) powders prepared by thermohydrolysis of $TiCl_4$ in aqueous chloride solutions. *Colloids and Surfaces A: Physicochemical and Engineering Aspects* 317(1-3): 366-376.

Dresselhaus, G., Dresselhaus, M.S. and Saito, R., (1998). *Physical properties of carbon nanotubes*.World Scientific Publishing, London.

Duan, Y., Liu, J., Ma, L., Li, N., Liu, H., Wang, J., Zheng, L., Liu, C., Wang, X., Zhao, X. and Yan, J., (2010).Toxicological characteristics of nanoparticulate anatase titanium dioxide in mice. *Biomaterials* 31(5): 894-899.

Ducker, W.A., Senden, T.J. and Pashley, R.M., (1991). Direct measurement of colloidal forces using an atomic force microscope. *Nature* 353(6341):239-241.

Elgh, B., Yuan, N., Cho, H.S., Magerl, D., Philipp, M., Roth, S.V., Yoon, K.B., Müller-Buschbaum, P., Terasaki, O. and Palmqvist, A.E., (2014). Controlling morphology, mesoporosity, crystallinity, and photocatalytic activity of ordered mesoporous TiO_2 films prepared at low temperature. *APL Materials* 2(11): 113313.

Escárcega González, C.E., Rodríguez Vázquez, M.L., Jaramillo Juárez, F., Martínez Ruvalcaba, H., Silva Briano, M., Adabache Ortíz, A. and Posadas del Río, F.A., (2015). The renal effects of a single and intravenous dose of titanium dioxide nanoparticles in adult male rats. *Revista mexicana de ciencias farmacéuticas* 46(1): 47-55.

Favi, P.M., Gao, M., Johana Sepúlveda Arango, L., Ospina, S.P., Morales, M., Pavon, J.J. and Webster, T.J., (2015). Shape and surface effects on the cytotoxicity of nanoparticles: Gold nanospheres versus gold nanostars. *Journal of Biomedical Materials Research Part A* 103(11): 3449-3462.

Feng, Q., Li, Y., Wang, N., Hao, Y., Chang, J., Wang, Z., Zhang, X., Zhang, Z. and Wang, L., (2020). A biomimetic nanogenerator of reactive nitrogen species based on battlefield transfer strategy for enhanced immunotherapy. *Small* 16(25): 2002138.

Ferancová, A., Ovádeková, R., Vaníčková, M., Šatka, A., Viglaský, R., Zima, J., Barek, J. and Labuda, J., (2006). DNA-Modified Screen-Printed Electrodes with Nanostructured Films of Multiwall Carbon Nanotubes, Hydroxyapatite and Montmorillonite. *Electroanalysis: An International Journal Devoted to Fundamental and Practical Aspects of Electroanalysis* 18(2): 163-168.

Flygare, M. and Svensson, K., (2019). Quantifying crystallinity in carbon nanotubes and its influence on mechanical behaviour. *Materials Today Communications* 18: 39-45.

Francis, A.P. and Devasena, T., (2018). Toxicity of carbon nanotubes: A review. *Toxicology and industrial health* 34(3): 200-210.

Fu, Peter P., Xia, Q., Hwang, H.M., Ray, P.C. and Yu, H., (2014). Mechanisms of nanotoxicity: generation of reactive oxygen species. *Journal of food and drug analysis* 22(1): 64-75.

Gao, Chenghao., Cheng, H., Xu, N., Li, Y., Chen, Y., Wei, Y., Gao, B., Fu, J., Huo, K. and Xiong, W., (2019). Poly (dopamine) and Ag nanoparticle-loaded TiO2 nanotubes with optimized antibacterial and ROS-scavenging bioactivities. *Nanomedicine* 14(7): 803-818.

Gao, T., Fjellvåg, H. and Norby, P., (2009). Crystal structures of titanate nanotubes: a Raman scattering study. *Inorganic chemistry* 48(4): 1423-1432.

Gao, X. and Matsui, H., (2005). Peptide-based nanotubes and their applications in bionanotechnology. *Advanced Materials* 17(17): 2037-2050.

Garcés, M., Cáceres, L., Chiappetta, D., Magnani, N. and Evelson, P., (2021). Current understanding of nanoparticle toxicity mechanisms and interactions with biological systems. *New Journal of Chemistry* 45(32): 14328-14344.

Geim, A.K. and Novoselov, K.S., (2010). The rise of graphene. *Nanoscience and technology: a collection of reviews from nature journals*: 11-19.

Geiser, M., Rothen-Rutishauser, B., Kapp, N., Schürch, S., Kreyling, W., Schulz, H., Semmler, M., Hof, V.I., Heyder, J. and Gehr, P., (2005). Ultrafine particles cross cellular membranes by nonphagocytic mechanisms in lungs and in cultured cells. *Environmental health perspectives* 113(11): 1555-1560.

Gerischer, H. and Tributsch, H., (1968). Elektrochemische Untersuchungen zur spektralen Sensibilisierung von ZnO-Einkristallen. *Berichte der Bunsengesellschaft für physikalische Chemie* 72(3): 437-445.

Ghicov, A., Albu, S.P., Macak, J.M. and Schmuki, P., 2008. High-Contrast Electrochromic Switching Using Transparent Lift-Off Layers of Self-Organized TiO_2 Nanotubes. *Small 4*(8): 1063-1066.

Ghorbanpour, M. and Hadian, J., (2015). Multi-walled carbon nanotubes stimulate callus induction, secondary metabolites biosynthesis and antioxidant capacity in medicinal plant Saturejakhuzestanica grown in vitro. *Carbon* 94: 749-759.

Granqvist, C.G. and Buhrman, R.A., (1976). Ultrafine metal particles. *Journal of applied Physics* 47(5): 2200-2219.

Grissa, I., Elghoul, J., Ezzi, L., Chakroun, S., Kerkeni, E., Hassine, M., El Mir, L., Mehdi, M., Cheikh, H.B. and Haouas, Z., (2015). Anemia and genotoxicity induced by sub-chronic intragastric treatment of rats with titanium dioxide nanoparticles. *Mutation research/genetic toxicology and environmental mutagenesis* 794: 25-31.

Gross, J.L., Morrison, R.S., Eidsvoog, K., Herblin, W.F., Kornblith, P.L. and Dexter, D.L., (1990). Basic fibroblast growth factor: a potential autocrine regulator of human glioma cell growth. *Journal of neuroscience research* 27(4): 689-696.

Gupta, S. and Tripathi, M., (2012). A review on the synthesis of TiO_2 nanoparticles by solution route. *Open Chemistry* 10(2): 279-294.

Hall, A.H., Smolinske, S.C., Conrad, F.L., Wruk, K.M., Kulig, K.W., Dwelle, T.L. and Rumack, B.H., (1986). Ibuprofen overdose: 126 cases. *Annals of emergency medicine* 15(11): 1308-1313.

Han, Y.K., Lee, T.G., Yom, S.S., Son, M.H., Kim, E.K., Min, S.K. and Lee, J.Y., (1998). Comparison between TiO_2 thin films on InP and GaAs substrates by metalorganic chemical vapor deposition. *Journal of the Korean Physical Society* 32: 1697-1699.

He, Z., Que, W., Chen, J., He, Y. and Wang, G., (2013). Surface chemical analysis on the carbon-doped mesoporous TiO_2 photocatalysts after post-thermal treatment: XPS and FTIR characterization. *Journal of Physics and Chemistry of Solids* 74(7): 924-928.

Heinrich, U., Fuhst, R., Rittinghausen, S., Creutzenberg, O., Bellmann, B., Koch, W. and Levsen, K., (1995). Chronic inhalation exposure of Wistar rats and two different strains of mice to diesel engine exhaust, carbon black, and titanium dioxide. *Inhalation toxicology* 7(4): 533-556.

Hewitt, R.E., Vis, B., Pele, L.C., Faria, N. and Powell, J.J., (2017). Imaging flow cytometry assays for quantifying pigment grade titanium dioxide particle internalization and interactions with immune cells in whole blood. *Cytometry Part A* 91(10): 1009-1020.

Hong, C., An, S., Son, M., Hong, S.S., Lee, D.H. and Lee, C., (2012). In-vitro cell tests using doxorubicin-loaded polymeric TiO_2 nanotubes used for cancer photothermotherapy. *Anti-Cancer Drugs* 23(5): 553-560.

Horváti, K., Gyulai, G., Csámpai, A., Rohonczy, J., Kiss, E. and Bősze, S., (2018). Surface Layer modification of poly (d, l-lactic-co-glycolic acid) nanoparticles with targeting peptide: a convenient synthetic route for Pluronic F127–Tuftsin conjugate. *Bioconjugate chemistry* 29(5): 1495-1499.

Hussain, S.M., Hess, K.L., Gearhart, J.M., Geiss, K.T. and Schlager, J.J., (2005). In vitro toxicity of nanoparticles in BRL 3A rat liver cells. *Toxicology in vitro* 19(7): 975-983.

Iijima, S. and Ichihashi, T., (1993). Single-shell carbon nanotubes of 1-nm diameter. *Nature* 363(6430): 603-605.

Jaccard, N., Griffin, L.D., Keser, A., Macown, R.J., Super, A., Veraitch, F.S. and Szita, N., (2014). Automated method for the rapid and precise estimation of adherent cell culture characteristics from phase contrast microscopy images. *Biotechnology and bioengineering* 111(3): 504-517.

Jackman, H., Krakhmalev, P. and Svensson, K., (2015). Mechanical behavior of carbon nanotubes in the rippled and buckled phase. *Journal of Applied Physics* 117(8): 084318.

Jäkel, S. and Dimou, L., (2017). Glial cells and their function in the adult brain: a journey through the history of their ablation. *Frontiers in cellular neuroscience* 11: 24.

Jeng, H.A. and Swanson, J., (2006). Toxicity of metal oxide nanoparticles in mammalian cells. *Journal of Environmental Science and Health Part A* 41(12): 2699-2711.

Johnston, H.J., Hutchison, G., Christensen, F.M., Peters, S., Hankin, S. and Stone, V., (2010). A review of the in vivo and in vitro toxicity of silver and gold particulates: particle attributes and biological mechanisms responsible for the observed toxicity. *Critical reviews in toxicology* 40(4): 328-346.

Kang, Q., Yang, L. and Cai, Q., (2008). An electro-catalytic biosensor fabricated with Pt–Au nanoparticle-decorated titania nanotube array. *Bioelectrochemistry* 74(1): 62-65.

Karousis, N., Tagmatarchis, N. and Tasis, D., (2010). Current progress on the chemical modification of carbon nanotubes. *Chemical reviews* 110(9): 5366-5397.

Kasibhatla, S., Amarante-Mendes, G.P., Finucane, D., Brunner, T., Bossy-Wetzel, E. and Green, D.R., (2006). Acridine orange/ethidium bromide (AO/EB) staining to detect apoptosis. *Cold Spring Harbor Protocols* 2006 (3). DOI: 10.1101/pdb.prot4493.

Kasuga, T., Hiramatsu, M., Hoson, A., Sekino, T. and Niihara, K., (1998). Formation of titanium oxide nanotube. *Langmuir* 14(12): 3160-3163.

Kim, T.W., Kleitz, F., Paul, B. and Ryoo, R., (2005). MCM-48-like large mesoporous silicas with tailored pore structure: facile synthesis domain in a ternary triblock copolymer− butanol− water system. *Journal of the American Chemical Society* 127(20): 7601-7610.

Kis, A., Mihailovic, D., Remskar, M., Mrzel, A., Jesih, A., Piwonski, I., Kulik, A.J., Benoît, W. and Forró, L., (2003). Shear and Young's moduli of MoS2 nanotube ropes. *Advanced materials* 15(9): 733-736.

Koch, C.C., (2006) *Nanostructured materials: processing, properties and applications*. William Andrew Publishers, New York.

Kostarelos, K., Lacerda, L., Pastorin, G., Wu, W., Wieckowski, S., Luangsivilay, J., Godefroy, S., Pantarotto, D., Briand, J.P., Muller, S. and Prato, M., (2007). Cellular uptake of functionalized carbon nanotubes is independent of functional group and cell type. *Nature nanotechnology* 2(2): 108-113.

Law, M., Goldberger, J. and Yang, P., (2004). Semiconductor nanowires and nanotubes. *Annual Review of Material Research* 34: 83-122.

Li, C., Shuford, K.L., Park, Q.H., Cai, W., Li, Y., Lee, E.J. and Cho, S.O., (2007). High-yield synthesis of single-crystalline gold nano-octahedra. *AngewandteChemie* 119(18): 3328-3332.

Lie, D.C., Colamarino, S.A., Song, H.J., Désiré, L., Mira, H., Consiglio, A., Lein, E.S., Jessberger, S., Lansford, H., Dearie, A.R. and Gage, F.H., (2005). Wnt signalling regulates adult hippocampal neurogenesis. *Nature* 437(7063): 1370-1375.

Linsebigler, A.L., Lu, G. and Yates Jr, J.T., (1995). Photocatalysis on TiO_2 surfaces: principles, mechanisms, and selected results. *Chemical reviews* 95(3): 735-758.

Lüdtke-Buzug, K., Biederer, S., Sattel, T., Knopp, T. and Buzug, T.M., (2009). Preparation and characterization of dextran-covered Fe_3O_4 nanoparticles for magnetic particle imaging. *4th European Conference of the International Federation for Medical and Biological Engineering, Springer, Berlin, Heidelberg. pp.*2343-2346. DOI: 10.1007/978-3-540-89208-3-562.

Lynam, C., Moulton, S.E. and Wallace, G.G., (2007). Carbon-nanotube biofibers. *Advanced Materials* 19(9): 1244-1248.

Macak, J.M., Zlamal, M., Krysa, J. and Schmuki, P., (2007). Self-organized TiO_2 nanotube layers as highly efficient photocatalysts. *Small* 3(2): 300-304.

Magrez, A., Horváth, L., Smajda, R., Salicio, V., Pasquier, N., Forro, L. and Schwaller, B., (2009). Cellular toxicity of TiO_2-based nanofilaments. *Acs Nano* 3(8): 2274-2280.

Makino, H., Emi, H., Yamaguchi, A., Iritani, E., Namiki, N., Myojo, T. and Yamamoto, K., (2008). Environmental and safety issues with nanoparticles, *Nanoparticle Technology*

Handbook, Elsevier Academic Press, Cambridge pp. 385-417. DOI: 10.1016/B978-044453122-3.50010-6.

Mansoori, G.A., (2005) *Principles of nanotechnology: molecular-based study of condensed matter in small systems*. Principles of Nanotechnology. World Scientific Publishing, Singapore.

Mansoori, G.A., (2015). *Energy: Sources, Utilization, Legislation, Sustainability, Illinois as Model State*. World Scientific Publishers, Illinois.

Mansoori, G.A., (2017). An introduction to nanoscience and nanotechnology. *Nanoscience and Plant–Soil Systems*, Springer Soil Biology Series, Chicago, pp. 3-20.

Marchand, R., Brohan, L. and Tournoux, M., (1980). TiO_2 (B) a new form of titanium dioxide and the potassium octatitanate K2Ti8O17. *Materials Research Bulletin* 15(8): 1129-1133.

Meena, R. and Kajal, K., (2015). Cytotoxic and genotoxic effects of titanium dioxide nanoparticles in testicular cells of male wistar rat. *Applied Biochemistry and Biotechnology* 175(2): 825-840.

Mirabolghasemi, H., Liu, N., Lee, K. and Schmuki, P., (2013). Formation of 'single walled'TiO_2 nanotubes with significantly enhanced electronic properties for higher efficiency dye-sensitized solar cells. *Chemical Communications* 49(20): 2067-2069.

Mohammadinejad, R., Moosavi, M.A., Tavakol, S., Vardar, D.Ö., Hosseini, A., Rahmati, M., Dini, L., Hussain, S., Mandegary, A. and Klionsky, D.J., (2019). Necrotic, apoptotic and autophagic cell fates triggered by nanoparticles. *Autophagy* 15(1): 4-33.

Moon, E.Y., Yi, G.H., Kang, J.S., Lim, J.S., Kim, H.M. and Pyo, S., (2011). An increase in mouse tumor growth by an in vivo immunomodulating effect of titanium dioxide nanoparticles. *Journal of immunotoxicology* 8(1): 56-67.

Morgado Jr, E., (2007). dr Abreu, MAS; Moure, GT; Marinkovic, BA; Jardium, PM; Araujo, AS Characterization of Nanostructured Titanates Obtained by Alkali Treatment of TiO_2-Anatases with Distinct Crystal Sizes. *Chemistry of. Materials* 19: 665-676.

Moriguchi, I., Ozono, A., Mikuriya, K., Teraoka, Y., Kagawa, S. and Kodama, M., (1999). Micelle-templated mesophases of phenol-formaldehyde polymer.*Chemistry Letters* 1999(11): 1171-1172.

Moron, M.S., Depierre, J.W. and Mannervik, B., (1979). Levels of glutathione, glutathione reductase and glutathione S-transferase activities in rat lung and liver. *Biochimica et biophysica acta (BBA)-general subjects* 582(1): 67-78.

Mosdam, T., (1983). Rapid colorimetric assay for cellular growth and survival: Application to proliferation and cytotoxic assay. *Journal of Immunological Methods* 65: 55-63.

Mostafa, N.Y. and El-Bahy, Z.M., (2015). Effect of microwave heating on the structure, morphology and photocatalytic activity of hydrogen titanate nanotubes. *Journal of Environmental Chemical Engineering* 3(2): 744-751.
Mun, K.S., Alvarez, S.D., Choi, W.Y. and Sailor, M.J., (2010). A stable, label-free optical interferometric biosensor based on TiO_2 nanotube arrays. *Acs Nano* 4(4): 2070-2076.

Murata, K., Kaneko, K., Kokai, F., Takahashi, K., Yudasaka, M. and Iijima, S., (2000). Pore structure of single-wall carbon nanohorn aggregates. *Chemical physics letters* 331(1): 14-20.

Nielsch, K., Choi, J., Schwirn, K., Wehrspohn, R.B. and Gösele, U., (2002). Self-ordering regimes of porous alumina: the 10 porosity rule. *Nano letters* 2(7): 677-680.
Ohkawa, H., Ohishi, N. and Yagi, K., (1979). Assay for lipid peroxides in animal tissues by acid reaction. *Analytical biochemistry* 95(2): 351-358.

Oliveira, W.F., Arruda, I.R., Silva, G.M., Machado, G., Coelho, L.C. and Correia, M.T., (2017). Functionalization of titanium dioxide nanotubes with biomolecules for biomedical applications. *Materials Science and Engineering: C* 81: 597-606.

Orazizadeh, M., Fakhredini, F., Mansouri, E. and Khorsandi, L., (2014). Effect of glycyrrhizic acid on titanium dioxide nanoparticles-induced hepatotoxicity in rats. *Chemico-biological interactions* 220: 214-221.

O'Regan, B., Schwartz, D.T., Zakeeruddin, S.M. and Grätzel, M., (2000). Electrodeposited Nanocomposite n–p Heterojunctions for Solid-State Dye-Sensitized Photovoltaics.*Advanced Materials* 12(17): 1263-1267.

Pandurangan, M., Enkhtaivan, G., Young, J.A., Hoon, H.J., Lee, H., Lee, S. and Kim, D.H., (2016). In vitro therapeutic potential of Tio2 nanoparticles against human cervical carcinoma cells. *Biological trace element research* 171(2): 293-300.

Pandurangan, M., Enkhtaivan, G., Young, J.A., Hoon, H.J., Lee, H., Lee, S. and Kim, D.H., (2016). In vitro therapeutic potential of Tio2 nanoparticles against human cervical carcinoma cells. *Biological trace element research* 171(2): 293-300.

Panessa-Warren, B.J., Warren, J.B., Wong, S.S. and Misewich, J.A., (2006). Biological cellular response to carbon nanoparticle toxicity. *Journal of Physics: Condensed Matter* 18(33):2185.

Paramasivam, I., Avhale, A., Inayat, A., Bösmann, A., Schmuki, P. and Schwieger, W., (2009). MFI-type (ZSM-5) zeolite-filled TiO_2 nanotubes for enhanced photocatalytic activity. *Nanotechnology* 20(22): 225607.

Park, J., Bauer, S., von der Mark, K. and Schmuki, P., (2007). Nanosize and vitality: TiO_2 nanotube diameter directs cell fate. *Nano letters* 7(6): 1686-1691.

Peng, L., Barczak, A.J., Barbeau, R.A., Xiao, Y., LaTempa, T.J., Grimes, C.A. and Desai, T.A., (2010). Whole genome expression analysis reveals differential effects of TiO_2 nanotubes on vascular cells. *Nano letters* 10(1): 143-148.

Peng, L., Eltgroth, M.L., LaTempa, T.J., Grimes, C.A. and Desai, T.A., (2009). The effect of TiO_2 nanotubes on endothelial function and smooth muscle proliferation.*Biomaterials* 30(7): 1268-1272.

Peng, L., Mendelsohn, A.D., LaTempa, T.J., Yoriya, S., Grimes, C.A. and Desai, T.A., (2009). Long-term small molecule and protein elution from TiO_2 nanotubes.*Nano letters* 9(5): 1932-1936.

Peterson, G.L., (1977). A simplification of the protein assay method of Lowry et al. which is more generally applicable. *Analytical biochemistry* 83(2): 346-356.

Poliskie, M. and Clevenger, J.O., (2008). Fourier transform infrared (FTIR) spectroscopy for coating characterization and failure analysis. *Metal finishing* 106(5): 44-47.

Popat, K.C., Eltgroth, M., LaTempa, T.J., Grimes, C.A. and Desai, T.A., (2007). Decreased Staphylococcus epidermis adhesion and increased osteoblast functionality on antibiotic-loaded titania nanotubes. *Biomaterials* 28(32): 4880-4888.

Popat, K.C., Leoni, L., Grimes, C.A. and Desai, T.A., (2007). Influence of engineered titania nanotubular surfaces on bone cells. *Biomaterials* 28(21): 3188-3197.

Pothukuchi, S., Li, Y. and Wong, C.P., (2004). Formulation of different shapes of nanoparticles and their incorporation into polymers. In *9th International Symposium on Advanced Packaging Materials: Processes, Properties and Interfaces,* Institute of Electric and Electronics Engineers, Atlanta, Georgia. *pp.*200-203.

Prasad, R., Pandey, R. and Barman, I., (2016). Engineering tailored nanoparticles with microbes. *Wiley Interdisciplinary Reviews: Nanomedicine and Nanobiotechnology* 8(2): 316-330.

Punitha, V.N., Vijayakumar, S., Sakthivel, B. and Praseetha, P.K., (2020). Protection of neuronal cell lines, antimicrobial and photocatalytic behaviours of eco-friendly TiO_2 nanoparticles. *Journal of Environmental Chemical Engineering* 8(5): 104343.

Pushkar, S., Philip, A., Pathak, K. and Pathak, D., (2006). Dendrimers: Nanotechnology derived novel polymers in drug delivery. *Indian Journal of Pharmaceutical Education and Research*, 40(3): 153.

Ramakrishnan, V.M., Muthukumarasamy, N., Balraju, P., Pitchaiya, S., Velauthapillai, D. and Pugazhendhi, A., (2020).Transformation of TiO_2 nanoparticles to nanotubes by simple

solvothermal route and its performance as dye-sensitized solar cell (DSSC) photoanode. *International Journal of Hydrogen Energy* 45(31): 15441-15452.

Reshma, V.G. and Mohanan, P.V., (2017). Cellular interactions of zinc oxide nanoparticles with human embryonic kidney (HEK 293) cells. *Colloids and Surfaces B: Biointerfaces* 157: 182-190.

Roy, P., Berger, S. and Schmuki, P., (2011). TiO_2 nanotubes: synthesis and applications. *Angewandte Chemie International Edition* 50(13): 2904-2939.

Sahay, R., Reddy, V.J. and Ramakrishna, S., (2014). Synthesis and applications of multifunctional composite nanomaterials. *International Journal of Mechanical and Materials Engineering* 9(1): 25.

Saikumari, N., Dev, S.M. and Dev, S.A., (2021). Effect of calcination temperature on the properties and applications of bio extract mediated titania nano particles. *Scientific Reports* 11(1): 1-17.

Salzman, G.C., (1999). Light scatter: detection and usage. *Current protocols in cytometry* 9(1): 1-13.

Saquib, Q., Al-Khedhairy, A.A., Siddiqui, M.A., Abou-Tarboush, F.M., Azam, A. and Musarrat, J., (2012). Titanium dioxide nanoparticles induced cytotoxicity, oxidative stress and DNA damage in human amnion epithelial (WISH) cells. *Toxicology in vitro* 26(2): 351-361.

Schneider, J., Matsuoka, M., Takeuchi, M., Zhang, J., Horiuchi, Y., Anpo, M. and Bahnemann, D.W., (2014). Understanding TiO_2 photocatalysis: mechanisms and materials.*Chemical reviews* 114(19): 9919-9986.

Seo, D.S., Kim, H., Jung, H.C. and Lee, J.K., (2003). Synthesis and characterization of TiO_2 nanocrystalline powder prepared by homogeneous precipitation using urea. *Journal of materials research* 18(3): 571-577.

Shi, H., He, X., Yuan, Y., Wang, K. and Liu, D., (2010). Nanoparticle-based biocompatible and long-life marker for lysosome labeling and tracking. *Analytical chemistry* 82(6): 2213-2220.

Shrestha, N.K., Macak, J.M., Schmidt-Stein, F., Hahn, R., Mierke, C.T., Fabry, B. and Schmuki, P., (2009). Magnetically guided titania nanotubes for site-selective photocatalysis and drug release. *Angewandte Chemie International Edition* 48(5): 969-972.

Shukla, R.K., Kumar, A., Gurbani, D., Pandey, A.K., Singh, S. and Dhawan, A., (2013). TiO_2 nanoparticles induce oxidative DNA damage and apoptosis in human liver cells. *Nanotoxicology* 7(1): 48-60.

Shukla, S., Jadaun, A., Arora, V., Sinha, R.K., Biyani, N. and Jain, V.K., (2015). In vitro toxicity assessment of chitosan oligosaccharide coated iron oxide nanoparticles. *Toxicology reports* 2: 27-39.

Sies, H. and Akerboom, T.P., (1984). Glutathione disulfide (GSSG) efflux from cells and tissues. In *Methods in enzymology* 105:445-451).

Smital, K., Niharika, S. and Mansee, T., (2020). Sub-acute toxicity assessment of green synthesized hematite nanoparticles (α-Fe2O3 NPs) using Wistar rat. *Research Journal of Biotechnology* 15: 4.

Smolinske, S.C., Hall, A.H., Vandenberg, S.A., Spoerke, D.G. and McBride, P.V., (1990). Toxic effects of nonsteroidal anti-inflammatory drugs in overdose. *Drug Safety* 5(4): 252-274.

Song, Y.Y., Schmidt-Stein, F., Berger, S. and Schmuki, P., (2010). TiO_2 Nano Test Tubes as a Self-Cleaning Platform for High-Sensitivity Immunoassays. *Small* 6(11): 1180-1184.

Suttiponparnit, K., Jiang, J., Sahu, M., Suvachittanont, S., Charinpanitkul, T. and Biswas, P., (2011). Role of surface area, primary particle size, and crystal phase on titanium dioxide nanoparticle dispersion properties. *Nanoscale Research Letters* 6(1): 1-8.

Suzuki, H., Toyooka, T. and Ibuki, Y., (2007). Simple and easy method to evaluate uptake potential of nanoparticles in mammalian cells using a flow cytometric light scatter analysis. *Environmental science & technology* 41(8): 3018-3024.

Suzuki, H., Toyooka, T. and Ibuki, Y., (2007). Simple and easy method to evaluate uptake potential of nanoparticles in mammalian cells using a flow cytometric light scatter analysis. *Environmental science & technology* 41(8): 3018-3024.

Svenson, S. and Tomalia, D.A., (2012). Dendrimers in biomedical applications—reflections on the field. *Advanced drug delivery reviews* 64: 102-115.

Takahashi, Y., Shibata, Y., Maeda, M., Miyano, Y., Murai, K. and Ohmori, A., (2014). August.Plasma-spraying synthesis of high-performance photocatalytic TiO_2 coatings. *IOP Conference Series: Materials Science and Engineering,* International Symposium on Interfacial Joining and Surface Technology, Osaka, Japan, pp.012039.

Tamilselvan, A. and Balakumar, S., (2016). Anatase TiO_2 nanotube by electrochemical anodization method: effect of tubes dimension on the supercapacitor application. *Ionics* 22(1): 99-105.

Tang, H., Prasad, K., Sanjines, R., Schmid, P.E. and Levy, F., (1994). Electrical and optical properties of TiO_2 anatase thin films. *Journal of applied physics* 75(4): 2042-2047.

Tang, J., Xiong, L., Wang, S., Wang, J., Liu, L., Li, J., Yuan, F. and Xi, T., (2009). Distribution, translocation and accumulation of silver nanoparticles in rats. *Journal of nanoscience and nanotechnology* 9(8): 4924-4932.

Tekmen, S. and Alım, Z., (2018). Ethics in Nanotechnology and Society Perception, *Nanotoxicology* 19-33.

Tenne, R., (1995). Doped and heteroatom-containing fullerene-like structures and nanotubes. *Advanced Materials* 7(12): 965-995.

Thostenson, E.T., Ren, Z. and Chou, T.W., (2001). Advances in the science and technology of carbon nanotubes and their composites: a review. *Composites science and technology* 61(13): 1899-1912.

Tian, A., Wu, Y. and Mao, K., (2017). Enhanced performance of surface modified TiO_2 nanotubes for the decomposition of perfluorooctanoic acid. *AIP Conference Proceedings*. International conference on Material Science, Resource and Environmental Engineering, New York, pp. 1794(1):020029.

Vamanu, C.I., Cimpan, M.R., Høl, P.J., Sørnes, S., Lie, S.A. and Gjerdet, N.R., (2008). Induction of cell death by TiO2 nanoparticles: studies on a human monoblastoid cell line. *Toxicology in Vitro* 22(7): 1689-1696.

Vander Wal, R.L., Berger, G.M. and Ticich, T.M., (2003). Carbon nanotube synthesis in a flame using laser ablation for in situ catalyst generation. *Applied Physics A* 77(7): 885-889.

Vardharajula, S., Ali, S.Z., Tiwari, P.M., Eroğlu, E., Vig, K., Dennis, V.A. and Singh, S.R., (2012). Functionalized carbon nanotubes: biomedical applications. *International journal of nanomedicine* 7: 5361.

Venkatesh, N., Bhowmik, H. and Kuila, A., (2018). Metallic nanoparticle: a review. *Biomedical Journal of Scientific & Technical Research* 4(2): 3765-3775.

Verma, M.L., (2018). Critical evaluation of toxicity tests in context to engineered nanomaterials: an introductory overview. *Nanotoxicology: toxicity evaluation, risk assessment and management. CRC Press, Boca Raton,* pp. 1-17.

Vevers, W.F. and Jha, A.N., (2008). Genotoxic and cytotoxic potential of titanium dioxide (TiO_2) nanoparticles on fish cells in vitro. *Ecotoxicology* 17(5): 410-420.

Vidu, R., Rahman, M., Mahmoudi, M., Enachescu, M., Poteca, T.D. and Opris, I., (2014). Nanostructures: a platform for brain repair and augmentation. *Frontiers in systems neuroscience* 8: 91.

Von Bohlen Und Halbach, O., (2007). Immunohistological markers for staging neurogenesis in adult hippocampus. *Cell and tissue research* 329(3): 409-420.

Vu, T.H.T., Au, H.T., Tran, L.T., Nguyen, T.M.T., Tran, T.T.T., Pham, M.T., Do, M.H. and Nguyen, D.L., (2014). Synthesis of titanium dioxide nanotubes via one-step dynamic hydrothermal process. *Journal of materials science* 49(16): 5617-5625.

Wan, C.P., Myung, E. and Lau, B.H., (1993). An automated micro-fluorometric assay for monitoring oxidative burst activity of phagocytes. *Journal of Immunological Methods* 159(1-2): 131-138.

Wang, Q., Wang, Y., Duan, B. and Zhang, M., (2016). Modified sol-gel synthesis of carbon nanotubes supported titania composites with enhanced visible light induced photocatalytic activity. *Journal of Nanomaterials 2016*: 1.

Wang, R., Shi, M., Xu, F., Qiu, Y., Zhang, P., Shen, K., Zhao, Q., Yu, J. and Zhang, Y., 2020. Graphdiyne-modified TiO_2 nanofibers with osteoinductive and enhanced photocatalytic antibacterial activities to prevent implant infection. *Nature communications* 11(1): 1-12.

Wang, Y., Cui, H., Zhou, J., Li, F., Wang, J., Chen, M. and Liu, Q., (2015). Cytotoxicity, DNA damage, and apoptosis induced by titanium dioxide nanoparticles in human non-small cell lung cancer A549 cells. *Environmental Science and Pollution Research* 22(7): 5519-5530.

Wani, M.Y., Hashim, M.A., Nabi, F. and Malik, M.A., (2011). Nanotoxicity: dimensional and morphological concerns. *Advances in Physical Chemistry* 2011. DOI: 10.1155/2011/450912.

Wei, M., Konishi, Y., Zhou, H., Sugihara, H. and Arakawa, H., (2004). A simple method to synthesize nanowires titanium dioxide from layered titanate particles. *Chemical Physics Letters* 400(1-3): 231-234.

Whittaker, E.J.W. and Zussman, J., (1956). The characterization of serpentine minerals by X-ray diffraction. *Mineralogical Magazine and Journal of the Mineralogical Society* 31(233): 107-126.

Wilder, J.W., Venema, L.C., Rinzler, A.G., Smalley, R.E. and Dekker, C., (1998). Electronic structure of atomically resolved carbon nanotubes. *Nature* 391(6662): 59-62.

Wu, G.S., Xie, T., Yuan, X.Y., Li, Y., Yang, L., Xiao, Y.H. and Zhang, L.D., (2005). Controlled synthesis of ZnO nanowires or nanotubes via sol–gel template process.*Solid State Communications* 134(7): 485-489.

Wu, Z., Guo, C., Liang, S., Zhang, H., Wang, L., Sun, H. and Yang, B., (2012). A pluronic F127 coating strategy to produce stable up-conversion NaYF4: Yb, Er (Tm) nanoparticles in culture media for bioimaging. *Journal of Materials Chemistry* 22(35): 18596-18602.

Yamamoto, T., Murakami, Y., Motoyanagi, J., Fukushima, T., Maruyama, S. and Kato, M., (2009). An analytical system for single nanomaterials: combination of capillary electrophoresis with Raman spectroscopy or with scanning probe microscopy for individual single-walled carbon nanotube analysis. *Analytical chemistry* 81(17): 7336-7341.

Yan, X. and Chen, X., (2015). Titanium dioxide nanomaterials. *Encyclopedia of inorganic and bioinorganic chemistry*: 1-38. DOI: 10.1002/9781119951438.eibc2335.

Yilmaz, E. and Soylak, M., (2020). Functionalized nanomaterials for sample preparation methods. *Handbook of Nanomaterials in Analytical Chemistry*, Elsevier Publishers, New York, pp. 375-413.

Ying, L., Hon, L.S., White, T., Withers, R. and Hai, L.B., (2003). Controlled nanophase development in photocatalytic titania. *Materials Transactions* 44(7): 1328-1332.

Yoshida, R., Suzuki, Y. and Yoshikawa, S., (2005). Syntheses of TiO_2 (B) nanowires and TiO_2 anatase nanowires by hydrothermal and post-heat treatments. *Journal of solid state Chemistry* 178(7): 2179-2185.

You DG, Deepagan VG, Um W, Jeon S, Son S, Chang H, Yoon HI, Cho YW, Swierczewska M, Lee S, Pomper MG., (2016). ROS-generating TiO_2 nanoparticles for non-invasive sonodynamic therapy of cancer. *Scientific report* 6(1):1-2.

Younes, N.R.B., Amara, S., Mrad, I., Ben-Slama, I., Jeljeli, M., Omri, K., El Ghoul, J., El Mir, L., Rhouma, K.B., Abdelmelek, H. and Sakly, M., (2015). Subacute toxicity of titanium dioxide (TiO_2) nanoparticles in male rats: emotional behavior and pathophysiological examination. *Environmental Science and Pollution Research* 22(11): 8728-8737.

Yu, Q., Wang, H., Peng, Q., Li, Y., Liu, Z. and Li, M., (2017). Different toxicity of anatase and rutile TiO_2 nanoparticles on macrophages: involvement of difference in affinity to proteins and phospholipids. *Journal of hazardous materials* 335: 125-134.

Yuan, Z.Y. and Su, B.L., (2004). Titanium oxide nanotubes, nanofibers and nanowires. *Colloids and Surfaces A: Physicochemical and Engineering Aspects* 241(1-3): 173-183.

Zavala, M.Á.L., Morales, S.A.L. and Ávila-Santos, M., (2017). Synthesis of stable TiO_2 nanotubes: effect of hydrothermal treatment, acid washing and annealing temperature. *Heliyon* 3(11): 00456.

Zhang, S., Peng, L.M., Chen, Q., Du, G.H., Dawson, G. and Zhou, W.Z., (2003). Formation Mechanism of $H_2Ti_3O_7$ Nanotubes. *Physical Review Letters* 91(25): 256103.

Zhao, J., Bowman, L., Zhang, X., Vallyathan, V., Young, S.H., Castranova, V. and Ding, M., (2009). Titanium dioxide (TiO_2) nanoparticles induce JB6 cell apoptosis through activation of the caspase-8/Bid and mitochondrial pathways. *Journal of toxicology and environmental health, part A* 72(19): 1141-1149.

Zhou, S.M., Zhang, X.H., Meng, X.M., Zou, K., Fan, X., Wu, S.K. and Lee, S.T., (2004). The fabrication and optical properties of highly crystalline ultra-long Cu-doped ZnO nanowires.*Nanotechnology* 15(9): 1152.

Zhu, K., Vinzant, T.B., Neale, N.R. and Frank, A.J., (2007). Removing structural disorder from oriented TiO_2 nanotube arrays: reducing the dimensionality of transport and recombination in dye-sensitized solar cells. *Nano Letters* 7(12): 3739-3746.

Zhu, X., Han, S., Feng, W., Kong, Q., Dong, Z., Wang, C., Lei, J. and Yi, Q., (2018). The effect of heat treatment on the anatase–rutile phase transformation and photocatalytic activity of Sn-doped TiO_2 nanomaterials. *RSC advances* 8(26): 14249-14257.

Zhu, Y., Murali, S., Cai, W., Li, X., Suk, J.W., Potts, J.R. and Ruoff, R.S., (2010). Graphene and graphene oxide: synthesis, properties, and applications. *Advanced materials* 22(35): 3906-3924.

Zhu, Y.Q., Sekine, T., Brigatti, K.S., Firth, S., Tenne, R., Rosentsveig, R., Kroto, H.W. and Walton, D.R., (2003). Shock-wave resistance of WS_2 nanotubes. *Journal of the American Chemical Society* 125(5): 1329-1333.

Zoccal, J.V.M., Arouca, F.O. and Gonçalves, J.A.S., (2010). Synthesis and characterization of TiO_2 nanoparticles by the method pechini. *Materials science forum* 660: 385-390.

Zoroddu, M.A., Medici, S., Ledda, A., Nurchi, V.M., Lachowicz, J.I. and Peana, M., (2014). Toxicity of nanoparticles. *Current Medicinal Chemistry* 21(33): 3837-3853.

Zucker, R.M. and Daniel, K.M., (2012). Detection of TiO_2 nanoparticles in cells by flow cytometry. *Nanoparticles in biology and medicine*, Humana Press, Totowa, New Jersey, pp. 497-509.

ANNEXURE

LIST OF PUBLICATIONS

1. **Athira SS**, Biby ET, Mohanan PV (2020) Dextran stabilized fullerene soot induced toxicity on Alveolar epithelial cells (A549 cells). *Environmental Research*. 118: 109716.

2. **Athira SS**, Biby TE, Mohanan PV (2020) Effect of polymer functionalized fullerene soot on C6 glial cells. *European Polymer Journal*. 127: 10957.

3. Sudhakaran S, **Athira SS**, Suresh Babu S, Varma HK, Mohanan PV (2019) Determination of the bioavailability of zinc oxide nanoparticles using ICP-AES and associated toxicity, *Colloids and surface B: Biointerfaces*. 188: 110767.

4. Sruthi S, **Athira SS**, Mohanan PV (2018) ZnO nanoparticle induced neurotoxic potential upon interaction with primary astrocytes. *Neurotoxicology*. 73:213-227.

5. Prajitha N, **Athira SS**, Mohanan PV (2018) Bio-interactions and risks of engineered nanoparticles. *Environmental Research*. 172:98-108.

6. **Athira SS**, Prajitha N, Mohanan PV (2018) Interaction of nanoparticles with central nervous system and its consequences. *American Journal Of Research In Medical Sciences*. 4(1):1-32.

7. Prajitha N, **Athira SS**, Mohanan PV (2018) Pyrogens, a polypeptide produces fever by metabolic changes in hypothalamus: mechanisms and detections. *Immunology letters.* 204:38-46.

8. **S.S. Athira,** P. V. Mohanan, Comparative neurotoxicity evaluation of bare and Pluronic F127 functionalized TiO_2 nanotubes (Submitted).

Online reports

1. **Athira S S**, Mohanan P V (2020) Fullerene soot nanoparticles impose threat to glial cell community. Atlas of Science https://atlasofscience.org/fullerene-soot-nanoparticles-impose-threat-to-glial-cell-community/

2. **Athira S S,** Mohanan PV (2019) Sympathy of Nanoparticles With Primary Astrocytes Leads To Neurotoxicity. Science Trends https://pubmed.ncbi.nlm.nih.gov/31028760/
3. **Athira SS**, Prajitha N, Mohanan PV (2018) Can Nanoparticles Form An Alliance With The Central Nervous System? Science Trends https://sciencetrends.com/can-nanoparticles-form-an-alliance-with-the-central-nervous-system/

4. Sruthi S, **Athira SS**, Mohanan PV (2018) Melatonin play wonders in Zinc oxide nanoparticle induced toxicity. Atlas of Science https://atlasofscience.org/melatonin-play-wonders-in-zinc-oxide-nanoparticle-induced-toxicity/

Book Chapters

1. **Athira, S.S**., Akhil, V., Joseph, X., Ashtami, J. and Mohanan, P.V., 2020. 2D Hollow Nanomaterials. Layered 2D Advanced Materials and Their Allied Applications (pp. 211-248), Wiley-Scrivener publisher. https://onlinelibrary.wiley.com/doi/abs/10.1002/9781119655190.ch10

2. Ashtami, J., Joseph, X., Akhil, V., **Athira, S.S**. and Mohanan, P.V., 2020. 2D Layered Double Hydroxides. Layered 2D Advanced Materials and Their Allied Applications (pp. 249-281), Wiley-Scrivener publisher. https://onlinelibrary.wiley.com/doi/abs/10.1002/9781119655190.ch11

3. J Ashtami, **SS Athira,** VG Reshma, PV Mohanan (2019) Black phosphorus based nanodevices. Black Phosphorus (pp. 31-58), Springer, Cham. https://link.springer.com/chapter/10.1007/978-3-030-29555-4_2

CONFERENCE PRESENTATIONS

1. **Athira SS**, Mohanan PV (2019) Synthesis, physico-chemical characterization and neurotoxic effects of titanium dioxide nanoparticles. Poster presented at International conference on emerging advancement in science and technology (ICEAST 2019), New Delhi, 5^{th}-6^{th} September 2019.

2. **Athira SS**, Prajitha N, Syama S, Mohanan PV (2018) Consequences of graphene oxide nanoparticles in HEK293 cells. Presented at the 'International Conference on the Role of Toxicology in Public Health & 38^{th} Annual Conference of Society of Toxicology, India, Sri Balaji Vidyapeeth, Puducherry, India, 12-14 December 2018.

.

3. **Athira SS**, Prajitha N, Mohanan PV (2018) Adverse effects of Graphene oxide nanoparticles in HEK293 cells. Presented at 28^{th} Swedeshi Science Congress, National Institute for Interdisciplinary Sciences and Technology, Thiruvananthapuram, Kerala, India, 7-9 November 2018.